

# A 3D Printed Ballistic Drug Delivery System for Wildlife Administration

---

**Jingjunjiao (Abbey) Long**

Drug Delivery Research Group

School of Science

Faculty of Health and Environmental Sciences

Auckland University of Technology

*A thesis submitted to Auckland University of Technology in fulfilment of the requirements for the degree of Doctor of Philosophy, 2019.*

# Abstract

Overpopulation of wildlife, especially in pest-prone territories, is a major ecological problem. Culling is the most effective population control approach but drug-induced contraception is also common for protected species. The administration of contraception in the wild has been restricted to conventional methods such as surgery which require capturing and handling often large numbers of incorporative or dangerous animals. This thesis proposed a new approach for wildlife contraception by utilising three-dimensional (3D) printing technology to fabricate a novel ballistic drug delivery system (BDDS) capable of remotely administering contraceptives amongst any other required drug(s).

A literature review was conducted focusing on the use and application of fused deposition modelling (FDM) method of 3D printing in drug delivery (Chapter 2). In chapter 3, A ballistic projectile for short-term (seasonal) progesterone (P4)-induced contraception was developed using FDM. A sustained drug release (over five months) was achieved with the projectile providing sufficient kinetic energy to penetrate thin and medium-thickness skins. Subsequently, this projectile was modified to a multi-compartment model capable of loading and delivering multiple drugs, including anti-inflammatory dexamethasone (DEX), local anaesthetic lidocaine hydrochloride (LDC) and contraceptive levonorgestrel (LNG). The drug formulations were independently developed in the following chapters: DEX was formulated in poly (vinyl alcohol) (PVA) hydrogels, and a sustained release was achieved over one month (Chapter 4), LDC was incorporated with chitosan-pectin (CS-PEC) hydrogel and manufactured as a customised 3D printed wound dressing that released LDC in 5h (Chapter 5), LNG was incorporated within a combined system of CS

microspheres and PVA hydrogels, achieving controlled release for over two years (Chapter 6). The above formulations, can be easily incorporated into a multiple-compartment projectile as a BDDS or could be used individually for other clinical applications. The new knowledge created by this thesis provide new insights into ballistic delivery to wildlife, and make a major contribution to advance the application of 3D printing technology in drug delivery.

# Table of Contents

<b>Abstract.....</b>	<b>i</b>
<b>List of tables.....</b>	<b>x</b>
<b>List of figures.....</b>	<b>xii</b>
<b>Attestation of Authorship .....</b>	<b>xviii</b>
<b>Co-author contributions .....</b>	<b>xix</b>
<b>Acknowledgments .....</b>	<b>xxiii</b>
<b>Chapter 1 .....</b>	<b>1</b>
<i>Introduction and thesis framework .....</i>	<i>1</i>
1.1. General introduction.....	2
1.1.1. Wildlife contraception.....	2
1.1.2. Remote drug delivery systems (RDDS).....	4
1.1.3. 3D printing .....	7
1.2. Thesis motivation .....	8
1.3. Thesis Aims .....	10
1.4. Thesis structure.....	12
1.5. Chapter contents and rationales.....	13
1.6. Research outputs arising from this thesis .....	19
1.6.1. Conference presentations .....	19
1.6.2. Publications arising from this thesis .....	20

1.6.3. Other Publications .....	21
1.7. References .....	22
<b>Chapter 2 .....</b>	<b>- 24 -</b>
<i>A Literature Review: Application of Fused Deposition Modelling (FDM) Method of 3D Printing in Drug Delivery .....</i>	<i>- 24 -</i>
2.1. Introduction .....	- 25 -
2.2. 3D Printing .....	- 28 -
2.2.1. Computer aided design.....	- 28 -
2.2.2. 3D printing Techniques applied in drug delivery systems.....	- 28 -
2.2.3. Fused deposition modelling (FDM) in drug delivery .....	- 30 -
2.3. Printing material .....	- 35 -
2.3.1. Suitable polymers in FDM system.....	- 35 -
2.3.2. Drug loading into the filament .....	- 39 -
2.4. Application of FDM in drug delivery.....	- 41 -
2.4.1. 3D printed tablets .....	- 41 -
2.4.2. 3D printed devices.....	- 45 -
2.5. Limitation and future application .....	- 48 -
2.6. References .....	- 50 -
<b>Chapter 3 .....</b>	<b>- 57 -</b>
<i>Development of customised 3D printed biodegradable projectile for administering extended-release contraceptive to wildlife.....</i>	<i>- 57 -</i>

3.1.	Introduction .....	- 58 -
3.2.	Materials and methods.....	- 62 -
3.2.1.	Materials.....	- 62 -
3.2.2.	Preparation of PLA filament loaded with P4 with HME .....	- 62 -
3.2.3.	3D printing of biodegradable projectiles.....	- 62 -
3.2.4.	Characterisation.....	- 63 -
3.3.	Results and discussion.....	- 67 -
3.3.1.	Evaluation of drug loading by HME and its distribution within the host polymer - 67 -	
3.3.2.	Metrological studies of 3D printed biodegradable projectiles .....	- 68 -
3.3.3.	DSC analyses of the influence of extrusion/printing process and drug additive on thermal transition of polymer.....	- 70 -
3.3.4.	FTIR analyses: evidence of chemical interactions between the drug additive and the host polymer.....	- 73 -
3.3.5.	Studies on <i>in vitro</i> drug release .....	- 76 -
3.3.6.	Ballistic penetration analysis .....	- 78 -
3.4.	Conclusion.....	- 81 -
3.5.	References .....	- 82 -
<b>Chapter 4</b>	<b>.....</b>	<b>- 92 -</b>
	<i>Controlled release of dexamethasone from poly (vinyl alcohol) hydrogel.....</i>	<i>- 92 -</i>
4.1.	Introduction .....	- 93 -

4.2.	Materials and methods.....	- 96 -
4.2.1.	Materials.....	- 96 -
4.2.2.	Preparation of DEX loaded hydrogels .....	- 96 -
4.2.3.	Viscosity measurements.....	- 97 -
4.2.4.	Swelling studies .....	- 98 -
4.2.5.	Porosity measurement .....	- 98 -
4.2.6.	Apparent density .....	- 99 -
4.2.7.	Fourier transform infrared (FTIR) spectroscopy.....	- 99 -
4.2.8.	<i>In vitro</i> drug release .....	- 100 -
4.2.9.	Scanning Electron Microscopy (SEM) .....	- 100 -
4.2.10.	Release kinetics .....	- 100 -
4.2.11.	Statistical analysis. ....	- 102 -
4.3.	Results .....	- 103 -
4.3.1.	Hydrogel preparation .....	- 103 -
4.3.2.	Swelling and water absorption .....	- 104 -
4.3.3.	Porosity and density .....	- 107 -
4.3.4.	FTIR .....	- 109 -
4.3.5.	<i>In vitro</i> drug release .....	- 111 -
4.3.6.	Morphology.....	- 117 -
4.4.	Conclusion.....	- 119 -
4.5.	Reference:.....	- 120 -

<b>Chapter 5 .....</b>	<b>- 128 -</b>
<i>A 3D printed chitosan-pectin hydrogel wound dressing for lidocaine hydrochloride delivery.....</i>	<i>- 128 -</i>
5.1. Introduction .....	- 129 -
5.2. Materials and methods.....	- 132 -
5.2.1. Materials.....	- 132 -
5.2.2. Hydrogel preparation .....	- 132 -
5.2.3. 3D printing of hydrogel scaffold.....	- 132 -
5.2.4. Metrological parameters and porosity of scaffolds .....	- 133 -
5.2.5. Swelling and water absorption .....	- 134 -
5.2.6. Bio-adhesion strength.....	- 135 -
5.2.7. Spectral analysis of chemical interactions .....	- 136 -
5.2.8. Thermal properties .....	- 136 -
5.2.9. <i>In vitro</i> drug release .....	- 136 -
5.2.10. Drug release kinetics .....	- 137 -
5.2.11. Statistical analysis .....	- 139 -
5.3. Results and discussion.....	- 140 -
5.3.1. Evaluation of feasibility of fabricating hydrogel scaffolds using 3D printing	
- 140 -	
5.3.2. Effect of encapsulation of drug on the morphology, swelling and water	
absorption of hydrogel .....	- 141 -



5.3.3.	Bio-adhesion strength.....	- 144 -
5.3.4.	Determination of molecular interactions between the drug and the hydrogel scaffold - 145 -	
5.3.5.	Evaluation of <i>in vitro</i> drug release studies .....	- 151 -
5.4.	Conclusion.....	- 155 -
5.5.	Reference:.....	- 157 -
<b>Chapter 6</b>	.....	<b>- 163 -</b>
	<i>Development of a long-term contraceptive implant with levonorgestrel loaded chitosan microspheres embedded in poly (vinyl alcohol) hydrogel</i> .....	- 163 -
6.1.	Introduction .....	- 164 -
6.2.	Materials and methods.....	- 169 -
6.2.1.	Materials.....	- 169 -
6.2.2.	Microspheres and hydrogel preparation.....	- 169 -
6.2.3.	Morphological assessment .....	- 170 -
6.2.4.	Drug loading .....	- 171 -
6.2.5.	Swelling and water absorption of PVA hydrogel .....	- 172 -
6.2.6.	<i>In vitro</i> drug release .....	- 173 -
6.2.7.	Kinetic models .....	- 174 -
6.2.8.	Spectral analysis of chemical interactions .....	- 174 -
6.2.9.	Differential scanning calorimetry (DSC) analysis .....	- 175 -
6.3.	Results and discussion.....	- 176 -

6.3.1.	Characterisation of CS microspheres .....	- 176 -
6.3.2.	Characterisation of the hydrogel .....	- 180 -
6.3.3.	Swelling studies .....	- 182 -
6.3.4.	<i>In vitro</i> drug release .....	- 187 -
6.3.5.	Spectral analysis .....	- 192 -
6.3.6.	Thermal analysis .....	- 195 -
6.4.	Conclusion .....	- 199 -
6.5.	Reference .....	- 201 -
<b>Chapter 7</b>	.....	<b>- 208 -</b>
	<i>General discussion</i> .....	- 208 -
7.1.	Thesis summary .....	- 209 -
7.2.	Core chapter philosophies .....	- 211 -
7.3.	Limitations .....	- 215 -
7.3.1.	<i>In vivo</i> studies for individual formulations .....	- 215 -
7.3.2.	Characterisation of the assembled projectile .....	- 216 -
7.4.	Future work .....	- 217 -
7.5.	Conclusion .....	- 219 -
7.6.	References .....	- 220 -
<b>Reference list</b>	.....	<b>- 221 -</b>

# List of tables

Table 1-1. Physicochemical properties of the drugs used in this thesis.....	16
Table 2-1. Typical polymers used in FDM 3D printing .....	- 36 -
Table 3-1. Drug Loading (DL), Incorporation Efficiency (IE) and Relative standard Deviation Percent (%RSD) of drug content in HME filaments and 3D printed biodegradable projectiles with theoretical P4 loadings of 2, 5 and 10% w/w (PLA2, PLA5 and PLA10 respectively) (n=3±SD). ....	- 68 -
Table 3-2. Metrological properties (diameter, length and weight) of 3D printed biodegradable projectiles with different formulations (n=3±SD).....	- 70 -
Table 3-3. DSC analysis of pure P4 and 3D printed PLA biodegradable projectiles with different concentrations of P4: 0, 2, 5 and 10% w/w. ....	- 72 -
Table 3-4. Minimum specific kinetic energy required to penetrate thin and medium-thickness hides (Ek,p). ....	- 79 -
Table 3-5. Range of specific energy required to penetrate muscle (Em,p).....	- 79 -
Table 3-6. Range of total energy required to deliver projectile 4 mm into muscle. ...	- 80 -
Table 4-1. Composition and designation of PVA hydrogels. ....	- 97 -
Table 4-2. Kinetics parameters of DEX release from PVA hydrogels. ....	- 116 -
Table 5-1. Average physical dimensions and weights of 3D printed and lyophilised mesh scaffolds along with wet and dry weights (n=3± SD).....	- 141 -
Table 5-2. Mathematical model of kinetics parameters of lidocaine hydrochloride (LDC) release from 3D printed chitosan-pectin (CS-PEC) hydrogel scaffolds. ....	- 154 -

Table 6-1. Particle size parameters of levonorgestrel (LNG)-loaded chitosan (CS) microspheres. ....	- 179 -
---	---------

Table 6-2. Drug loading of chitosan (CS) microspheres and poly (vinyl alcohol) (PVA) hydrogels. ....	- 180 -
--	---------

# List of figures

Figure 1-1. Diagrams of a two-chambered compress gas dart (A) and a powder explosive powered dart (B) (West et al., 2014).....	5
Figure 1-2. Design of the improved projectile and illustration of drug compartments...	15
Figure 2-1. A): CAD design, B): Capsule designed in CAD and C): Capsule printed.-	28
-	
Figure 2-2. Schematic illustration of FDM system. ....	32 -
Figure 2-3. Schematic image of hot melt extrusion (HME) system: A): HME (Noztek Pro, UK), B): digital-control motor, C): screw barrel, D): control panel, E): nozzle, F): heater band & fan, G): screw and H): hopper. ....	40 -
Figure 3-1. Biodegradable projectile design: for 0.177 calibre 900FPS air-rifle sized 35 mm length $\times$ 4.5 mm diameter with a 15 mm cone tip. ....	63 -
Figure 3-2. Photograph of 3D printed biodegradable projectiles: (a) pure poly (lactic acid) (PLA), (b) PLA2 (2% progesterone loading), (c) PLA5 (5% progesterone loading) and (d) PLA10 (10% progesterone loading). ....	68 -
Figure 3-3. SEM images of 3D printed PLA10 projectiles: (a) surface and (b) cross section. ....	69 -
Figure 3-4. DSC curves of A: (a) printed pure poly (lactic acid) (PLA), (b) printed PLA with 2% progesterone loading, (c) printed PLA with 5% progesterone loading, (d) printed PLA with 10% progesterone loading and (e) pure progesterone; B: (a) pure PLA, (b) physical mixture of PLA and progesterone and (c) pure progesterone. ....	73 -
Figure 3-5. FTIR spectra of (a) progesterone (b) printed pure poly (lactic acid) (PLA) and printed PLA with (c) 2%, (d) 5% and (e) 10% progesterone loading. ....	74 -

Figure 3-6. Chemical interaction of poly (lactic acid) (PLA) polymer and progesterone. - 75 -	
Figure 3-7. SEM cross section images of PLA10 projectiles: (a) before and (b) after the dissolution study. .... - 77 -	
Figure 3-8. <i>In vitro</i> drug release profiles of P4 from 3D printed PLA biodegradable projectiles (n=3±SD). .... - 78 -	
Figure 4-1. Crosslinking reaction of poly (vinyl alcohol) (PVA) and glutaraldehyde (GA). .... - 97 -	
Figure 4-2. Rheological behaviour of poly (vinyl alcohol) (PVA) hydrogels crosslinked by different concentrations of glutaraldehyde (GA). .... - 103 -	
Figure 4-3. Poly (vinyl alcohol) (PVA) hydrogels with different concentrations of glutaraldehyde (GA) (0.125, 0.250, 0.375, 0.500, 0.625 and 0.750% respectively): a1) wet dexamethasone (DEX)-free PVA hydrogels, a2) dried DEX-free PVA hydrogels, b1) wet DEX-loaded PVA hydrogels and b2) dried DEX-loaded PVA hydrogels. .... - 104 -	
Figure 4-4. Swelling kinetics of poly (vinyl alcohol) (PVA) hydrogels at $37 \pm 2^\circ\text{C}$ in PBS buffer with increasing concentrations of glutaraldehyde (GA): a). dexamethasone (DEX)-free PVA hydrogels and b) DEX-loaded PVA hydrogels (n=3±SD). .... - 105 -	
Figure 4-5. Equilibrium water content (EWC) of dexamethasone (DEX)-free and -loaded poly (vinyl alcohol) (PVA) hydrogels at different concentrations of crosslinker glutaraldehyde (GA) (n=3±SD). .... - 106 -	
Figure 4-6. Physical properties of dexamethasone (DEX)-free and -loaded poly (vinyl alcohol) (PVA) hydrogels with increasing concentrations of glutaraldehyde (GA): a) porosity and b) apparent density (n=3±SD). *: p<0.05. .... - 108 -	
Figure 4-7. FTIR spectra of (a) pure dexamethasone (DEX), (b) DEX-loaded poly (vinyl alcohol) (PVA) hydrogel (DEX concentration: 2.5mg/mL, glutaraldehyde (GA) concentration: 0.25%), (c) DEX-free PVA hydrogel (GA concentration: 0.25%) and (d) DEX & GA free PVA. .... - 109 -	

Figure 4-8. <i>In vitro</i> drug release of dexamethasone (DEX) from poly (vinyl alcohol) (PVA) hydrogels with different glutaraldehyde (GA) concentrations (n=3±SD). ....	113 -
Figure 4-9. SEM images of the transverse sections of dexamethasone (DEX)-loaded poly (vinyl alcohol) (PVA) hydrogel: a) DEX-375 before release dissolution (DEX crystals were circled as white), b) DEX-125 after release dissolution, c) DEX-375 after release dissolution and d) DEX-750 after release dissolution. ....	118 -
Figure 5-1. A digital 3D mesh scaffold design (unit: mm). ....	133 -
Figure 5-2. Digital 3D design of 3D printed poly (lactic acid) (PLA) mesh holder for swelling and water absorption studies of 3D printed chitosan-pectin (CS-PEC) hydrogel scaffold. ....	135 -
Figure 5-3. The chromatogram obtained with LCD peak eluting at 1.121 mins. ....	137 -
Figure 5-4. 3D printed chitosan-pectin (CS-PEC) hydrogel scaffold: a) freshly printed, b) lyophilised and c) flexibility of a lyophilised scaffold. ....	140 -
Figure 5-5. SEM micrographs of the cross section of 3D printed chitosan-pectin (CS-PEC) hydrogel scaffolds: a) lidocaine hydrochloride free (LDC-0), b) LDC-2, c) LDC-5 and d) LDC-10. ....	142 -
Figure 5-6. Equilibrium swelling ratio (ESR) of chitosan-pectin (CS-PEC) hydrogel scaffolds as a function of lidocaine hydrochloride (LDC) content (n=3± SD). ....	144 -
Figure 5-7. Bioadhesion strength of 3D printed hydrogel scaffolds as a function of lidocaine hydrochloride (LDC) content (n=3± SD). **: p<0.01. ....	145 -
Figure 5-8. DSC curves of (a) chitosan (CS), (b) pectin (PEC), (c) CS-PEC scaffold, (d) 10% w/v lidocaine hydrochloride-loaded (LDC-10) CS-PEC scaffold and (e) LDC.-	147 -
Figure 5-9. FTIR spectra of: (a) chitosan (CS), (b) pectin (PEC) and (c) CS-PEC scaffold. ....	147 -

Figure 5-10. Physical interactions between chitosan (CS) and pectin (PEC) polysaccharides. ....	- 149 -
Figure 5-11. FTIR spectra of: (a) lidocaine hydrochloride-free (LDC-0), (b) 2% w/v LDC-loaded (LDC-2), (c) 5% w/v LDC-loaded (LDC-5), (d) 10% w/v LDC-loaded (LDC-10) chitosan-pectin (CS-PEC) scaffolds and (e) LDC. ....	- 150 -
Figure 5-12. <i>In vitro</i> drug release of lidocaine hydrochloride (LDC) drug from 3D printed chitosan-pectin (CS-PEC) hydrogel scaffolds with different amount of drug loadings (n=3± SD). ....	- 152 -
Figure 6-1. The chromatogram obtained with LNG peak eluting at 2.370 mins. ....	- 172 -
Figure 6-2. Aldehyde-crosslinking reaction of chitosan (CS) by glutaraldehyde (GA). ...	- 176 -
Figure 6-3. SEM micrograph of Levonorgestrel (LNG)-loaded and glutaraldehyde (GA)-crosslinked chitosan (CS) microspheres in the size range of 125-300 µm. ....	- 177 -
Figure 6-4. SEM micrographs of a) levonorgestrel (LNG)-free chitosan (CS) microsphere, b) LNG-loaded CS microsphere, c) surface of LNG-free CS microsphere, d) surface of LNG-loaded CS microsphere, e) LNG-loaded CS microsphere embedded in poly (vinyl alcohol) (PVA) hydrogel and f) cross-section of LNG-CS microsphere.-	- 178 -
Figure 6-5. Particle size distribution of levonorgestrel (LNG)-loaded chitosan (CS) microsphere from different size ranges: dotted line represents microspheres < 63 µm, dashed line represents microspheres of 63-125 µm and solid line represents microspheres of 125-300 µm.....	- 179 -
Figure 6-6. Poly (vinyl alcohol) (PVA) hydrogel scaffolds (PVA concentration:15%): a) Microsphere-free fresh hydrogel after five freeze-thaw cycles, b) Microsphere-free dried hydrogel after annealing, c) microspheres-loaded (125-300 µm) fresh hydrogel after five freeze-thaw cycles and d) microspheres-loaded (125-300 µm) dried hydrogel after annealing. ....	- 182 -



Figure 6-7. SEM micrographs of dried and annealed poly (vinyl alcohol) (PVA) hydrogels prepared with different PVA concentrations: a) 10%, b) 15% and c) 20% w/v.

..... - 182 -

Figure 6-8. Equilibrium water content (EWC) of poly (vinyl alcohol) (PVA) hydrogels: solid bars correspond to the unannealed PVA hydrogels without microspheres, gradient-filled bars correspond to the annealed PVA hydrogels without microspheres and dot-filled bars correspond to the annealed PVA hydrogels with microspheres ( $n=3\pm SD$ ). \*\*:  $p<0.01$ .

..... - 184 -

Figure 6-9. Equilibrium swelling ratio (ESR) of unannealed poly (vinyl alcohol) (PVA) hydrogels prepared by five cycles of freeze-thawing without microspheres: dotted line represents 10% PVA hydrogel, dashed line represents 15% PVA hydrogel and solid line represents 20% PVA hydrogel ( $n=3\pm SD$ ). .....

- 185 -

Figure 6-10. Equilibrium swelling ratio (ESR) of freeze-thawed followed by annealed hydrogels without microspheres: dotted line represents 10% PVA hydrogel, dashed line represents 15% PVA hydrogel and solid line represents 20% PVA hydrogel ( $n=3\pm SD$ ).-

186 -

Figure 6-11. Equilibrium swelling ratio (ESR) of annealed poly (vinyl alcohol) (PVA) hydrogels prepared by five cycles of freeze-thawing with levonorgestrel (LNG)-chitosan (CS) microspheres: dotted line represents 10% PVA hydrogel, dashed line represents 15% PVA hydrogel and solid line represents 20% PVA hydrogel ( $n=3\pm SD$ ). .....

- 187 -

Figure 6-12. *In vitro* release of levonorgestrel (LNG) from microsphere system based on different size ranges of microspheres: dotted line represents microspheres  $< 63\ \mu\text{m}$ , dashed line represents microspheres of  $63\text{-}125\ \mu\text{m}$  and solid line represents microspheres of  $125\text{-}300\ \mu\text{m}$  ( $n=3\pm SD$ ). .....

- 188 -

Figure 6-13. *In vitro* release of levonorgestrel (LNG) from microsphere-hydrogel system based on different poly (vinyl alcohol) (PVA) concentrations: dotted line represents 10% PVA hydrogel, dashed line represents 15% PVA hydrogel and solid line represents 20% PVA hydrogel ( $n=3\pm SD$ ). .....

- 190 -

Figure 6-14. SEM micrographs of samples after dissolution test: a) levonorgestrel (LNG)-loaded chitosan (CS) microsphere, b) 10% poly(vinyl alcohol) (PVA) hydrogel, c) 15% PVA hydrogel and d) 20% PVA hydrogel. .... - 192 -

Figure 6-15. FTIR spectra of (a) chitosan (CS), (b) levonorgestrel (LNG)-free chitosan (CS) microspheres, (c) LNG-loaded CS microsphere, (d) LNG-loaded CS microsphere (125-300  $\mu\text{m}$ ) embedded in 20% poly (vinyl alcohol) (PVA) hydrogel , (e) 20% PVA hydrogel, (f) PVA and (g) LNG. .... - 193 -

Figure 6-16. Aldehyde crosslinking reaction of chitosan by glutaraldehyde..... - 194 -

Figure 6-17. DSC thermograms of (a) chitosan (CS), (b) levonorgestrel (LNG)-loaded CS microspheres, (c) annealed 20% poly(vinyl alcohol) (PVA) hydrogel with LNG-loaded CS microspheres, (d) annealed 20% PVA hydrogel, (e) unannealed 20% PVA hydrogel, (f) PVA and (g) LNG. .... - 196 -

Figure 6-18. Crosslinked poly (vinyl alcohol) (PVA) hydrogel by hydrogen bonding and crystallisation by annealing..... - 198 -

# Attestation of Authorship

“I hereby declare that this submission is my own work and that, to the best of my knowledge and belief, it contains no material previously published or written by another person (except where explicitly define in acknowledgements), nor material which to a substantial extent has been submitted for the award of any other degree or diploma of a university or other institution of higher learning.”

Signed: 




Date: 01.30.2019

# Co-author contributions

The contribution of literature review in this thesis has been broken down into four parts, each of which has been given a proportion (%time) to produce the completed output:

Concept & structure	= 10%
Article retrieval & assessments	= 5%
Writing	= 75%
Reviewing & editing	= 10%

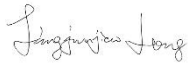


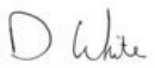



## Chapter 2: Literature review (*Long et al. 2017*)

	Contribution	Proportion	Total	Signature
Jingjunjiao Long	Concept & structure	40%	81.75%	
	Article retrieval & assessments	90%		
	Writing	95%		
	Reviewing & editing	20%		
Hamideh Gholizadeh	Article retrieval & assessments	10%	5.75%	
	Writing	5%		
	Reviewing & editing	15%		
Jun Lu	Reviewing & editing	5%	0.5%	
Craig Bunt	Reviewing & editing	10%	1%	
Ali Seyfoddin	Concept & structure	60%	11%	
	Reviewing & editing	50%		

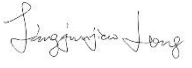



The contributions of experimental manuscripts in this thesis have been broken down into four parts, each of which have been given a proportion (%time) to produce the completed output:

Experimental design	= 10%
Sample collection	= 20%
Data analysis	= 20%
Writing	= 40%
Reviewing & editing	= 10%







### Chapter 3: Experimental manuscript (*Long et al. 2018*)

Author	Contribution	Proportion	Total	Signature
Jingjunjiao Long	Experimental design	60%	82.4%	
	Sample collection	96%		
	Data analysis	96%		
	Writing	95%		
Ashveen V. Nand	Reviewing & editing	10%	1%	
Sudip Ray	Sample collection	2%	1.8%	
	Data analysis	2%		
	Reviewing & editing	10%		
Sam Mayhew	Sample collection	2%	0.8%	CC 
	Data analysis	2%		
David White	Writing	5%	3%	
	Reviewing & editing	10%		
Craig R. Bunt	Reviewing & editing	10%	1%	
Ali Seyfoddin	Experimental design	40%	10%	
	Reviewing & editing	60%		



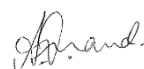




#### Chapter 4: Experimental manuscript (*Long et al. accepted*)

Author	Contribution	Proportion	Total	Signature
Jingjunjiao Long	Experimental design	70%	85%	
	Sample collection	100%		
	Data analysis	90%		
	Writing	100%		
Ashveen V. Nand	Experimental design	10%	3%	
	Reviewing & editing	20%		
Craig R. Bunt	Reviewing & editing	20%	2%	
Ali Seyfoddin	Experimental design	20%	10%	
	Data analysis	10%		
	Reviewing & editing	60%		

#### Chapter 5: Experimental manuscript (*Long et al. submitted*)

Author	Contribution	Proportion	Total	Signature
Jingjunjiao Long	Experimental design	80%	85%	
	Sample collection	95%		
	Data analysis	90%		
	Writing	100%		
Alaitz Etxabide	Experimental design	10%	3%	
Etxeberria	Reviewing & editing	20%		
Ashveen V. Nand	Reviewing & editing	10%	1%	
Craig R. Bunt	Reviewing & editing	10%	1%	
Sudip Ray	Sample collection	5%	2%	
	Reviewing & editing	10%		
Ali Seyfoddin	Experimental design	10%	8%	
	Data analysis	10%		
	Reviewing & editing	50%		

Chapter 6: Experimental manuscript (*Long et al. Submitted*)

Author	Contribution	Proportion	Total	Signature
Jingjunjiao Long	Experimental design	80%	84%	
	Sample collection	90%		
	Data analysis	90%		
	Writing	100%		
Alaitz Etxabide	Experimental design	10%	2%	
Etxeberria	Reviewing & editing	10%		
Ashveen V. Nand	Reviewing & editing	10%	1%	
Craig R. Bunt	Reviewing & editing	10%	1%	
Caroline Kornelseng	Sample collection	5%	1%	
Sudip Ray	Sample collection	5%	2%	
	Reviewing & editing	10%		
Ali Seyfoddin	Experimental design	10%	9%	
	Data analysis	10%		
	Reviewing & editing	60%		

# Acknowledgments

First and foremost, I would like to express my sincere gratitude to my primary supervisor Dr. Ali Seyfoddin for his constant support, patience, motivation and encouragements throughout my Ph.D. He spent countless hours proofreading my research papers and thesis, giving me valuable suggestions which always led to improvement of my work. Moreover, he has taught me how to do research and given me plenty of opportunities to present my work in front of experts at international and domestic conferences. I would like to thank him for inspiring my research in many ways and for allowing me to grow to an independent researcher.

Special thanks to my second supervisor, A/Prof. Craig R. Bunt, for his invaluable insights and immense knowledge. He constantly gave me valuable suggestions that greatly boosted my determination and research progress. I really appreciate his contributions, time and efforts in supervising me from distance.

My heartfelt gratitude is reserved for Dr. Ashveen V. Nand, for his willingness to be my third supervisor with endless encouragements and guidance to overcome the multitude of challenges and difficulties in this journey.

Many thanks to all the research scholars especially Dr. Sudip Ray from the University of Auckland and Dr. David White from the BioDesign Lab at AUT, who offered so much help with my experiments, contributed to my papers and provided guidance with the technical aspects of my research. I am extremely grateful to Dr. Alaitz



Etxabide Etxeberria, as a postdoctoral research fellow in Ali's team, who shared her experiences, constructive ideas and insightful suggestions to improve my work.

I would like to take this opportunity to thank all my friends in Drug Delivery Research Group at AUT and my flatmates. The journey of pursuing a PhD degree is sometimes difficult and lonely. However, your generous support, in personal or academic ways, brought so much light into my journey.

I would also like to thank all the staff at the School of Science who helped and supported me during these years.

Finally, I want to document my special gratitude to my family- Zhongchao Long, Hongjing Chen, Shimiao Yu, Jianxin Yu and Shuguang Chen. Many thanks to all of you for the constant and unconditional support in my career and life. Your love and the faith you had on me have been a constant inspiration to me, motivating me to strive towards my goal and make me who I am today.

# Chapter 1

*Introduction and thesis framework*

## 1.1. General introduction

### 1.1.1. Wildlife contraception

The overpopulation of a number of wild animals as a result of unsuccessful species introduction or a shift in the ecosystem has become a burden as it is associated with increased risk of disease transmission to livestock and competition with endangered species. This is especially relevant to New Zealand and Australia as countries with a large number of livestock and growing pest/wildlife problems. The disease transmission associated with overpopulation of wildlife has raised concerns as human beings are often exposed to transmittable pathogens from wildlife and infected livestock (Treanor et al., 2010). It is therefore essential to develop effective approaches to control wildlife population.

Contraception has been widely used in wildlife management especially when it comes to protected animals such as kangaroos (M. E. Wilson & Coulson, 2016), koalas (Smith, 2017) and feral horses (Beever, Huntsinger, & Petersen, 2018; Hall, Nixon, & Aitken, 2017). However, population control by contraception in non-domestic species remains a challenge due to the difficulties in targeting and delivering contraceptive drug(s).

Conventional drug delivery to wildlife is challenging due to difficulties in treating large numbers, inefficiency of the delivery methods and lacking animal species specificity. Conventional drug delivery methods include oral administration, hand-held injections or pole syringes and implants which often require restraining and animal handling (West et al., 2014). The common drawback of all these approaches is the safety concerns for both rangers and animals. The complexity of preparing and

delivering procedures along with the inapplicability to target large numbers of animals has further limited the use of these systems. Other simplistic delivery methods, such as medicated oral baits are also limited by the lack of specificity for target animals and the drug/dosage form stability problems in the field.

To give an example, in 1920, 18 koalas were released in the Kangaroo Island just off the mainland of South Australia, southwest of Adelaide. Originally introduced to stop Australia's diminishing koala population from going extinct they turned into feral but protected pests with a population exceeding 50,000 in 2015 (Wahlquist, 2017). This became a major threat to the local ecosystem as koalas eat up the regrowth leaves on the very top of eucalyptus, leading to suffocation and death of those trees. This in turn adversely affects all animals whose life depends on those trees, including parrots, possums, wrens, bees and the koalas themselves starving. Some strategies, such as capturing, relocation and sterilisation, have been deployed to control the increasing koala population. One the most effective sterilisation method used for this purpose is to insert an under-skin hormone contraceptive implant to the captured koala, which is quicker, less labour intensive and cheaper than de-sex surgeries (Wahlquist, 2017). However, it is still difficult, time consuming and costly to capture koalas from high eucalyptus trees, which can reach a height of 100 meters. Moreover, other wild animals, compared to tree bound koalas, may be much more difficult and risky to capture and treat. In such scenarios, novel treatment strategies such as remote or ballistic drug delivery systems (RDDS or BDDS) find important applications.

The development of an effective drug delivery method for wildlife with the ability to effectively and safely administer medicines to free-ranging species are therefore significant tasks that need to be addressed.

#### 1.1.2. Remote drug delivery systems (RDDS)

In 1950s, while working on introduced wild goat, deer and tahr population in New Zealand, Christchurch born pharmacist, veterinarian and inventor Sir Collin A. Murdoch came up with an idea of developing a remote or ballistic drug delivery system to tranquilise animals. Having experience with repairing and modifying rifles in World War II, Murdoch invented various rifles, darts and pistols which have been an important part of animal studies/treatment/control around the globe. He established the Paxarms Limited which still sells various ballistic tranquilising systems.

Generally, a RDDS contains a projector and a dart with four components, including a storage space for drug(s), an injective part for loading drug, a needle to penetrate the skin and a stabiliser for ballistic accuracy (West, Heard, & Caulkett, 2014). Such systems can deliver the medicines to wild animals at a safe distance, avoiding the risks of anaesthetisation and direct contact with animals.

##### 1.1.2.1. Darts

Several types of darts have been developed for remote drug delivery, two typical types are two-chambered compress gas darts and powder explosive powered darts (Figure 1-1) (Wiedner, Lindsay, & Isaza, 2012).

Two-chambered compressed gas darts are lightweight plastic darts with dual chambers divided by a movable syringe plunger in the centre (see Figure 1-1 A), examples include blow darts and moulded nylon darts (West et al., 2014). Blow darts

are constructed of lightweight medical-grade plastic and the sharp needle enables the penetration into various types of animal skin. Moulded nylon darts have heavier and made from moulded nylon, an opaque synthetic polymer, suitable for outdoors with long ballistic ranges.

Powder explosive powered darts are heavyweight darts consisted of a powder explosive cap, a chamber for drug loading and a movable central syringe plunger to separate the drug from the explosive unit and trigger the mechanism (see Figure 1-1 B) (Hendricks & Treadway, 2015; West et al., 2014).



Figure 1-1. Diagrams of a two-chambered compress gas dart (A) and a powder explosive powered dart (B) (West et al., 2014).

Many other darts have also been used such as chemical powered, spring powered, solid drug darts and biobullets (Falconer, Christie, Pollard, Olsen, & Grainger, 2016; Kreeger, 1997; West et al., 2014).

#### 1.1.2.2. Projectors

The selection of projectors for remote delivery system depends on the type of darts. The most popular type is compressed gas projector that includes blowpipes, blowguns, air and CO<sub>2</sub> rifles and pistols. Blowpipes are the most versatile, economic and lightweight projectors available in the market (Bush, 1992; West et al., 2014). The key advantage of blowpipe is minimal trauma to the animal due to its low velocity (Kreeger, 1997; West et al., 2014). However, blowpipe requires practical experience

and has limited effective range (about 0.5 to 10 meters) (Kreeger, 1997; West et al., 2014). Blowgun is similar to blowpipe but uses compressed gas to project the dart (Bush, 1992; Haigh & Hopf, 1976; West et al., 2014). This projector has higher accuracy, easier operation and longer range (about 5 to 30 meters) (Brockelman & Kobayashi, 1971; West et al., 2014). Air and CO<sub>2</sub> rifles and pistols are a group of projectors with a barrel mounted onto a triggered compressed gas power, which are suitable for long-distance shooting as it may cause trauma at short range (Bush, 1992; Kreeger, 1997; West et al., 2014). There are other projectors appropriate for remote drug delivery, such as powder loaded rifles (Christie et al., 2006; Kreeger, 1997; West et al., 2014), crossbows, bows (Kreeger, 1997; West et al., 2014) and injection collars (Bush, 1992; Kreeger, 1997; West et al., 2014).

#### 1.1.2.3. Advantages and limitations of RDDS

Using a RDDS for wildlife delivery offers the following advantages: i) target specific; ii) dose tailorability based on the body weight; iii) various formulations can be administered; iv) short-distance contact with wildlife is avoided and v) economical cost per animal (Kreeger, 1997).

However, there are still some limitations of current RDDS that need to be improved for the purpose of delivering contraceptive drugs: i) the formulations are limited to liquid or powder forms with a fast release of incorporated drug not suitable for long-term contraception; ii) recycling of the needle/syringe is difficult in the field and iii) dart size/shape cannot be customised based on animal species or projectors.

To overcome the above shortcomings, this thesis aims to develop a novel BDDS capable of loading and delivering specific dosages of multiple drugs with both

immediate and sustained release profiles to wild animals using biodegradable and biocompatible materials tailor-made in different shapes and sizes.

### 1.1.3. 3D printing

3D printing technology has gained significant interests as a fabrication method in pharmaceutical and medical area since the first 3D printed medicine Spritam was approved by US Food and Drug Administration (FDA) in 2015 (Long, Gholizadeh, Lu, Bunt, & Seyfoddin, 2017). 3D printing, also known as additive manufacturing, is a fabrication process whereby a 3D object is created layer-by-layer by depositing a feed stock material from a nozzle-based deposition system (Tan, Maniruzzaman, & Nokhodchi, 2018). Micro and macro sized models with high precision and controllability can be created, modified, optimised and analysed by computer-aided design (CAD) software, which facilitate the possibility of developing customised medicines with different drug(s), dosages, sizes, geometries and materials. Flexible materials, such as hydrogels and plastic polymers can be 3D printed making it possible to manufacture drug-loaded scaffolds with various release profiles from immediate to extended release behaviours. 3D printing facilitates the development of customised medicines with adjustable drug dosages or formulations. Besides, rapid prototyping and cost-effective materials bring additional benefits for 3D printing in pharmaceutical and medical applications. Therefore, 3D printing was chosen in this thesis to fabricate a BDDS for wildlife with the advantages of i) target animal specificity; ii) flexibility to include solid, semisolid or liquid formulations; iii) drug/dosage diversity based on animal sizes/ species; iv) adjustable projectile size for different animals and v) diverse shapes to fit different projectors.



## 1.2. Thesis motivation

In my undergraduate studies, I chose bioscience as my major in Huazhong University of Science and Technology, that opened a window for me to realise the beauty of life and diversity, from genotype to phenotype, from microorganism to biocoenosis. Systemic principles and technologies in biological sciences, bioinformatics, medicine and computer science learned in my bachelor laid the cornerstone of my PhD project, allowing me to understand the requirements and design pharmaceutical formulations. After bachelor graduation, I went to The University of Manchester in UK to obtain a master degree in biotechnology. There, I learned about polymer chemistry and computer modelling in medicine. My master thesis title was ‘Modelling the interactions between polymers for drug delivery in human cells’. This lead to my PhD and I was pleased to take up this challenge and utilise my knowledge to contribute to wildlife management and drug delivery development.

In the last two decades, drug delivery has emerged as a branch of science that aims to enhance existing drug formulations and to design novel delivery systems for increased therapeutic efficiency. Thousands of formulations and dosage forms have been developed, however, there still exists many gaps for personalised or customised medicines. The development of 3D printing brings new opportunities for improving customised drug formulations and with the first 3D printed drug approved by FDA in 2015, opportunities appear endless. Besides, there remains a paucity of investigations on developing a BDDS for long-term contraception in wildlife. Therefore, I wanted to employ 3D printing technology to develop a novel BDDS, which combines the benefits of customisation and formulation diversity. Furthermore, this theses aims to establish individual application for the formulations developed in each core chapter,

providing additional potential for future practicality. The outputs arising from this thesis bring us one step closer to solving the problem of wildlife contraception, and contribute to the development of controlled drug delivery in general.

### 1.3. Thesis Aims

The primary aim of this thesis is to create a novel 3D printed BDDS to load and deliver multiple drugs with specific dosages and release profiles to wild animals. The second aim is to develop different customised formulations for each drug which they can be assembled as a BDDS for wildlife or used individually for their specific applications.

The specific objectives of this thesis are:

- i. To develop a 3D printed projectile with poly (lactic acid) (PLA) polymer for ballistic drug delivery of progesterone (P4) with sustained release profiles.
- ii. To modify the prototype projectile into an improved multi-compartment model applicable for delivering three drugs with both immediate and sustained release profiles.
- iii. To formulate dexamethasone (DEX), as an anti-inflammatory medicine to control inflammation and trauma caused by bullet penetration, with chemically crosslinked poly (vinyl alcohol) (PVA) hydrogel systems. This formulation can also be used individually as an anti-inflammatory implant with a sustained release of DEX over one month.
- iv. To formulate lidocaine hydrochloride (LDC), a local anaesthetic to reduce the pain of the trauma, with physically crosslinked chitosan-pectin (CS-PEC) hydrogels and subsequently 3D print it as a flexible mesh scaffold. The individual application of this formulation is as a customised 3D printed hydrogel wound dressing with pain relief function through immediate release of LDC.
- v. To formulate levonogestrel (LNG), a progestin contraceptive, with a combined system consists of CS microspheres embedded into PVA hydrogels to prolong the

drug release profile. This formulation can be used individually as a long-term contraceptive implant.

## 1.4. Thesis structure

This thesis consists of a general introduction (Chapter 1), a literature review (Chapter 2), four experimental papers (Chapter 3-6), a final thesis synthesis, discussion and conclusion (Chapter 7), and a comprehensive reference list. Chapter 2-6 are prepared as individual publications and are presented in this thesis as they would appear for publication, with minor modifications in satisfaction of Auckland University of technology (AUT) postgraduate rules and regulation. The contents and rationales of core chapters are described in the following section.

## 1.5. Chapter contents and rationales

**Chapter 2- Literature review:** *Application of fused deposition modelling (FDM) method of 3D printing in drug delivery.*

Fused deposition modelling (FDM), which is currently the most common and accessible 3D printing technology, was considered as our first choice of 3D printing to be employed in this thesis. FDM utilises thermoplastic filaments as printing materials to create a 3D object by melting the filaments and depositing in sequential layers, whereby biodegradable polymers can be used to print a customised projectile with the required physical properties and accuracy. Besides, using hot melt extrusion (HME) to fabricate drug-loaded filaments for FDM 3D printing adds additional benefits in pharmaceutical and medical applications as it brings possibility to develop customised medical implants/scaffolds with specific drug(s) and release behaviours. Thus, a literature review on FDM and HME, which were employed in the following Chapter 3, was carried out at the start of this thesis.

**Chapter 3- Research paper:** *Development of customised 3D printed biodegradable projectile for administering extended-release contraceptive to wildlife.*

After summarising the literature of FDM in pharmaceutical area, we wanted to confirm the feasibility and suitability of using this 3D printing technology to fabricate a ballistic projectile. Therefore, a prototype 3D printed projectile loaded with contraceptive drug progesterone (P4) were developed. In this study, three concentrations of P4 (2, 5 and 10% w/w) with PLA polymer was prepared as 1.75mm filaments by HME and subsequently printed as biodegradable projectiles using FDM 3D printing. These 3D printed projectiles were characterised to assess their potential

as a BDDS. The *in vitro* drug release study indicated that P4 loaded in the projectiles exhibited controlled release behaviours over a five-month period. Penetration assessment confirmed the drug loaded PLA projectiles provided sufficient specific kinetic energy required to penetrate thin and medium-thickness skins. This work demonstrates the feasibility of using FDM 3D printing for manufacturing customised ballistic drug delivery devices.

However, as a prototype, some limitations were noticed: i) P4, as a natural hormone, requires a relatively high dose to achieve effective contraception. Considering the limited loading capability by HME, this device is not suitable for long-term contraception, ii) the projectile model in this study can only incorporate and deliver a single contraceptive drug with no space for loading anti-inflammatory and local anaesthetic drugs in the projectile. Based on these limitations, the prototype was improved into a multi-compartment model, which is applicable for delivering three drugs in a single projectile.

### **Prototype improvement- Multi-compartment model**

After confirming the feasibility of 3D printing technology in Chapter 3, a multi-compartment model capable of delivering more drugs was designed. The improvement of the projectile prototype was based on the consideration that the trauma caused by the projectile penetration cannot be avoided in a BDDS where an anti-inflammatory drug needs to be incorporated to control the inflammation around the trauma and a local anaesthetic to numb the surrounding tissue to reduce the pain. Besides, considering the difficulties in targeting and managing wild animals, it is desirable to reduce the frequency of drug administration. Therefore, this thesis aimed

to develop long-term contraception by using LNG, a potent synthetic progestin, to achieve a controlled release for years instead of months. Based on these considerations, an improved model was designed (Figure 1-2), which can be loaded with and deliver three drugs from a single projectile. The projectile would be expanded after the penetration impact; the broken structure would allow the diffusion of the drug(s). Additionally, the 3D printed case is micro-porous, which is deposited layer-by-layer allowing fluid movement in and out of the scaffold and drug release by diffusion.

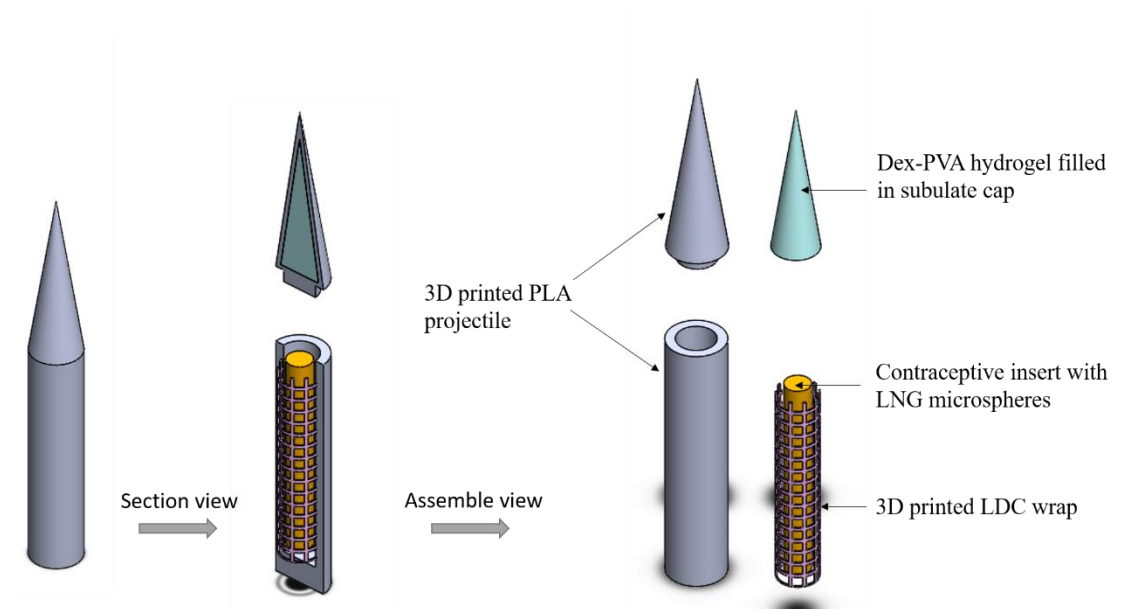


Figure 1-2. Design of the improved projectile and illustration of drug compartments.

In the improved design, the projectile had two hollow parts: a subulate cap and a cylindrical body. The projectile was designed to be printed with PLA polymer by FDM 3D printer, whereby the size and shape can be altered for different animals and projectors. The sharp cap acts as the bullet and is loaded with anti-inflammatory DEX formulated in PVA hydrogels. The cylindrical body with hollow structure provides the required space to accommodate the long-term LNG contraceptive insert wrapped



with a flexible 3D printed LDC hydrogel mesh. The physicochemical properties of the drugs used in this thesis are summarised in Table 1-1. The drug formulation were independently developed in the following chapters.

Table 1-1. Physicochemical properties of the drugs used in this thesis.

Drug	Formula	Molar mass (g/mol)	Melting point (°C)	Log P	Solubility
Progesterone (P4)	C <sub>21</sub> H <sub>30</sub> O <sub>2</sub>	314.46	128-132	4.04	16.8 µg /mL in water and 15.1 µg /mL in 0.9% aqueous saline.
Dexamethasone (DEX)	C <sub>22</sub> H <sub>29</sub> FO <sub>5</sub>	392.461	262-264	1.83	0.0505 mg/mL in water; soluble in ethanol, methanol, acetone, dioxane, and slightly soluble in chloroform
Lidocaine hydrochloride (LDC)	C <sub>14</sub> H <sub>23</sub> ClN <sub>2</sub> O	270.80	77-78	2.44	4100 mg/L in water; Very soluble in alcohol, chloroform; freely soluble in ether, benzene. Dissolves in oils
Levonorgestrel (LNG)	C <sub>21</sub> H <sub>28</sub> O <sub>2</sub>	312.45	240	3.8	2.05 mg/L in water; soluble in ethanol (1 in 120), chloroform (1 in 15), diethyl ether (1 in 400) and dioxane.

**Chapter 4- Research paper:** *Controlled release of dexamethasone from poly (vinyl alcohol) hydrogel.*

This study investigated a chemically crosslinked PVA hydrogel controlled drug delivery system to deliver anti-inflammatory DEX, which would be accommodated in the hollow space in the subulate cap of the projectile. Controlled and sustained release of DEX were achieved over 33 days and the release behaviours were shown to be controlled by the crosslinking densities. PVA hydrogel was chosen in this study as a drug delivery system for DEX because of its biocompatibility and controllability of drug release by easily adjustment of crosslinking density. The sol-gel property of hydrogel system makes it easy to be injected into the hollow space in the projectile when it is in the solution state, and stored in the projectile cap after gelation and drying.

After the delivery of the projectile, the PVA hydrogels can be rehydrated and swelled by absorbing body fluids to give a controlled and sustained release of incorporated DEX to provide effective control of inflammation around trauma.

The individual application of this DEX-PVA formulation is to be used as an anti-inflammatory implant to reduce acute and chronic inflammations after surgery or implantation.

**Chapter 5- Research paper:** *A 3D printed chitosan-pectin hydrogel wound dressing for lidocaine e delivery*

In this study, a chitosan-pectin (CS-PEC) biopolymeric hydrogel drug delivery system was investigated for the local anaesthetic drug lidocaine hydrochloride (LDC) delivery using 3D printing technology. This formulation was 3D printed as a flexible mesh, which would be wrapped around the contraceptive cylindrical insert and then inserted in the hollow space of the projectile body. It is designed to provide an immediate release of LDC around the trauma for effective pain management. The hydrogels prepared by physical crosslinking of CS and PEC polysaccharides present high swelling ratio and water absorption ability, indicating a great potential for absorbing exudates and maintaining moist environment for wound healing of the trauma. An extrusion-based 3D printer was employed to fabricate a mesh scaffold of CS-PEC hydrogels with good flexibility that can be wrapped around the inner wall of the cylindrical body of the projectile. 3D printed hydrogel drug delivery system also brings the possibility of adjusting the scaffold size, thickness and shape, which can be customised based on the animal's size/specie and the projectile size/shape.

The individual application of this chapter is to be used as a customised wound dressing for wounds that require immediate pain relief and moist environment.

**Chapter 6- Research paper:** *Development of a long-term contraceptive implant with levonorgestrel loaded chitosan microspheres embedded in poly (vinyl alcohol) hydrogel*

This study reports on the fabrication and characterisation of a controlled release system designed as a CS microspheres embedded in PVA matrix for delivery of LNG for long-term contraception. This formulation was moulded as a cylindrical insert to be accommodated in the projectile body, providing a long-term release of contraception (3-5 years). LNG is a synthetic progestin that provides effective contraception with a much lesser dose than P4, which capable for long-term contraception. A combined system consists of CS microspheres and PVA hydrogels were developed in this study to prolong the release of LNG at year level and control the drug release as a zero-order release pattern with minimum burst release, which is deemed necessary for a variety of drug delivery applications.

The individual application of this chapter is to provide a promising biodegradable delivery system for long-term contraception with a controlled zero-order drug release profile.

## 1.6. Research outputs arising from this thesis

### 1.6.1. Conference presentations

**Long, J.,** Nand, A. V., Bunt, C., Seyfoddin, A. (2018, August). 3D printed ballistic drug delivery system for wildlife applications. Queenstown Research Week 2018, Queenstown, New Zealand.

**Long, J.,** Nand, A. V., Ray, S., Mayhew, S., White, D., Bunt, C., Seyfoddin, A. (2018, July). 3D printed biopolymeric vehicle for contraceptive delivery to wildlife. MACRO 2018, Queensland, Australia.

**Long, J.,** Bunt, C., & Seyfoddin, A (2017, November). A 3D printed remote drug delivery system for wildlife contraception. New Zealand-Australian Controlled Release Society 2017 Joint Workshop (CRS), Auckland, New Zealand.

Seyfoddin, A., **Long, J.,** & Bunt, C. (2016, December). Remote drug delivery devices for wild life administration. Paper presented at Australasian Wildlife Management Society (AWMS), Auckland, New Zealand.

**Long, J.,** Kim, J. H., Bunt, C., & Seyfoddin, A. (2016, September). A 3D Printed Veterinary Drug Delivery Device: *In Vitro* Characterisation. Emerging Polymer Technologies Summit 2016, Melbourne, Australia.

Seyfoddin, A., **Long, J.,** Gholizadeh, H., & Bunt, C. (2016, September). 3D printed poly (lactic acid) ballistic contraceptive device for wildlife administration. Emerging Polymer Technologies Summit 2016, Melbourne, Australia.

Bunt, C., Pickering, K., **Long, J.**, Gholizadeh, H., & Seyfoddin, A. (2016, July). Physical assessment of a 3D printed poly (lactic acid) dart for wildlife contraceptive delivery. Paper presented at Controlled Release Society (CRS), Seattle, Washington, U.S.A..

#### 1.6.2. Publications arising from this thesis

**Long, J.**, Nand, A. V., Bunt, C., & Seyfoddin, A. (2019). Controlled release of dexamethasone from poly (vinyl alcohol) hydrogel. *Pharmaceutical development and technology*, 1-10.

**Long, J.**, Nand, A. V., Ray, S., Mayhew, S., White, D., Bunt, C. R., & Seyfoddin, A. (2018). Development of customised 3D printed biodegradable projectile for administering extended-release contraceptive to wildlife. *International journal of pharmaceutics*, 548(1), 349-356.

**Long, J.**, Gholizadeh, H., Lu, J., Bunt, C., & Seyfoddin, A. (2017). Application of fused deposition modelling (FDM) method of 3D printing in drug delivery. *Current pharmaceutical design*, 23(3), 433-439.

**Long, J.**, Etxabide, A. E., Nand, A. V., Bunt, C. R., Ray, S., & Seyfoddin, A.. 3D printed chitosan-pectin hydrogel wound dressing for lidocaine hydrochloride delivery. Submitted to the Journal of *Materials Science and Engineering C*, under review.

**Long, J.**, Etxabide, A. E., Nand, A. V., Bunt, C. R., Kornelsen, C., Ray, S., & Seyfoddin, A.. Development of a long-term contraceptive implant with levonorgestrel loaded chitosan microspheres embedded in poly (vinyl alcohol) hydrogel. Submitted

to the Journal of *American Chemical Society (ACS) Applied Bio Materials*, under review.

### 1.6.3. Other Publications

Etxabide, A., **Long, J.**, Stevenson M., de la Caba, K., Guerrero, P., & Seyfoddin, A.. Development and characterization of ribose-crosslinked gelatin products prepared by indirect 3D printing. *Food Hydrocolloids*, accepted.

Etxabide, A., **Long, J.**, Guerrero, P., de la Caba, K., & Seyfoddin, A. (2019). 3D printed lactose-crosslinked gelatin scaffolds as a drug delivery system for dexamethasone. *European Polymer Journal*, 114, 90-97.

Sharma, M., **Long, J.**, & Seyfoddin, A. (2018). Thermosensitive Hydrogels for Drug Delivery and Tissue Engineering. *Hydrogels: Design, Synthesis and Application in Drug Delivery and Regenerative Medicine*, 184.

## 1.7. References

- Beever, E. A., Huntsinger, L., & Petersen, S. L. (2018). Conservation challenges emerging from free-roaming horse management: A vexing social-ecological mismatch. *Biological conservation*, 226, 321-328.
- Brockelman, W. Y., & Kobayashi, N. K. (1971). Live capture of free-ranging primates with a blowgun. *The Journal of Wildlife Management*, 852-855.
- Bush, M. (1992). Remote drug delivery systems. *Journal of Zoo and Wildlife Medicine*, 159-180.
- Christie, R., Findley, D., Dunfee, M., Hansen, R., Olsen, S., & Grainger, D. (2006). Photopolymerized hydrogel carriers for live vaccine ballistic delivery. *Vaccine*, 24(9), 1462-1469.
- Falconer, J. L., Christie, R. J., Pollard, E. J., Olsen, S. C., & Grainger, D. W. (2016). Live RB51 vaccine lyophilized hydrogel formulations with increased shelf life for practical ballistic delivery. *International journal of pharmaceutics*, 498(1), 187-194.
- Haigh, J., & Hopf, H. (1976). The blowgun in veterinary practice: its uses and preparation. *Journal of the American Veterinary Medical Association*, 169(9), 881-883.
- Hall, S. E., Nixon, B., & Aitken, R. J. (2017). Non-surgical sterilisation methods may offer a sustainable solution to feral horse (*Equus caballus*) overpopulation. *Reproduction, Fertility and Development*, 29(9), 1655-1666.
- Hendricks, M. D., & Treadway, L. N. (2015). Dart gun: Google Patents.
- Kreeger, T. J. (1997). Overview of delivery systems for the administration of contraceptives to wildlife. *Contraception in wildlife management*. Washington, DC: US Government Printing Office, 29-48.

- Long, J., Gholizadeh, H., Lu, J., Bunt, C., & Seyfoddin, A. (2017). Review: Application of Fused Deposition Modelling (FDM) Method of 3D Printing in Drug Delivery. *Current pharmaceutical design*, 23(3), 433-439.
- Smith, K. (2017). Assessing koala (*Phascolarctos cinereus*) population density for management on French Island, Victoria.
- Tan, D., Maniruzzaman, M., & Nokhodchi, A. (2018). Advanced pharmaceutical applications of Hot-Melt Extrusion coupled with Fused Deposition Modelling (FDM) 3D printing for personalised drug delivery. *Pharmaceutics*, 10(4), 203.
- Treanor, J. J., Johnson, J. S., Wallen, R. L., Cilles, S., Crowley, P. H., Cox, J. J., . . . Plumb, G. E. (2010). Vaccination strategies for managing brucellosis in Yellowstone bison. *Vaccine*, 28, F64-F72.
- Wahlquist, C. (2017). Kangaroo Island koala cull rejected by South Australian government. Retrieved from <https://www.theguardian.com/australia-news/2017/aug/28/kangaroo-island-koala-cull-rejected-by-south-australian-government>.
- West, G., Heard, D., & Caulkett, N. (2014). *Zoo animal and wildlife immobilization and anesthesia*: John Wiley & Sons.
- Wiedner, E., Lindsay, W., & Isaza, R. (2012). Management of zebras and zebra hybrids (zebroids). *Compendium*, 34, E1-E4.
- Wilson, M. E., & Coulson, G. (2016). Comparative efficacy of levonorgestrel and deslorelin contraceptive implants in free-ranging eastern grey kangaroos (*Macropus giganteus*). *Wildlife Research*, 43(3), 212-219.



## Chapter 2

### *A Literature Review: Application of Fused Deposition Modelling (FDM) Method of 3D Printing in Drug Delivery*

Published as:

Long, J., Gholizadeh, H., Lu, J., Bunt, C., & Seyfoddin, A. (2017). Application of fused deposition modelling (FDM) method of 3D printing in drug delivery. *Current pharmaceutical design*, 23(3), 433-439.

## 2.1. Introduction

Drug delivery is defined as the method or process of administering pharmaceutical compounds into the human or animal body to achieve a therapeutic effect (Tiwari et al., 2012). Drug delivery systems are designed to provide controlled drug release profiles to achieve maximum distribution and absorption of the drug in the target tissue, which ultimately enhances therapeutic efficacy, safety and patient compliance (Tiwari et al., 2012).

The route of administration is the path by which a drug is administered in the body and can be generally classified into drugs that are: taken orally, given by injection or implants (Rossi, Perale, & Masi, 2016) administered through sublingual, buccal, vaginal, transdermal, ocular or nasopulmonary routes. Therapeutic concerns and drug physicochemical and pharmacokinetic properties are major factors in selecting the route of administration for a drug (Seyfoddin, Shaw, & Al-Kassas, 2010).

Tablets and capsules are the most common drug delivery devices. Direct tableting and capsule filling are the conventional drug fabrication methods designed for immediate drug release (Jonathan & Karim, 2016).

Due to the need of controlling the rate of drug release, drug fabrication has gradually developed towards multi-step technologies such as coating, granulation and extrusion. Recent advances in biotherapy and individually tailored medicine have created new concepts in drug formulation such as nano-scale medicines (Kunasekaran & Krishnamoorthy, 2015) and more complex multi-compartment manufacturing methods (Tiwari et al., 2012).

New materials and methods inventions for drug delivery, particularly for controlled delivery to the target area is an expanding field in pharmaceutical science. In addition, rapid prototyping of new drugs during development stages, and reducing the economic costs and risks of upscale should be especially considered (Jonathan & Karim, 2016). Solid freeform fabrication is a rapid prototyping method in biomanufacturing of implants and scaffolds by 3D printing (Leong, Cheah, & Chua, 2003). This printing process uses designs produced by computer aided design (CAD) software in stereolithography (.stl) format to fabricate a digitally controlled layer-by-layer deposition until completion of the solid freeform.

The great flexibility and eminent fabrication capability have made 3D printing suitable for manufacturing custom-designed scaffolds (Ang et al., 2002; Karageorgiou & Kaplan, 2005; Moroni, de Wijn, & van Blitterswijk, 2006), tissue engineering (Farzadi et al., 2015) and drug delivery systems (Jonathan & Karim, 2016). In 2015, the first 3D-printed drug Spritam was approved by US Food and Drug Administration (FDA) (Fitzgerald, 2015). Currently 3D printing is under investigation for fabrication of tablets and implantable systems with immediate-release or sustained-release properties.

Macro and micro sized structures for drug delivery produced using 3D printing technologies can enable drug delivery scientists to deposit precise quantities of therapeutic substances along with structural and scaffolding materials to form complex multi-compartmental systems that are otherwise difficult to fabricate (C. Zhang et al., 2008). Such systems allow incorporation of concentrated ingredients and other spatial patterns of drug deposition within the polymer matrix capable of solving

long-standing clinical problems and difficulties (Chung et al., 2013; Ferris, Gilmore, & Wallace, 2013).

This article provides an overview of fused deposition modelling (FDM) based 3D printing applied in drug delivery. Key-words such as 3D printing, FDM, drug delivery and polymer alone or in combination were used to find relative articles in many databases such as PRISMA guidelines, Medline, Embase, Science Direct, Springer Link, Google Scholar and university databases. This review contains a general introduction of FDM printing technology, identifies suitable polymers and applications in fabricating personalised drug-delivery devices. Also, the advancements, advantages, limitations and the possible future applications of FDM 3D printing in drug delivery systems will be addressed.

## 2.2. 3D Printing

### 2.2.1. Computer aided design

Computer-aided design (CAD) software facilitates the creation, modification, optimisation and analysis of 2D and 3D designs in the form of an electronic file as output. The 3D printable models are capable of modification to reduce the errors prior to printing. The CAD created models are often produced in stl. format which is suitable for 3D printing. For example, Figure 2-1 shows the process of designing and printing a capsule drug delivery system in our lab. Images B and C in Figure 2-1 illustrate the level of accuracy and flexibility of design in CAD for a given drug delivery device.

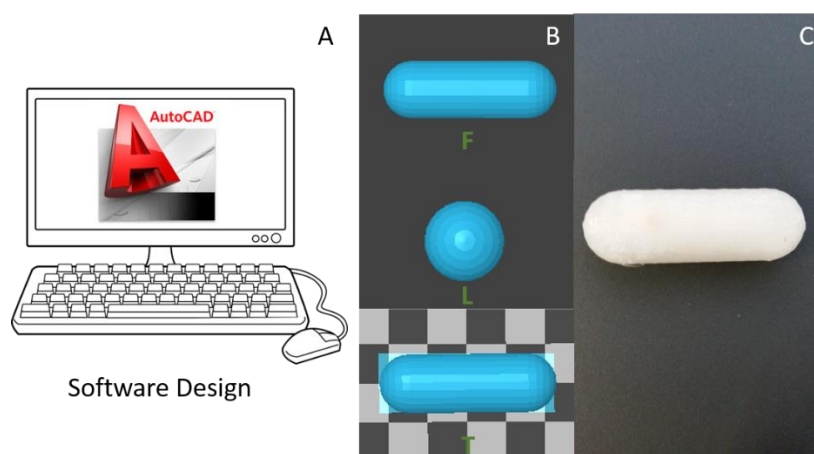


Figure 2-1. A): CAD design, B): Capsule designed in CAD and C): Capsule printed.

### 2.2.2. 3D printing Techniques applied in drug delivery systems

3D printing techniques for the fabrication of solid free forms of drugs can be divided into three categories. Although methods of fabrication are different, all of them use layer by layer deposition to produce the designed object.

### 2.2.2.1. 3D printing inkjet-based system

Inject printing was invented in 1978 and is based on Lord Rayleigh's instability theory (Prasad & Smyth, 2015). Traditional desktop printers use the concept in continuous jet and drop on demand printing (Gross, Erkal, Lockwood, Chen, & Spence, 2014). In continuous printing, a stream of droplets is produced by a pressurised flow that pushes the droplets to the substrate by electrostatic plates.

The drop on demand 3D printing technique dispenses micro-droplets at desired positions in additive layers to produce the entire 3D structure model. Micro deposition of the materials and non-contact reduces wastage and lowers risk of contamination and mechanical depreciation of the print head (L. Li et al., 2009). Drop on demand is more precise, because it produces desirable droplet sizes at high speed (Jonathan & Karim, 2016).

### 2.2.2.2. 3D printing extrusion-based deposition systems

In this method, the nozzle deposits melted or solid materials to fabricate the designed object layer-by-layer, including fused deposition modelling (FDM), 3D plotting, multiphase jet solidification (MJS) and precise extrusion manufacturing (PEM) (Hutmacher, Sittinger, & Risbud, 2004). For example, FDM uses melting material whereas other deposition methods are assisted by a pressurised micro-syringe that pushes other non-melted liquid material out of the nozzle (Jonathan & Karim, 2016).

### 2.2.2.3. 3D laser-based printing system

In this technique, a pulsed laser induces the transfer of material from a source film onto a substrate in contact or close proximity to the film (Arnold, Serra, & Piqué, 2007). The beam of an ultrafast laser focuses tightly into the material to locally

polymerise it. A CAD model leads the movement of the beam to fabricate a realistic model of the design (Selimis, Mironov, & Farsari, 2015).

#### 2.2.2.4. 3D printing powder-based distribution system

In powder-based 3D printing technology, the object is created by selectively spraying a liquid binder on a powder bed (Butscher, Bohner, Hofmann, Gauckler, & Müller, 2011). The liquid acts as i) a binder with low viscosity and rapid rate of drying or curing, for example the silicate systems, in which the powder particles are combined together by the polymerisation of silicic acid or its salts in aqueous solution (Sachs, Cima, Williams, Brancazio, & Cornie, 1992); ii) stimulant of a reaction to solidify or bond the powder, such as a crystallisation reaction (Butscher et al., 2011). This method is widely used in tissue engineering scaffold due to its flexibility for powder materials (Butscher et al., 2011; Warnke et al., 2010).

#### 2.2.3. Fused deposition modelling (FDM) in drug delivery

Fused deposition modelling (FDM) is one of the most widely used 3D printing techniques to make solid objects and offers accurate dosage by adjusting the parameters in CAD. Rapid prototyping, precision of quantity, and versatility in incorporation of concentration gradients within the polymer matrix are the advantages of this technique (Moulton & Wallace, 2014). This technology can lead to innovative drug delivery ideas that can overcome the limitations and disadvantages of traditional drug delivery systems. The increasing use of FDM based 3D printing technologies in drug delivery systems is attributed to its numerous advantages, such as the possibility to manufacture patient-tailored tablets (Goyanes, Buanz, Hatton, Gaisford, & Basit, 2014a; Goyanes et al., 2015; Skowrya, Pietrzak, & Alhnan, 2015) or capsules with

high accuracy and fabrication of various geometric devices (Espalin et al., 2010; Teo et al., 2011; Zein, Hutmacher, Tan, & Teoh, 2002) with immediate and controlled drug release properties.

FDM is a thermo-based technique, so heat transfer characteristics and rheology of melted polymers are significant criteria influencing selection of a suitable material for the intended purpose. Thermoplastic polymers are dominant in FDM applications due to their low melting temperature. The main characteristics of most common polymers are discussed in the polymer section. Along with the development of 3D printing technology, various polymers are emerging to fit diverse requirements of biomedical applications and drug delivery systems. Numerous polymers have been explored for the fabrication of scaffolds and implants but, limited polymers are investigated for drug delivery systems. The most commonly used polymers for FDM drug delivery systems are poly (vinyl alcohol) (PVA) (Skowrya et al., 2015), poly (lactic acid) (PLA) (Skowrya et al., 2015; Wittbrodt & Pearce, 2015) and ethylene vinyl acetate (EVA) (Genina et al., 2016).

#### 2.2.3.1. How FDM systems work

FDM is a nozzle-based deposition system that allows direct printing of an object designed in CAD to create a 3D pattern layer by layer. In this technique, torque and pinch system pushes precise amounts of thermoplastic polymer filament into the heater or liquefier block. The temperature of the liquefier block is set based on the type of filament and its melting and glass transition temperature. Then, the molten filament is extruded through a high temperature nozzle and thereafter solidifies onto the previous layer on the build plate (Chia & Wu, 2015). The nozzle controls the flow



of the polymer and the diameter of the extruded material. Figure 2-2 demonstrates a schematic process of FDM.

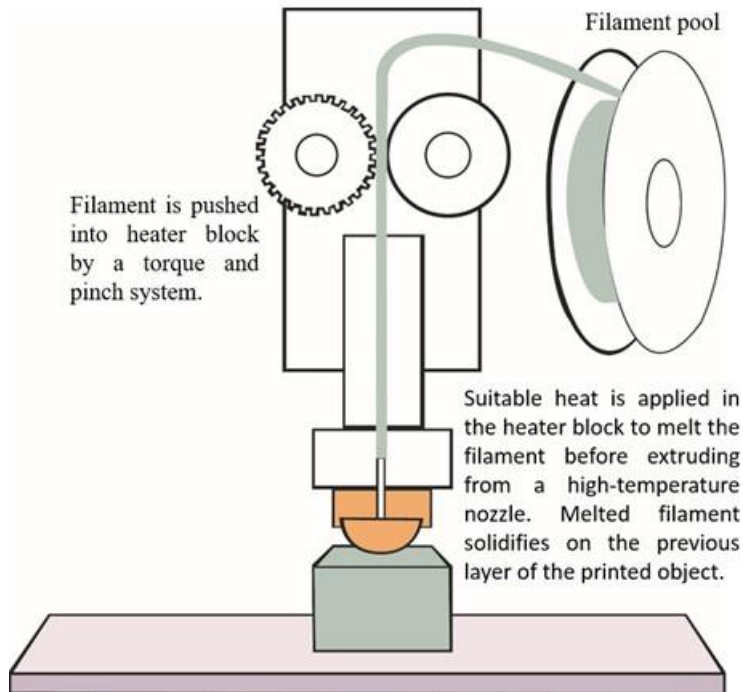


Figure 2-2. Schematic illustration of FDM system.

It is possible to have more than one nozzle to print an object by FDM. Two or more polymers with different medicines can be printed at the same time to fabricate drug delivery systems with multiple medicines. Also, it is possible to use a different filament or save the drug in drug-loaded filaments by using drug free filament for support material. In this model, each nozzle is controlled by its individual software settings working independently.

#### 2.2.3.2. Practical considerations with FDM

Physical and mechanical properties of a 3D printed object are important. Heat transfer characteristics and rheology of the materials used as filament are the most important criteria in material selection (Zein et al., 2002). Thickness of the layers, angle and gap width between layers are controllable variables in the 3D printer software (H. Chen,

Fuhlbrigge, Zhang, & Masood, 2007; Chia & Wu, 2015). Other variables include infill density, extrusion speed, height of the layers, the temperature of the nozzle and the height of build platform (Goyanes et al., 2015; Pietrzak, Isreb, & Alhnan, 2015; Skowrya et al., 2015). The infill density refers to the degree to which the printer will fill in the void space with polymer with the range of 0,empty to 100, solid (Goyanes, Buanz, Basit, & Gaisford, 2014b). Control of these variables in scaffolds results in desired pore size, interconnectivity and morphology of the object (Chia & Wu, 2015). The raster (the matrix which is composed of the printed lines) gap and raster angle are controllable in the FDM printing process and which contribute to the porosity and the pore distribution in the matrix (H. Chen et al., 2007). The characteristics of the build plate, also, significantly influence successful printing of prototypes. For example, adherence of the extruded materials to the build plate is essential to fix the base and support materials. Adherence to the build platform must be sufficient to hold the print object in place during printing but not too great to restrict separation from the build plate once printing has been completed.

Column strength is a significant property of a filament. Low column strength results in bending or buckling of the filament above the liquefier and preventing the flow of the melt through the nozzle. Filament diameter, tensile and flexural strengths are responsible for column strength of the filament (Genina et al., 2016). In addition to column strength, pressure drop in the nozzle determines the required force to push the melt through the nozzle and it depends on the geometry of the print head and the melt viscosity. The melt index and drop pressure have inverse relationship, therefore low melting index of the filament causes a high drop in pressure inhibiting filament fed

into the liquefier. In contrast, a high melting index facilitates filament feeding , but causes discontinuous flow of the extrude (Genina et al., 2016).

## 2.3. Printing material

### 2.3.1. Suitable polymers in FDM system

As mentioned in the previous section, melting point, glass transition, and the flow behaviour of the molten filament are important in selection of a suitable material for a specific purpose in 3D printing. Thermoplastic polymers are common materials used in FDM technique, because they can be formed into filaments with specific dimensions. Also, the polymers have relatively low melting points and suitable viscosity during the process of melt to build. The main properties of the most common polymers are briefly explained and a summary of their characteristics applied in drug delivery is presented in Table 2-1.

Generally, in FDM techniques the polymers are used as drug-loaded filaments providing flexibility in controlled release of drugs. Firstly, Acrylonitrile butadiene styrene (ABS) synthesised from three monomeric chemicals: acrylonitrile, butadiene and styrene (Rutkowski & Levin, 1986). It is a common engineering thermoplastic polymer which was one of the earliest polymers applied in FDM (Genina et al., 2016). However, it is not widely used in medical or pharmaceutical area due to its low biocompatibility (McCullough & Yadavalli, 2013) and toxicity (Rutkowski & Levin, 1986).

Table 2-1. Typical polymers used in FDM 3D printing

Materials	Melting Point	Glass Transition Point	Biodegradability	Physical Property	Application	Reference
Acrylo-nitrile butadiene styrene (ABS)	105°C	105°C	No	Soluble in esters, ketones, ethylene dichloride and acetone.	Matrix model/ microfluidic device	(H. Chen et al., 2007; McCullough & Yadavalli, 2013)
Poly (lactic acid) (PLA)	150~160°C	60-65°C	Yes	Soluble in chlorinated solvents, hot benzene, tetrahydrofuran and dioxane.	Tablets	(Melocchi et al., 2015)
Polycaprolactone (PCL)	60°C	-60°C	Yes	Soluble in chloroform, dichloromethane, tetrahydrofuran	Scaffold/mesh/contraceptive implants	(Holländer et al., 2016; Rai, Teoh, Hutmacher, Cao, & Ho, 2005; Teo et al., 2011)
Ethylene vinyl acetate (EVA)	59~185°C	-53~-23°C	No	Insoluble white solid in pellet, pill or powder form	Contraceptive implants	(Genina et al., 2016)
Poly (methyl methacrylate) (PMMA)	160°C	105°C	No	Soluble in many organic solvents	Bone cement beads	(Seeley et al., 2004)
Poly (vinyl alcohol) (PVA)	180~228°C	85°C	Yes	Water-soluble; Incompressible	Tablets	(Goyanes et al., 2014b; Goyanes et al., 2014a; Goyanes et al., 2015; Goyanes et al., 2015b; Pietrzak et al., 2015; Skowrya et al., 2015)

Poly (lactic acid) (PLA) is a biodegradable, high-strength, high-modulus polymer that belongs to the family of aliphatic polyesters (Garlotta, 2001). The relative lower melting temperature of PLA, ranging from 150°C to 160°C, makes it energy saving during the fabrication process (Skowrya et al., 2015; Wittbrodt & Pearce, 2015). In addition, the biocompatible and biodegradable PLA polymer is a safer alternative to non-degradable ABS filament (Groenendyk & Gallant, 2013). The physical properties of PLA polymer such as density, heat capacity, mechanical and rheological properties are dependent on its transition temperatures (Mohanty, Misra, & Drzal, 2005). In the solid state, PLA exists in either amorphous or semicrystalline status. For amorphous PLA, the glass transition temperature ( $T_g$ ) determines the upper temperature for its applications; for semicrystalline PLA, both  $T_g$  and melting temperature ( $T_m$ ) are the fundamental factors to determine the temperatures used in its application (Mohanty et al., 2005).

Polycaprolactone (PCL) has been considered a promising candidate for medical applications due to its excellent biodegradability. It has a relatively lower melting temperature (60 °C) which requires much lower energy during the melting process (Labet & Thielemans, 2009). Its good tensile strength, elongation and great compatibility with many other polymers (E. G. Kim, Kim, & Kim, 2007) make PCL appropriate for 3D printing.

Ethylene vinyl acetate (EVA) is a biocompatible and non-toxic polymer consisted of ethylene and vinyl acetate (VA), which is commonly used with polydimethylsiloxane (PDMS) in implantable controlled release devices (Genina et al., 2016). Different proportions of VA component can affect the crystallinity, stiffness, softening and

melting temperature of EVA, which make it suitable for FDM processing when mixed with thermos-setting polymer PDMS (Genina et al., 2016; Henderson, 1993).

Poly (methyl methacrylate) (PMMA) has been used to manufacture reconstructive materials, such as dental implants, craniofacial reconstructions, bone implants and ocular prostheses (Baino et al., 2016; Espalin et al., 2010). PMMA was used as the filament for FDM based 3D printing for the fabrication of porous patient-tailored implants for craniofacial reconstructions and orthopaedic spacers (Espalin et al., 2010). An example of PMMA-based copolymer is the Eudragit, comprising methacrylic acid and methacrylic/acrylic esters and their derivatives (Thakral, Thakral, & Majumdar, 2013). Eudragits have been widely used in pharmaceutical applications for their varying degrees of solubility (Nikam et al., 2011). Pietrzak et al (2015) printed controlled-release theophylline tablets by loading the drug into three types of Eudragit polymers (Eudragit RL, RS and E) via hot melt extrusion (Pietrzak et al., 2015).

Poly vinyl alcohol (PVA) is the most widely used commercial polymer in 3D printed drug delivery systems due to its excellent biocompatibility, biodegradability and good water-solubility; these properties make PVA appropriate for oral administration such as customised tablets (Goyanes et al., 2014b; Goyanes et al., 2014a; Goyanes et al., 2015; Goyanes et al., 2015b; Pietrzak et al., 2015; Skowrya et al., 2015), transdermal patches (Wan & Lim, 1992) and ocular devices (Davies, Fair, Hadgraft, & Kellaway, 1991; C. Wilson, Olejnik, & Hardy, 1983). The melting point of PVA may range from 180 °C (partially hydrolysed) to 228 °C (fully hydrolysed) depending on the degree of hydrolysis of the acetate groups (Jonathan & Karim, 2016). Goyanes et al. (Goyanes

et al., 2015b) indicated that the percentage of PVA component may affect the release rate of the loaded drug as the PVA matrix drives the drug release behaviour.

### 2.3.2. Drug loading into the filament

Prior to fabricate the drug delivery devices with FDM 3D printing, the target drug(s) should be loaded into the polymeric filament. The simplest and traditional way of loading active drug(s) into filament is impregnation, which is depended on passive diffusion of a potent drug into filament matrix (Goyanes et al., 2014b; Goyanes et al., 2014a; Skowrya et al., 2015). The filament is placed in a high-concentration drug solution (generally a non-solvent for the polymer such as ethanol or methanol) for 24h with stirring followed by a drying process to ensure drug entrapment within the polymer matrix (Goyanes et al., 2014b; Goyanes et al., 2014a; Jonathan & Karim, 2016; Skowrya et al., 2015). However, the impregnation process requires a high concentration of drug solution and significant time due to the inherent nature of passive diffusion; this progress makes this drug-loading method expensive and inefficient as only limited active drug molecules could be trapped into the polymer matrix by passive diffusion (Farzadi et al., 2015; Jonathan & Karim, 2016).





Figure 2-3. Schematic image of hot melt extrusion (HME) system: A): HME (Noztek Pro, UK), B): digital-control motor, C): screw barrel, D): control panel, E): nozzle, F): heater band & fan, G): screw and H): hopper.

An alternative manufacturing method, hot melt extrusion (HME), has been applied to enhance drug loading (Goyanes et al., 2015; Goyanes et al., 2015b; Pietrzak et al., 2015). HME is a common method of fabricating filaments for FDM based 3D printing processes. During HME, pressure and heat are applied to melt the raw material and then extrude it out of a nozzle at an elevated temperature (Maniruzzaman, Boateng, Snowden, & Douroumis, 2012). As shown in Figure 2-3, during HME the drug and melted polymer are loaded through the hopper and then physically mixed in the screw before extruding from the nozzle as a filament with defined shape and diameter suitable for the FDM 3D printing.

## 2.4. Application of FDM in drug delivery

### 2.4.1. 3D printed tablets

Along with the development of novel treatments for specific diseases, personalised tablets have gained increasing attention. FDM based 3D printing technology offers considerable advantages in the fabrication of individualised tablets such as simplifying the manufacture process, improving on the inherent properties and delivery of dosage forms (Goyanes et al., 2014a).

Goyanes et al. (Goyanes et al., 2014a) explored the feasibility of using FDM to manufacture modified-release tablets loaded with two drugs for the treatment of inflammatory bowel disease (IBD): 5-aminosalicylic acid (5-ASA, mesalazine) and 4-aminosalicylic acid (4-ASA) (Goyanes et al., 2014a). These drugs were loaded via impregnation achieving a final drug loading of 0.06% w/w and 0.25% w/w for 5-ASA and 4-ASA respectively. The final tablets with varying infill percentages of drug-loaded polymer (10%, 50% and 90%) were achieved by encoding the surface data and determining the thickness of desired tablets in CAD. Through differential scanning calorimetry (DSC) and thermogravimetric analysis (TGA), Goyanes et al. found that almost half of the loaded drug 4-ASA was thermally degraded by the heated extrusion process at 210°C (from 0.25% w/w to 0.12% w/w) while there was no notable reduction in the content of 5-ASA; this indicates that FDM 3D printing is more suitable for a drug with degradation points higher than the printing temperature. The drug release profiles, obtained using a USP-II apparatus in Hank's bicarbonate buffer, reveal that the less infill percentage of drug (10%) lead to faster release profile when comparing to 50% and 90% infill percentages of 4-ASA/5-ASA in the tablets. This

finding indicates that the drug release rate of 3D printed tablets could be controlled by optimising the processing parameters in FDM 3D printing.

Similar 3D printed tablets with controlled-release profiles were prepared with fluorescein dye loaded PVA, fluorescein was chosen for its thermo stability and easy quantification (Goyanes et al., 2014b). The fluorescein was loaded into PVA filament by impregnation with a load amount of 0.29% w/w. The tablets of various infill percentages (0%, 10%, 25%, 50% or 90%, 100%) were printed with pre-loaded PVA filament. The analysis of dye content in printed tablets showed no significant change after printing which confirms that the dye was not thermally degraded likely being due to the printing temperature (220°C) being less than its degradation temperature (320°C). The dissolution test also showed similar trends to 4-ASA/5-ASA tablets, confirming that faster release profile was due to a lower infill percentage.

Extended-release personalised prednisolone tablets were formulated with FDM 3D printing by Skowrya et al. (2015). Similar to the above, the drug prednisolone was loaded into PVA polymeric matrix by impregnation. The PVA filament was incubated in a saturated methanolic solution of prednisolone and the load of prednisolone approximate 1.9% w/w was achieved. To assess the accuracy of control over the dosage of FDM 3D printed tablets, Skowrya et al. explored difference of theoretical doses based on the tablet mass and measured the dose of prednisolone in the tablet. The results showed that the dose accuracy was between 88.7-107% for the tablets with drug contents of 2, 3, 4, 5, 7.5 and 10 mg, which indicates the feasibility of fabricating personalised tablets with various drug dosages can be achieved by designing tablets with different mass. DSC and x-ray powder diffraction pattern (XRPD) results

identified that the prednisolone in the printed tablets existed in an amorphous form among the PVA polymeric matrix. *In vitro* drug release assessment, using a pH-change flow-through cell dissolution system, showed that tablets with different weights had a similar *in vitro* release profile and the release of prednisolone was extended up to 24h. This study demonstrated that FDM based 3D printing is a promising method for fabricating extended-release tablets and patient-tailored controlled release tablets can be its future products.

In a similar study, a controlled-release budesonide tablet was prepared using FDM 3D printing (Goyanes et al., 2015). The drug was loaded into PVA filaments for the fabrication of a 9 mg budesonide modified-release tablet by using an enhanced drug loading method HME. The Eudragit L100(for gastro-resistance) coated tablet showed a sustained release profile in simulated colonic conditions. The release rate of drug could be controlled by changing the concentration of PVA in the filament. In comparison with two commercial budesonide medicines Entocort® and Cortiment® (Uceris®), the 3D printed budesonide tablet exhibited a controlled intermediate release profile in comparing with immediate-released Entocort ® and slow-released Cortiment® (Uceris®).

By applying HME drug loading method, Pietrzak et al. (Pietrzak et al., 2015) fabricated patient-tailored immediate and extended release tablets with FDM based 3D printing by loading a thermo-stable drug theophylline into three methacrylic polymers (Eudragit RL, RS and E) as well as a cellulose-based polymer hydroxypropyl cellulose (HPC SSL). Pietrzak et al. also suggested that the temperature of 3D printing should be approximately 40-50°C higher than that of HME

processing to ensure suitable melt/flow properties. This is because for FDM printing process, heating is at a much faster rate but for a very much shorter time than that during HME.

It has been reported that thermo-labile filaments may degrade if the printing temperature is higher than their melting point. To overcome the degradation problem, a high melting point material, example a model drug, was incorporated into the filament to increase the melting temperature of the mixture. In Goyanes et al.'s study, theophylline with a melting point of 273°C was loaded in a Rudragit RL filament and printed at a lower temperature of 170°C (Goyanes et al., 2014a). According to DSC and XRPD analysis, theophylline mostly existed in a crystalline form after HME and 3D printing. *In vitro* release of theophylline from Eudragit RL-printed tablets was extended over 16h. To control the drug release profile, immediate-released polymers (HPC SSL and Eudragit E) were used in place of Eudragit RL and *in vitro* release showed that the majority of theophylline was released within 25 min and the release rate could be slowed down by adding a sustained-released polymer Eudragit RS.

3D printing has the potential to create multi-compartmental drug delivery caplets. Novel designs for multiple drugs and release profiles were engineered by FDM based 3D printing in combination with HME for drug loading (Goyanes et al., 2015b). Two unique caplets were designed: i) multilayer caplets with alternate layers (1 mm layer thickness) and ii) DuoCaplets with a capsule-shaped core embedded within a larger caplet, with each layer containing a different drug. Two drugs commonly used in combination, paracetamol and caffeine, were loaded into PVA filaments by HME at 4.3% and 8.2% for paracetamol and 4.7% and 9.5% for caffeine. TGA analysis

indicated that the drugs were not detectably degraded during both HME and the 3D printing processes. 2-dimensional hyper spectral arrays across the entire surface of the tablets were determined by Raman Spectroscopy and the result showed that there was a definitive separation between the different layers or components. XRPD and DSC data showed that paracetamol was present in an amorphous state while caffeine was in a crystalline form: the amorphous vs crystalline state perhaps maybe due to the different hydrogen bonding interactions between the drug(s) and the PVA polymer. The release profiles of these two caplets were different. For the multilayer caplets, both paracetamol and caffeine exhibited similar release profiles, reaching 100% release within 360 min. Increasing drug content enhanced drug release rate which maybe have been due to the lower concentration of PVA matrix. For the DuoCaplet, drug load in the external layer was released first and the internal layer only release the drug when the external layer was practically dissolved. The drug in the internal core showed a lag time of 50 to 135 min. This study established the feasibility of achieving immediate and delayed release profiles for multiple drugs in a single oral caplet printed by FDM based 3D printer.

#### 2.4.2. 3D printed devices

Teo et al. (Teo et al., 2011) investigated the feasibility of a solvent-free system for the antibiotic gentamycin. They fabricated a mesh wound dressing with various concentrations of gentamycin sulphate (GS) (5, 15 and 25% w/w) incorporated in polycaprolactone-tricalcium phosphate (PCL-TCP) using FDM. Efficacy of the mesh against bacteria, elution efficiency and cytotoxicity were examined. 25% w/w loading demonstrated the largest antibacterial activity, but highest cytotoxicity. Based on the *in vitro* analysis, the mesh loaded with 15% GS (PT15) was used for antibacterial

activity and healing effect on infected wound in the mice model. The *in vivo* analysis indicated that the dressing could effectively combat bacteria in the infected area to below detectable limits in one day. In addition, almost complete closure of the wound area was observed on day 14 of the treatment. In this study, about 93% of the incorporated GS was released in 14 days; while in a similar study conducted by Miyai et al. (Miyai et al., 2008) (manufactured by a moulding process) only about half of the incorporated antibiotic drug was released over 56 days. The researchers believed that compared to the Miyai et al. model, fabrication of the mesh by FDM provided a higher specific surface area and enhanced the speed of drug diffusion. Additionally, the burst release pattern of the model was desirable for infection treatment applications. In addition to desired release profile and short healing time, the anti-adhesive property of the mesh fabricated by FDM helps expelling from healed wound and prevents disturbance and bleeding of the site after removal of the dressing.

FDM has been also used to manufacture implantable contraceptive drug delivery systems. Genina et al. (Genina et al., 2016) investigated the feasibility of using a range of Ethyl vinyl alcohols (EVAs) with different vinyl alcohol content (9, 12, 16, 18, 28 and 33%) to load indomethacin as a model drug to fabricate a T-shaped intrauterine device (IUS) and a subcutaneous rod (SR) by using FDM. Drug free and drug loaded filaments were extruded using 1.5 to 2.5 mm die and a temperature range of 15 to 40°C above the melting point of the copolymer (60 to 102°C) to be used for fabrication of model prototypes. HME processes of EVA copolymers at various temperatures demonstrated that various grades of EVA have specific melting point, melting index, viscosity and swelling ability. These characteristics influence the choice of the die size, extrusion and print settings of the filaments; for example, the extrusion

temperature close to the melting point of the copolymer increased the viscosity of the filament making the extrusion easier by the smaller die. Based on the results of this study, it was found that not all grades of EVA are not suitable for the contraceptive purpose, so optimisation of the parameters involved in the process for various grades of EVA is required. Therefore, Genina et al. found drug-loaded and drug-free filaments containing 16% VA were the most successfully printed filaments at 165°C, speed of 10 to 40 mm/s, 0.1 mm layer thickness and 3 shells. In addition, the filaments containing 15% drug was the easiest to process.

In terms of print process parameters, drug and VA content of the filaments influenced thermal behaviour and printing temperature of the objects. Column strength of the filament was one of the significant parameters towards bending and print quality. In terms of printing speed, printing temperature, viscosity and melt index of the filament melt, the geometry of the print head and pressure drop in the nozzle were important parameters. Therefore, the relationship between the mentioned behaviours of the filament and printing settings are critical factors for a successful 3D printing process.



## 2.5. Limitation and future application

Compared to established drug delivery device fabrication methods, FDM based 3D printing offers competitive advantages. However, similar to many emerging technologies, the limitations of FDM 3D printing also need to be identified and addressed. Firstly, the drug loading methods prior to FDM remain a concern due to the use of heat. Even though HME could offer higher and more adjustable drug loading, drug candidates are restricted to thermo-stable substances. Thermo-sensitive medicines are not suitable for FDM based printing limiting its biomedical and pharmaceutical applications. In addition, the thermoplastic properties of the polymer filaments can be modified when an additive is incorporated into the polymeric matrix that may lead to a change of their viscosities and flexibilities. Secondly, high temperatures are required for the printing process to melt the filament at the point of extrusion building the object, which may cause physical instability and degradation issues. Thirdly, support structures that need to be constructed as the base support for printed objects contribute to material wastage especially when the object has complex geometry or large base area. Additionally, it is difficult to remove the inner support required to support hollow objects in scaled-up procedures.

In summary, FDM based 3D printing is a low-cost and efficient manufacture process, which provides good flexibility and accuracy. The main advantage of FDM 3D printing is that unique-designed tablets or devices with personalised dosages can be easily designed and printed. The release profiles of the loaded drug can be controlled and adjusted due to the possibility of printing objects in diverse geometries and proportions of drugs and polymers (Jonathan & Karim, 2016). These advantages make

FDM printing a promising emerging technology for the fabrication of customised tablets and other drug delivery devices.

## 2.6. References

- Ang, T. H., Sultana, F. S. A., Hutmacher, D. W., Wong, Y. S., Fuh, J. Y. H., Mo, X. M., . . . Teoh, S. H. (2002). Fabrication of 3D chitosan–hydroxyapatite scaffolds using a robotic dispensing system. *Materials Science and Engineering: C*, 20(1–2), 35-42.
- Arnold, C. B., Serra, P., & Piqué, A. (2007). Laser direct-write techniques for printing of complex materials. *Materials Research Society Bulletin*, 32(01), 23-31.
- Baino, F., Ferraris, S., Miola, M., Perero, S., Verné, E., Coggiola, A., . . . Ferraris, M. (2016). Novel antibacterial ocular prostheses: Proof of concept and physico-chemical characterization. *Materials Science and Engineering: C*, 60, 467-474.
- Butscher, A., Bohner, M., Hofmann, S., Gauckler, L., & Müller, R. (2011). Structural and material approaches to bone tissue engineering in powder-based three-dimensional printing. *Acta Biomaterialia*, 7(3), 907-920.
- Chen, H., Fuhlbrigge, T., Zhang, G., & Masood, S. (2007). Application of fused deposition modelling in controlled drug delivery devices. *Assembly automation*, 27(3), 215-221.
- Chia, H. N., & Wu, B. M. (2015). Recent advances in 3D printing of biomaterials. *Journal of biological engineering*, 9(1), 1.
- Chung, J. H., Naficy, S., Yue, Z., Kapsa, R., Quigley, A., Moulton, S. E., & Wallace, G. G. (2013). Bio-ink properties and printability for extrusion printing living cells. *Biomaterials Science*, 1(7), 763-773.
- Davies, N. M., Fair, S. J., Hadgraft, J., & Kellaway, I. W. (1991). Evaluation of mucoadhesive polymers in ocular drug delivery. I. Viscous solutions. *Pharmaceutical research*, 8(8), 1039-1043.

- Espalin, D., Arcaute, K., Rodriguez, D., Medina, F., Posner, M., & Wicker, R. (2010). Fused deposition modeling of patient-specific polymethylmethacrylate implants. *Rapid Prototyping Journal*, 16(16), 164-173.
- Farzadi, A., Waran, V., Solati-Hashjin, M., Rahman, Z. A. A., Asadi, M., & Osman, N. A. A. (2015). Effect of layer printing delay on mechanical properties and dimensional accuracy of 3D printed porous prototypes in bone tissue engineering. *Ceramics International*, 41(7), 8320-8330.
- Ferris, C. J., Gilmore, K. J., & Wallace, G. G. (2013). Modified gellan gum hydrogels for tissue engineering applications. *Soft Matter*, 9(14), 3705-3711.
- Fitzgerald, S. (2015). FDA Approves First 3D-Printed Epilepsy Drug Experts Assess the Benefits and Caveats. *Neurology Today*, 15(18), 26-27.
- Garlotta, D. (2001). A Literature Review of Poly (Lactic Acid). *Journal of Polymers & the Environment*, 9(2), 63-84.
- Genina, N., Holländer, J., Jukarainen, H., Mäkilä, E., Salonen, J., & Sandler, N. (2016). Ethylene vinyl acetate (EVA) as a new drug carrier for 3D printed medical drug delivery devices. *European Journal of Pharmaceutical Sciences*, 90, 53-63.
- Goyanes, A., Buanz, A. B. M., Basit, A. W., & Gaisford, S. (2014b). Fused-filament 3D printing (3DP) for fabrication of tablets. *International journal of pharmaceutics*, 476(1–2), 88-92.
- Goyanes, A., Buanz, A. B. M., Hatton, G. B., Gaisford, S., & Basit, A. W. (2014a). 3D printing of modified-release aminosalicylate (4-ASA and 5-ASA) tablets. *European Journal of Pharmaceutics and Biopharmaceutics*, 89, 157-162.
- Goyanes, A., Chang, H., Sedough, D., Hatton, G. B., Wang, J., Buanz, A., . . . Basit, A. W. (2015). Fabrication of controlled-release budesonide tablets via desktop (FDM) 3D printing. *International journal of pharmaceutics*, 496(2), 414-420.

- Goyanes, A., Wang, J., Buanz, A., Martínez-Pacheco, R., Telford, R., Gaisford, S., & Basit, A. W. (2015b). 3D printing of medicines: Engineering novel oral devices with unique design and drug release characteristics. *Molecular pharmaceutics*, 12(11), 4077-4084.
- Groenendyk, M., & Gallant, R. (2013). 3D printing and scanning at the Dalhousie University Libraries: a pilot project. *Library Hi Tech*, 31(1), 34-41.
- Gross, B. C., Erkal, J. L., Lockwood, S. Y., Chen, C., & Spence, D. M. (2014). Evaluation of 3D printing and its potential impact on biotechnology and the chemical sciences. *Analytical chemistry*, 86(7), 3240-3253.
- Henderson, A. M. (1993). Ethylene-vinyl acetate (EVA) copolymers: a general review. *The Institute of Electrical and Electronics Engineers Electrical Insulation Magazine*, 9(1), 30-38.
- Holländer, J., Genina, N., Jukarainen, H., Khajeheian, M., Rosling, A., Mäkilä, E., & Sandler, N. (2016). Three-dimensional printed PCL-based implantable prototypes of medical devices for controlled drug delivery. *Journal of pharmaceutical sciences*, 105(9), 2665-2676.
- Hutmacher, D. W., Sittering, M., & Risbud, M. V. (2004). Scaffold-based tissue engineering: rationale for computer-aided design and solid free-form fabrication systems. *Trends in Biotechnology*, 22(7), 354-362.
- Jonathan, G., & Karim, A. (2016). 3D printing in pharmaceuticals: A new tool for designing customized drug delivery systems. *International Journal of Pharmaceutics*, 499(1-2), 376-394.
- Karageorgiou, V., & Kaplan, D. (2005). Porosity of 3D biomaterial scaffolds and osteogenesis. *Biomaterials*, 26(27), 5474-5491.

- Kim, E. G., Kim, B. S., & Kim, D. S. (2007). Physical properties and morphology of polycaprolactone/starch/pine- leaf composites. *Journal of applied polymer science*, 103(2), 928-934.
- Kunasekaran, V., & Krishnamoorthy, K. (2015). Experimental Design for the Optimization of Nanoscale Solid Lipid Particles Containing Rasagiline Mesylate. *Journal of Young Pharmacists Vol*, 7(4), 285.
- Labet, M., & Thielemans, W. (2009). Synthesis of polycaprolactone: a review. *Chemical Society Reviews*, 38(12), 3484-3504.
- Leong, K., Cheah, C., & Chua, C. (2003). Solid freeform fabrication of three-dimensional scaffolds for engineering replacement tissues and organs. *Biomaterials*, 24(13), 2363-2378.
- Li, L., Saedan, M., Feng, W., Fuh, J., Wong, Y., Loh, H., . . . Lu, L. (2009). Development of a multi-nozzle drop-on-demand system for multi-material dispensing. *Journal of Materials Processing Technology*, 209(9), 4444-4448.
- Maniruzzaman, M., Boateng, J. S., Snowden, M. J., & Douroumis, D. (2012). A review of hot-melt extrusion: process technology to pharmaceutical products. *International Scholarly Research Notices pharmaceuticals*, 2012.
- McCullough, E. J., & Yadavalli, V. K. (2013). Surface modification of fused deposition modeling ABS to enable rapid prototyping of biomedical microdevices. *Journal of Materials Processing Technology*, 213(6), 947-954.
- Melocchi, A., Parietti, F., Loreti, G., Maroni, A., Gazzaniga, A., & Zema, L. (2015). 3D printing by fused deposition modeling (FDM) of a swellable/erodible capsular device for oral pulsatile release of drugs. *Journal of Drug Delivery Science and Technology*, 30, 360-367.

- Miyai, T., Ito, A., Tamazawa, G., Matsuno, T., Sogo, Y., Nakamura, C., . . . Satoh, T. (2008). Antibiotic-loaded poly- $\epsilon$ -caprolactone and porous  $\beta$ -tricalcium phosphate composite for treating osteomyelitis. *Biomaterials*, 29(3), 350-358.
- Mohanty, A. K., Misra, M., & Drzal, L. T. (2005). *Natural fibers, biopolymers, and biocomposites*: Chemical Rubber Company Press.
- Moroni, L., de Wijn, J. R., & van Blitterswijk, C. A. (2006). 3D fiber-deposited scaffolds for tissue engineering: Influence of pores geometry and architecture on dynamic mechanical properties. *Biomaterials*, 27(7), 974-985.
- Moulton, S. E., & Wallace, G. G. (2014). 3-dimensional (3D) fabricated polymer based drug delivery systems. *Journal of Controlled Release*, 193, 27-34.
- Nikam, V. K., Kotade, K. B., Gaware, V. M., Dhamak, R., Somwanshi, S. B., & Khadse, A. N. (2011). Eudragit a versatile polymer: a review. *Pharmacol online*, 1(1), 152-164.
- Pietrzak, K., Isreb, A., & Alhnan, M. A. (2015). A flexible-dose dispenser for immediate and extended release 3D printed tablets. *European Journal of Pharmaceutics and Biopharmaceutics*, 96, 380-387.
- Prasad, L. K., & Smyth, H. (2015). 3D Printing technologies for drug delivery: a review. *Drug development and industrial pharmacy*, 42(7), 1019-1031.
- Rai, B., Teoh, S.-H., Hutmacher, D., Cao, T., & Ho, K. (2005). Novel PCL-based honeycomb scaffolds as drug delivery systems for rhBMP-2. *Biomaterials*, 26(17), 3739-3748.
- Rutkowski, J. V., & Levin, B. C. (1986). Acrylonitrile–butadiene–styrene copolymers (ABS): Pyrolysis and combustion products and their toxicity—a review of the literature. *Fire and materials*, 10(3- 4), 93-105.

- Sachs, E., Cima, M., Williams, P., Brancazio, D., & Cornie, J. (1992). Three dimensional printing: rapid tooling and prototypes directly from a CAD model. *Journal of Engineering for Industry*, 114(4), 481-488.
- Seeley, S. K., Seeley, J. V., Telehowski, P., Martin, S., Tavakoli, M., Colton, S. L., . . . Atkinson, P. J. (2004). Volume and surface area study of tobramycin-polymethylmethacrylate beads. *Clinical orthopaedics and related research*, 420, 298-303.
- Selimis, A., Mironov, V., & Farsari, M. (2015). Direct laser writing: Principles and materials for scaffold 3D printing. *Microelectronic Engineering*, 132, 83-89.
- Seyfoddin, A., Shaw, J., & Al-Kassas, R. (2010). Solid lipid nanoparticles for ocular drug delivery. *Drug delivery*, 17(7), 467-489.
- Skowrya, J., Pietrzak, K., & Alhnan, M. A. (2015). Fabrication of extended-release patient-tailored prednisolone tablets via fused deposition modelling (FDM) 3D printing. *European Journal of Pharmaceutical Sciences*, 68, 11-17.
- Teo, E. Y., Ong, S.-Y., Chong, M. S. K., Zhang, Z., Lu, J., Moochhala, S., . . . Teoh, S.-H. (2011). Polycaprolactone-based fused deposition modeled mesh for delivery of antibacterial agents to infected wounds. *Biomaterials*, 32(1), 279-287.
- Thakral, S., Thakral, N. K., & Majumdar, D. K. (2013). Eudragit®: a technology evaluation. *Expert opinion on drug delivery*, 10(1), 131-149.
- Tiwari, G., Tiwari, R., Sriwastawa, B., Bhati, L., Pandey, S., Pandey, P., & Bannerjee, S. K. (2012). Drug delivery systems: An updated review. *International journal of pharmaceutical investigation*, 2(1), 2.
- Wan, L. S., & Lim, L. (1992). Drug release from heat-treated polyvinyl alcohol films. *Drug development and industrial pharmacy*, 18(17), 1895-1906.



- Warnke, P. H., Seitz, H., Warnke, F., Becker, S. T., Sivananthan, S., Sherry, E., . . . Douglas, T. (2010). Ceramic scaffolds produced by computer- assisted 3D printing and sintering: Characterization and biocompatibility investigations. *Journal of Biomedical Materials Research Part B: Applied Biomaterials*, 93(1), 212-217.
- Wilson, C., Olejnik, O., & Hardy, J. (1983). Precorneal drainage of polyvinyl alcohol solutions in the rabbit assessed by gamma scintigraphy. *Journal of Pharmacy and Pharmacology*, 35(7), 451-454.
- Wittbrodt, B., & Pearce, J. M. (2015). The effects of PLA color on material properties of 3-D printed components. *Additive Manufacturing*, 8, 110-116.
- Zein, I., Hutmacher, D. W., Tan, K. C., & Teoh, S. H. (2002). Fused deposition modeling of novel scaffold architectures for tissue engineering applications. *Biomaterials*, 23(4), 1169-1185.
- Zhang, C., Zhao, K., Hu, T., Cui, X., Brown, N., & Boland, T. (2008). Loading dependent swelling and release properties of novel biodegradable, elastic and environmental stimuli-sensitive polyurethanes. *Journal of Controlled Release*, 131(2), 128-136.

## Chapter 3

*Development of customised 3D printed biodegradable projectile for administering extended-release contraceptive to wildlife*

Published as:

Long, J., Nand, A. V., Ray, S., Mayhew, S., White, D., Bunt, C. R., & Seyfoddin, A. (2018). Development of customised 3D printed biodegradable projectile for administering extended-release contraceptive to wildlife. *International journal of pharmaceutics*, 548(1), 349-356.

### 3.1. Introduction

There is a crisis as a result of overpopulation of some wildlife species and it is increasing at an alarming rate. Conventional drug delivery to wildlife is challenging due to the difficulties in treating large numbers, inefficiency of the delivery methods and lack of animal species specificity. Traditional drug delivery methods, such as oral administration or injections which often require restraining with animal handling and risk negative outcomes (West et al., 2014). The complexity of preparing and delivering procedures along with the inability to target large numbers of wildlife has limited the use of these traditional systems. Other simplistic delivery methods such as the medical baits, by mixing the drugs into baits to be distributed in the animals' habitat, are also limited by the lack of specificity for targeting the desired animals and drug/bait stability problems encountered in the field (Shapiro et al., 2016).

Wildlife ballistic drug delivery allows the remote administration of pharmaceuticals without the need to restrain the animal and has been shown to be bioequivalent to parenteral delivery (Olsen, Christie, Grainger, & Stoffregen, 2006). Compared to medical baits, ballistic delivery offers pronounced specificity as the pharmaceuticals delivered by this system can be targeted on single individuals. Therefore, the drug(s) and its dosage can be appropriately administered based on the animal's species, sex, age, body weight, and health status. Additionally, various formulations be selected for ballistic delivery and tailored to the pharmacokinetic and pharmacodynamics characteristics of the drug(s). Ballistic delivery method enables the drug(s) to be effectively delivered to unrestrained or un-cooperative animals at a safe distance, avoiding the need for anaesthetisation that further reduces both the associated risks and costs.

Satisfactory drug-eluting projectile delivery requires optimisation of two opposing requirements. Firstly, it is highly desirable that the projectile has enough kinetic energy to penetrate the potentially tough animal hide and realise sufficient penetration of the underlying soft tissue so as to not be subsequently dislodged or ejected from the body. This requirement is counterbalanced by the need to minimise impact damage to the underlying soft tissue to cause the least physical trauma and animal distress. While the use of compressed-air propelled hypodermic syringes for wild animal pharmaceutical delivery meets both of these constraints, environmental concerns around syringe disposal or persistence in the environment and lack of effective range are motivating investigations into seeking an alternative means of animal drug delivery.

Mammalian skin is an anisotropic material (Kalra, Lowe, & Al-Jumaily, 2016) which is comprised of three primary layers: the epidermis, the dermis and hypodermis. Beneath epidermis layer, the dermis provides connective tissue that contains blood vessels and is the typical injection site target. The deeper hypodermis layer has excellent shock absorbing qualities making it ideal to slow down the projectile. Both the hypodermis and underlying superficial muscles are well vasculated making this an ideal site for sustained drug delivery (El Maghraby, Barry, & Williams, 2008). In this investigation, the effect of different projectile tips on the penetration depth of intact medium and thin-skinned mammal hides were assessed.

Customised medication has become an important concept in the modern development of pharmaceutical and medical applications as large scale manufacturers of medicines are unable to fabricate complex formulations or specific doses to meet an individual's

therapeutic need (Goole & Karim, 2016; Khaled, Burley, Alexander, Yang, & Roberts, 2015; Scoutaris, Alexander, Gellert, & Roberts, 2011). Use of 3D printing technology for drug delivery is an emerging and promising research and application area for customised pharmaceutical therapy. 3D printing is a rapid prototyping method to fabricate 3D designs with a digitally controlled layer-by-layer deposition technique using computer aided design (CAD) software (Long et al., 2017). One of the most widely used 3D printing systems is fused deposition modelling (FDM) which provides the advantages of rapid prototyping, precision of quantity and versatility in incorporation of concentration gradients within the polymer matrix when compared to the other techniques (Moulton & Wallace, 2014). A 3D printed BDDS offers the following potential advantages: i) potential for multiple pharmaceutical delivery, ii) flexibility to create hollow reservoirs to accommodate solid, semisolid or liquid formulations, iii) customised dosages for each individual, iv) target animal specificity, v) possibility of marking the animal with colours or electrical identification devices along with the administration of the therapeutics, vi) low treatment costs, vii) minimum direct contact with wild animals, and viii) no anaesthetisation requirement.

In this work, poly (lactic acid) (PLA) is chosen as the filament due to its biodegradable, biocompatible, high-strength, high-modulus and non-toxic properties (Sébastien, Stéphane, Copinet, & Coma, 2006). The relatively low melting temperature of PLA 160°C also facilitates the melt fabrication and printing processes. Prior to filament-fused 3D printing, the target drug needs to be loaded into the polymer filament. Impregnation by diffusion is the simplest and traditional way to incorporate drug(s) into the filament however this technique has limitations, such as the necessary of a high concentration of drug solution, low and inaccurate drug

loading, and significant processing time (Long et al., 2017). An alternative loading method, hot melt extrusion (HME), was chosen in this work due to its enhanced drug loading and fast processing time. During HME, drug(s) and polymer are physically mixed and melted within the extrusion screw and subsequently extruded from the nozzle as a filament at a controlled diameter (generally 1.75-3.00mm) for subsequent 3D printing (Long et al., 2017).

The contraceptive drug progesterone, a common contraceptive known as pregn-4-ene-3,20-dione or P4, is an endogenous steroid hormone released from corpus luteum in human and mammal females (King & Brucker, 2010). In this study, P4 was chosen for its thermo-stability and effectively contraceptive function achieved by thickening the sticky mucus produced at the neck of cervix (Villanueva, 2007).

The specific aims of this research here were to i) explore the feasibility of 3D printed biodegradable projectiles loaded with contraceptive P4 via HME and FDM 3D printing; ii) to identify the stabilities of both drug and polymer during HME and 3D printing processes; iii) to explore the interactions between P4 and polymer, iv) to evaluate *in vitro* drug release performance; and v) to simulate ballistic performance of PLA printed projectiles in penetrating animal hides.

## 3.2. Materials and methods

### 3.2.1. Materials

Poly (lactic acid) (PLA, 2003D grade) pellets were kindly supplied from Clariant Limited (Auckland, New Zealand), and progesterone (P4) was kindly gifted from Dairy Equipment Company (Hamilton, New Zealand). Dichloromethane, absolute ethanol and methanol of HPLC grade were purchased from Fisher Scientific UK (Loughborough, UK).

### 3.2.2. Preparation of PLA filament loaded with P4 with HME

Accurately weighed P4 powder was mixed with PLA pellets to prepare P4-PLA filaments with different amount of drug loadings of 2, 5 and 10%. The mixtures were loaded into a single-screw HME extruder (Noztek Pro filament extruder, Noztek, UK) and then extruded at 150°C through a 1.75 mm nozzle at 15 rpm. The extruded filaments were collected and grinded into powder by a commercial grinder (BCG200, Breville, New Zealand). The powders were re-extruded to better distribute P4 within the filament.

### 3.2.3. 3D printing of biodegradable projectiles

Biodegradable projectiles of 4.5 mm diameter x 35 mm long with a 15 mm Spitzer style cone tip (for 0.177" calibre) were designed using AutoCAD (Autodesk Inc, USA) (Figure 3-1) and fabricated with the drug-loaded filaments via a FDM 3D printer (Figure 3-1) (UP Mini 3D printer, 3D printing Systems, New Zealand). The printing settings used were as follows: fine quality with solid fill, printing speed of 10 cm<sup>3</sup>/h, 0.4 mm nozzle outlet diameter, Z resolution (layer thickness) of 0.15 mm and extrusion temperature of 200°C.

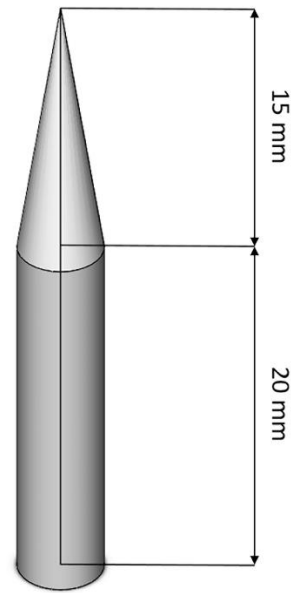


Figure 3-1. Biodegradable projectile design: for 0.177 calibre 900FPS air-rifle sized 35 mm length  $\times$  4.5 mm diameter with a 15 mm cone tip.

### 3.2.4. Characterisation

#### 3.2.4.1. Metrological data

The diameters and lengths of the printed biodegradable projectiles were measured by a Vernier calliper. The weights of the biodegradable projectiles were measured using an electronic balance (AUW220D, SHIMADZU, Japan). Surface and cryo-fractured cross-section images of the HME filaments, printed biodegradable projectiles and samples after *in vitro* release test were obtained using a Schottky field emission SEM (SU-70, Hitachi, UK) under a working voltage of 2 kV. Prior to SEM, samples were placed on metallic stubs and coated with platinum under vacuum for 100 seconds using an ion sputter coater (E-1045, Hitachi, UK) for visualisation.

#### 3.2.4.2. Thermal analysis

Thermal properties of the 3D printed projectiles were determined using differential scanning calorimetry (DSC) (DSC Q1000, TA Instruments, NZ). An accurate amount of samples were weighed (5 mg) and subsequently sealed in aluminium pans. The



tests were performed under nitrogen atmosphere at a heating rate of 10°C/min between the temperature range of 30-220°C.

#### 3.2.4.3. Fourier transform infrared spectroscopy (FTIR)

Fourier transform infrared spectroscopy (FTIR) was performed on 3D printed biodegradable projectiles using a Thermo Scientific Nicolet iS10 FTIR spectrophotometer in attenuated total reflectance (ATR) mode using diamond crystal.

#### 3.2.4.4. Uniformity test

To calculate drug uniformity within the filament, 20 cm length from the initial, middle and end sections of filaments loaded with 2, 5 and 10% P4 were cut and ground into powder. The three groups of drug-loaded filaments were completely dissolved in a solvent system consisting of dichloromethane and methanol (5:3). The amount of P4 within the PLA polymeric matrix were then determined by UV spectrophotometry (Ultrospec 7000, BIOCHROM, UK) using a calibration curve at an absorption wavelength of 244 nm (calibration equation was  $y = 0.0812x + 0.0088$ ,  $R^2=0.9991$ ). The drug loading (DL), incorporation efficiency (IE) and relative standard deviation percent (%RSD) were calculated as typically reported (D. Li et al., 2013).

In order to assess the P4 contents in the printed projectiles, each projectile was accurately weighed and completely dissolved in dichloromethane and methanol (5:3). The loading amount of P4 in each projectile was determined with the same method.

#### 3.2.4.5. *In vitro* drug release test

*In vitro* drug release tests were performed in 100 mL release media selected to maintain sink conditions, comprised of 62.5% ethanol and 37.5% double distilled water in 250 mL screw-capped bottles, shaken at 100 rpm on a benchtop shaker (SK-

300, Lab Companion, Korea) in an incubator room maintained at  $35 \pm 2^\circ\text{C}$  for a period of 164 days. At predefined time points, 2 mL of the incubation media from each sample was collected and equal amount of fresh media was added into each release system to maintain the total volume and sink condition. The concentration of P4 in samples was determined by UV spectrophotometry (Ultrospec 7000, BIOCHROM, UK) using a calibration curve at an absorption wavelength of 244 nm (calibration equation was  $y = 0.0487x - 0.0062$ ,  $R^2=0.9994$ ). The percentage cumulative amount of P4 released was plotted against square-root-of-time for each sample. Three duplicates ( $n=3$ ) were performed and the results were presented as mean value  $\pm$  SD.

#### 3.2.4.6. Ballistic penetration study

This investigation compares the specific kinetic energy required to penetrate thin and medium-thickness skins and correlates this to desired projectile mass and velocity to realise the desired penetration depth. A simple pendulum system enabled different masses to be dropped from a known height to impact a Spitzer tipped projectile forcing it into freshly excised thin and medium-thickness skins of sheep and horse hides respectively. Other projectile tips were tested, including flat, tiered and round, but were found to require energy levels beyond that normally available from an air rifle. Behind each intact skin was a synthetic muscle supporting structure made from open-cell foam that had been encapsulated in a thin silicon layer (Whittle et al., 2008). The purpose of this study was to identify the projectile tip and least kinetic energy levels required to penetrate the hide so as to minimise impact damage to the underlying soft tissue.

#### 3.2.4.7. Statistical analysis.

Data were subjected to one-way analysis of variant (ANOVA) with the level of significance set at  $P < 0.05$ .

### 3.3. Results and discussion

#### 3.3.1. Evaluation of drug loading by HME and its distribution within the host polymer

For drug loading methods, discussed previously (Long et al., 2017), HME is an auspicious alternative to impregnation as it overcomes major disadvantages of impregnation such as long processing time, concentrated drug solution and low loading amount by passive diffusion (Goole & Karim, 2016; Goyanes et al., 2014b; Goyanes et al., 2015; Skowrya et al., 2015). All filaments manufactured by HME with different drug loadings had smooth and translucent appearance. As seen in Table 3-1, the uniformity indicated that P4 was distributed well in the PLA polymeric matrix with all %RSD values below 6.0%, the upper limit of the USP specification (Hill, Varker, Karlage, & Myrdal, 2009). A double-extrusion procedure was employed in this study as it significantly reduced the %RSD value in PLA5 group from 6.27 (initial extrusion) to 1.06 (second extrusion) in the preliminary optimisation trial. The drug loading of each filament increased with increasing concentrations of P4, while the incorporation efficiency of all three formulations are lower than theoretical values. It was observed during HME processing drug powder appeared to adhere to and remain of the wall of mixing chamber and on the screw surface.

Table 3-1. Drug Loading (DL), Incorporation Efficiency (IE) and Relative standard Deviation Percent (%RSD) of drug content in HME filaments and 3D printed biodegradable projectiles with theoretical P4 loadings of 2, 5 and 10% w/w (PLA2, PLA5 and PLA10 respectively) (n=3±SD).

	Formulation	Position	DL ± SD (%)	IE ± SD (%)	%RSD
Filament	PLA2	Initial	1.58 ± 0.00	79.05 ± 0.19	4.76
		Middle	1.73 ± 0.02	86.70 ± 0.91	
		End	1.56 ± 0.01	78.03 ± 0.36	
	PLA5	Initial	3.57 ± 0.02	71.37 ± 0.50	1.06
		Middle	3.53 ± 0.02	70.63 ± 0.41	
		End	3.62 ± 0.01	72.48 ± 0.15	
	PLA10	Initial	9.38 ± 0.01	93.83 ± 0.07	4.97
		Middle	8.84 ± 0.04	88.44 ± 0.38	
		End	8.31 ± 0.09	83.06 ± 0.94	
Biodegradable projectile	PLA2		1.43 ± 0.08	71.33 ± 3.98	5.93
	PLA5		3.49 ± 0.08	69.76 ± 1.61	4.68
	PLA10		7.54 ± 0.24	75.42 ± 2.38	1.81

### 3.3.2. Metrological studies of 3D printed biodegradable projectiles

Biodegradable projectiles were printed using a benchtop FDM printer. The photographs of the printed biodegradable projectiles are presented in Figure 3-2, while the weights and physical dimensions are listed in Table 3-2.

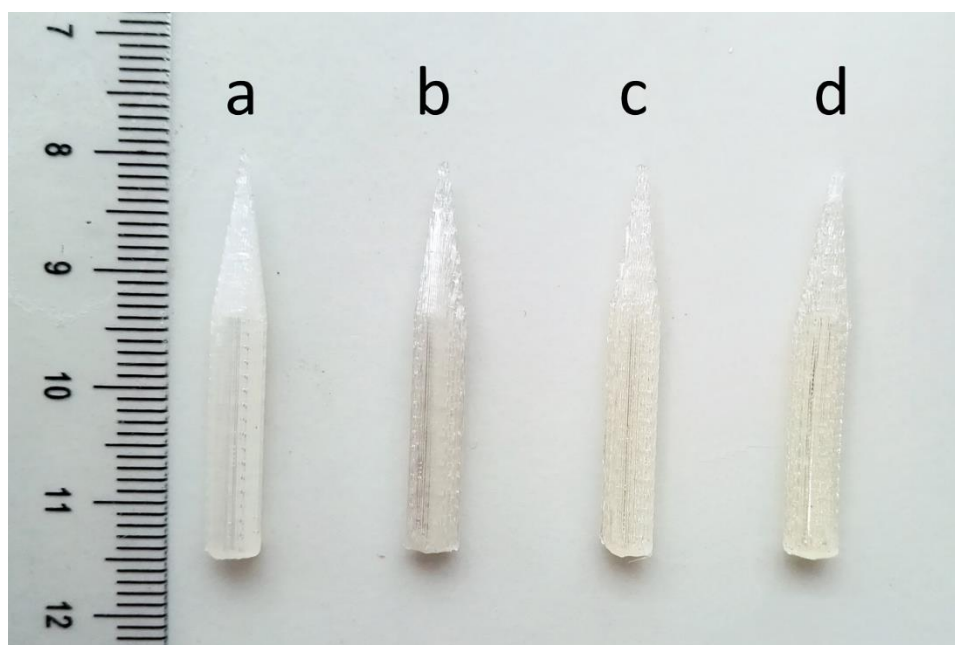


Figure 3-2. Photograph of 3D printed biodegradable projectiles: (a) pure poly (lactic acid) (PLA), (b) PLA2 (2% progesterone loading), (c) PLA5 (5% progesterone loading) and (d) PLA10 (10% progesterone loading).

The 3D printed biodegradable projectiles with various P4 loadings showed no significant difference between physical dimensions in millimetre (diameter  $p=0.056$ , length  $p=0.094$ ) and weight (weight  $p=0.060$ ). The visual appearance of the projectiles printed with PLA filaments of 2, 5 and 10% P4 were similar to a blank (no P4) projectile. The DL and IE of medical projectiles, given in Table 3-1, showed a trend similar to that of HME filament. The %RSD values of the biodegradable projectiles in Table 3-1 demonstrated that these printed medicines had a high degree of repeatability and precision in drug content. The morphological properties of 3D printed biodegradable projectiles were observed using SEM. As shown in Figure 3-3, no drug particle was visible in PLA matrix after HME and 3D printing. P4 was mixed within the host polymer matrix by thermal processing. The SEM images show that after cooling down, re-aggregation of P4 within the polymer matrix did not occur, indicating that P4 is miscible and well dispersed in the polymer matrix. This signified the potential of 3D printing to fabricate solid medicines with a considerable range of doses responding to individual needs.

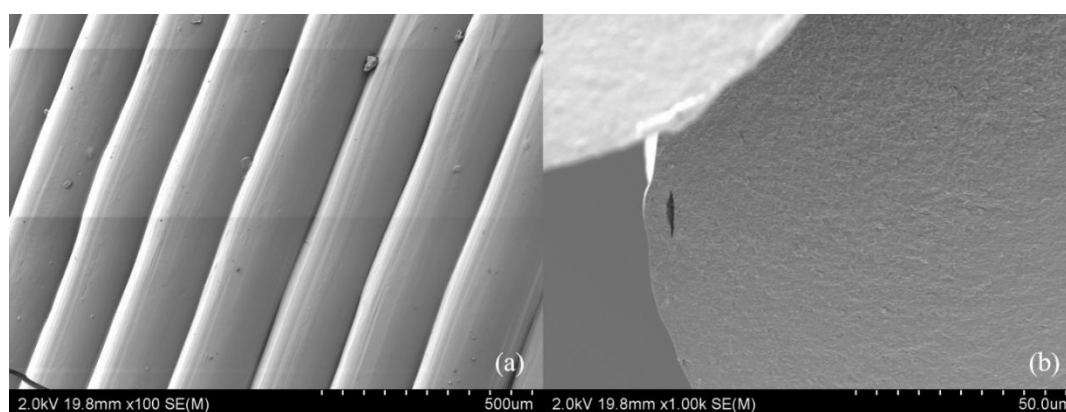


Figure 3-3. SEM images of 3D printed PLA10 projectiles: (a) surface and (b) cross section.

Table 3-2. Metrological properties (diameter, length and weight) of 3D printed biodegradable projectiles with different formulations ( $n=3\pm SD$ ).

Formulation	Diameter $\pm SD$ (mm)	Length $\pm SD$ (mm)	Weight $\pm SD$ (g)
PLA2	4.23 $\pm$ 0.07	33.20 $\pm$ 0.06	0.333 $\pm$ 0.021
PLA5	4.18 $\pm$ 0.05	33.34 $\pm$ 0.16	0.362 $\pm$ 0.026
PLA10	4.16 $\pm$ 0.03	33.37 $\pm$ 0.22	0.344 $\pm$ 0.021

### 3.3.3. DSC analyses of the influence of extrusion/printing process and drug additive on thermal transition of polymer

Manufacturing technologies involving heating and cooling can affect the properties of the polymers as materials undergo changes in the degree of molecular motion during the process cycle. These thermal transitions are associated with amorphous and crystalline components of the polymers. Incorporation of additives in the polymer system, could further influence these thermal transitions of polymers, hence, DSC studies were performed on 3D printed biodegradable projectiles containing P4 at different loadings. The results of these studies were compared with the DSC thermograms of P4 or 3D printed biodegradable projectile to determine the influence of P4 on thermal changes of the host polymer as a measure of glass transition ( $T_g$ ), crystallisation ( $T_c$ ) and melting ( $T_m$ ) temperature of PLA (Table 3-3).

The characteristic sharp endothermic peak of P4 at 131°C was noted which corresponds to its crystalline melting temperature. The printed PLA sample without P4 additive, showed a  $T_g$  at 60°C and endothermic crystalline melting peak ( $T_c$ ) at 166°C respectively. Also, the broad exothermic peak due to the cold-crystallisation occurred at 93°C suggesting some of the amorphous structure in the material had undergone molecular ordering and converted to a structured nature leading to crystalline formations during the heating process (Senatov et al., 2016). However, the

area of this exothermic crystalline peak is less than the endothermic melting peak indicating the presence of original crystal in addition to this cold-crystalline structure.

For PLA samples containing P4 at different loadings, the absence of the endothermal peak of P4 confirms the absence of local concentrations of drug within the host matrix. This finding also suggests that P4 was evenly distributed within the host polymer matrix as no crystalline material was present even at the highest P4 loading. The physical mixture also confirms the hypothesis of disappearance of crystalline peak of drug sample due to melting of drug and then finely dispersed at the polymer matrix during processing.

Interestingly, incorporation of only 2% P4 in PLA significantly shifted the cold-crystallisation peak towards higher temperature from 93 to 112°C. Thus, P4 was able to decrease the molecular chain mobility and structure formation of PLA during heating, which impede the process of crystallisation and leads to higher values of  $T_c$ . The dispersed P4 could possibly act as nucleation site during the ordering of PLA molecular chains during the heating process. Similar shifting of this exothermic peak was noted at 5% and 10% P4 loadings, however, the peak position and intensity did not change markedly at higher loadings, indicating that the P4-induced crystallisation had reached a maximum even at low loading levels.

Conversely, the effect of the drug additive on glass transition of polymer was not so profound. Addition of 10% P4 in PLA showed a mild plasticisation effect as the  $T_g$  of PLA was reduced to 56°C from 60°C (Table 3-3). At lower loadings of P4, this plasticisation effect was quite trivial with the additive primarily affecting the crystalline component of the polymer. In addition to exothermic transitions, the



addition of P4 also significantly influenced the endothermic melting transition of PLA. Thus, at 2% P4 loading, the  $T_m$  of PLA was reduced to 145°C from 166°C. Also, the enthalpy of fusion ( $\Delta H_f$ ), as a measure of energy required for polymer melting transition was reduced from 48 J/g to 26 J/g. These findings suggests that FDM based printing technology enables the diffusion of the drug additive into the free volume of PLA, between the polymer chains and could possibly undergo molecular interactions with the polymer. The formation of bimodal crystalline melt transition within the printed drug loaded polymer samples implies the formation of different size and crystalline lamellae structures. The ingress of P4 disrupts the inter/intra molecular interactions within PLA and thereby reduces the thickness of lamellae, disordering its lamellate structures and consequently decreasing the amount of polymer crystalline formation. It also depresses the melting point with the changes in  $T_m$  being not so evident when increasing P4 loading. This indicates that the P4 induced crystallisation equilibrium of PLA with as little as 2% drug loading. Thermal processing of PLA at higher temperature may pose the risk of polymer degradation so depressing the melting point of PLA by incorporating this drug additive would be advantageous for material processing (Ray & Cooney, 2012).

Table 3-3. DSC analysis of pure P4 and 3D printed PLA biodegradable projectiles with different concentrations of P4: 0, 2, 5 and 10% w/w.

Proportion	$T_g$ (°C)	$T_c$ (°C)	$\Delta H_f$ (J/g)	$T_m$ (°C)
Pure PLA	60.43	93.44	47.88	166.04
PLA-2%P4	59.19	111.77	25.86	145.33
PLA-5%P4	57.85	112.18	28.56	144.91
PLA-10%P4	56.39	109.57	29.62	142.48
Pure P4	NA	NA	84.65	130.68

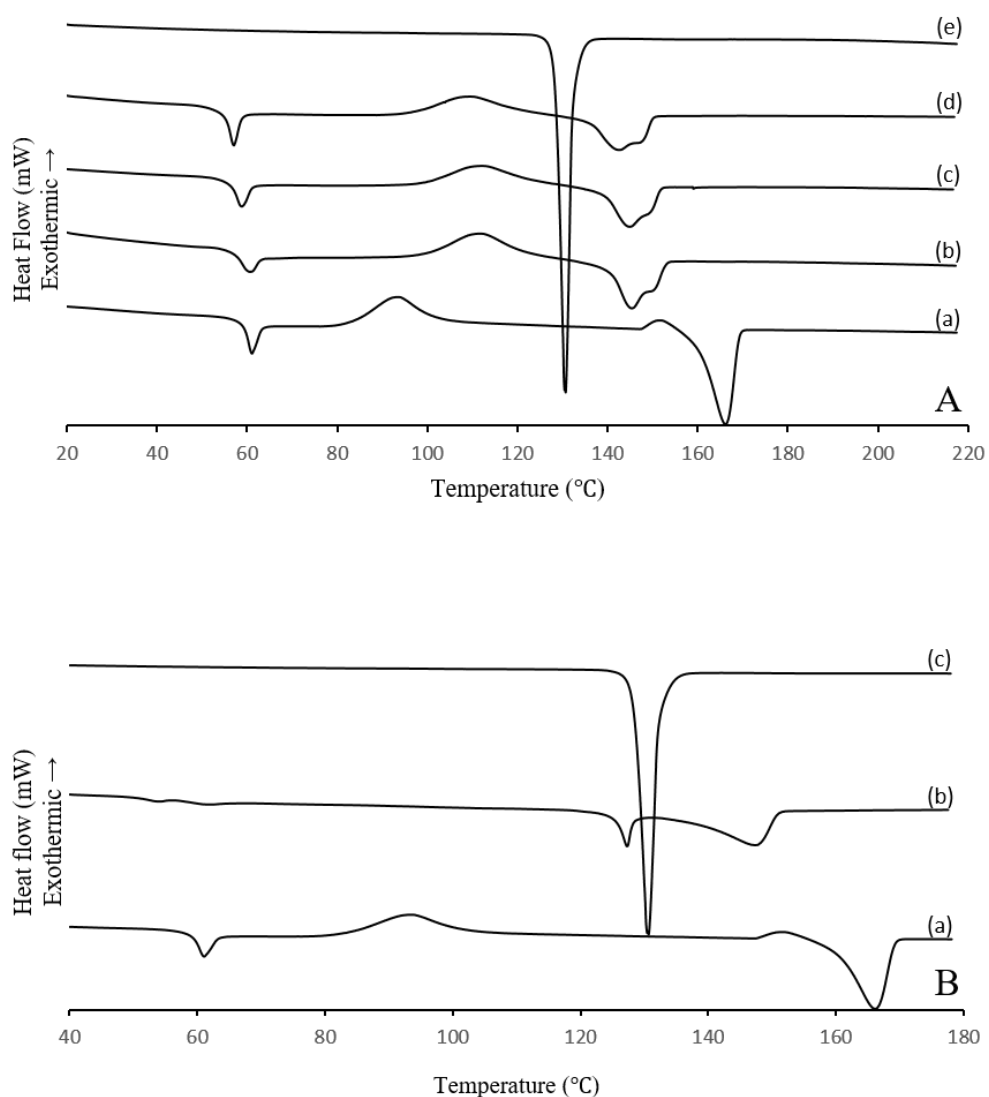


Figure 3-4. DSC curves of A: (a) printed pure poly (lactic acid) (PLA), (b) printed PLA with 2% progesterone loading, (c) printed PLA with 5% progesterone loading, (d) printed PLA with 10% progesterone loading and (e) pure progesterone; B: (a) pure PLA, (b) physical mixture of PLA and progesterone and (c) pure progesterone.

### 3.3.4. FTIR analyses: evidence of chemical interactions between the drug additive and the host polymer

FTIR spectra of 3D printed biodegradable PLA, PLA loaded with P4 projectiles and pure P4 are presented in Figure 3-5.

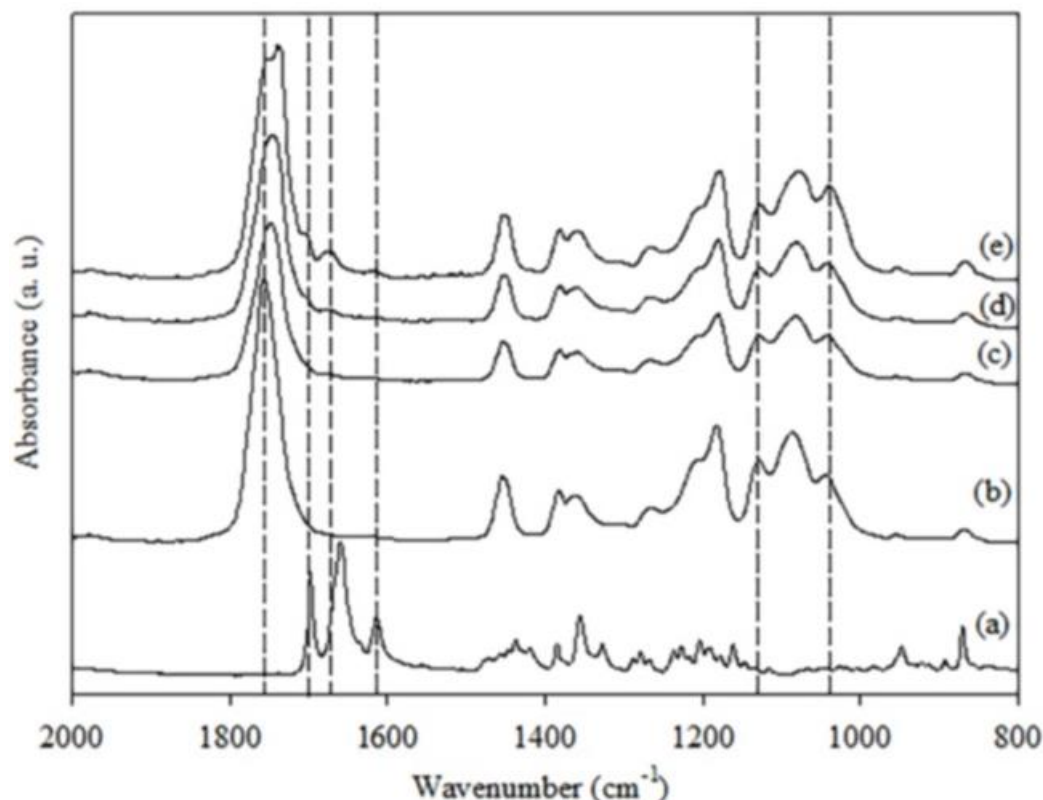


Figure 3-5. FTIR spectra of (a) progesterone (b) printed pure poly (lactic acid) (PLA) and printed PLA with (c) 2%, (d) 5% and (e) 10% progesterone loading.

The spectrum of P4 exhibited characteristic absorbance bands at  $1660\text{ cm}^{-1}$  and  $1698\text{ cm}^{-1}$ , attributed to C=O stretching vibration linked to C3-cyclic and C20 linked to methyl group respectively (Cerchiara, Luppi, Bigucci, & Zecchi, 2003). Moreover, the C=C stretching appeared at  $1615\text{ cm}^{-1}$  while the =C-H bending of P4 appeared at  $870\text{ cm}^{-1}$  (Leimann et al., 2015).

Appearance of these C=O stretching bands at  $1675\text{ cm}^{-1}$  and  $1700\text{ cm}^{-1}$  in 10% P4 loaded sample (Figure 3-5) indicates the presence of the P4 additive in the PLA matrix. Shifting of C=O linked to C3-cyclic group indicates possible hydrogen bonding type chemical interaction between this additive and the polymer (Figure 3-6). However, at lower drug loadings, the intensity of above bands became very weak.

The major peaks in the spectrum of PLA can be assigned to C=O stretching at 1756  $\text{cm}^{-1}$ , -C-H bending at 1455 and 1382  $\text{cm}^{-1}$  and various ester related bands at 1182 and 1087  $\text{cm}^{-1}$  (C-O-C stretching), 1044  $\text{cm}^{-1}$  (C-CH<sub>3</sub> stretching) and 1128  $\text{cm}^{-1}$  (CH<sub>3</sub> asymmetrical rocking) (Oliveira et al., 2013; Wrona, Cran, Nerín, & Bigger, 2017). The P4 loaded PLA printed projectile samples exhibited all spectral features of PLA, however, P4 peaks were not seen when the drug loading was low. Mashak, Mobedi, and Mahdavi (2015) have also reported this phenomenon elsewhere (Mashak et al., 2015). The bulk polymer is expected to mask or dilute FTIR contributions of additives when the loading level is low (Nand, Ray, Travas-Sejdic, & Kilmartin, 2012). Nevertheless, with increasing drug loading, peaks additional to those of PLA, were observed at 1615  $\text{cm}^{-1}$  and 1675  $\text{cm}^{-1}$  and a shoulder peak was also observed at about 1700  $\text{cm}^{-1}$ . These features could be attributed to contributions from P4 and therefore could be used to ascertain the presence of P4 in the printed projectiles. The spectra of P4 loaded PLA projectiles were very similar to that of PLA, indicating no significant chemical changes occurred in the polymer backbone upon melt extrusion and the incorporation of the drug. The notable changes however, were the red shift of the PLA band at 1756  $\text{cm}^{-1}$  to 1735  $\text{cm}^{-1}$  and the increase in intensity of the 1040  $\text{cm}^{-1}$  band compared to the 1127  $\text{cm}^{-1}$  band upon incorporation of P4. These observations suggest some interaction of the drug with the polymer matrix, a phenomenon also supported by DSC results.

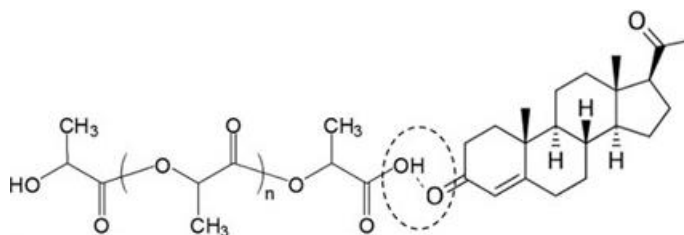


Figure 3-6. Chemical interaction of poly (lactic acid) (PLA) polymer and progesterone.

### 3.3.5. Studies on *in vitro* drug release

*In vitro* release of P4 from the biodegradable projectiles was performed in a release assessment media containing 62.5% ethanol and 37.5% double distilled water. Ethanol was used to maintain sink conditions that would otherwise be difficult to maintain due to poor water solubility of P4. The drug release data presented in Figure 3-8 indicates that all the formulations showed sustained release over a period of 164 days as our target delivery timing. The patterns of drug release were diverse with respect to the drug loading. Faster and greater drug release was observed with the higher percentage of steroidal P4 loaded. These results are consistent with those of D. Li et al. (2013) who explored the release behaviour of a steroid drug (dexamethasone) from PLA filaments fabricated by HME. The highest loading projectiles, PLA10, had a faster release (up to 48.4%) in first 53 days followed by a sustained release in the subsequent 69 days and finally reached a plateau in the last 42 days. The PLA2 and PLA5 biodegradable projectiles exhibited similar release behaviours in the early stage (16.2% and 16.7% of P4 released in 32 days, respectively), following by continuous release profiles with the released percentages of 63.5% and 74.4% respectively. At the end of the study period, 71.0% and 85.0% drug were released from PLA2 and PLA5, while 97.8% was released from the PLA10 projectiles. This result suggests that during the solvent treatment the drug incorporated in the polymeric matrix facilitates pore formation from the surface to bulk, which promotes solvent uptake and drug dissolution (Figure 3-7).

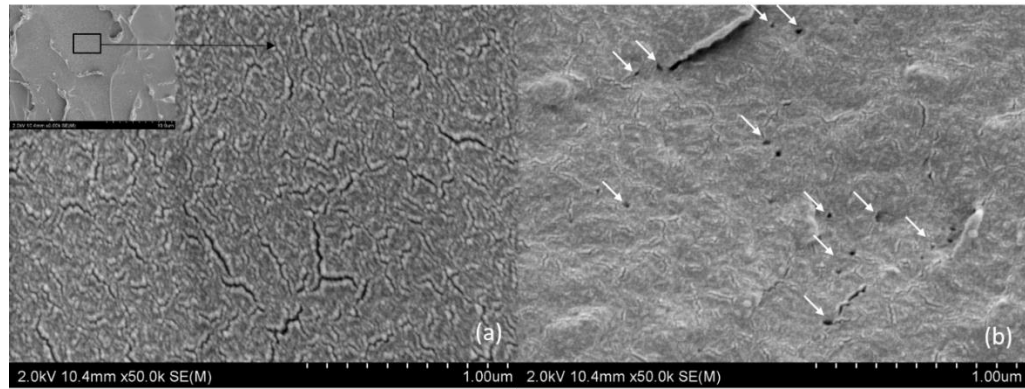


Figure 3-7. SEM cross section images of PLA10 projectiles: (a) before and (b) after the dissolution study.

Mathematical models of *in vitro* drug release behaviours are essential for defining the drug release mechanism (Dash, Murthy, Nath, & Chowdhury, 2010; Shaikh, Kshirsagar, & Patil, 2015; Singhvi & Singh, 2011). The *in vitro* drug release data for P4-PLA biodegradable projectiles was fitted into zero-order and Higuchi models (Dash et al., 2010). PLA2 and PLA5 were best modelled by zero-order model ( $R^2$  values: 0.9801 and 0.9835, respectively) in which the release rate of incorporated drug is independent of its concentration (as shown in Eq.(3-1)). Essentially, the drug was more likely to be surrounded by PLA and most of the drug was released by passive diffusion which was controlled by the concentration gradient between the device and surrounding medium.

$$C = C_0 - K_0 t \quad (3-1)$$

where  $C$  is the amount of drug released,  $C_0$  is the initial amount of drug in solution,  $K_0$  is the zero order rate constant and  $t$  is the time (Shaikh et al., 2015).

For PLA10, the Higuchi model ( $R^2$  value: 0.9843) was found to be a better fit followed by zero order ( $R^2$  value: 0.9725), indicating that the P4 released from the PLA matrix in this device was mainly controlled by the micro-pores diffusion as well as passive

diffusion (as shown in Eq.(3-2)). The formation of pores in the cross section of PLA10 sample noted in Figure 3-7 (b) further support the observed Higuchi kinetics, representing that channels were formed for facilitating the solvent intake and P4 dissolution. This is in accord with the findings that at the higher drug loaded samples showed a higher and faster release than the lower drug-loading projectiles.

$$C = [D(2qt - C_s)C_s t]^{1/2} \quad (3-2)$$

where  $C$  is the total amount of drug release per unit area of the matrix,  $D$  is the diffusion coefficient for the drug in the matrix,  $qt$  is the total amount of drug in a unit volume of matrix,  $C_s$  is the dimensional solubility of drug in the polymer matrix and  $t$  is the time (Shaikh et al., 2015).

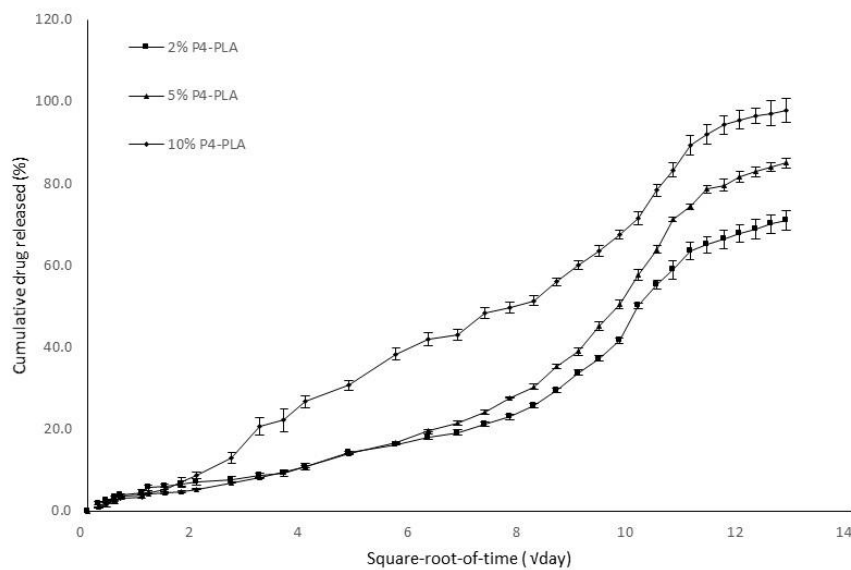


Figure 3-8. *In vitro* drug release profiles of P4 from 3D printed PLA biodegradable projectiles (n=3±SD).

### 3.3.6. Ballistic penetration analysis

Minimum specific kinetic energy required to penetrate thin and medium-thickness hides ( $E_{k,p}$ ) are presented in Table 3-4. Results from 177 and 22 calibre projectile

testing demonstrated the sharp pointed Spitzer was capable of penetrating the two different hide types within the range of that delivered by an air rifle (Table 3-4). This was based on the maximum available energy of 9.4 J, determined from the typical muzzle velocity of 255 m/s achieved by a 0.289 g projectile fired from this type of gun. From these results, it can be seen that lower specific energy levels are required to penetrate the medium thickness skin however, it should be noted that these skins are also thicker than the thin hides and therefore the projectile requires a higher energy to penetrate through this layer.

Table 3-4. Minimum specific kinetic energy required to penetrate thin and medium-thickness hides ( $E_{k,p}$ ).

Projectile Tip	$E_{k,p}$ Sheep (thin skin)	$E_{k,p}$ Horse (medium skin)
177 Spitzer	0.89 J/mm	0.68 J/mm
22 Spitzer	2.11 J/mm	1.00 J/mm

The energy required to penetrate into the muscle can be determined by correlating the force required to realise muscle shear rupture for each projectile size to unit depth penetration. In our calculations we used muscle shear rupture stress range of 39 kPa to 48.5 kPa (Catkins & Sullivan 2007) that yielded a muscle specific energy penetration ( $E_{m,p}$ ) for 177 and 22 calibre projectiles, shown in Table 3-5.

Table 3-5. Range of specific energy required to penetrate muscle ( $E_{m,p}$ ).

Projectile Tip	$E_{m,p}$ range
177 Spitzer	0.62 J/mm to 0.77 J/mm
22 Spitzer	1.10 J/mm to 1.37 J/mm

From these results it becomes possible to estimate the air rifle firing pressure required to deliver a projectile to a desired penetration depth by knowing the animal hide classification (thin or medium) and calculating the total kinetic energy required ( $E_{tot}$ ). This is calculated from an estimated hide thickness (X) and intended depth of muscle penetration (Y) using Eq.(3-3).



$$E_{tot} = XE_{h,p} + YE_{m,p} \quad (3-3)$$

Assuming the drug-eluting projectile penetrates the skin of a thin-hide animal (2 mm thick), or that of a medium-hide animal (4 mm), and in both cases the projectile is intended to be delivered into muscle 2 mm below the hypodermis layer. Lower and upper bound solutions representing the range of variance in muscle specific energy penetration are shown in Table 3-6.

Table 3-6. Range of total energy required to deliver projectile 4 mm into muscle.

Projectile Tip	Thin-hide animal	Medium-hide animal
177 Spitzer	4.26 J - 4.86 J	4.58 J - 5.80 J
22 Spitzer	8.62 J - 9.70 J	8.45 J - 9.48 J

A simple comparison shows that lead is nine times as dense as PLA; a biodegradable and bioactive thermoplastic aliphatic polyester that is a suitable candidate for ballistic drug delivery. Assuming a contact velocity of 255 m/s, the impact energy of 177 and 22 calibre lead projectiles, having a mass of 1.03 g and 2.60 g, equates to an impact energy of 33.49 J and 84.53 joules respectively. A drug-loaded PLA 177 and 22 calibre projectile having an approximate mass of 0.114 g and 0.289 g respectively, and travelling at the same velocity of 255m/s, would be capable of delivering 3.71 J and 9.40 J of work on the animal. These two values compare well to the total energy required to deliver a projectile 4 mm into muscle in both thin and medium hide animals, shown in Table 3-6. Variation in calibre and adjustment in projectile velocity through variation in rifle air-pressure provides a range of depth penetration that can be predicted using the findings of this investigation.

### 3.4. Conclusion

Biodegradable projectiles containing different loadings of the contraceptive drug P4 using 3D printing and HME techniques to demonstrate the feasibility of using 3D printing as a prototyping tool for fabricating and delivering customised medicines. Particularly, the viability of combining FDM 3D printing and HME in manufacturing P4-PLA biodegradable projectiles with particular dosages was assessed. We have found that the re-extrusion HME method was adequate to prepare uniformed filaments with different drug loadings. Additionally, FDM 3D printing can be considered as a potent tool to fabricate tailored medicines with different drugs, dosages, sizes, shapes and polymers to fulfil the needs of personalised care and treatment. The Spectroscopic studies showed that P4 was successfully entrapped into PLA matrix without chemical changes. Thermal analysis studies suggested that the incorporation of P4 weakened the polymer-polymer interactions in PLA and thereby reduced the cold-crystallisation and melting temperature of PLA. Formation of micro-pores in solvent treated projectiles were evident from microscopic studies, which is more pronounced at higher drug loaded sample. The *in vitro* release study demonstrated that the printed projectiles could deliver a sustained release of drug for more than five months with defined release mechanisms. The ballistic study also showed that a range of depth penetration in hide and muscle can be achieved by adjusting the projectile velocity.

In principle, the present work confirms the potential and feasibility of HME and FDM 3D printing techniques as a promising platform to bring more flexible and appropriate solutions for pharmaceutical and medical applications.

### 3.5. References

- Ang, T. H., Sultana, F. S. A., Hutmacher, D. W., Wong, Y. S., Fuh, J. Y. H., Mo, X. M., . . . Teoh, S. H. (2002). Fabrication of 3D chitosan–hydroxyapatite scaffolds using a robotic dispensing system. *Materials Science and Engineering: C*, 20(1–2), 35-42.
- Arnold, C. B., Serra, P., & Piqué, A. (2007). Laser direct-write techniques for printing of complex materials. *Materials Research Society Bulletin*, 32(01), 23-31.
- Baino, F., Ferraris, S., Miola, M., Perero, S., Verné, E., Coggiola, A., . . . Ferraris, M. (2016). Novel antibacterial ocular prostheses: Proof of concept and physico-chemical characterization. *Materials Science and Engineering: C*, 60, 467-474.
- Butscher, A., Böhner, M., Hofmann, S., Gauckler, L., & Müller, R. (2011). Structural and material approaches to bone tissue engineering in powder-based three-dimensional printing. *Acta Biomaterialia*, 7(3), 907-920.
- Cerchiara, T., Luppi, B., Bigucci, F., & Zecchi, V. (2003). Effect of chitosan on progesterone release from hydroxypropyl- $\beta$ -cyclodextrin complexes. *International journal of pharmaceutics*, 258(1), 209-215.
- Chen, H., Fuhlbrigge, T., Zhang, G., & Masood, S. (2007). Application of fused deposition modelling in controlled drug delivery devices. *Assembly automation*, 27(3), 215-221.
- Chia, H. N., & Wu, B. M. (2015). Recent advances in 3D printing of biomaterials. *Journal of biological engineering*, 9(1), 1.
- Chung, J. H., Naficy, S., Yue, Z., Kapsa, R., Quigley, A., Moulton, S. E., & Wallace, G. G. (2013). Bio-ink properties and printability for extrusion printing living cells. *Biomaterials Science*, 1(7), 763-773.

- Dash, S., Murthy, P. N., Nath, L., & Chowdhury, P. (2010). Kinetic modeling on drug release from controlled drug delivery systems. *Acta Poloniae Pharmaceutica*, 67(3), 217-223.
- Davies, N. M., Fair, S. J., Hadgraft, J., & Kellaway, I. W. (1991). Evaluation of mucoadhesive polymers in ocular drug delivery. I. Viscous solutions. *Pharmaceutical research*, 8(8), 1039-1043.
- El Maghraby, G. M., Barry, B. W., & Williams, A. C. (2008). Liposomes and skin: from drug delivery to model membranes. *European Journal of Pharmaceutical Sciences*, 34(4), 203-222.
- Espalin, D., Arcaute, K., Rodriguez, D., Medina, F., Posner, M., & Wicker, R. (2010). Fused deposition modeling of patient-specific polymethylmethacrylate implants. *Rapid Prototyping Journal*, 16(16), 164-173.
- Farzadi, A., Waran, V., Solati-Hashjin, M., Rahman, Z. A. A., Asadi, M., & Osman, N. A. A. (2015). Effect of layer printing delay on mechanical properties and dimensional accuracy of 3D printed porous prototypes in bone tissue engineering. *Ceramics International*, 41(7), 8320-8330.
- Ferris, C. J., Gilmore, K. J., & Wallace, G. G. (2013). Modified gellan gum hydrogels for tissue engineering applications. *Soft Matter*, 9(14), 3705-3711.
- Fitzgerald, S. (2015). FDA Approves First 3D-Printed Epilepsy Drug Experts Assess the Benefits and Caveats. *Neurology Today*, 15(18), 26-27.
- Garlotta, D. (2001). A Literature Review of Poly (Lactic Acid). *Journal of Polymers & the Environment*, 9(2), 63-84.
- Genina, N., Holländer, J., Jukarainen, H., Mäkilä, E., Salonen, J., & Sandler, N. (2015). Ethylene vinyl acetate (EVA) as a new drug carrier for 3D printed medical drug delivery devices. *European Journal of Pharmaceutical Sciences*, 90, 53-63.

- Goole, J., & Karim, A. (2016). 3D printing in pharmaceuticals: A new tool for designing customized drug delivery systems. *International journal of pharmaceuticals*, 499(1-2), 376-394.
- Goyanes, A., Buanz, A. B. M., Basit, A. W., & Gaisford, S. (2014b). Fused-filament 3D printing (3DP) for fabrication of tablets. *International journal of pharmaceuticals*, 476(1-2), 88-92.
- Goyanes, A., Buanz, A. B. M., Hatton, G. B., Gaisford, S., & Basit, A. W. (2014a). 3D printing of modified-release aminosalicylate (4-ASA and 5-ASA) tablets. *European Journal of Pharmaceuticals and Biopharmaceuticals*, 89, 157-162.
- Goyanes, A., Chang, H., Sedough, D., Hatton, G. B., Wang, J., Buanz, A., . . . Basit, A. W. (2015). Fabrication of controlled-release budesonide tablets via desktop (FDM) 3D printing. *International journal of pharmaceuticals*, 496(2), 414-420.
- Goyanes, A., Wang, J., Buanz, A., Martínez-Pacheco, R., Telford, R., Gaisford, S., & Basit, A. W. (2015b). 3D printing of medicines: Engineering novel oral devices with unique design and drug release characteristics. *Molecular pharmaceuticals*, 12(11), 4077-4084.
- Groenendyk, M., & Gallant, R. (2013). 3D printing and scanning at the Dalhousie University Libraries: a pilot project. *Library Hi Tech*, 31(1), 34-41.
- Gross, B. C., Erkal, J. L., Lockwood, S. Y., Chen, C., & Spence, D. M. (2014). Evaluation of 3D printing and its potential impact on biotechnology and the chemical sciences. *Analytical chemistry*, 86(7), 3240-3253.
- Henderson, A. M. (1993). Ethylene-vinyl acetate (EVA) copolymers: a general review. *The Institute of Electrical and Electronics Engineers Electrical Insulation Magazine*, 9(1), 30-38.

- Hill, S., Varker, A. S., Karlage, K., & Myrdal, P. B. (2009). Analysis of drug content and weight uniformity for half-tablets of 6 commonly split medications. *Journal of Managed Care Pharmacy*, 15(3), 253-261.
- Holländer, J., Genina, N., Jukarainen, H., Khajeheian, M., Rosling, A., Mäkilä, E., & Sandler, N. (2016). Three-dimensional printed PCL-based implantable prototypes of medical devices for controlled drug delivery. *Journal of pharmaceutical sciences*, 105(9), 2665-2676.
- Hutmacher, D. W., Sittering, M., & Risbud, M. V. (2004). Scaffold-based tissue engineering: rationale for computer-aided design and solid free-form fabrication systems. *Trends in Biotechnology*, 22(7), 354-362.
- Jonathan, G., & Karim, A. (2016). 3D printing in pharmaceuticals: A new tool for designing customized drug delivery systems. *International Journal of Pharmaceutics*, 499(1–2), 376-394.
- Kalra, A., Lowe, A., & Al-Jumaily, A. (2016). Mechanical Behaviour of Skin: A Review. *Journal of Material Science & Engineering*, 5(4), 254-260.
- Karageorgiou, V., & Kaplan, D. (2005). Porosity of 3D biomaterial scaffolds and osteogenesis. *Biomaterials*, 26(27), 5474-5491.
- Khaled, S. A., Burley, J. C., Alexander, M. R., Yang, J., & Roberts, C. J. (2015). 3D printing of tablets containing multiple drugs with defined release profiles. *International journal of pharmaceutics*, 494(2), 643-650.
- Kim, E. G., Kim, B. S., & Kim, D. S. (2007). Physical properties and morphology of polycaprolactone/starch/pine- leaf composites. *Journal of applied polymer science*, 103(2), 928-934.
- King, T. L., & Brucker, M. C. (2010). *Pharmacology for women's health*: Jones & Bartlett Publishers.

- Kunasekaran, V., & Krishnamoorthy, K. (2015). Experimental Design for the Optimization of Nanoscale Solid Lipid Particles Containing Rasagiline Mesylate. *Journal of Young Pharmacists Vol*, 7(4), 285.
- Labet, M., & Thielemans, W. (2009). Synthesis of polycaprolactone: a review. *Chemical Society Reviews*, 38(12), 3484-3504.
- Leimann, F. V., Biz, M. H., Kaufmann, K. C., Maia, W. J., Honçalves, O. H., Cardozo Filho, L., . . . Araújo, P. H. H. d. (2015). Characterization of progesterone loaded biodegradable blend polymeric nanoparticles. *Ciência Rural*, 45(11), 2082-2088.
- Leong, K., Cheah, C., & Chua, C. (2003). Solid freeform fabrication of three-dimensional scaffolds for engineering replacement tissues and organs. *Biomaterials*, 24(13), 2363-2378.
- Li, D., Guo, G., Fan, R., Liang, J., Deng, X., Luo, F., & Qian, Z. (2013). PLA/F68/dexamethasone implants prepared by hot-melt extrusion for controlled release of anti-inflammatory drug to implantable medical devices: I. Preparation, characterization and hydrolytic degradation study. *International journal of pharmaceutics*, 441(1), 365-372.
- Li, L., Saedan, M., Feng, W., Fuh, J., Wong, Y., Loh, H., . . . Lu, L. (2009). Development of a multi-nozzle drop-on-demand system for multi-material dispensing. *Journal of Materials Processing Technology*, 209(9), 4444-4448.
- Long, J., Gholizadeh, H., Lu, J., Bunt, C., & Seyfoddin, A. (2017). Application of fused deposition modelling (FDM) method of 3D printing in drug delivery. *Current pharmaceutical design*, 23(3), 433-439.
- Maniruzzaman, M., Boateng, J. S., Snowden, M. J., & Douroumis, D. (2012). A review of hot-melt extrusion: process technology to pharmaceutical products. *International Scholarly Research Notices pharmaceutics*, 2012.

- Mashak, A., Mobedi, H., & Mahdavi, H. (2015). A Comparative Study of Progesterone and Lidocaine Hydrochloride Release from Poly (L-lactide) Films. *Pharmaceutical Sciences*, 21(2), 77.
- McCullough, E. J., & Yadavalli, V. K. (2013). Surface modification of fused deposition modeling ABS to enable rapid prototyping of biomedical microdevices. *Journal of Materials Processing Technology*, 213(6), 947-954.
- Melocchi, A., Parietti, F., Loreti, G., Maroni, A., Gazzaniga, A., & Zema, L. (2015). 3D printing by fused deposition modeling (FDM) of a swellable/erodible capsular device for oral pulsatile release of drugs. *Journal of Drug Delivery Science and Technology*, 30, 360-367.
- Miyai, T., Ito, A., Tamazawa, G., Matsuno, T., Sogo, Y., Nakamura, C., . . . Satoh, T. (2008). Antibiotic-loaded poly- $\epsilon$ -caprolactone and porous  $\beta$ -tricalcium phosphate composite for treating osteomyelitis. *Biomaterials*, 29(3), 350-358.
- Mohanty, A. K., Misra, M., & Drzal, L. T. (2005). *Natural fibers, biopolymers, and biocomposites*: Chemical Rubber Company Press.
- Moroni, L., de Wijn, J. R., & van Blitterswijk, C. A. (2006). 3D fiber-deposited scaffolds for tissue engineering: Influence of pores geometry and architecture on dynamic mechanical properties. *Biomaterials*, 27(7), 974-985.
- Moulton, S. E., & Wallace, G. G. (2014). 3-dimensional (3D) fabricated polymer based drug delivery systems. *Journal of Controlled Release*, 193, 27-34.
- Nand, A. V., Ray, S., Travas-Sejdic, J., & Kilmartin, P. A. (2012). Characterization of polyethylene terephthalate/polyaniline blends as potential antioxidant materials. *Materials Chemistry and Physics*, 134(1), 443-450.



- Nikam, V. K., Kotade, K. B., Gaware, V. M., Dhamak, R., Somwanshi, S. B., & Khadse, A. N. (2011). Eudragit a versatile polymer: a review. *Pharmacol online*, 1(1), 152-164.
- Oliveira, J. E., Medeiros, E. S., Cardozo, L., Voll, F., Madureira, E. H., Mattoso, L. H. C., & Assis, O. B. G. (2013). Development of poly (lactic acid) nanostructured membranes for the controlled delivery of progesterone to livestock animals. *Materials Science and Engineering: C*, 33(2), 844-849.
- Olsen, S. C., Christie, R., Grainger, D., & Stoffregen, W. (2006). Immunologic responses of bison to vaccination with *Brucella abortus* strain RB51: Comparison of parenteral to ballistic delivery via compressed pellets or photopolymerized hydrogels. *Vaccine*, 24(9), 1346-1353.
- Pietrzak, K., Isreb, A., & Alhnan, M. A. (2015). A flexible-dose dispenser for immediate and extended release 3D printed tablets. *European Journal of Pharmaceutics and Biopharmaceutics*, 96, 380-387.
- Rai, B., Teoh, S.-H., Hutmacher, D., Cao, T., & Ho, K. (2005). Novel PCL-based honeycomb scaffolds as drug delivery systems for rhBMP-2. *Biomaterials*, 26(17), 3739-3748.
- Ray, S., & Cooney, R. P. (2012). Thermal degradation of polymer and polymer composites *Handbook of environmental degradation of materials* (Second ed.).
- Rossi, F., Perale, G., & Masi, M. (2016). *Controlled Drug Delivery Systems: Towards New Frontiers in Patient Care*: Springer.
- Rutkowski, J. V., & Levin, B. C. (1986). Acrylonitrile–butadiene–styrene copolymers (ABS): Pyrolysis and combustion products and their toxicity—a review of the literature. *Fire and materials*, 10(3- 4), 93-105.

- Sachs, E., Cima, M., Williams, P., Brancazio, D., & Cornie, J. (1992). Three dimensional printing: rapid tooling and prototypes directly from a CAD model. *Journal of Engineering for Industry*, 114(4), 481-488.
- Scoutaris, N., Alexander, M. R., Gellert, P. R., & Roberts, C. J. (2011). Inkjet printing as a novel medicine formulation technique. *Journal of Controlled Release*, 156(2), 179-185.
- Sébastien, F., Stéphane, G., Copinet, A., & Coma, V. (2006). Novel biodegradable films made from chitosan and poly (lactic acid) with antifungal properties against mycotoxinogen strains. *Carbohydrate polymers*, 65(2), 185-193.
- Seeley, S. K., Seeley, J. V., Telehowski, P., Martin, S., Tavakoli, M., Colton, S. L., . . . Atkinson, P. J. (2004). Volume and surface area study of tobramycin-polymethylmethacrylate beads. *Clinical orthopaedics and related research*, 420, 298-303.
- Selimis, A., Mironov, V., & Farsari, M. (2015). Direct laser writing: Principles and materials for scaffold 3D printing. *Microelectronic Engineering*, 132, 83-89.
- Senatov, F., Niaza, K., Zadorozhnyy, M. Y., Maksimkin, A., Kaloshkin, S., & Estrin, Y. (2016). Mechanical properties and shape memory effect of 3D-printed PLA-based porous scaffolds. *Journal of the mechanical behavior of biomedical materials*, 57, 139-148.
- Seyfoddin, A., Shaw, J., & Al-Kassas, R. (2010). Solid lipid nanoparticles for ocular drug delivery. *Drug delivery*, 17(7), 467-489.
- Shaikh, H. K., Kshirsagar, R., & Patil, S. (2015). Mathematical models for drug release characterization: a review. *World Journal Of Pharmacy And Pharmaceutical Sciences*, 4(04), 324-338.

- Shapiro, L., Eason, C., Bunt, C., Hix, S., Aylett, P., & MacMorran, D. (2016). Efficacy of encapsulated sodium nitrite as a new tool for feral pig management. *Journal of pest science*, 89(2), 489-495.
- Singhvi, G., & Singh, M. (2011). In-vitro drug release characterization models. *International Journal of Pharmaceutical Studies and Research*, 2(1), 77-84..
- Skowrya, J., Pietrzak, K., & Alhnan, M. A. (2015). Fabrication of extended-release patient-tailored prednisolone tablets via fused deposition modelling (FDM) 3D printing. *European Journal of Pharmaceutical Sciences*, 68, 11-17.
- Teo, E. Y., Ong, S.-Y., Chong, M. S. K., Zhang, Z., Lu, J., Moochhala, S., . . . Teoh, S.-H. (2011). Polycaprolactone-based fused deposition modeled mesh for delivery of antibacterial agents to infected wounds. *Biomaterials*, 32(1), 279-287.
- Thakral, S., Thakral, N. K., & Majumdar, D. K. (2013). Eudragit®: a technology evaluation. *Expert opinion on drug delivery*, 10(1), 131-149.
- Tiwari, G., Tiwari, R., Sriwastawa, B., Bhati, L., Pandey, S., Pandey, P., & Bannerjee, S. K. (2012). Drug delivery systems: An updated review. *International journal of pharmaceutical investigation*, 2(1), 2.
- Villanueva, J. M. (2007). Vaginal health products: Google Patents.
- Wan, L. S., & Lim, L. (1992). Drug release from heat-treated polyvinyl alcohol films. *Drug development and industrial pharmacy*, 18(17), 1895-1906.
- Warnke, P. H., Seitz, H., Warnke, F., Becker, S. T., Sivananthan, S., Sherry, E., . . . Douglas, T. (2010). Ceramic scaffolds produced by computer- assisted 3D printing and sintering: Characterization and biocompatibility investigations. *Journal of Biomedical Materials Research Part B: Applied Biomaterials*, 93(1), 212-217.

- West, G., Heard, D., & Caulkett, N. (2014). *Zoo animal and wildlife immobilization and anesthesia*: John Wiley & Sons.
- Whittle, K., Kieser, J., Ichim, I., Swain, M., Waddell, N., Livingstone, V., & Taylor, M. (2008). The biomechanical modelling of non-ballistic skin wounding: blunt-force injury. *Forensic science, medicine, and pathology*, 4(1), 33-39.
- Wilson, C., Olejnik, O., & Hardy, J. (1983). Precorneal drainage of polyvinyl alcohol solutions in the rabbit assessed by gamma scintigraphy. *Journal of Pharmacy and Pharmacology*, 35(7), 451-454.
- Wittbrodt, B., & Pearce, J. M. (2015). The effects of PLA color on material properties of 3-D printed components. *Additive Manufacturing*, 8, 110-116.
- Wrona, M., Cran, M. J., Nerín, C., & Bigger, S. W. (2017). Development and characterisation of HPMC films containing PLA nanoparticles loaded with green tea extract for food packaging applications. *Carbohydrate polymers*, 156, 108-117.
- Zein, I., Hutmacher, D. W., Tan, K. C., & Teoh, S. H. (2002). Fused deposition modeling of novel scaffold architectures for tissue engineering applications. *Biomaterials*, 23(4), 1169-1185.
- Zhang, C., Zhao, K., Hu, T., Cui, X., Brown, N., & Boland, T. (2008). Loading dependent swelling and release properties of novel biodegradable, elastic and environmental stimuli-sensitive polyurethanes. *Journal of Controlled Release*, 131(2), 128-136.

## Chapter 4

*Controlled release of dexamethasone from poly (vinyl alcohol) hydrogel*

Manuscript prepared as:

Long, J., Nand, A. V., Bunt, C., & Seyfoddin, A. (2019). Controlled release of dexamethasone from poly (vinyl alcohol) hydrogel. *Pharmaceutical development and technology*, 1-10.

## 4.1. Introduction

A drug delivery system, which considers the drug's physicochemical and pharmacokinetic properties, generally plays a significant role in controlling the pharmacological action of a drug (Perrie & Rades, 2010). Hydrogels are one of the forthcoming types of polymer-based controlled drug release systems. Polymeric hydrogels are crosslinked networks of hydrophilic macromolecules that can be used as multipurpose materials (N. Peppas & Simmons, 2004). Crosslinked hydrogels possess the abilities of swelling and imbibing a large amount of water, while also maintaining their 3D structures (Gehrke & Lee, 1990). Characteristics of hydrogels, such as high water content, softness and rubbery consistency, make them resemble living tissues more than other synthesised biomaterials (P. Gupta, Vermani, & Garg, 2002). The drug release rate from hydrogels can be controlled by adjusting the pore volume fraction, the pore size, the type and strength of interactions between incorporated drug and polymer chains (Hoffman, 2012). The biocompatibility of hydrogels and their controllability of drug release make them ideal candidates for applications in biomedicine (Hoffman, 2012; N. A. Peppas, Hilt, Khademhosseini, & Langer, 2006) and pharmaceuticals (N. Peppas, Bures, Leobandung, & Ichikawa, 2000). The major applications of using hydrogel as drug carriers are limited to hydrophilic drugs due to the hydrophilic nature of hydrogels. However, there has been numerous studies of developing strategies to enable hydrogels for delivering hydrophobic drugs (Gu, O'Connor, GH Qiao, & Ladewig, 2017; Larrañeta, Barturen, Ervine, & Donnelly, 2018; Larrañeta, Stewart, Ervine, Al-Kasasbeh, & Donnelly, 2018; McKenzie et al., 2015).

DEX is a corticosteroid used as an anti-inflammatory agent in a variety of pathophysiological conditions. DEX can inhibit the production of essential factors in generating inflammatory response, such as vasoactive and chemo-attractive factors, lipolytic and proteolytic enzymes, and the extraversion of leukocytes to the wound (ElHag, Coghlan, Christmas, Harvey, & Harris, 1985; Hickey, Kreutzer, Burgess, & Moussy, 2002; Wood & Barnes, 1995; Yin, Yamamoto, & Gaynor, 1998). However, DEX can cause serious systemic side effects particularly with high doses (Heimdal, Hirschberg, Slettebø, Watne, & Nome, 1992). Subsequently, it is imperative that controlled, sustained release systems for local delivery of DEX be designed and applied. DEX release systems based on polymeric hydrogels (Fiorica, Palumbo, Pitarresi, Bongiovì, & Giammona, 2017; Salgado, Rodríguez-Rojo, Reis, Cocero, & Duarte, 2017; Shen & Burgess, 2012), supramolecular nanofibers of DEX derivatives (Z. Zhang et al., 2018) and inorganic materials such as silica (Numpilai, Witton, Chareonpanich, & Limtrakul, 2017) and laponite (Roozbahani, Kharaziha, & Emadi, 2017) are reported in the literature.

Poly (vinyl alcohol) (PVA), a non-toxic, non-carcinogenic and water soluble polyhydroxy polymer, offers hydrophilic surfaces compatible with living tissues (Islam & Yasin, 2012). Furthermore, the porosity of PVA networks can be tailored by physical or chemical crosslinking (Alemzadeh & Vossoughi, 2002; N. Peppas & Simmons, 2004; N. A. Peppas & Wright, 1998). These properties have promoted PVA to be applied in biomedical applications such as drug delivery, wound dressing and tissue engineering (Kayal & Ramanujan, 2010; Kokabi, Sirousazar, & Hassan, 2007; Schmedlen, Masters, & West, 2002; Tavakoli & Tang, 2017). Glutaraldehyde (GA) crosslinked polymer systems have been utilised for biomedical applications

(Nuttelman, Mortisen, Henry, & Anseth, 2001; Paradossi, Cavalieri, Chiessi, Spagnoli, & Cowman, 2003; Shah, Shah, & Pradhan, 1997; T. Wang, Turhan, & Gunasekaran, 2004; Yu et al., 2017; X. Zhang, Tang, & Zheng, 2016). In this study, a controlled release system for DEX has been developed by embedding the drug into GA crosslinked PVA hydrogel matrix to control the release behaviours. The aim of this work is to develop a controlled release system for DEX based entirely on a PVA hydrogel matrix. The specific objectives of this work are: i) to develop PVA hydrogel drug delivery systems with different levels of crosslinking; ii) to study the effects of loading DEX on hydrogel properties; iii) to investigate the release patterns of DEX controlled by different levels of crosslinking of PVA hydrogel.



## 4.2. Materials and methods

### 4.2.1. Materials

DEX ( $\log P=1.83$ ) was purchased from Flem Pharma (Shanghai, China). PVA powder (hydrolysis: 78.5-81.5 mole%, Mw: 120,000-132,000) was kindly gifted by Chemiplas (Auckland, New Zealand). Glutaraldehyde (GA) (Grade II, 25% in H<sub>2</sub>O) and phosphate buffered saline (PBS) tablets were purchased from Sigma-Aldrich (Auckland, New Zealand). Hydrochloric acid (36%) was purchased from ECP Ltd (Auckland, New Zealand). Absolute ethanol of HPLC grade was purchased from Fisher Scientific UK (Loughborough, UK).

### 4.2.2. Preparation of DEX loaded hydrogels

A 5% (w/v) PVA solution was prepared by dissolving PVA in deionised water under continuous mechanical stirring for 2h at 95°C. The solution was cooled to room temperature before further treatment. DEX powder was added to the PVA solution to obtain a final concentration of 2.5 mg/mL under continuous string to yield a well-dispersed suspension. Varying amounts of GA, a crosslinker, was slowly added to the PVA/ DEX suspension under mechanical stirring. Glutaraldehyde residues may have some toxicity however, only low concentrations of GA were used in this study (0.125-0.725% v/v). Based on the molar ratios calculated in Table 4-1 (PVA:GA in the range of 72:1-12:1), GA should be fully consumed in the crosslinking reaction as complete reaction between GA and PVA should occur at the molar ratio of PVA:GA=2:1. Considering PVA is more than sufficient in this reaction, the residue of GA can be regarded as negligible. The reaction between GA and PVA chains, leading to a 3-dimensional crosslinked macromolecular structure, is presented in Figure 4-1. Hydrochloric acid (0.1% v/v) was added to create an acid environment for gel

formation. DEX-free hydrogels were prepared as control. The detailed compositions of hydrogels are listed in Table 4-1.

Table 4-1. Composition and designation of PVA hydrogels.

Formula Code	GA concentration (% v/v)	GA (mL)	PVA solution (mL)	Molar ratio PVA:GA	DEX (mg)
Cr-125	0.125	0.3	60	72:1	-
Cr-250	0.250	0.6	60	36:1	-
Cr-375	0.375	0.9	60	24:1	-
Cr-500	0.500	1.2	60	18:1	-
Cr-625	0.625	1.5	60	14.4:1	-
Cr-750	0.750	1.8	60	12:1	-
DEX-125	0.125	0.6	120	72:1	300
DEX-250	0.250	1.2	120	36:1	300
DEX-375	0.375	1.8	120	24:1	300
DEX-500	0.500	2.4	120	18:1	300
DEX-625	0.625	3.0	120	14.4:1	300
DEX-750	0.750	3.6	120	12:1	300

The pre-gel mixtures were poured into petri dishes and immediately placed in 50°C oven for 5 minutes to accelerate hydrogel formation in order to avoid sedimentation of DEX. The hydrogels were dried in dark conditions at room temperature overnight and further vacuum dried at 40°C for 2 days to obtain solid films.

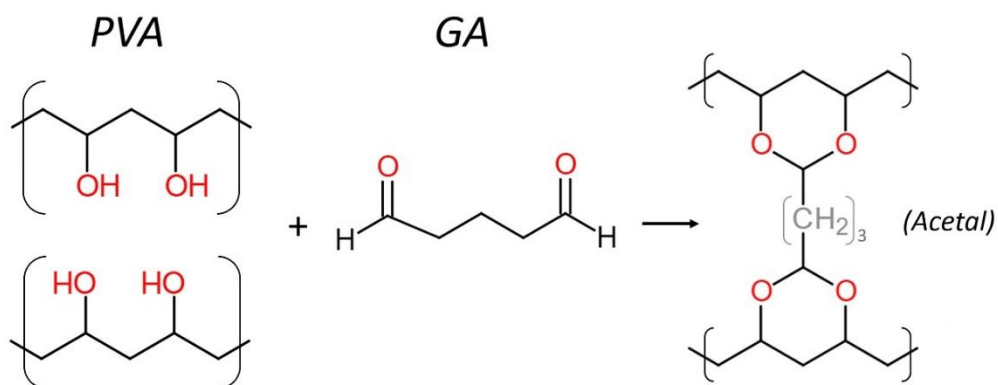


Figure 4-1. Crosslinking reaction of poly (vinyl alcohol) (PVA) and glutaraldehyde (GA).

#### 4.2.3. Viscosity measurements

The viscosity of pre-gel solutions were determined as a function of time using a RST Coaxial Cylinder Rheometer (Brookfield, USA) equipped with a coaxial cylinder spindle geometry. 20 mL of pre-gel solution was placed in the cylinder and viscosity

(Pa.s) was measured at room temperature and at pre-determined time points during the gelation.

#### 4.2.4. Swelling studies

The equilibrium swelling ratio (ESR) of PVA hydrogels in PBS buffer (pH 7.4) with 0.5% Tween 20 at  $37 \pm 2^\circ\text{C}$  were determined using a gravimetric method (Khurma, Rohindra, & Nand, 2006). Dried samples were weighed and placed in stainless steel wire mesh. The mesh container was submersed into the swelling buffer maintained at  $37 \pm 2^\circ\text{C}$  in a water bath. At predetermined time intervals, the samples were withdrawn and blotted with tissue paper to remove the surface water. The blotted samples were immediately weighed to determine the wet weight. The experiments were continued until equilibrium was achieved. The ESR was calculated using Eq.(4-1) (n=3):

$$E_{SR}(\%) = \frac{W_t - W_d}{W_d} \times 100 \quad (4-1)$$

where  $W_t$  is the weight of wet hydrogel at a particular time (t),  $W_d$  is the weight of dry hydrogel before soaking. The equilibrium water content (EWC) was calculated using Eq.(4-2) (n=3):

$$E_{WC}(\%) = \frac{W_e - W_d}{W_e} \times 100 \quad (4-2)$$

where  $W_e$  is the weight of hydrogel at equilibrium state.

#### 4.2.5. Porosity measurement

The porosity of PVA hydrogels were determined by the solvent replacement method (Gemeinhart, Chen, Park, & Park, 2000). Dried hydrogel samples were weighed and immersed in absolute ethanol at room temperature overnight to ensure the porous

structures were filled with the solvent. The soaked samples were weighed immediately after blotting with tissue paper to remove the surface ethanol. The porosity was calculated using Eq.(4-3) (n=3):

$$\text{Porosity (\%)} = \frac{W_{se} - W_d}{\rho V} \times 100 \quad (4-3)$$

where  $W_{se}$  is the weight of hydrogel after soaking in absolute ethanol,  $W_d$  is the weight of dried hydrogel before soaking,  $\rho$  is the density of absolute ethanol,  $V$  is the volume of the hydrogel.

#### 4.2.6. Apparent density

For measuring apparent density of hydrogels, the samples were accurately weighed after soaking in distilled water at room temperature overnight (X. Li, Bian, Li, Lian, & Jin, 2011; Nanda, Sood, Reddy, & Markandeywar, 2013). The apparent densities of the hydrogels were calculated using Eq.(4-4) (n=3):

$$\rho = \frac{4W_{sw}}{\pi d^2 h} \quad (4-4)$$

where  $\rho$  is the apparent density of hydrogel ( $\text{g/cm}^3$ ),  $W_{sw}$  is the mass of hydrogel after saturation with water,  $d$  is the diameter and  $h$  is the height of hydrogel after saturation with water.

#### 4.2.7. Fourier transform infrared (FTIR) spectroscopy

FTIR spectra was obtained to characterise the presence of specific chemical groups in the samples using a Nicolet iS10 FTIR spectrophotometer (Thermo Scientific, USA) in attenuated total reflectance (ATR) mode using a diamond ATR crystal. The

spectra of the samples were recorded in the range of 4000-400  $\text{cm}^{-1}$  with an average of 32 scans at a resolution of 4  $\text{cm}^{-1}$ .

#### 4.2.8. *In vitro* drug release

The *in vitro* DEX release from PVA hydrogels was studied in 100 mL PBS buffer (pH=7.4) with 0.5% Tween 20 in a 250 mL screw-capped bottle, at 100 rpm on a benchtop shaker (SK-300, Lab Companion, Korea) in an incubator room maintained at  $35 \pm 2^\circ\text{C}$  for a period of 33 days. At predetermined time intervals, 2 mL of the incubation media from each sample was collected, and an equal amount of fresh media was added into each release system to maintain the total volume and sink condition. The concentration of DEX in the release media was determined by UV spectrophotometry (Ultrospec 7000, BIOCHROM, UK) against a calibration curve at an absorption wavelength of 242nm. The cumulative amount of DEX was plotted against release time for each sample. Three duplicates were performed and the results were presented as mean value  $\pm$  SD.

#### 4.2.9. Scanning Electron Microscopy (SEM)

Cryo-fractured cross-section images of DEX-loaded PVA hydrogel samples after *in vitro* release test were obtained with a Schottky field emission SEM (SU-70, Hitachi, UK) under a working voltage of 5 kV. Prior to imaging, air dried samples were placed on metallic stubs and coated with platinum under vacuum for 20 seconds using an ion sputter coater (E-1045, Hitachi, UK) for visualisation.

#### 4.2.10. Release kinetics

To study the release kinetics and mechanism of DEX release from PVA hydrogel formulations, data was fitted to the models below.

Zero-order model (Dash et al., 2010):

$$Q_t = Q_0 + K_0 t \quad (4-5)$$

where  $Q_t$  is the amount of drug released at time  $t$ ,  $Q_0$  is the initial amount of drug in the solution, and  $K_0$  is the zero order release constant expressed in the units of concentration/time. Zero-order model describes the system where the release rate of incorporated drug is independent of its concentration (Shaikh et al., 2015).

First-order model (Dash et al., 2010):

$$\log Q = \log Q_0 - K_1 t / 2.303 \quad (4-6)$$

where  $Q_0$  is the initial concentration of drug,  $K_1$  is first order rate constant expressed in units of  $\text{time}^{-1}$ , and  $t$  is the time. First-order model describes the dependency on the drug concentration in the polymer networks (Desai, Simonelli, & Higuchi, 1965).

Higuchi model (Dash et al., 2010):

$$Q_t = K_H \times t^{1/2} \quad (4-7)$$

where  $Q_t$  is amount of drug released in time  $t$ ,  $K_H$  is the Higuchi dissolution constant expressed in the units of concentration/time. Higuchi model is proposed to describe the drug release from a matrix system with different geometrics and porous structure (Higuchi, 1963).

Hixson-Crowell model (Dash et al., 2010):

$$Q_0^{1/3} - Q_{tr}^{1/3} = K_{HC} t \quad (4-8)$$

where  $Q_0$  is the initial amount of drug in the pharmaceutical dosage form,  $Q_{tr}$  is the remaining amount of drug in the pharmaceutical dosage form at time  $t$  and  $K_{HC}$  is a constant incorporating the surface-volume relation. This equation describes the release from systems where there is a change in surface area and diameter of particles (Niebergall, Milosovich, & Goyan, 1963).

Korsmeyer–Peppas model (Dash et al., 2010):

$$Q_t/Q_\infty = K_{KP}t^n \quad (4-9)$$

where  $Q_t/Q_\infty$  is a fraction of drug released at time  $t$ ,  $K_{KP}$  is the release rate constant and  $n$  is the release exponent. This relationship describes drug release from a polymeric system such as hydrogel. Data up to 60% drug release was used to fit into this kinetic model.

#### 4.2.11. Statistical analysis.

Data were subjected to one-way analysis of variant (ANOVA) with the level of significance set at  $P < 0.05$ .

## 4.3. Results

### 4.3.1. Hydrogel preparation

Viscometry was used to study the gelation of the hydrogels. Time versus viscosity plots of the hydrogel systems are presented in Figure 4-2. The gelation time decreased as the concentration of crosslinker in the matrix increased. A higher polymer/crosslinker ratio led to more interactions between the polymer chains and crosslinker molecules, thus decreasing the gelation time. The reaction between PVA and GA, as shown in Figure 4-1, yielded hydrogels of appreciable mechanical strength.

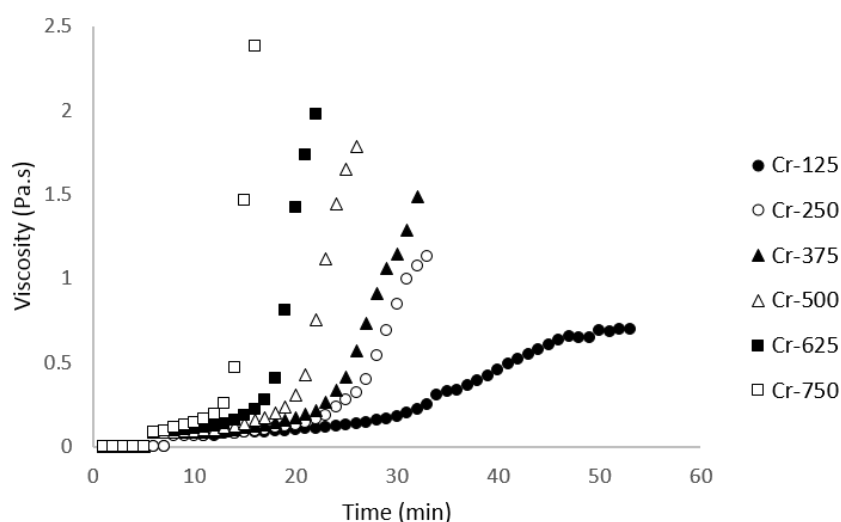


Figure 4-2. Rheological behaviour of poly (vinyl alcohol) (PVA) hydrogels crosslinked by different concentrations of glutaraldehyde (GA).

The wet and dried PVA hydrogels with/without DEX were obtained as shown in Figure 4-3. The vacuum drying process caused shrinkage of the hydrogels due to the water-loss. As shown in Figure 4-3 b1 and b2, the DEX loaded hydrogels showed uniform distribution of the drug within the polymer matrices. It is evident from Figure 4-3 that the diameters of wet hydrogel films decreased with the increasing concentrations of GA. A reasonable explanation for this may be that the introduction of more crosslinker reduces the free volume in PVA matrix (Yeom & Lee, 1996).



Therefore, the higher concentrations of GA produced smaller volume of wet PVA hydrogels as the water in the matrix pores was squeezed out.

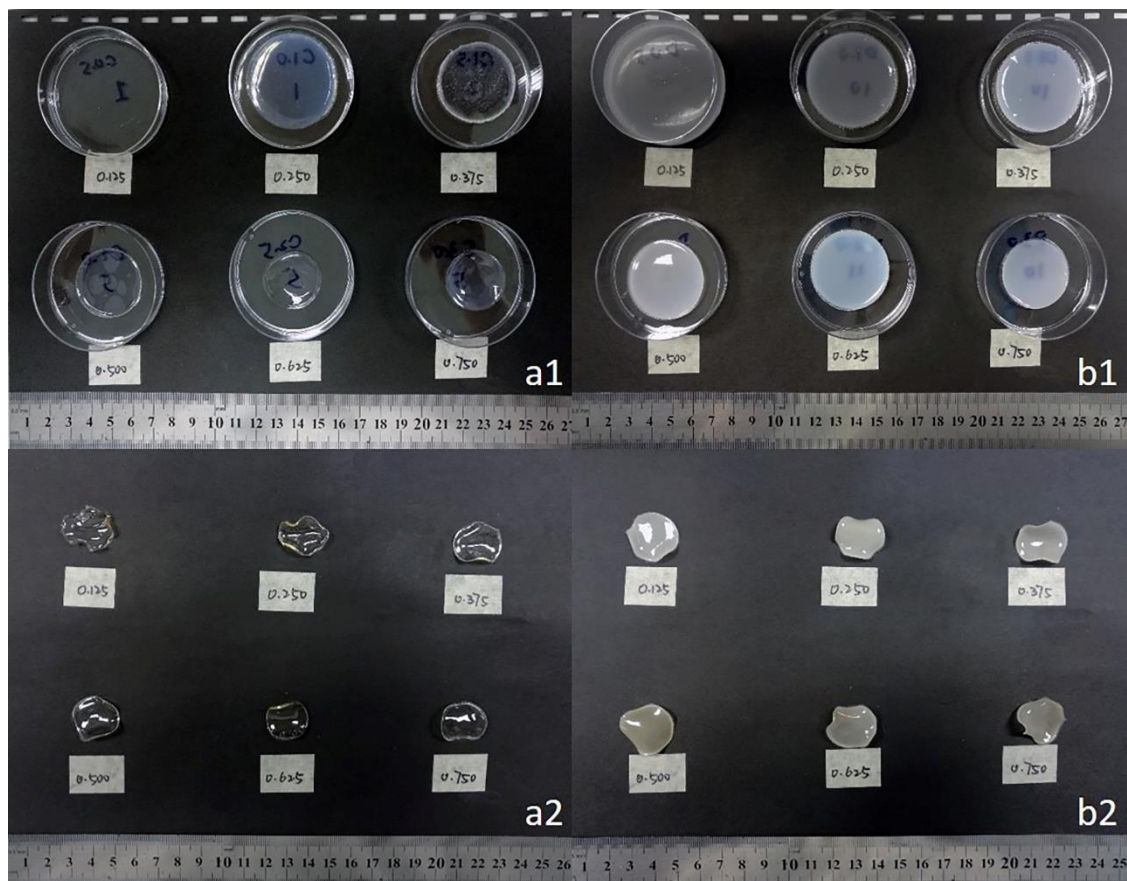


Figure 4-3. Poly (vinyl alcohol) (PVA) hydrogels with different concentrations of glutaraldehyde (GA) (0.125, 0.250, 0.375, 0.500, 0.625 and 0.750% respectively): a1) wet dexamethasone (DEX)-free PVA hydrogels, a2) dried DEX-free PVA hydrogels, b1) wet DEX-loaded PVA hydrogels and b2) dried DEX-loaded PVA hydrogels.

#### 4.3.2. Swelling and water absorption

Time dependent swelling responses of drug free and DEX loaded PVA hydrogels in PBS buffer (pH=7.4) are shown in Figure 4-4. All hydrogels swelled rapidly and reached an equilibrium state by about 45 minutes. The increasing amount of crosslinker decreased and slowed the swelling response in all samples. It can be seen from Figure 4-4 that when crosslinker density increased in PVA hydrogels, the swelling rate and ESR decreased. Highest ESR values were obtained (110.6% and

104.6% in DEX and control groups respectively) at the lowest concentration of GA (0.125%) with the fastest swelling in 15 minutes.

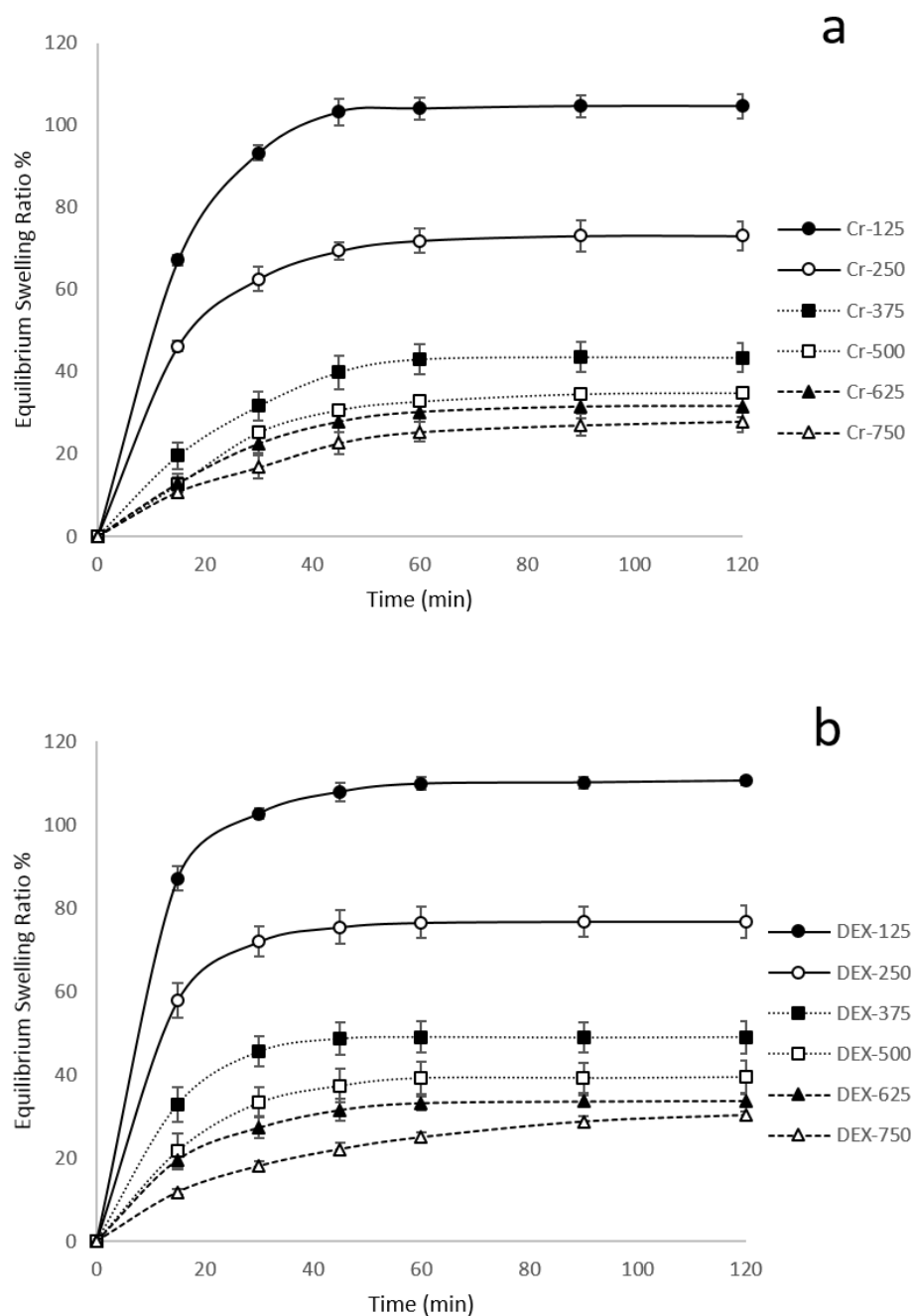


Figure 4-4. Swelling kinetics of poly (vinyl alcohol) (PVA) hydrogels at  $37 \pm 2^\circ\text{C}$  in PBS buffer with increasing concentrations of glutaraldehyde (GA): a). dexamethasone (DEX)-free PVA hydrogels and b) DEX-loaded PVA hydrogels ( $n=3\pm\text{SD}$ ).

The water absorption of PVA hydrogels, as shown in Figure 4-5, were obtained as equilibrium water content (EWC) in each sample. The EWC of all the hydrogels decreased with the increasing concentration of crosslinker GA and the maximum EWC (51.53% and 52.51% for control and DEX loaded hydrogels, respectively) was obtained at lowest concentration of GA at 0.125%. Loading of DEX had no significant effect on the hydrogel swelling behaviour or water absorption ( $p=0.8028$ ).

The swelling behaviour and water absorption of the hydrogels depend on the crosslinker concentration as more GA molecules reacting with -OH groups of PVA leave a reduced number of unreacted hydroxyl groups to attract water molecules. A higher crosslinking density also means a more compact 3-dimensional macromolecular network with less free volume. The lower porosity reduced the space for free water to be absorbed in the hydrogel matrix so decreased swelling was observed.

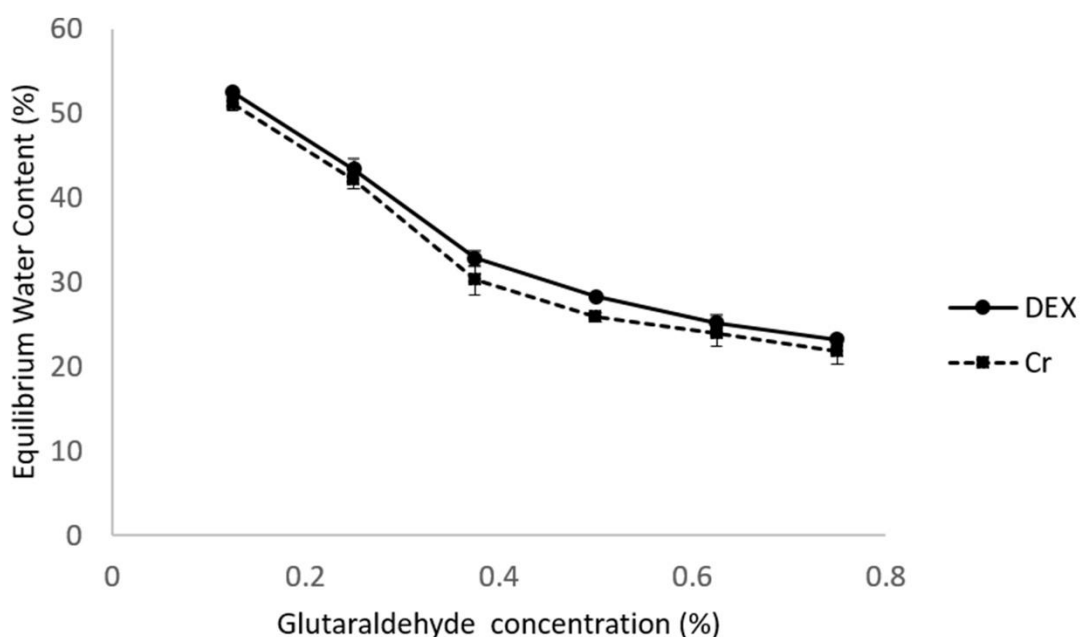


Figure 4-5. Equilibrium water content (EWC) of dexamethasone (DEX)-free and -loaded poly (vinyl alcohol) (PVA) hydrogels at different concentrations of crosslinker glutaraldehyde (GA) ( $n=3\pm SD$ ).

#### 4.3.3. Porosity and density

The porosity, measured as the volume of pores present in the matrix, of all hydrogel samples were shown in Figure 4-6 a. The porosity of all hydrogel samples showed a decreasing trend with the increasing concentration of GA, ranging from 4.58% to 2.33% in control group and 3.66% to 1.85% in DEX loaded group. This could be attributed to the possibility of higher amount of crosslinker leading to formation of compact structures. This was also confirmed in the swelling and apparent density assessment, the more dense formation of interconnected pores, in lightly crosslinked hydrogels, allowed the hydrogel to absorb more water resulting in greater swelling ability and lower apparent density.

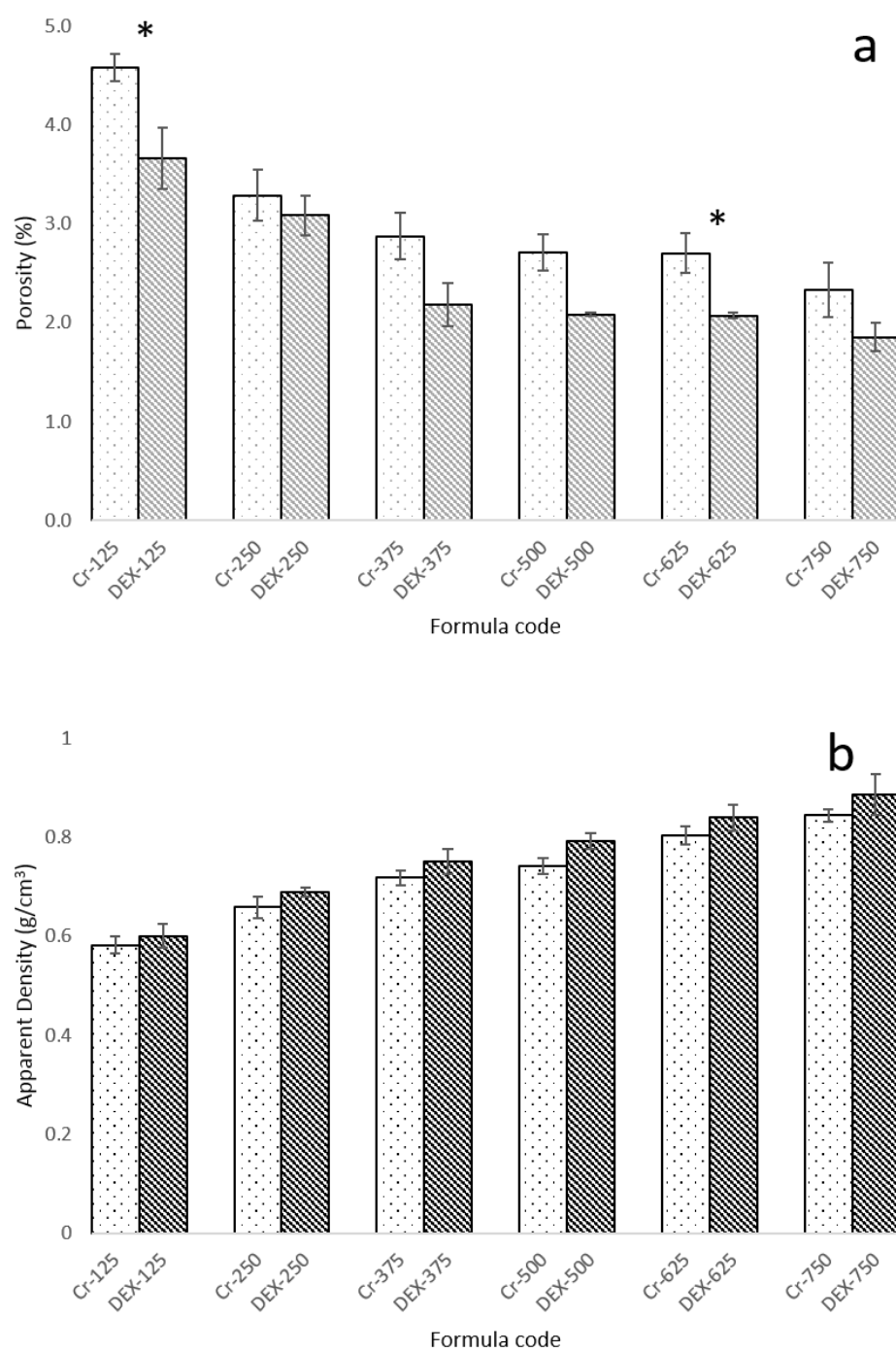


Figure 4-6. Physical properties of dexamethasone (DEX)-free and -loaded poly (vinyl alcohol) (PVA) hydrogels with increasing concentrations of glutaraldehyde (GA): a) porosity and b) apparent density ( $n=3\pm SD$ ). \*:  $p<0.05$ .

The apparent density of wet hydrogels was obtained as shown in Figure 4-6 b. The apparent density is an important parameter of hydrogels as it provides the information about pore size and distribution, permeability, and presence of structural defects in

polymer structures (Nanda et al., 2013). Following the addition of GA, an increasing trend of apparent density in the hydrogels was recorded in both control and drug-loaded samples. The minimum apparent density ( $0.582$  and  $0.601 \text{ g/cm}^3$  in control and DEX-loaded samples) was attained at the highest concentration of GA. This is due to the incorporation of higher crosslinker density conducting to form more compact matrix as the porosity of hydrogel network reduced, leading to the increase of apparent density. Similar to swelling test, there was no significant difference was observed between the control and drug-loaded groups in both porosity and density assessments ( $p$  value =  $0.207$  and  $0.979$  for porosity and density, correspondingly), indicating that the incorporation of DEX has no detectable effect on the physical structure of PVA hydrogels.

#### 4.3.4. FTIR

FTIR spectra of GA/DEX-free PVA, DEX-free PVA hydrogel, DEX-loaded PVA hydrogel and pure DEX are presented in Figure 4-7.

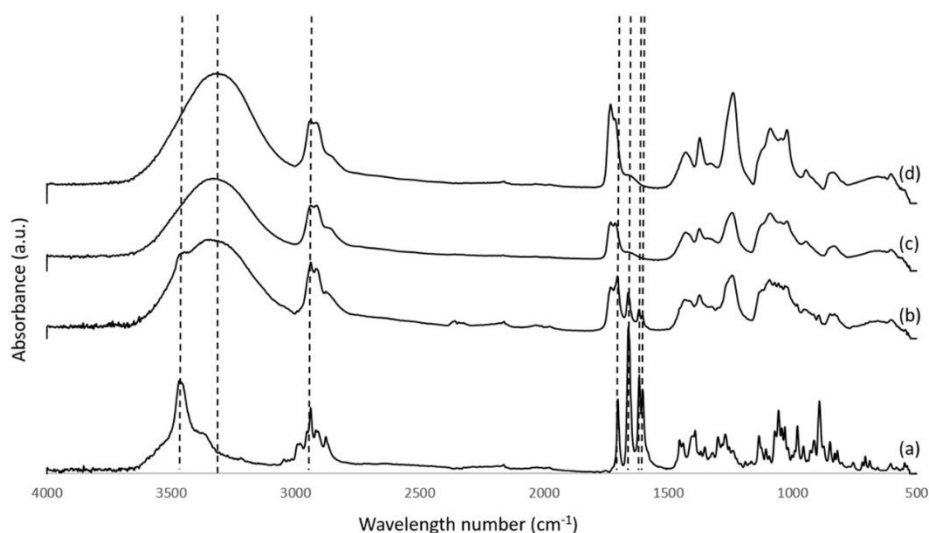


Figure 4-7. FTIR spectra of (a) pure dexamethasone (DEX), (b) DEX-loaded poly (vinyl alcohol) (PVA) hydrogel (DEX concentration:  $2.5 \text{ mg/mL}$ , glutaraldehyde (GA) concentration:  $0.25\%$ ), (c) DEX-free PVA hydrogel (GA concentration:  $0.25\%$ ) and (d) DEX & GA free PVA.

The major peaks related to hydroxyl and acetate groups were observed in the PVA spectrum. A broad band around  $3311\text{ cm}^{-1}$  was linked to the stretching O–H from the hydrogen bonded band (Andrade, Barbosa-Stancioli, Mansur, Vasconcelos, & Mansur, 2008; Figueiredo, Alves, & Borges, 2009; Mansur, Sadahira, Souza, & Mansur, 2008; E. F. d. Reis et al., 2006). Intermolecular and intramolecular hydrogen bonds are expected to occur among PVA chains owing to the high hydrophilic forces (E. F. d. Reis et al., 2006). The vibrational bands between  $2840$  and  $3000\text{ cm}^{-1}$  related to the stretching C–H of alkyl groups (Figueiredo et al., 2009; Mansur et al., 2008). The peaks occurred between  $1750$ – $1735\text{ cm}^{-1}$  refer to the stretching C=O and C–O from acetate group remaining from PVA in the saponification reaction (Andrade et al., 2008; Mansur et al., 2008).

The reaction of the PVA with crosslinker GA (as shown in Figure 4-1) contributes to a reduction in the amount of hydroxyl groups, indicating the –OH groups were consumed to form acetal bridges (see Figure 4-1). A relative decrease in aldehyde groups (C=O between  $1740$ – $1720\text{ cm}^{-1}$ ) was observed with the addition of GA to PVA matrix. This can be possibly explained as GA involved in bimodal reaction, the free aldehyde linked to the branches in the PVA chain when GA/PVA mass ratio stayed at low level (Figueiredo et al., 2009).

The spectrum of DEX exhibited characteristic absorbance bands at  $1706$ ,  $1660$  and  $1616\text{ cm}^{-1}$ , attributed to –C=O stretching vibration linked to C3-cyclic and C20 carbonyl group, and double bond framework conjugated to –C=O bonds (Rodrigues et al., 2009). Besides, two more characteristic absorption bands of  $3468\text{ cm}^{-1}$  and  $1270$

$\text{cm}^{-1}$  were expressed due to the stretching vibration of O-H and C-F bonds, respectively (Chiang, Yu, Chao, & Dong, 2012; Rodrigues et al., 2009).

The typical characteristic peaks from DEX were all observed in DEX loaded PVA hydrogel sample, including the -OH stretching band at  $3446\text{ cm}^{-1}$ , methyl and methylene groups between  $3000$  and  $2850\text{ cm}^{-1}$ , and carbonyl groups between  $1820$  and  $1670\text{ cm}^{-1}$ . The appearance of these groups ensures the presence of the DEX additive in the PVA matrix. Compared to pure DEX, a small shifting of -OH group from  $3468\text{ cm}^{-1}$  to  $3446\text{ cm}^{-1}$  was observed in DEX-loaded PVA hydrogel sample, indicating GA and PVA may have interacted with DEX via hydrogen bonding. However, this slight shifting also indicates that those hydrogen bonds introduced by DEX presented at a weak level as only small amount of DEX was dissolved to interact with GA/PVA due to its low solubility. The spectrum of DEX-loaded PVA sample was very similar to that of PVA, indicating no significant chemical changes occurred in the polymer backbone. These observations suggest DEX existed in the PVA hydrogel matrix with possible interactions between the drug, crosslinker and polymer.

#### 4.3.5. *In vitro* drug release

*In vitro* release studies of DEX from PVA hydrogel films were performed with respect to the concentrations of the crosslinker GA. The release data presented in

Figure 4-8 indicates that all of formulations showed sustained release over a period of 33 days as expected. As predicted from the swelling study and FTIR assessment, the patterns of drug release were controlled according to the concentrations of the crosslinker. The increasing crosslinker density decreased the drug release rate. This is possibly due to i) the drug was partially crosslinked by GA in the PVA hydrogels



so lesser and slower release was observed with higher crosslinking density; ii) the porous structure controlled by crosslinker density being responsible for water absorbance and swelling behaviours, and the water-filled channels are expected to act as the conduits for solvent uptake and DEX dissolution. This result is consistent with previous study which found the same effects of crosslinker concentration on the drug release rate (Kumar, Pandey, Koshy, & Saraf, 2010; Malana & Zohra, 2013).

All formulations showed a burst release in the first 6 h, reaching 39.0, 32.5, 24.8, 21.5, 11.2 and 4.9 % from DEX 125, 250, 375, 500, 625 and 750 formulations, respectively. The burst release effect was mainly due to the release of the surface-bound drug as no washing process was used. The free drug, which is not bonded with GA/PVA, can also contribute to the burst release as the porous structure of swelled PVA hydrogel provides channels for medium uptake and free drug dissolution. After burst release, a sustained release followed in the succeeding 25 days and finally reached plateau in the last 8 days. For the two formulations with highest crosslinker density, DEX 625 and DEX 750, continuous release was obtained during a period of 33 days. This result may be explained by the fact that the porous structure was relatively minor as the increasing crosslinker generated a more imperforate hydrogel structure, resulting a slower and longer drug release profile. This is also confirmed in the SEM images that the pores in DEX 6 formulation were less evident. By the end of the study period, 89.2, 84.6, 79.0, 71.9, 55.8 and 49.1% of DEX was released from DEX 125, 250, 375, 500, 625 and 750 PVA hydrogels, respectively. This result could be attributed to that the lower amount of crosslinker involved in the hydrogel matrix leading to lesser binding of the drug, so more free drug were released with faster release rate. Lesser crosslinker also produce more pores in the hydrogel matrix that promote the solvent

uptake and drug dissolution. This finding confirmed the possibility of using different crosslinker density in PVA hydrogels to control the drug release rate.

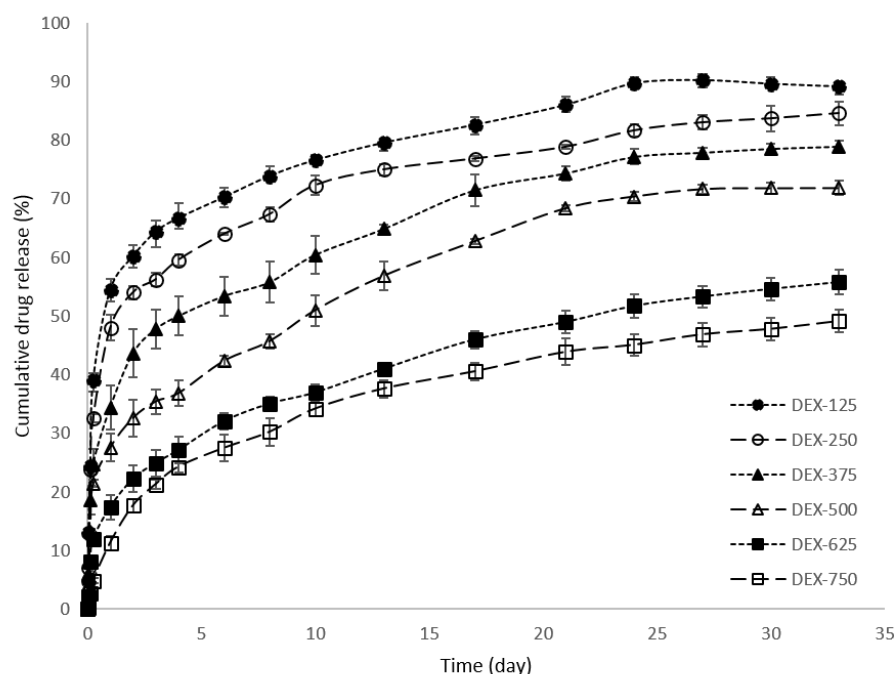


Figure 4-8. *In vitro* drug release of dexamethasone (DEX) from poly (vinyl alcohol) (PVA) hydrogels with different glutaraldehyde (GA) concentrations ( $n=3\pm SD$ ).

Mathematical models of *in vitro* drug release behaviours are essential for defining the drug release mechanism ((Dash et al., 2010; Shaikh et al., 2015; Singhvi & Singh, 2011). Several mathematical equations, as listed in Section 4.2.10, have been proposed to define the kinetics of the drug release from controllable release formulations. The drug release data were fitted into these models to analyse its release kinetics and mechanism from the PVA hydrogel formulations. The values of the kinetic rate constant ( $k$ ), the correlation coefficient ( $R^2$ ) and the release exponent ( $n$ ) are tabulated in Table 4-2.

Generally, the fitness levels for the investigated models ranked in the following order: Higuchi > Korsmeyer–Peppas > first-order > Hixson-Crowell > zero-order. The

release behaviour better fitted in Higuchi model than Korsmeyer–Peppas with the increasing crosslinker density. The Higuchi model is used to describe a system where Fickian diffusion is the rate limiting step and the predominant release mechanism under the following conditions: i) negligible edge effect, ii) initial concentration of drug in the matrix is much higher than the drug solubility, iii) the drug particles are much smaller than the thickness of the film and finely dispersed in the film, iv) swelling of matrix is negligible and v) constant drug diffusivity (Saurí et al., 2014). The PVA hydrogels in this study are solid thin films with negligible edge effect for drug diffusion. All hydrogel films finished swelling in 2 h (Figure 4-4), demonstrating the swelling of matrix were also negligible considering the release last for more than one month. The high correlation coefficients in Higuchi model for the hydrogels with higher crosslinker density suggested a greater contribution of Fickian diffusion with regard to the hydrogel erosion in the control of drug release kinetic behaviour, as more crosslinking formed to reduce the erosion when more GA reacted.

The PVA hydrogel formulations were also fitted to the Korsmeyer–Peppas model (with  $R^2$  ranging from 0.8828 to 0.9604), especially in PVA films with lower GA concentration. The Korsmeyer–Peppas model (also called The Power Law) to describe the diffusion of a penetrant and solute in a swellable polymer slab. This model is typically applied to the case of a hydrophilic polymer that sorbs the penetrant (water or solvent) and desorbs the incorporated drug (J Siepmann & Peppas, 2001). The values of the diffusional exponent “n” determined the mechanism of DEX released from crosslinker controlled PVA hydrogels. The exponent “n”, obtained from the slopes of the Korsmeyer–Peppas model, are used to describe the relative importance of Fickian diffusion. For cylindrical devices, i) when n approximates to

0.45, a Fickian transport (anomalous) is implied, indicating that the release is controlled by diffusion; ii) when  $0.45 < n < 0.89$ , a superposition of both phenomena (anomalous transport) is suggested; iii) when  $n=0.89$ , zero order (case II transport) applied (Korsmeyer, Gurny, Doelker, Buri, & Peppas, 1983). In this study, the values of the exponent “n” ranged from 0.4498 to 0.599, indicating that anomalous transport can be considered in the formulations.

Table 4-2. Kinetics parameters of DEX release from PVA hydrogels.

Formulation	Zero-order		First-order		Higuchi		Hixson-Crowell		Korsmeyer-Peppas *		
	K <sub>o</sub>	R <sup>2</sup>	K <sub>1</sub>	R <sup>2</sup>	K <sub>H</sub>	R <sup>2</sup>	K <sub>HC</sub>	R <sup>2</sup>	n	K <sub>KP</sub>	R <sup>2</sup>
DEX-125	0.0854	0.5995	0.0028	0.8556	2.7891	0.8133	0.0025	0.7763	0.4949	142.62	0.9278
DEX-250	0.0828	0.6214	0.0021	0.8342	2.6890	0.8322	0.0023	0.7659	0.5226	48.635	0.8828
DEX-375	0.0845	0.7260	0.0018	0.8880	2.6516	0.9090	0.0021	0.8397	0.4614	60.711	0.9006
DEX-500	0.0828	0.8109	0.0016	0.9203	2.5212	0.9557	0.0020	0.8892	0.4498	37.232	0.9064
DEX-625	0.0646	0.8368	0.0009	0.9096	1.9553	0.9732	0.0013	0.8857	0.4777	8.6411	0.9297
DEX-700	0.0600	0.8309	0.0009	0.8901	1.8224	0.9740	0.0012	0.8713	0.5990	1.3811	0.9604

\*: For Korsmeyer-Peppas model, the first 60% of the normalised drug was considered in calculation.

#### 4.3.6. Morphology

Microstructure and morphology of PVA hydrogel samples were evaluated by SEM. Figure 4-9 shows representative micrographs of PVA hydrogel with different concentrations of GA. Interior micro-pores can be seen in the transverse sections. It is noticed that the pore size and density visibly decreased with increasing GA ratio. As more GA was introduced, the surplus PVA hydroxyl groups were consumed to form increasing interactions and acetal bridges within the hydrogel matrix, resulting a more compact structure with reduced porosity. The ratio of GA and PVA effected the morphological structure and pores density of hydrogel matrix, which modulated the swelling and release behaviour. At lower GA concentration, the hydrogel films were more swellable with increased porous structure. This supported that the drug release behaviours in those PVA films were more fitted in Korsmeyer–Peppas model as the larger pores promoted the diffusion of water into the matrix and the swelling of the hydrogel when water enters. Conversely, the swelling ability and porous structure were decreased in the PVA films with higher GA concentration. This is accordant with the result that the release profiles in those PVA films were lesser fitted with Korsmeyer–Peppas model but more fitted with Higuchi model, where the matrix swelling is negligible and drug diffusion is constant.

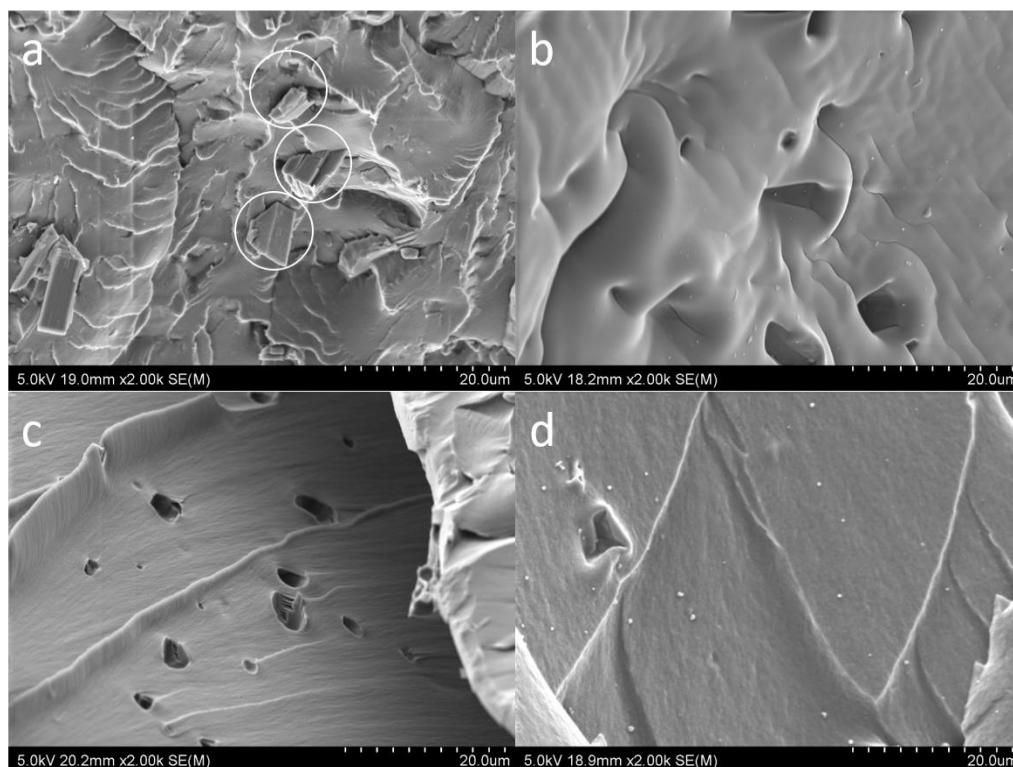


Figure 4-9. SEM images of the transverse sections of dexamethasone (DEX)-loaded poly (vinyl alcohol) (PVA) hydrogel: a) DEX-375 before release dissolution (DEX crystals were circled as white), b) DEX-125 after release dissolution, c) DEX-375 after release dissolution and d) DEX-750 after release dissolution.

#### 4.4. Conclusion

A PVA hydrogel drug delivery system has been synthesised and crosslinked with different concentrations of GA. The increased density of GA in PVA matrix showed reduced swelling behaviours and water absorption. FTIR analysis confirmed the existence of DEX in the PVA hydrogels with some possible interactions between the drug, crosslinker and polymer, indicating both DEX and PVA were crosslinked by GA through hydrogen bonding. The *in vitro* release assessment of DEX showed a burst release within 6h and followed by a sustained release for 25 days. PVA hydrogels with higher GA concentrations presented a slower and lesser release of incorporated DEX due to the increasing crosslinking level. Release data was fitted into Higuchi and Korsmeyer–Peppas models, suggesting a greater contribution of Fickian diffusion was dominant in the release kinetics. In principle, the present work confirms the potential and feasibility of PVA hydrogels crosslinked by different density of GA as a controlled release system in pharmaceutical and medical applications.



#### 4.5. Reference:

- Alemzadeh, I., & Vossoughi, M. (2002). Controlled release of paraquat from poly vinyl alcohol hydrogel. *Chemical Engineering and Processing: Process Intensification*, 41(8), 707-710.
- Andrade, G. I., Barbosa-Stancioli, E. F., Mansur, A. A. P., Vasconcelos, W. L., & Mansur, H. S. (2008). Small-angle X-ray scattering and FTIR characterization of nanostructured poly (vinyl alcohol)/silicate hybrids for immunoassay applications. *Journal of materials science*, 43(2), 450-463.
- Chiang, Z.-C., Yu, S.-H., Chao, A.-C., & Dong, G.-C. (2012). Preparation and characterization of dexamethasone-immobilized chitosan scaffold. *Journal of bioscience and bioengineering*, 113(5), 654-660.
- Dash, S., Murthy, P. N., Nath, L., & Chowdhury, P. (2010). Kinetic modeling on drug release from controlled drug delivery systems. *Acta Poloniae Pharmaceutica*, 67(3), 217-223.
- Desai, S. J., Simonelli, A., & Higuchi, W. (1965). Investigation of factors influencing release of solid drug dispersed in inert matrices. *Journal of pharmaceutical sciences*, 54(10), 1459-1464.
- ElHag, M., Coghlan, K., Christmas, P., Harvey, W., & Harris, M. (1985). The anti-inflammatory effects of dexamethasone and therapeutic ultrasound in oral surgery. *British journal of oral and maxillofacial surgery*, 23(1), 17-23.
- Figueiredo, K., Alves, T. L., & Borges, C. P. (2009). Poly (vinyl alcohol) films crosslinked by glutaraldehyde under mild conditions. *Journal of applied polymer science*, 111(6), 3074-3080.
- Fiorica, C., Palumbo, F. S., Pitarresi, G., Bongiovì, F., & Giammona, G. (2017). Hyaluronic acid and beta cyclodextrins films for the release of corneal epithelial cells and dexamethasone. *Carbohydrate polymers*, 166, 281-290.

- Gehrke, S. H., & Lee, P. I. (1990). Hydrogels for drug delivery systems. *Drugs and the pharmaceutical sciences*, 41, 333-392.
- Gemeinhart, R. A., Chen, J., Park, H., & Park, K. (2000). pH-sensitivity of fast responsive superporous hydrogels. *Journal of Biomaterials Science, Polymer Edition*, 11(12), 1371-1380.
- Gu, D., O'Connor, A. J., GH Qiao, G., & Ladewig, K. (2017). Hydrogels with smart systems for delivery of hydrophobic drugs. *Expert opinion on drug delivery*, 14(7), 879-895.
- Gupta, P., Vermani, K., & Garg, S. (2002). Hydrogels: from controlled release to pH-responsive drug delivery. *Drug discovery today*, 7(10), 569-579.
- Heimdal, K., Hirschberg, H., Slettebø, H., Watne, K., & Nome, O. (1992). High incidence of serious side effects of high-dose dexamethasone treatment in patients with epidural spinal cord compression. *Journal of neuro-oncology*, 12(2), 141-144.
- Hickey, T., Kreutzer, D., Burgess, D., & Moussy, F. (2002). Dexamethasone/PLGA microspheres for continuous delivery of an anti-inflammatory drug for implantable medical devices. *Biomaterials*, 23(7), 1649-1656.
- Higuchi, T. (1963). Mechanism of sustained-action medication. Theoretical analysis of rate of release of solid drugs dispersed in solid matrices. *Journal of pharmaceutical sciences*, 52(12), 1145-1149.
- Hoffman, A. S. (2012). Hydrogels for biomedical applications. *Advanced drug delivery reviews*, 64, 18-23.
- Islam, A., & Yasin, T. (2012). Controlled delivery of drug from pH sensitive chitosan/poly (vinyl alcohol) blend. *Carbohydrate polymers*, 88(3), 1055-1060.

- Kayal, S., & Ramanujan, R. (2010). Doxorubicin loaded PVA coated iron oxide nanoparticles for targeted drug delivery. *Materials Science and Engineering: C*, 30(3), 484-490.
- Khurma, J. R., Rohindra, D. R., & Nand, A. V. (2006). Synthesis and properties of hydrogels based on chitosan and poly (vinyl alcohol) crosslinked by genipin. *Journal of Macromolecular Science, Part A: Pure and Applied Chemistry*, 43(4-5), 749-758.
- Kokabi, M., Sirousazar, M., & Hassan, Z. M. (2007). PVA–clay nanocomposite hydrogels for wound dressing. *European Polymer Journal*, 43(3), 773-781.
- Korsmeyer, R. W., Gurny, R., Doelker, E., Buri, P., & Peppas, N. A. (1983). Mechanisms of solute release from porous hydrophilic polymers. *International journal of pharmaceutics*, 15(1), 25-35.
- Kumar, A., Pandey, M., Koshy, M., & Saraf, S. A. (2010). Synthesis of fast swelling superporous hydrogel: effect of concentration of crosslinker and acidol on swelling ratio and mechanical strength. *International Journal of Drug Delivery*, 2(2), 135-140.
- Larrañeta, E., Barturen, L., Ervine, M., & Donnelly, R. F. (2018). Hydrogels based on poly (methyl vinyl ether-co-maleic acid) and Tween 85 for sustained delivery of hydrophobic drugs. *International journal of pharmaceutics*, 538(1-2), 147-158.
- Larrañeta, E., Stewart, S., Ervine, M., Al-Kasasbeh, R., & Donnelly, R. F. (2018). Hydrogels for Hydrophobic Drug Delivery. Classification, Synthesis and Applications. *Journal of functional biomaterials*, 9(1), 13.
- Li, X., Bian, W., Li, D., Lian, Q., & Jin, Z. (2011). Fabrication of porous beta-tricalcium phosphate with microchannel and customized geometry based on gel-casting and rapid prototyping. *Proceedings of the institution of mechanical engineers, Part H: journal of engineering in medicine*, 225(3), 315-323.

- Malana, M. A., & Zohra, R. (2013). The release behavior and kinetic evaluation of tramadol HCl from chemically cross linked Ter polymeric hydrogels. *DARU Journal of Pharmaceutical Sciences*, 21(1), 10.
- Mansur, H. S., Sadahira, C. M., Souza, A. N., & Mansur, A. A. (2008). FTIR spectroscopy characterization of poly (vinyl alcohol) hydrogel with different hydrolysis degree and chemically crosslinked with glutaraldehyde. *Materials Science and Engineering: C*, 28(4), 539-548.
- McKenzie, M., Betts, D., Suh, A., Bui, K., Kim, L. D., & Cho, H. (2015). Hydrogel-based drug delivery systems for poorly water-soluble drugs. *Molecules*, 20(11), 20397-20408.
- Nanda, S., Sood, N., Reddy, B., & Markandeywar, T. S. (2013). Preparation and characterization of poly (vinyl alcohol)-chondroitin sulphate hydrogel as scaffolds for articular cartilage regeneration. *Indian Journal of Materials Science*, 2013.
- Niebergall, P., Milosovich, G., & Goyan, J. (1963). Dissolution rate studies II. Dissolution of particles under conditions of rapid agitation. *Journal of pharmaceutical sciences*, 52(3), 236-241.
- Numpilai, T., Witoon, T., Chareonpanich, M., & Limtrakul, J. (2017). Impact of physicochemical properties of porous silica materials conjugated with dexamethasone via pH-responsive hydrazone bond on drug loading and release behavior. *Applied Surface Science*, 396, 504-514.
- Nuttelman, C. R., Mortisen, D. J., Henry, S. M., & Anseth, K. S. (2001). Attachment of fibronectin to poly (vinyl alcohol) hydrogels promotes NIH3T3 cell adhesion, proliferation, and migration. *Journal of Biomedical Materials Research*, 57(2), 217-223.

- Paradossi, G., Cavalieri, F., Chiessi, E., Spagnoli, C., & Cowman, M. K. (2003). Poly (vinyl alcohol) as versatile biomaterial for potential biomedical applications. *Journal of Materials Science: Materials in Medicine*, 14(8), 687-691.
- Peppas, N., Bures, P., Leobandung, W., & Ichikawa, H. (2000). Hydrogels in pharmaceutical formulations. *European Journal of Pharmaceutics and Biopharmaceutics*, 50(1), 27-46.
- Peppas, N., & Simmons, R. (2004). Mechanistic analysis of protein delivery from porous poly (vinyl alcohol) systems. *Journal of Drug Delivery Science and Technology*, 14(4), 285-289.
- Peppas, N. A., Hilt, J. Z., Khademhosseini, A., & Langer, R. (2006). Hydrogels in biology and medicine: from molecular principles to bionanotechnology. *Advanced materials*, 18(11), 1345-1360.
- Peppas, N. A., & Wright, S. L. (1998). Drug diffusion and binding in ionizable interpenetrating networks from poly (vinyl alcohol) and poly (acrylic acid). *European Journal of Pharmaceutics and Biopharmaceutics*, 46(1), 15-29.
- Perrie, Y., & Rades, T. (2010). *Pharmaceutics–Drug Delivery and Targeting: Fastrack*, Pharmaceutical Press: London.
- Reis, E. F. d., Campos, F. S., Lage, A. P., Leite, R. C., Heneine, L. G., Vasconcelos, W. L., . . . Mansur, H. S. (2006). Synthesis and characterization of poly (vinyl alcohol) hydrogels and hybrids for rMPB70 protein adsorption. *Materials Research*, 9(2), 185-191.
- Rodrigues, L. B., Leite, H. F., Yoshida, M. I., Saliba, J. B., Junior, A. S. C., & Faraco, A. A. (2009). In vitro release and characterization of chitosan films as dexamethasone carrier. *International journal of pharmaceutics*, 368(1), 1-6.

- Roobahani, M., Kharaziha, M., & Emadi, R. (2017). pH sensitive dexamethasone encapsulated laponite nanoplatelets: Release mechanism and cytotoxicity. *International journal of pharmaceutics*, 518(1-2), 312-319.
- Salgado, M., Rodríguez-Rojas, S., Reis, R. L., Cocero, M. J., & Duarte, A. R. C. (2017). Preparation of barley and yeast  $\beta$ -glucan scaffolds by hydrogel foaming: Evaluation of dexamethasone release. *The Journal of Supercritical Fluids*, 127, 158-165.
- Saurí, J., Millán, D., Suñé-Negre, J., Colom, H., Ticó, J., Miñarro, M., . . . García-Montoya, E. (2014). Quality by design approach to understand the physicochemical phenomena involved in controlled release of captopril SR matrix tablets. *International journal of pharmaceutics*, 477(1), 431-441.
- Schmedlen, R. H., Masters, K. S., & West, J. L. (2002). Photocrosslinkable polyvinyl alcohol hydrogels that can be modified with cell adhesion peptides for use in tissue engineering. *Biomaterials*, 23(22), 4325-4332.
- Shah, D., Shah, Y., & Pradhan, R. (1997). Development and evaluation of controlled-release diltiazem HCl microparticles using cross-linked poly (vinyl alcohol). *Drug development and industrial pharmacy*, 23(6), 567-574.
- Shaikh, H. K., Kshirsagar, R., & Patil, S. (2015). Mathematical models for drug release characterization: a review. *World Journal Of Pharmacy And Pharmaceutical Sciences*, 4(04), 324-338.
- Shen, J., & Burgess, D. J. (2012). Accelerated in vitro release testing of implantable PLGA microsphere/PVA hydrogel composite coatings. *International journal of pharmaceutics*, 422(1-2), 341-348.
- Siepmann, J., & Peppas, N. (2001). Modeling of drug release from delivery systems based on hydroxypropyl methylcellulose (HPMC). *Advanced drug delivery reviews*, 48(2-3), 139-157.

- Singhvi, G., & Singh, M. (2011). In-vitro drug release characterization models. *International Journal of Pharmaceutical Studies and Research*, 2(1), 77-84.
- Tavakoli, J., & Tang, Y. (2017). Honey/PVA hybrid wound dressings with controlled release of antibiotics: Structural, physico-mechanical and in-vitro biomedical studies. *Materials Science and Engineering: C*, 77, 318-325.
- Wang, T., Turhan, M., & Gunasekaran, S. (2004). Selected properties of pH-sensitive, biodegradable chitosan–poly (vinyl alcohol) hydrogel. *Polymer International*, 53(7), 911-918.
- Wood, A. J., & Barnes, P. J. (1995). Inhaled glucocorticoids for asthma. *New England Journal of Medicine*, 332(13), 868-875.
- Yeom, C.-K., & Lee, K.-H. (1996). Pervaporation separation of water-acetic acid mixtures through poly (vinyl alcohol) membranes crosslinked with glutaraldehyde. *Journal of membrane science*, 109(2), 257-265.
- Yin, M.-J., Yamamoto, Y., & Gaynor, R. B. (1998). The anti-inflammatory agents aspirin and salicylate inhibit the activity of I $\kappa$ B kinase- $\beta$ . *Nature*, 396, 77-80.
- Yu, S., Zhang, X., Tan, G., Tian, L., Liu, D., Liu, Y., . . . Pan, W. (2017). A novel pH-induced thermosensitive hydrogel composed of carboxymethyl chitosan and poloxamer cross-linked by glutaraldehyde for ophthalmic drug delivery. *Carbohydrate polymers*, 155, 208-217.
- Zhang, X., Tang, K., & Zheng, X. (2016). Electrospinning and crosslinking of COL/PVA nanofiber-microsphere containing salicylic acid for drug delivery. *Journal of Bionic Engineering*, 13(1), 143-149.
- Zhang, Z., Yu, J., Zhou, Y., Zhang, R., Song, Q., Lei, L., & Li, X. (2018). Supramolecular nanofibers of dexamethasone derivatives to form hydrogel for

topical ocular drug delivery. *Colloids and surfaces B: Biointerfaces*, 164, 436-443.



## Chapter 5

*A 3D printed chitosan-pectin hydrogel wound dressing for lidocaine hydrochloride delivery*

Manuscript prepared as:

Long, J., Etxeberria, A. E., Nand, A. V., Bunt, C. R., Ray, S., & Seyfoddin, A. (2019). A 3D printed chitosan-pectin hydrogel wound dressing for lidocaine hydrochloride delivery. Submitted to the Journal of *Materials Science and Engineering C*, under review.

## 5.1. Introduction

Wound healing is an intricate process related to the general phenomenon of growth and tissue regeneration, which is influenced by both intrinsic and extrinsic factors (Boateng, Matthews, Stevens, & Eccleston, 2008; Gethin, 2007). For a wound to be healed successfully, it requires diverse types of cells and reaction pathways to regenerate the injured tissue and replace lost tissue (Boateng et al., 2008; Shakespeare, 2001). Wound healing process is comprised of four integrated and overlapping phases: haemostasis, inflammation, proliferation and tissue remodelling or resolution (Gosain & DiPietro, 2004). These four phases must progress in order with sufficient time for each phase to avoid improper or impaired wound healing. Consequently, wound dressings and devices to assist and promote the wound healing process form a significant segment of wound care management. Wound dressing aims to establish and maintain optimum conditions for the reestablishment of the damaged tissue (Boateng et al., 2008). An ideal wound dressing should be non-allergenic and non-toxic, preserve moist environment, promote effective oxygen exchange, protect the wound against microbial organisms and absorb wound exudates (Croisier & Jérôme, 2013). Chitosan (CS) is a semi-crystalline polysaccharide that is commonly obtained by alkaline deacetylation of chitin and is widely used as a biomedical material due to its distinctive properties such as biocompatibility, biodegradability, non-toxicity, antimicrobial and anti-fungal effects (Ahmed & Ikram, 2016; Croisier & Jérôme, 2013). CS is also beneficial for wound healing as it simulates haemostasis and accelerates tissue generation (Ahmed & Ikram, 2016). Pectin (PEC) is an anionic polysaccharide extracted from plant cell walls, which shows valuable properties for

drug delivery such as biocompatibility and mucoadhesiveness (Neufeld & Bianco-Peled, 2017).

There are various methods to encapsulate the drug and bioactive compounds within the porous polymer matrix for biomedical applications (X. Huang & Brazel, 2001; Kumari, Yadav, & Yadav, 2010; C. P. Reis, Neufeld, & Veiga, 2017; Vellayappan et al., 2016; J. C.-C. Wu et al., 2014). Among these, hydrogels can provide moist environment and assists cleansing sloughy or necrotic tissue to promote proper healing and hence advantageous for wound dressing application (Boateng et al., 2008). Physically crosslinked hydrogels are specifically attractive for medical and pharmaceutical applications because their preparation can avoid chemical crosslinkers which are typically toxic. In this respect, some studies have shown that blending CS and PEC solutions at acidic conditions can form physically crosslinked thermoreversible hydrogels by lowering the temperature (Kowalonek, 2017; Nordby, Kjøniksen, Nyström, & Roots, 2003).

Most currently marketed wound dressing products are not customisable to suit specific conditions or provide a specific dose of medication(s) based on patient requirement. 3D printed drug delivery systems have the potential to provide customised innovative solutions in this space (Long et al., 2018). It is possible to rapidly prototype or customise using 3D printing to fabricate designs with a digitally controlled layer-by-layer deposition technique using computer-aided design (CAD). In this study, a piston-based mechanical dispensing system was used to extrude continuous material to print CS-PEC hydrogel mesh scaffold. Compared to other 3D printing systems, such as fused deposition modelling (FDM), this extrusion based

hydrogel 3D printing can easily incorporate different doses of drug(s) without the need of heat treatment (Long et al., 2017). 3D printed hydrogel scaffolds for wound healing offer numerous advantages: i) formulations or doses can be customised based on individual's needs; ii) dimensional properties of the wound dressing, such as the area, thickness or pore size, can be tailored; iii) simple drug loading process; iv) a wide range of materials can be used; v) the mesh design allows effective oxygen penetration and vi) the sponge-like structure of lyophilised hydrogel wound dressings can efficiently absorb the wound exudates and provide a moist environment for a proper wound healing.

In this study, a novel biodegradable 3D printed hydrogel was developed for wound dressing application. The specific aims of this study were: i) to design a LDC encapsulated system in CS-PEC hydrogels with an immediate release behaviour; ii) to explore the feasibility of 3D printing CS-PEC hydrogel scaffold; iii) to evaluate the suitability of 3D printed hydrogel scaffold for wound dressing; iv) to explore the molecular interactions between the host hydrogel system and the drug, and v) to evaluate *in vitro* drug release performance.

## 5.2. Materials and methods

### 5.2.1. Materials

LDC was purchased from FlemPharma (Shanghai, China). PEC from citrus peel (galacturonic acid  $\geq 74.0\%$ ), high molecular weight CS (MW: 310000-375000 Da), hydrochloric acid (36%) and phosphate buffered saline (PBS) tablets were purchased from Sigma-Aldrich (Auckland, New Zealand). All other chemicals were of analytical grade.

### 5.2.2. Hydrogel preparation

Polysaccharide solutions of PEC and CS (2% w/v, respectively) were separately prepared in 0.1M HCl at 65°C under magnetic stirring for 3h. Then, hydrogel samples were prepared by mixing PEC and CS solutions (pH=1.93) at a ratio of 1:4 at 65°C under magnetic stirring for 1h. The mixture (10 mL) was then transferred to 3D printing syringes and cooled to room temperature (25°C) to form the gel structure.

LDC-loaded hydrogel samples were prepared under the same conditions. Prior to blending PEC and CS solutions, a specific amount of LDC was dissolved in PEC solution under magnetic stirring for 10 min at room temperature. The final concentrations of LDC in hydrogel were prepared as 0, 2, 5 and 10 % w/w and named as LDC-0, LDC-2, LDC-5 and LDC-10, respectively.

### 5.2.3. 3D printing of hydrogel scaffold

A mesh scaffold model was designed using Solidworks (SOLIDWORDS 2016 x64 Edition, Dassault Systemes) and exported as a STL. file and sliced by Slic3r (Slic3r 1.2.9) G-code comments to interface with the printer hardware (Repetier-Host 2.1.3, Germany). The scaffold was designed as a cubic mesh scaffold (23.50 mm length x

23.50 mm width x 1.00 mm height) with a grid size of 2.50 mm x 2.50 mm and line width of 0.50 mm (Figure 5-1).

The scaffolds were fabricated with CS-PEC hydrogels with and without LDC using a BioBot1 3D printer (Allevi, Philadelphia PA, USA). The following settings were used: JG25-0.5HP nozzle with inner diameter of 0.2540 mm, layer height of 0.25 mm, printing speed of 6 mm/s, printing temperature of 25°C and printing pressure of 10.7-15.1 PSI. After printing, the samples were frozen (8 h at -20°C) and subsequently lyophilised (12 h at -75°C with 0.0014 mbar pressure).

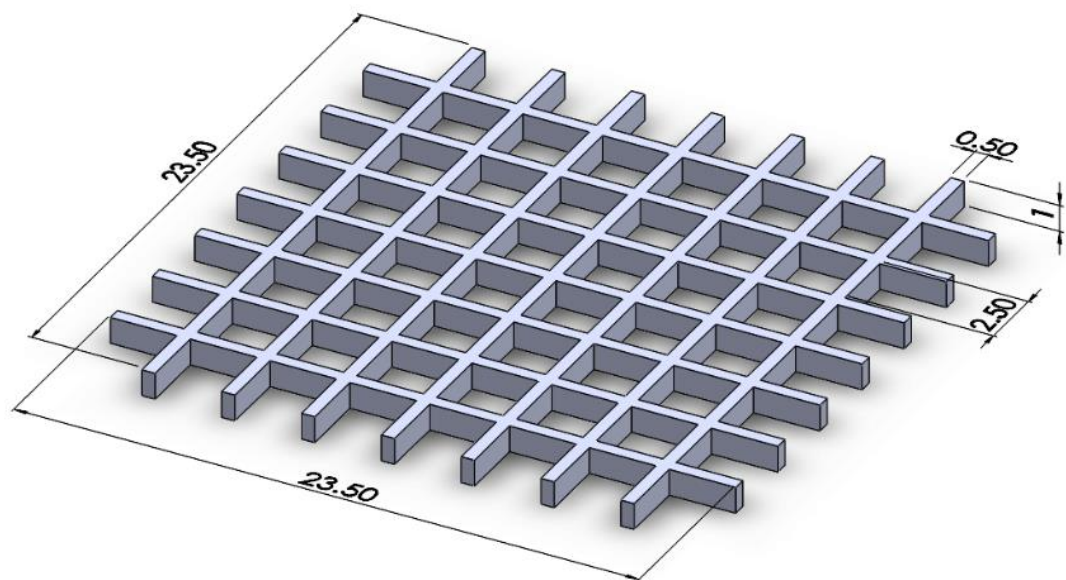


Figure 5-1. A digital 3D mesh scaffold design (unit: mm).

#### 5.2.4. Metrological parameters and porosity of scaffolds

The thickness, grid size, line width and total width of the lyophilised hydrogel scaffolds, presented in Figure 5-1, were measured by an electric Vernier caliper (TD2082, Jaycar Electronics, New Zealand). The weights of the wet and lyophilised hydrogel scaffolds were measured using an electronic balance (AUW220D, SHIMADZU, Japan) (n=3). Cryo-fractured cross-section images of the lyophilised

hydrogel scaffolds used to study the scaffold inner morphology, were obtained employing a Schottky field emission SEM (SU-70, Hitachi, United Kingdom) under a working voltage of 5 kV. Prior to SEM, samples were placed on metallic stubs and coated with platinum under vacuum for 100 seconds using an ion sputter coater (E-1045, Hitachi, United Kingdom) for visualisation.

#### 5.2.5. Swelling and water absorption

The equilibrium swelling ratio (ESR) of CS-PEC lyophilised hydrogel scaffolds in distilled water at room temperature was determined using a gravimetric method (Khurma et al., 2006). To avoid the breakage of the scaffold, a customised mesh holder (grid size: 2 mm x 2 mm) printed by an FDM 3D printer (UP Mini 3D printer, 3D printing Systems, New Zealand) with poly (lactic acid) (PLA) filament was used in the swelling and water absorption test (Figure 5-2). Dried samples were weighed and placed on the top of the mesh holder. The mesh holder was floated on the surface of distilled water, allowing the lyophilised hydrogel scaffold to absorb the water through the grid holes. At predetermined time intervals, the holder-sample systems were withdrawn and the bottom surface was blotted with tissue paper to remove excess water. Then, samples were immediately weighed to determine the wet weight. Three PLA mesh holders were used as control. The experiments were continued until equilibrium was achieved. The ESR was calculated using Eq.(5-1) (n=3):

$$E_{SR}(\%) = \frac{W_t - W_d}{W_d} \times 100 \quad (5-1)$$

where  $W_t$  is the weight of wet hydrogel at a particular time (t),  $W_d$  is the weight of dry hydrogel before swelling. The equilibrium water content (EWC) was calculated using Eq.(5-2) (n=3):

$$E_{wc} (\%) = \frac{W_e - W_d}{W_e} \times 100 \quad (5-2)$$

where  $W_e$  is the weight of hydrogel at equilibrium state.

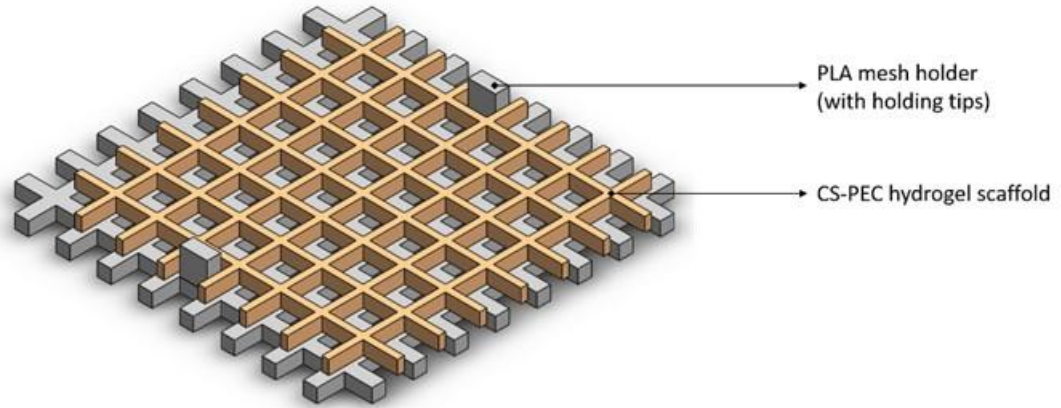


Figure 5-2. Digital 3D design of 3D printed poly (lactic acid) (PLA) mesh holder for swelling and water absorption studies of 3D printed chitosan-pectin (CS-PEC) hydrogel scaffold.

### 5.2.6. Bio-adhesion strength

The bioadhesive strength of the hydrogel scaffold on porcine skin after removing all the hair and fat (Jin et al., 2016) was measured using a texture analyser (TA.XT2, Stable Micro System, Haslemere, Surrey, UK). Before the test, the hydrogel samples were rehydrated by gradually dropping distilled water on the scaffold until it became transparent to simulate moisture wound condition. This skin was secured on the upper movable probe of the instrument while the hydrogel scaffold was attached to a glass slide on the lower fixed plate. The upper probe was lowered at a speed of 0.5 mm/s until the hydrogel made contact then hold with a force of 200 g for 30 s. Subsequently, the upper probe was lifted at a rate of 10 mm/s to a distance of 30 mm. The maximum force required to detach the hydrogel scaffold from the skin was considered the bioadhesive strength of that sample (n=3).



### 5.2.7. Spectral analysis of chemical interactions

Spectra obtained from Fourier-transform infrared (FTIR) spectroscopy were used to characterise the presence of specific chemical groups and their interactions in the scaffolds using a Nicolet iS10 FTIR spectrophotometer (Thermo Scientific, USA) in attenuated total reflectance (ATR) mode using a diamond ATR crystal. The spectra of the samples were recorded in the range of 4000-400  $\text{cm}^{-1}$  with an average of 64 scans at a resolution of 4  $\text{cm}^{-1}$ .

### 5.2.8. Thermal properties

Thermal properties of the 3D printed CS-PEC hydrogels were determined using differential scanning calorimetry (DSC) (DSC Q1000, TA Instruments, NZ). The samples (2-7 mg) were sealed in aluminium pans before the DSC test. The tests were performed under nitrogen atmosphere at a heating rate of 10  $^{\circ}\text{C}/\text{min}$  over the temperature range 30-180 $^{\circ}\text{C}$ .

### 5.2.9. *In vitro* drug release

The *in vitro* LDC release from CS-PEC hydrogels was studied in PBS buffer (pH=7.4) under sink conditions. The samples were inserted into a dialysis membrane (cut off 3500 MWCO) with 1 mL PBS buffer and then placed in a screwed bottle containing 99 mL PBS buffer that placed in a water bath maintained at 37 $^{\circ}\text{C}$  and under shaking (100 rpm). At predetermined time intervals, 1 mL of the release media from each sample was collected and an equal amount of fresh media was added into each release system to maintain the total volume and sink condition.

The concentration of LDC in the release media was determined by High-performance liquid chromatography (HPLC) using LC-20AT liquid chromatograph, LC-20AT HT

auto sampler, DGU-20A5 degasser, RF-10A XL UV/VIS detector (Shimadzu USA manufacturing Inc, USA) equipped with a GraceSmart RP 18, 3  $\mu\text{m}$ , 50 mm x 2.1 mm reverse phase chromatography column. A mixture of acetonitrile: 0.1% formic acid in water (5:95) was used as mobile phase, at a flow rate of 1 mL/min and injection volume of 2  $\mu\text{L}$  UV detection at 254 nm. A chromatogram of LDC peak is shown in Figure 5-3. A calibration curve ( $Y=5.054 \times 10^{-3}X$ ,  $R^2= 0.9999$ ) was prepared with standard solutions of 0, 6.25, 12.50, 25.00, 50.00 and 100.00  $\mu\text{g/mL}$ . The cumulative amount of LDC was plotted against release time for each sample.

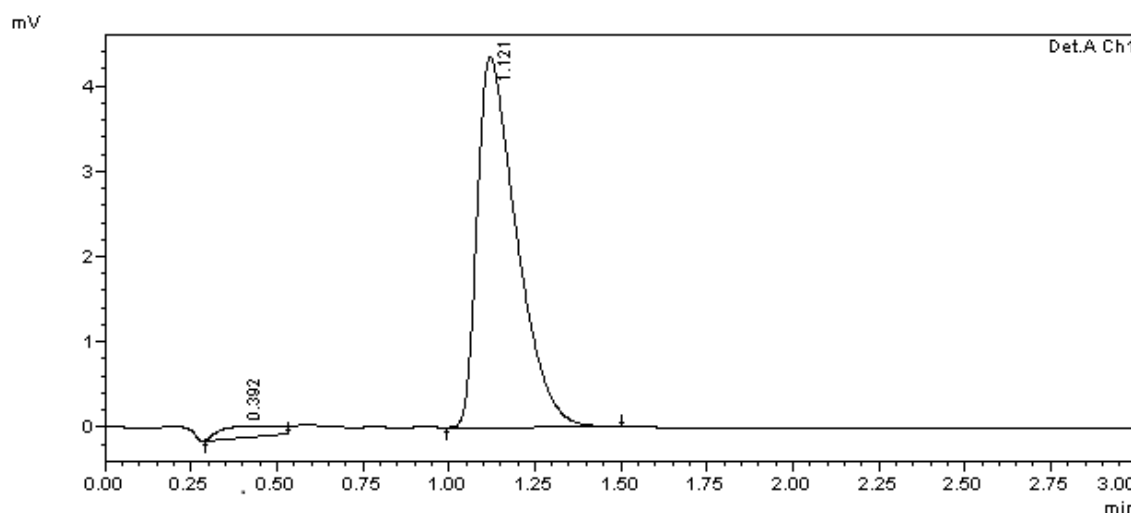


Figure 5-3. The chromatogram obtained with LCD peak eluting at 1.121 mins.

#### 5.2.10. Drug release kinetics

To study the release kinetics and mechanism of LDC release from CS-PEC hydrogels, data was fitted the following models.

Zero-order model (Dash et al. 2010):

$$Q_t = Q_0 + K_0 t \quad (5-3)$$

where  $Q_t$  is the amount of drug released at time  $t$ ,  $Q_0$  is the initial amount of drug in the solution, and  $K_0$  is the zero order release constant expressed in the units of

concentration/time. Zero-order model describes the system where the release rate of incorporated drug is independent of its concentration (Shaikh et al. 2015).

First-order model (Dash et al. 2010):

$$\log Q = \log Q_0 - K_1 t / 2.303 \quad (5-4)$$

where  $Q_0$  is the initial concentration of drug,  $K_1$  is first order rate constant expressed in units of  $\text{time}^{-1}$ , and  $t$  is the time. First-order model describes the dependency on the drug concentration in the polymer networks (Desai et al. 1965).

Higuchi model (Dash et al. 2010):

$$Q_t = K_H \times t^{1/2} \quad (5-5)$$

where  $Q_t$  is amount of drug released in time  $t$ ,  $K_H$  is the Higuchi dissolution constant expressed in the units of concentration/time. Higuchi model is proposed to describe the drug release from a matrix system with different geometrics and porous structure (Higuchi 1963).

Hixson-Crowell model (Dash et al. 2010):

$$Q_0^{1/3} - Q_{tr}^{1/3} = K_{HC} t \quad (5-6)$$

where  $Q_0$  is the initial amount of drug in the pharmaceutical dosage form,  $Q_{tr}$  is the remaining amount of drug in the pharmaceutical dosage form at time  $t$  and  $K_{HC}$  is a constant incorporating the surface-volume relation. This equation describes the release from systems where there is a change in surface area and diameter of particles (Niebergall et al. 1963).

Korsmeyer–Peppas model (Dash et al. 2010):

$$Q_t/Q_\infty = K_{KP}t^n \quad (5-7)$$

where  $Q_t/Q_\infty$  is a fraction of drug released at time  $t$ ,  $K_{KP}$  is the release rate constant and  $n$  is the release exponent. This relationship describes drug release from a polymeric system such as hydrogel. Data up to 60% drug release was used to fit into this kinetic model.

#### 5.2.11. Statistical analysis

Data were subjected to one-way analysis of variant (ANOVA) with the level of significance set at  $P < 0.05$  in Microsoft Excel.

### 5.3. Results and discussion

#### 5.3.1. Evaluation of feasibility of fabricating hydrogel scaffolds using 3D printing

One of the important criteria for designing hydrogels is to achieve adequate mechanical integrity, shape retention and flexibility of the scaffold system to ensure practical applicability. In this study, thermosensitive CS-PEC hydrogel scaffolds were printed using an extrusion-based benchtop 3D printer. The photographs of freshly printed and lyophilised hydrogel scaffolds are presented in Figure 5-4 (a & b), while the weights and physical dimensions of freeze-dried scaffolds are listed in Table 5-1.

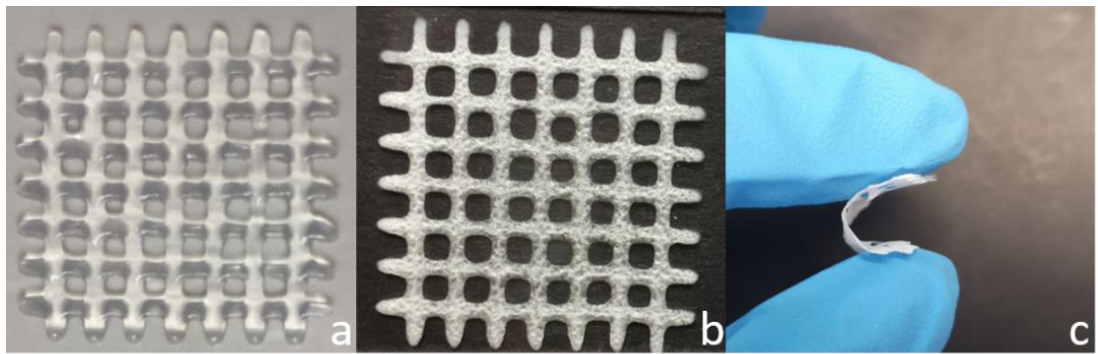


Figure 5-4. 3D printed chitosan-pectin (CS-PEC) hydrogel scaffold: a) freshly printed, b) lyophilised and c) flexibility of a lyophilised scaffold.

It is evident that all formulations were printable with good consistency in shape. As shown in Figure 5-4 (a & b) the CS-PEC hydrogels showed good printability with visible lines in the small grid and maintained its geometry and mechanical integrity after extrusion and lyophilisation processes. As shown in Figure 5-4 c, the lyophilised scaffolds exhibit good flexibility, which is beneficial for pain management allowing for physical activity and comfort during recovery as well as improving the contact with wound.

The measurements of physical dimensions and weights in Table 5-1 also confirmed the acceptable repeatability of those 3D printed CS-PEC hydrogel scaffolds. As shown in Table 5-1, the physical property maintained good consistency for each formulation. No significant difference ( $p>0.05$ ) was detected between each group. However, the thickness was reduced significantly ( $p<0.05$ ) after drying (from 1.00 mm to 0.29 mm) compared to hydrated hydrogels.

Viscosity of printing materials is an important parameter for extrusion-based 3D printing. The materials with ideal viscosity should be able to maintain a proper extrusion speed during printing without over-liquefying or blocking in the nozzle and to conserve the geometries after printing. CS-PEC hydrogel exhibits thermoreversible properties therefore, its viscosity can be adjusted by adjusting the surrounding temperature. Consequently, the viscosity of the fluid system was adjusted by tuning the processing temperature during 3D printing and thereby, the defined geometries after printing were maintained.

Table 5-1. Average physical dimensions and weights of 3D printed and lyophilised mesh scaffolds along with wet and dry weights ( $n=3\pm$  SD).

Formulation	Thickness $\pm$ SD (mm)	Grid size $\pm$ SD (mm)	Line width $\pm$ SD (mm)	Total width $\pm$ SD (mm)	Wet weight $\pm$ SD (mg)	Dry weight $\pm$ SD (mg)
Digital model	1.00	2.50	0.50	23.50	-	-
LDC-0	0.29 $\pm$ 0.04	2.06 $\pm$ 0.13	1.07 $\pm$ 0.09	21.64 $\pm$ 0.04	214.27 $\pm$ 5.19	4.47 $\pm$ 0.09
LDC-2	0.28 $\pm$ 0.05	2.12 $\pm$ 0.09	1.16 $\pm$ 0.16	22.61 $\pm$ 0.33	214.67 $\pm$ 13.01	4.60 $\pm$ 0.22
LDC-5	0.29 $\pm$ 0.01	1.99 $\pm$ 0.05	1.00 $\pm$ 0.07	21.54 $\pm$ 0.07	215.87 $\pm$ 6.22	4.67 $\pm$ 0.09
LDC-10	0.28 $\pm$ 0.01	2.03 $\pm$ 0.09	1.01 $\pm$ 0.06	22.57 $\pm$ 0.25	220.57 $\pm$ 15.70	4.67 $\pm$ 0.12

### 5.3.2. Effect of encapsulation of drug on the morphology, swelling and water absorption of hydrogel

Encapsulation of LDC in the CS-PEC hydrogel appeared to reduce hydrogel pore size as shown in cryo-fractured cross-sectional images of the lyophilised scaffolds (Figure 5-5). The drug-loaded samples form a more compact three-dimensional

macromolecular structure, as has been reported previously (Chen, Park, & Park, 1999; Kabiri & Zohuriaan-Mehr, 2004).

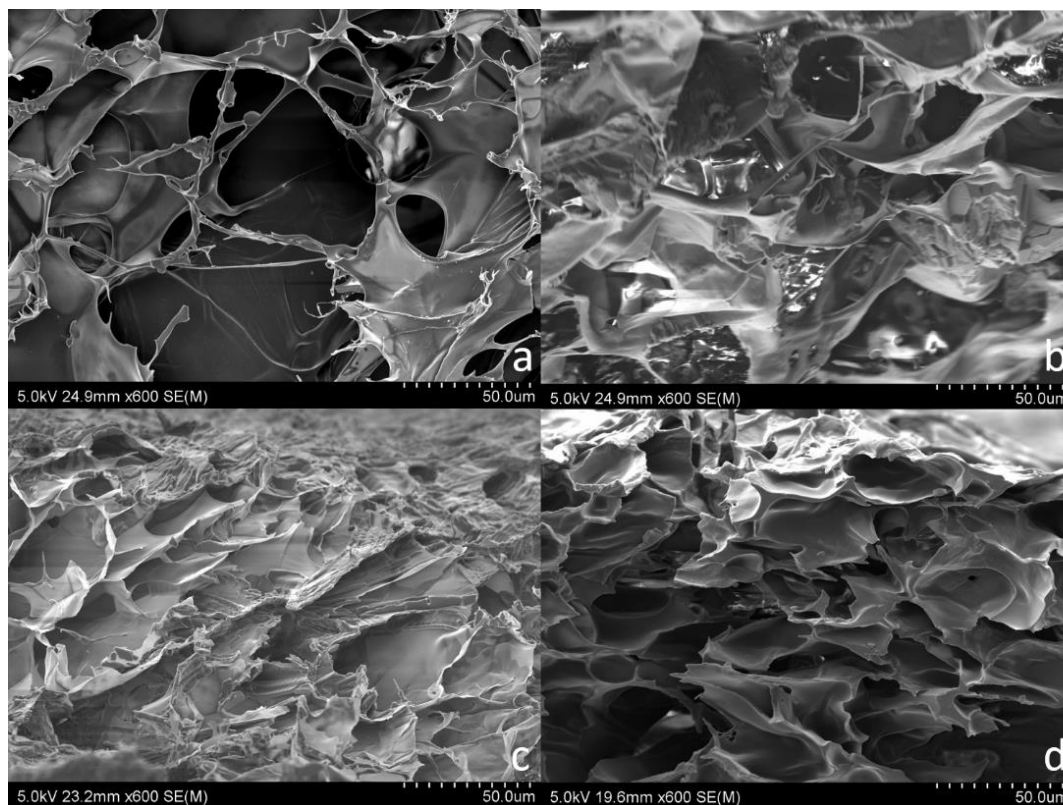


Figure 5-5. SEM micrographs of the cross section of 3D printed chitosan-pectin (CS-PEC) hydrogel scaffolds: a) lidocaine hydrochloride free (LDC-0), b) LDC-2, c) LDC-5 and d) LDC-10.

The equilibrium swelling ratio (ESR) of LDC-0 and LDC-10 samples are presented in Figure 5-6. All lyophilised hydrogel scaffolds swelled rapidly and reached an equilibrium state in about 2 h and 4 h for LDC-0 and LDC-loaded samples, respectively. The presence of the drug reduced the swelling behaviour of CS-PEC scaffolds. This may be related to a salting-out effect due to the  $\text{Cl}^-$  from LDC interfering with positively charged CS polymers. The neutralised polymer leads to decreased interactions with water, which results in reduced water absorbency (Mallepally, Bernard, Marin, Ward, & McHugh, 2013). It has been reported that introducing sodium chloride (NaCl) resulted in reduced swelling behaviours of the thermosensitive hydrogels made of N-vinylcaprolactam (NVCL) via a salting-out

effect (Lee & Bae, 2015). The compact structure with reduced pore size as observed in LDC-10 samples (Figure 5-5 d) may also contribute to the reduced swelling ratio. Consequently, the final ESR values were 2832% and 2265% for LDC-0 and LDC-10 samples, respectively. The high ESR values in CS-PEC hydrogels showed the likely suitability for absorbing wound exudates. Wound exudates contain tissue degrading enzymes that may obstruct the proliferation and activity of cells and break down extracellular matrix materials and growth factors (Boateng et al., 2008). Therefore, the absorption property of wound dressing is an essential factor as it can promote the local haemostasis at the open wound and subsequently remove the wound exudates which can delay the wound healing and macerate surrounding skin (Boateng et al., 2008).

The water absorption values, obtained as equilibrium water content (EWC) in each sample, were 97% and 96% for LDC-0 and LDC-10 hydrogels, respectively. The high EWC values in CS-PEC hydrogels indicate that a large volume of water was physically entrapped in the crosslinked CS-PEC hydrogels. The sponge-like structure of CS-PEC hydrogels provide benefits in absorbing and entrapping water, contributing to maintaining a moisture environment on the wound bed. A moist wound environment can prevent desiccation and cell death, enhance epidermal migration and promote tissue regeneration on wound area (Boateng et al., 2008; Okan, Woo, Ayello, & Sibbald, 2007; Sibbald et al., 2000; Snyder, Fife, & Moore, 2016).



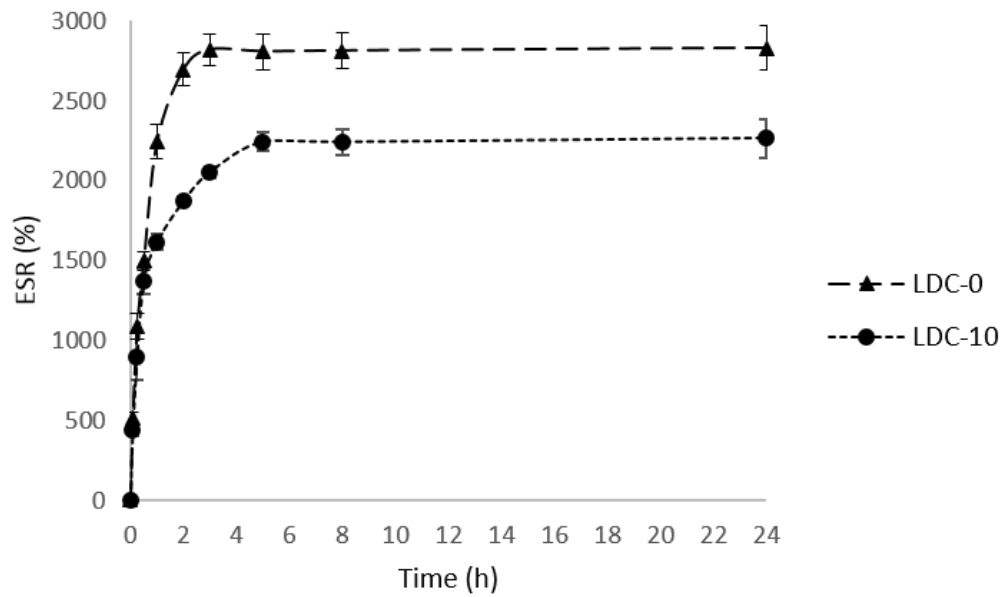


Figure 5-6. Equilibrium swelling ratio (ESR) of chitosan-pectin (CS-PEC) hydrogel scaffolds as a function of lidocaine hydrochloride (LDC) content ( $n=3 \pm \text{SD}$ ).

### 5.3.3. Bio-adhesion strength

In *ex vivo* bio-simulated conditions, bio-adhesion strength can be measured as the force required to detach a sample from the surface of porcine skin (Jin et al., 2016; Tamburic & Craig, 1997; Wittaya-areekul, Prahsarn, & Sungthongjeen, 2006). In this study, the adhesive strength of LDC-0 and LDC-loaded samples were measured by texture analyser as the detachment force. As shown in Figure 5-7, all hydrogel scaffolds showed adhesive strength in the range of 86.5-126.9 g (equal to 0.85-1.24 N), which is similar to the currently marketed wound dressings, such as those made of silicone (0.7 N), polyurethane (0.9 N) and acrylate (1.14 N) (Klode et al., 2011). The adhesive strength of LDC-0 was found to be significantly less ( $p=0.0027$ ), while there was no statistical difference ( $p=0.2894$ ) between LDC-loaded groups. This may be explained by the porosity changes in the LDC-loaded samples as the introduction of LDC contributed to more compact structures with increased mechanical interaction

and interlocking contact area, where stronger forces were required to detach the sample from skin.

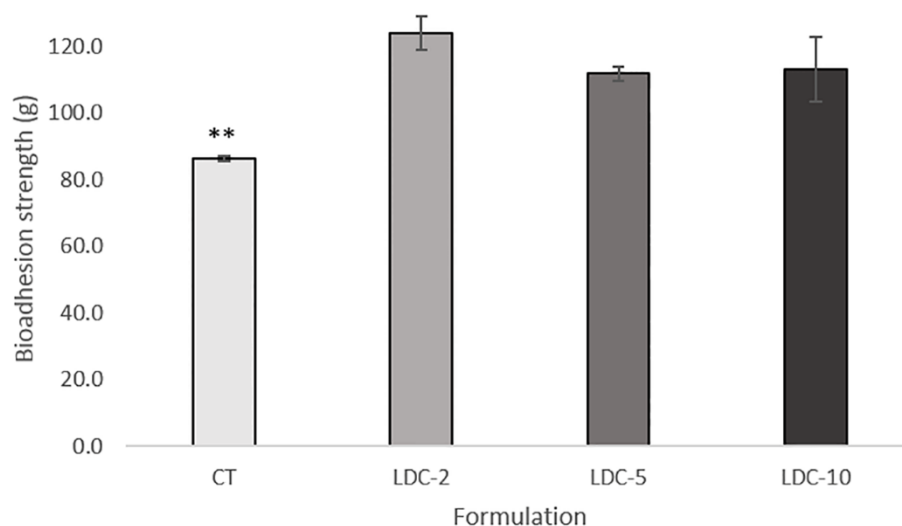


Figure 5-7. Bioadhesion strength of 3D printed hydrogel scaffolds as a function of lidocaine hydrochloride (LDC) content ( $n=3 \pm \text{SD}$ ). \*\*:  $p < 0.01$ .

An ideal wound dressing should be self-adhesive, easily removable and painless (Boateng et al., 2008). Appropriate adherence and easily removable dressings can protect the wound against further trauma and prevent damaging the newly generated tissue. As shown in Figure 5-7, the adhesion strength of the hydrogel scaffolds is in the range of 86.5-126.9 g, indicating that the 3D printed scaffold has sufficient adhesion to attach and hold itself to the skin. Such adhesion strengths can be easily peeled off without causing tissue damage or pain (Klode et al., 2011).

#### 5.3.4. Determination of molecular interactions between the drug and the hydrogel scaffold

Processes involving heating and cooling can affect the properties of crystalline substances as they undergo changes in the degree of molecular motion during the process cycle (Ray & Cooney, 2018). Incorporation of crystalline additives in the

polymer system, could further influence the recrystallisation process. Hence, DSC studies were performed on 3D printed lyophilised CS-PEC hydrogel containing crystalline drug LDC. The DSC thermograms of lyophilised hydrogels without and with drug-loading, LDC-0 and LDC-10 respectively, are shown in Figure 5-8. The results were compared with pristine polymers and drug i.e., CS, PEC and LDC respectively. CS and PEC showed wide endothermic peaks in the temperature range of 40-170°C, with endothermic enthalpy change of 330 and 388 J/g, respectively, representing the dehydration of the polymers (Archana, Dutta, & Dutta, 2013; Kaur & Kaur, 2012; Mishra, Datt, & Banthia, 2008; Neufeld & Bianco-Peled, 2017). An endothermic peak was also observed in the CS-PEC hydrogel with reduced endothermic enthalpy of 268.4 J/g. This result designates that the formation of hydrogen bonds between CS and PEC is correlated to a better organisation of polymer chains, as supported in SEM (Figure 5-5) where a crosslinked structure was observed. It also indicates that freeze-drying process successfully reduced the moisture content in the CS-PEC hydrogel.

LDC presented a single sharp endothermic peak at 78°C corresponding to its melting point ( $T_m$ ), confirming its crystalline state (Repka, Gutta, Prodduturi, Munjal, & Stodghill, 2005). In the drug-loaded CS-PEC hydrogel (LDC-10), the crystal endotherm from LDC was bimodal in nature with two small peaks at 67 and 74°C respectively. The bimodal crystalline melt transition within the printed drug loaded polymer samples implies the formation of different size and crystalline structures. Hence, the changes in  $T_m$  and bimodal crystalline transition of LDC were induced by the recrystallisation process and molecular interactions between the drug and the functional polymers CS and PEC.

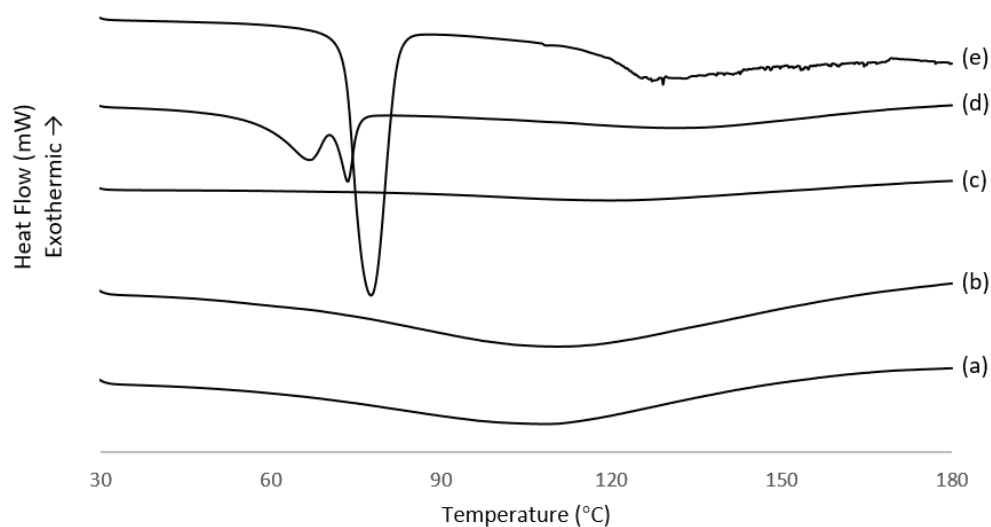


Figure 5-8. DSC curves of (a) chitosan (CS), (b) pectin (PEC), (c) CS-PEC scaffold, (d) 10% w/v lidocaine hydrochloride-loaded (LDC-10) CS-PEC scaffold and (e) LDC.

In order to evaluate the CS-PEC interaction in hydrogel, and the interaction between the drug LDC and CS-PEC hydrogel, samples were further analysed by FTIR spectroscopy.

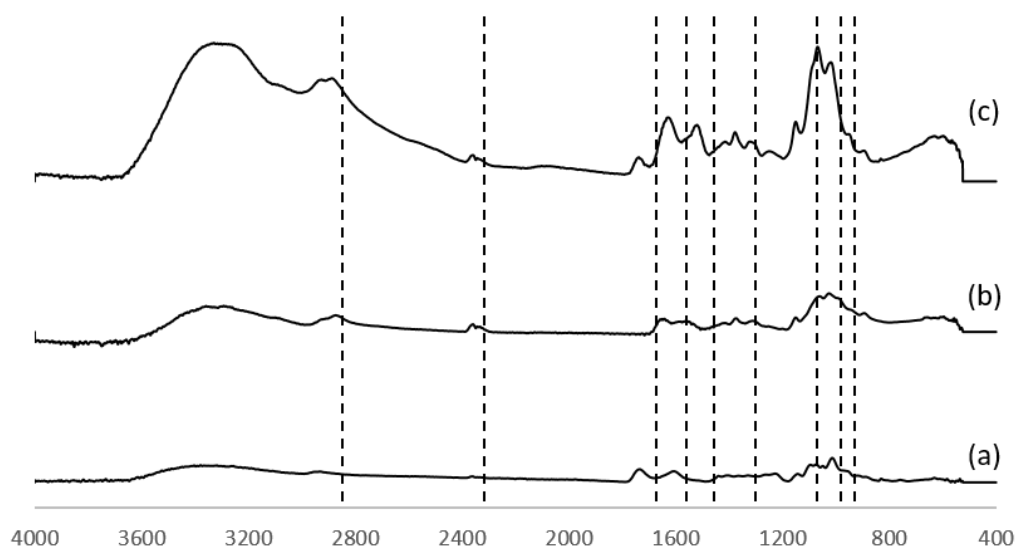


Figure 5-9. FTIR spectra of: (a) chitosan (CS), (b) pectin (PEC) and (c) CS-PEC scaffold.

The characteristic bands of CS showed NH stretching vibrations overlapped with hydrogen-bonded OH groups in the region of  $3700\text{--}3000\text{ cm}^{-1}$  while CH stretching vibrations at  $2909$  and  $2872\text{ cm}^{-1}$  in the region of  $3000\text{--}2800\text{ cm}^{-1}$ . The bands at  $1652\text{ cm}^{-1}$  and  $1590\text{ cm}^{-1}$  correspond to the carbonyl stretching (C=O) of amide I and N-H bending of amide II vibration, respectively (Kim et al., 2003; Kowalonek, 2017; Neufeld & Bianco-Peled, 2017; Tentor et al., 2017). For PEC, the broad band in the region of  $3700\text{--}3000\text{ cm}^{-1}$  indicates the presence of hydrogen-bonded OH groups. PEC showed the characteristic band of C=O vibration of methyl esterified carboxyl group at  $1738\text{ cm}^{-1}$ , strong absorption band around  $1606\text{ cm}^{-1}$  belonging to the asymmetric stretching vibration of  $\text{COO}^-$ , and the band around  $1408\text{ cm}^{-1}$  of  $-\text{COO}^-$  symmetric stretching vibration (Gnanasambandam & Proctor, 2000; T. H. Kim, Park, Kim, & Cho, 2003; Kowalonek, 2017; Neufeld & Bianco-Peled, 2017; Sinitsya, Čopíková, Prutyanov, Skoblya, & Machovič, 2000; Tentor et al., 2017). For the CS-PEC complex, the broadened and increased band intensity of the OH vibration region may indicate the formation of hydrogen bonds between OH groups of CS and PEC (Kowalonek, 2017), which is shown in Figure 5-10. The band at  $1738\text{ cm}^{-1}$  (C=O vibration from the ester groups in PEC) has no change in the position, indicating that the ester group did not participate in the molecular interaction (Kowalonek, 2017). The thermoreversible gelation mechanism of CS-PEC hydrogel (as shown in Figure 5-10) is possibly due to: i) formation of hydrogen bond when cooled and breakage of hydrogen bond when heated (Ventura & Bianco-Peled, 2015) and ii) electrostatic attractions between negatively charged carboxylate groups in PEC and positively charged amino groups in CS when pH is lower than the isoelectric points (IP) of CS (4.9-7.1) and higher than the IP of PEC (3.5) (Kowalonek, 2017). Considering the pH

of CS-PEC gel mixture is around 1.7, no polyelectrolyte complex is expected to form in this study as the both of CS and PEC chains are positively charged (Kowalonek, 2017; Nordby et al., 2003). The lack of change at  $1738\text{ cm}^{-1}$ , representing the ester groups in PEC, also confirms no electrostatic interactions were formed between CS and PEC chains. All these observations suggest that the gelation of CS-PEC hydrogel was due to hydrogen bond interaction as marked in Figure 5-10.

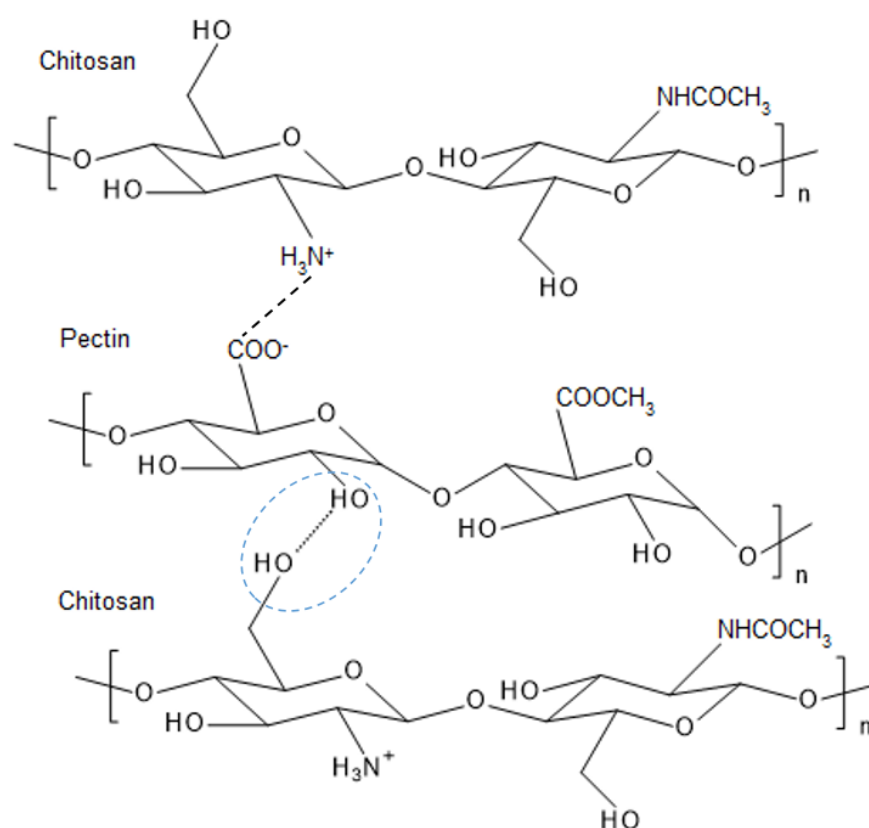


Figure 5-10. Physical interactions between chitosan (CS) and pectin (PEC) polysaccharides.

Regarding LDC, the drug showed a sharp band at  $1655\text{ cm}^{-1}$  representing the carbonyl group ( $\text{C}=\text{O}$ ) stretching of the amide group (Abu-Huwaij, Assaf, Salem, & Sallam, 2007; Kevadiya, Joshi, Mody, & Bajaj, 2011; Kochhar et al., 2013; Sawant, Luu, Ye, & Buchta, 2010). Other two characteristic bands of LDC at  $1477\text{ cm}^{-1}$  and  $1543\text{ cm}^{-1}$  were also observed, corresponding to C-N stretching and the one with higher energy

was due to the bond with higher inductive effect (O-C-N) (Abu-Huwaij et al., 2007; Kevadiya et al., 2011; Kochhar et al., 2013; Sawant et al., 2010). At higher drug loadings (LDC-5 and LDC-10), the characteristic bands of LDC become more prominent in the hydrogel-drug samples (Figure 5-11). All characteristic bands of LDC were presented in the LDC-loaded CS-PEC hydrogels without any noticeable change in band position indicating that LDC did not interact with CS and PEC polysaccharides. This result obtained from DSC and FTIR studies demonstrate that though the recrystallisation of drug was affected during the encapsulation, gel formation and freeze-drying processes, the drug was physically entrapped in the hydrogel matrix without losing the functional groups of LDC, indicating the functional stability of LDC was well maintained in the hydrogel carrier.

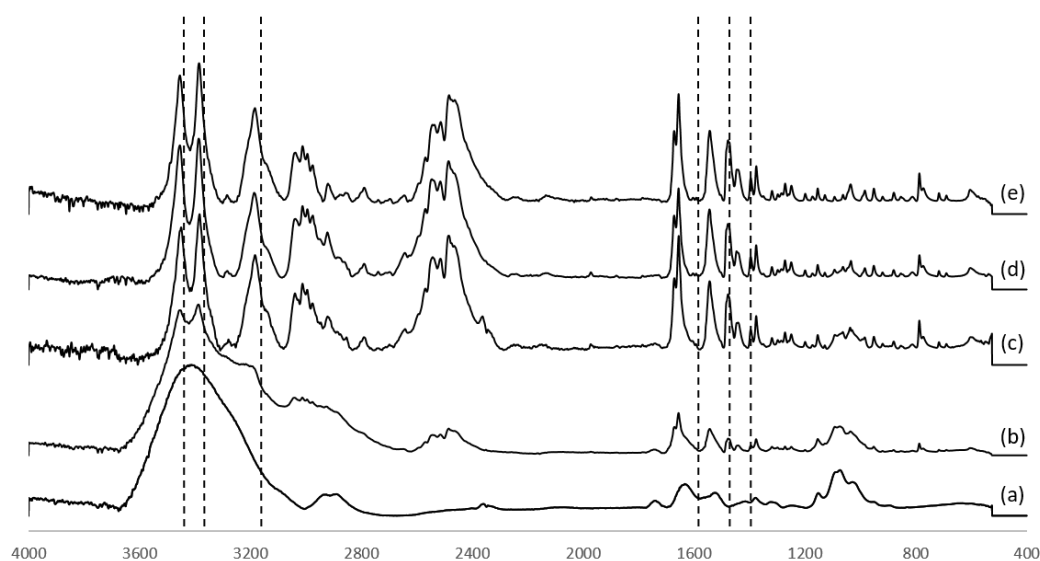


Figure 5-11. FTIR spectra of: (a) lidocaine hydrochloride-free (LDC-0), (b) 2% w/v LDC-loaded (LDC-2), (c) 5% w/v LDC-loaded (LDC-5), (d) 10% w/v LDC-loaded (LDC-10) chitosan-pectin (CS-PEC) scaffolds and (e) LDC.

### 5.3.5. Evaluation of *in vitro* drug release studies

*In vitro* drug release profiles of 3D printed CS-PEC lyophilised hydrogel scaffolds with different amounts of LDC were obtained in PBS buffer. The release data presented in Figure 5-12 indicates that all formulations are capable of controlling release of drug over a period about 4 h.

All formulations showed a burst release in 1 h, followed by a sustained release in the subsequent 4 h with final release reaching 88, 91 and 94% in LDC-2, LDC-5 and LDC-10, respectively. The burst release over 1 h in the formulations would provide an effective pain relief when applied to fresh wound. Considering the half-life of LDC (120 min), it would be recommended for fresh epidermal wounds which require an immediate pain management. The porous structure of CS-PEC hydrogel, as shown in Figure 5-5, contributes to the fast release of entrapped LDC as the pores form channels for solvent uptake leading to LDC dissolution. Meanwhile, the sponge-like structure of the hydrogel carrier also promotes the solvent uptake and controls the release of LDC for up to 5 h. Another contributing factor to the fast drug release is the degradation of CS-PEC hydrogels, which was observed along with the release study. Considering the degradation rate, it would be recommended to change the dressing every 2-4 hours after applying on wounds. Due to its thermosensitive nature, the raised temperature (37°C) leads to the partial breakage of hydrogen bonds between CS and PEC chains, resulting in the sectional dissolution of the CS-PEC hydrogel matrixes. This can bring a benefit that the adhesion of hydrogel dressings would be reduced during the drug release, which is ideal for wound dressings as they can be easily removed from the skin without incurring any trauma or damage to the newly formed sensitive epithelial cells (Boateng et al., 2008).



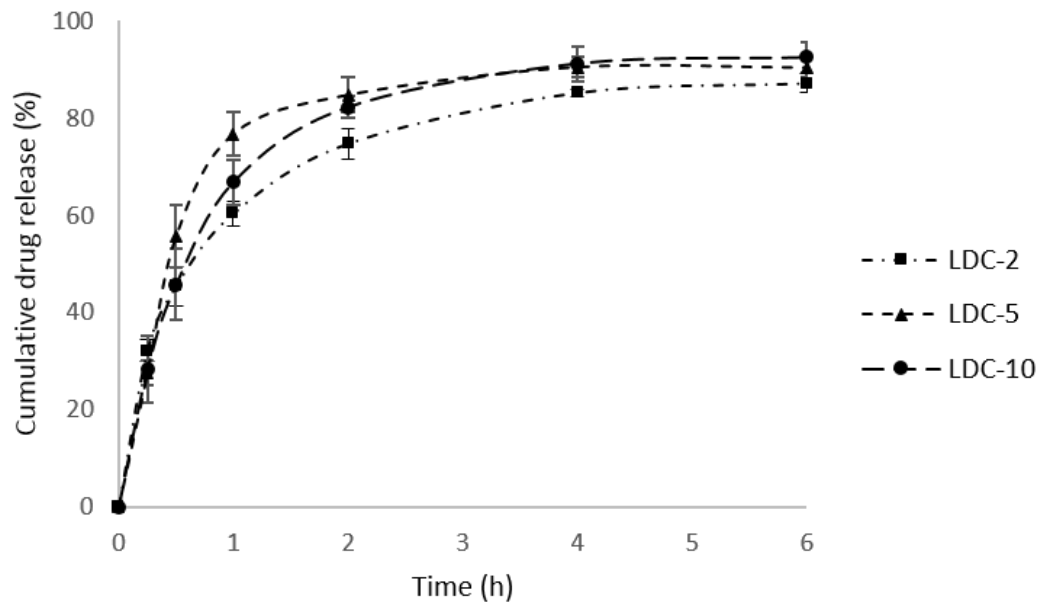


Figure 5-12. *In vitro* drug release of lidocaine hydrochloride (LDC) drug from 3D printed chitosan-pectin (CS-PEC) hydrogel scaffolds with different amount of drug loadings ( $n=3 \pm \text{SD}$ ).

The drug release data were fitted to the models to analyse release kinetics and mechanism from the 3D printed CS-PEC hydrogel formulations. The kinetic rate constant ( $k$ ), the correlation coefficient ( $R^2$ ) and the release exponent ( $n$ ) are reported in Table 5-2.

All formulations were best fitted in Korsmeyer–Peppas model ( $R^2=0.9656$ ,  $0.9992$  and  $0.9938$  for LDC-2, LDC-5 and LDC-10, respectively), which is used to describe the diffusion of a penetrant solute in a swellable polymer matrix (Dash et al., 2010; Shaikh et al., 2015; Juergen Siepmann & Peppas, 2011). Korsmeyer–Peppas model (also called The Power Law) is typically applied to a porous system of a swelled polymer that sorbs the solvent and desorbs the loaded drug along with the dissolution of the polymer matrix (Shaikh et al., 2015; J Siepmann & Peppas, 2001). The porous structure was identified by SEM in all formulations, while the swelling study showed a high water absorption ability which facilitates the solvent uptake and drug dissolution. Along with the release test, the dissolution of hydrogel scaffolds was

observed as the increased temperature (37°C) promotes the breakage of hydrogen bonds and correspondingly the partial degradation of CS-PEC hydrogels.

In this model, the value of exponent “ $n$ ” indicates the release mechanism of drug. For the case of thin film, i) when  $n=0.5$ , corresponds to a Fickian dissuasion mechanism; ii) when  $0.5 < n < 1$ , an anomalous transport (both Fickian and Case-II) is implied; iii) when  $n=1$ , a Case-II transport is suggested and iv) when  $n > 1$ , a supper Case-II transport applied (Ofokansi & Kenechukwu, 2013; Juergen Siepmann & Peppas, 2011). In this study, the values of the exponent “ $n$ ” were above 1, indicating a supper Case-II transport of erosion-controlled manner was dominated in the drug release. A reason that could account for the identified super Case-II transport is the thermosensitivity of CS-PEC hydrogel carrier, as the increased temperature at 37°C promoted the degradation and erosion of the hydrogel polymer matrix along with drug release.

Table 5-2. Mathematical model of kinetics parameters of lidocaine hydrochloride (LDC) release from 3D printed chitosan-pectin (CS-PEC) hydrogel scaffolds.

Formulation	Zero-order		First-order		Higuchi		Hixson-Crowell		Korsmeyer-Peppas		
	K <sub>o</sub>	R <sup>2</sup>	K <sub>1</sub>	R <sup>2</sup>	K <sub>H</sub>	R <sup>2</sup>	K <sub>HC</sub>	R <sup>2</sup>	n	K <sub>KP</sub>	R <sup>2</sup>
LDC-2	11.486	0.6658	0.3227	0.8752	34.702	0.8913	0.3432	0.8138	1.0500	1.1736	0.9656
LDC-5	11.522	0.5425	0.3678	0.7548	36.313	0.7904	0.3698	0.6843	1.1937	1.0114	0.9992
LDC-10	12.604	0.6546	0.4265	0.8826	38.15	0.8796	0.4185	0.8148	1.1549	1.0320	0.9938

\*: For Korsmeyer–Peppas model, the first 60% of the normalised drug was considered in calculation.

## 5.4. Conclusion

In this study, a 3D printed biodegradable thermosensitive CS-PEC scaffolds were developed for wound dressing applications. The CS-PEC scaffolds showed good printability and the final lyophilised wound dressings exhibited good physical integrity and flexibility. In the swelling and water absorption assessments, the 3D printed hydrogels showed the ability to absorb exudates and maintain a moist environment for wounds with high ESW values of 2832% and 2265%, as well as 97% and 96% of water absorption in absence (LDC-0) or presence of drug (LDC-10), respectively. Correspondingly, the higher porosity and reduction of pore size was observed in the LDC-10 samples. The 3D printed dressings also showed self-adhesion to skin with bioadhesion strength in the range of 86.5-126.9 g, which is matching the marketed wound dressings. DSC study showed formation of hydrogen bonds between CS and PEC results in a better organisation of polymer chains, and freeze-drying process successfully reduced the moisture content in the CS-PEC hydrogel and ensures the presence of LDC in the crystalline form within the lyophilised hydrogels. FTIR results indicate that the CS-PEC hydrogels were formed due to hydrogen bonding interactions, and LDC incorporated in the hydrogels maintained its functional stability as no significant interaction was detected between LDC and CS-PEC hydrogels. *In vitro* drug release assessment showed that all formulations presented a fast but controlled release of LDC over 5 h. The drug release kinetics of those formulations were best fitted the Korsmeyer–Peppas model, indicating the erosion of polymer along with drug release, which offers a benefit for wound dressing as the adhesion strength would reduce, therefore, minimising tissue damage or scar generation during changing of wound dressings. All these properties indicate that the

3D printed and lyophilised CS-PEC scaffolds could be used as a suitable candidate for wound dressings and could open up the opportunity for developing future personalised wound managements.

## 5.5. Reference:

- Abu-Huwaij, R., Assaf, S., Salem, M., & Sallam, A. (2007). Mucoadhesive dosage form of lidocaine hydrochloride: I. Mucoadhesive and physicochemical characterization. *Drug development and industrial pharmacy*, 33(8), 855-864.
- Ahmed, S., & Ikram, S. (2016). Chitosan based scaffolds and their applications in wound healing. *Achievements in the Life Sciences*, 10(1), 27-37.
- Archana, D., Dutta, J., & Dutta, P. (2013). Evaluation of chitosan nano dressing for wound healing: Characterization, in vitro and in vivo studies. *International journal of biological macromolecules*, 57, 193-203.
- Boateng, J. S., Matthews, K. H., Stevens, H. N., & Eccleston, G. M. (2008). Wound healing dressings and drug delivery systems: a review. *Journal of pharmaceutical sciences*, 97(8), 2892-2923.
- Croisier, F., & Jérôme, C. (2013). Chitosan-based biomaterials for tissue engineering. *European Polymer Journal*, 49(4), 780-792.
- Dash, S., Murthy, P. N., Nath, L., & Chowdhury, P. (2010). Kinetic modeling on drug release from controlled drug delivery systems. *Acta Poloniae Pharmaceutica*, 67(3), 217-223.
- Gethin, G. (2007). The significance of surface pH in chronic wounds. *Wounds uk*, 3(3), 52.
- Gnanasambandam, R., & Proctor, A. (2000). Determination of pectin degree of esterification by diffuse reflectance Fourier transform infrared spectroscopy. *Food chemistry*, 68(3), 327-332.
- Gosain, A., & DiPietro, L. A. (2004). Aging and wound healing. *World journal of surgery*, 28(3), 321-326.

- Huang, X., & Brazel, C. S. (2001). On the importance and mechanisms of burst release in matrix-controlled drug delivery systems. *Journal of Controlled Release*, 73(2-3), 121-136.
- Jin, S. G., Kim, K. S., Kim, D. W., Kim, D. S., Seo, Y. G., Go, T. G., . . . Choi, H.-G. (2016). Development of a novel sodium fusidate-loaded triple polymer hydrogel wound dressing: Mechanical properties and effects on wound repair. *International journal of pharmaceutics*, 497(1-2), 114-122.
- Kaur, A., & Kaur, G. (2012). Mucoadhesive buccal patches based on interpolymer complexes of chitosan–pectin for delivery of carvedilol. *Saudi Pharmaceutical Journal*, 20(1), 21-27.
- Kevadiya, B. D., Joshi, G. V., Mody, H. M., & Bajaj, H. C. (2011). Biopolymer–clay hydrogel composites as drug carrier: host–guest intercalation and in vitro release study of lidocaine hydrochloride. *Applied Clay Science*, 52(4), 364-367.
- Khurma, J. R., Rohindra, D. R., & Nand, A. V. (2006). Synthesis and properties of hydrogels based on chitosan and poly (vinyl alcohol) crosslinked by genipin. *Journal of Macromolecular Science, Part A: Pure and Applied Chemistry*, 43(4-5), 749-758.
- Kim, T. H., Park, Y. H., Kim, K. J., & Cho, C. S. (2003). Release of albumin from chitosan-coated pectin beads in vitro. *International journal of pharmaceutics*, 250(2), 371-383.
- Klode, J., Schöttler, L., Stoffels, I., Körber, A., Schadendorf, D., & Dissemond, J. (2011). Investigation of adhesion of modern wound dressings: a comparative analysis of 56 different wound dressings. *Journal of the European Academy of Dermatology and Venereology*, 25(8), 933-939.

- Kochhar, J. S., Lim, W. X. S., Zou, S., Foo, W. Y., Pan, J., & Kang, L. (2013). Microneedle integrated transdermal patch for fast onset and sustained delivery of lidocaine. *Molecular pharmaceutics*, 10(11), 4272-4280.
- Kowalonek, J. (2017). Studies of chitosan/pectin complexes exposed to UV radiation. *International journal of biological macromolecules*, 103, 515-524.
- Kumari, A., Yadav, S. K., & Yadav, S. C. (2010). Biodegradable polymeric nanoparticles based drug delivery systems. *Colloids and surfaces B: Biointerfaces*, 75(1), 1-18.
- Lee, C. H., & Bae, Y. C. (2015). Effect of salt on swelling behaviors of thermosensitive hydrogels: applicability of the nonrandom contact model. *Macromolecules*, 48(12), 4063-4072.
- Long, J., Gholizadeh, H., Lu, J., Bunt, C., & Seyfoddin, A. (2017). Application of fused deposition modelling (FDM) method of 3D printing in drug delivery. *Current pharmaceutical design*, 23(3), 433-439.
- Long, J., Nand, A. V., Ray, S., Mayhew, S., White, D., Bunt, C. R., & Seyfoddin, A. (2018). Development of customised 3D printed biodegradable projectile for administering extended-release contraceptive to wildlife. *International journal of pharmaceutics*, 548(1), 349-356.
- Mallepally, R. R., Bernard, I., Marin, M. A., Ward, K. R., & McHugh, M. A. (2013). Superabsorbent alginate aerogels. *The Journal of Supercritical Fluids*, 79, 202-208.
- Mishra, R. K., Datt, M., & Banthia, A. K. (2008). Synthesis and characterization of pectin/PVP hydrogel membranes for drug delivery system. *Aaps Pharmscitech*, 9(2), 395-403.



- Neufeld, L., & Bianco-Peled, H. (2017). Pectin–chitosan physical hydrogels as potential drug delivery vehicles. *International journal of biological macromolecules*, 101, 852-861.
- Nordby, M. H., Kjøniksen, A.-L., Nyström, B., & Roots, J. (2003). Thermoreversible gelation of aqueous mixtures of pectin and chitosan. *Rheology. Biomacromolecules*, 4(2), 337-343.
- Ofokansi, K. C., & Kenechukwu, F. C. (2013). Formulation development and evaluation of drug release kinetics from colon-targeted ibuprofen tablets based on Eudragit RL 100-chitosan interpolyelectrolyte complexes. *International Scholarly Research Notices: Pharmaceutics*, 2013.
- Okan, D., Woo, K., Ayello, E. A., & Sibbald, G. (2007). The role of moisture balance in wound healing. *Advances in skin & wound care*, 20(1), 39-53.
- Ray, S., & Cooney, R. P. (2018). Thermal degradation of polymer and polymer composites *Handbook of Environmental Degradation of Materials* (Third ed., pp. 185-206): Elsevier.
- Reis, C. P., Neufeld, R. J., & Veiga, F. (2017). Preparation of Drug-Loaded Polymeric Nanoparticles *Nanomedicine in Cancer* (pp. 197-240): Pan Stanford.
- Repka, M. A., Gutta, K., Prodduturi, S., Munjal, M., & Stodghill, S. P. (2005). Characterization of cellulosic hot-melt extruded films containing lidocaine. *European Journal of Pharmaceutics and Biopharmaceutics*, 59(1), 189-196.
- Sawant, P. D., Luu, D., Ye, R., & Buchta, R. (2010). Drug release from hydroethanolic gels. Effect of drug's lipophilicity (log P), polymer–drug interactions and solvent lipophilicity. *International journal of pharmaceutics*, 396(1-2), 45-52.

- Shaikh, H. K., Kshirsagar, R., & Patil, S. (2015). Mathematical models for drug release characterization: a review. *World Journal Of Pharmacy And Pharmaceutical Sciences*, 4(04), 324-338.
- Shakespeare, P. (2001). Burn wound healing and skin substitutes. *Burns*, 27(5), 517-522.
- Sibbald, R., Williamson, D., Orsted, H., Campbell, K., Keast, D., Krasner, D., & Sibbald, D. (2000). Preparing the wound bed--debridement, bacterial balance, and moisture balance. *Ostomy/Wound Management*, 46(11), 14-22.
- Siepmann, J., & Peppas, N. (2001). Modeling of drug release from delivery systems based on hydroxypropyl methylcellulose (HPMC). *Advanced drug delivery reviews*, 48(2-3), 139-157.
- Siepmann, J., & Peppas, N. A. (2011). Higuchi equation: derivation, applications, use and misuse. *International journal of pharmaceutics*, 418(1), 6-12.
- Sinitsya, A., Čopíková, J., Prutyanov, V., Skoblya, S., & Machovič, V. (2000). Amidation of highly methoxylated citrus pectin with primary amines. *Carbohydrate polymers*, 42(4), 359-368.
- Snyder, R. J., Fife, C., & Moore, Z. (2016). Components and quality measures of DIME (devitalized tissue, infection/inflammation, moisture balance, and edge preparation) in wound care. *Advances in skin & wound care*, 29(5), 205.
- Tamburic, S., & Craig, D. Q. (1997). A comparison of different in vitro methods for measuring mucoadhesive performance. *European Journal of Pharmaceutics and biopharmaceutics*, 44(2), 159-167.
- Tentor, F. R., de Oliveira, J. H., Scariot, D. B., Lazarin-Bidoia, D., Bonafe, E. G., Nakamura, C. V., . . . Martins, A. F. (2017). Scaffolds based on chitosan/pectin

thermosensitive hydrogels containing gold nanoparticles. *International journal of biological macromolecules*, 102, 1186-1194.

Vellayappan, M., Venugopal, J., Ramakrishna, S., Ray, S., Ismail, A., Mandal, M., . . . Jaganathan, S. (2016). Electrospinning applications from diagnosis to treatment of diabetes. *Royal Society of Chemistry Advances*, 6(87), 83638-83655.

Ventura, I., & Bianco-Peled, H. (2015). Small-angle X-ray scattering study on pectin–chitosan mixed solutions and thermoreversible gels. *Carbohydrate polymers*, 123, 122-129.

Wittaya-areekul, S., Prahsarn, C., & Sungthongjeen, S. (2006). Development and in vitro evaluation of chitosan-Eudragit RS 30D composite wound dressings. *AAPS PharmSciTech*, 7(1), E215-E220.

Wu, J. C.-C., Ray, S., Gizdavic-Nikolaidis, M., Uy, B., Swift, S., Jin, J., & Cooney, R. P. (2014). Nanostructured bioactive material based on polycaprolactone and polyaniline fiber-scaffolds. *Synthetic Metals*, 198, 41-50.

## Chapter 6

*Development of a long-term contraceptive implant with levonorgestrel loaded chitosan microspheres embedded in poly (vinyl alcohol) hydrogel*

Manuscript prepared as:

Long, J., Etxeberria, A. E., Nand, A. V., Bunt, C. R., Kornelsen, C., Ray, S., & Seyfoddin, A. (2019). Development of a long-term contraceptive implant with levonorgestrel loaded chitosan microspheres embedded in poly (vinyl alcohol) hydrogel. Submitted to the Journal of *American Chemical Society (ACS) Applied Bio Materials*, under review. .

## 6.1. Introduction

Oral hormonal contraceptives have been used for women fertility control for more than five decades (Shulman, 2011) using a combination of progestogen and oestrogen or the progestogen-only pill. A preference for the progestogen-only pill has emerged as a result of increased risk of venous thrombosis associated with oestrogen use (Shulman, 2011; Stegeman et al., 2013). Both of these oral contraceptives require daily dosing and are associated with variable plasma concentrations. Therefore, several extended release formulations of progesterone/progestin have been developed to address the above issues over the past five decades. Long-term contraceptives, such as intravaginal rings (IVRs), intrauterine devices (IUDs), subdermal implants and transdermal patches, have been designed to effectively prevent unplanned pregnancy and improve female reproductive health (Friend, 2016). However, these implants may be associated with the following drawbacks: i) devices, such as IUDs, are expensive and can cause discomfort to patients (Manoukian et al., 2018) and ii) non-biodegradable implants require surgical removal and the retrieval surgery may be more traumatic than the initial insertion (Croxatt, 2002; Ma, Song, Sun, Yang, & Leng, 2006; Shulman, 2011; Shulman, Nelson, & Darney, 2004). Thus, recent efforts have focused on the development of long-term biodegradable contraceptive devices that can avoid both daily ingestion and eliminate the requirement of retrieval.

Biodegradable microsphere drug reservoirs, formulated using natural or synthetic polymers, have been used for sustained release of different contraceptive drugs (Freiberg & Zhu, 2004; Friend, 2016; Manoukian et al., 2018; L. Wu, Janagam, Mandrell, Johnson, & Lowe, 2015). Emulsion-based crosslinking methods have been widely used to prepare microspheres for controlled drug delivery systems, including

i) short-term release microspheres such as pullulan-PVA microspheres emulsion crosslinked by GA to release pirfenidone in lung in 24 hours (Soni & Ghosh, 2017), CS microspheres crosslinked by GA for pirfenidone nasal delivery in six hours (Kashikar, Dhole, Kandekar, & Khose, 2014), and acrylamide grafted locust bean gum (Am-g-LBG) and PVA microspheres for buflomedil hydrochloride oral delivery in 12 hours; ii) sustained release microspheres such as poly( $\epsilon$ -caprolactone) (PCL) microspheres with LNG for long-term release of 120 days (Dhanaraju, Vema, Jayakumar, & Vamsadhara, 2003; Manoukian et al., 2018), poly(lactic-co-glycolic acid) (PLGA) microspheres coated with PVA hydrogel for sustained DEX release in one month (Hickey et al., 2002). The drug release behaviour from microsphere systems, such as the release rate, duration of action, initial burst release and overall *in vitro/in vivo* correlation, can be altered by the microsphere composition, crosslinking method/density, particle size, shape, molecular weight, the drug loading and distribution, and the fabrication and sterilisation processes (Buntner et al., 1998; Jameela, Kumary, Lal, & Jayakrishnan, 1998; Machado, Lunardi, Tristão, & Marchetti, 2009; S. Wang et al., 2005; L. Wu et al., 2015). Taking above-mentioned into account, in this study CS, a natural biodegradable polysaccharide obtained by alkaline deacetylation of chitin, was crosslinked by GA and synthesised as a microsphere reservoir for the contraceptive drug LNG. The aldehyde-crosslinking of CS introduced by GA was used to decrease the biodegradation rate of the polymer matrix and so, to control LNG release behaviour from the microspheres since it has been reported that GA-crosslinked CS can be used as a long acting drug carriers (Ahsan et al., 2017; El-Feky, Sharaf, El Shafei, & Hegazy, 2017; Jameela et al., 1998;

Poon, Wilson, & Headley, 2014; Sinha et al., 2004; Szymańska & Winnicka, 2015; Yu et al., 2017; Zou, Zhao, Ye, Wang, & Li, 2015).

Diffusion- and/or erosion-controlled release mechanisms from microsphere reservoirs can lead to extended release of loaded drugs for a period of weeks or months. However, microspheres alone generally lack the ability to precisely deliver drugs for long-term due to their relatively large surface area leading to increased drug release as well as increased degradation rates (Manoukian et al., 2018; L. Wu et al., 2015). Additionally, the possible migration of injectable microspheres from the site of injection may be a concern (L. Wu et al., 2015). To overcome these disadvantages, in this study the LNG-CS microspheres were furthermore compartmentalised into a PVA hydrogel matrix. There is a growing interest in using biodegradable polymers as the host matrix for encapsulating drug and bioactive compounds (Long et al., 2018; Vellayappan et al., 2016; Wu et al., 2014). In fact, PVA is a hydrophilic, non-toxic, biodegradable and biocompatible polymer and its hydrogels have found various pharmaceutical and biomedical uses as synthetic articular cartilages (Hassan & Peppas, 2000; Kenawy, Kamoun, Eldin, & El-Meligy, 2014; Kobayashi, Chang, & Oka, 2005), wound dressings (Fan, Yang, Yang, Peng, & Hu, 2016; Kamoun, Kenawy, & Chen, 2017) and drug delivery systems (G. Chang et al., 2015; Wei Chen, Hou, Tu, Gao, & Haag, 2017; J. K. Li, Wang, & Wu, 1998; Mallapragada, Peppas, & Colombo, 1997; West et al., 2014). Furthermore, PVA hydrogels have been used as coatings for microspheres to prolong or modify the release behaviours of the incorporated drugs (Bhardwaj, Sura, Papadimitrakopoulos, & Burgess, 2007; Bhardwaj, Sura, Papadimitrakopoulos, & Burgess, 2010; Galeska et al., 2005; Shen & Burgess, 2012). In this study, PVA hydrogel was physically crosslinked by a

repeated cycle of freezing at  $-20^{\circ}\text{C}$  and thawing at room temperature followed by an annealing treatment at  $130^{\circ}\text{C}$  to increase the crystallinity and stability of the matrix. Annealing is a heat treatment that can alter physical and/or chemical properties and in this case can increase the mechanical strength of PVA (K. Chen et al., 2018). It has been reported that freeze-thaw crosslinked and annealed PVA hydrogels can enhance mechanical properties and stability of the final product (Fukumori & Nakaoki, 2013, 2015).

That said, the aim of this study was to develop an optimised formulation with zero-order drug release pattern for long-term contraceptive delivery and to evaluate the effect of different controlling factors on optimising the formulation. The specific objectives of this study were: i) to incorporate LNG into GA crosslinked CS microspheres; ii) to synthesise physically crosslinked and annealed PVA hydrogel to incorporate LNG-CS microspheres and iii) to optimise the formulations by characterising the physical/chemical properties of this system and evaluating *in vitro* drug release.

In this study, the following two aspects were primarily investigated as control parameters: i) influence of microsphere size and PVA concentration on drug loading and drug release rate; and ii) influence of post-processing (annealing) on gel swelling. Based on these two aspects, an optimised formulation and processing condition is suggested as an outcome of this study: LNG-CS microspheres in the size range of  $125\text{-}300\text{ }\mu\text{m}$  embedded in 20% PVA hydrogel treated with five cycles of freeze-thaw process and annealing treatment. After optimisation, FTIR and DSC were used to



characterise and investigate the effect of crosslinking, crystallinity on gel swelling and drug release rate as well as possible interaction between the drug and polymers.

## 6.2. Materials and methods

### 6.2.1. Materials

Levonorgestrel (LNG) was purchased from Flem Pharma (Shanghai, China), PVA powder (hydrolysis: 98.5-99.2%) from Hangzhou Colorcom Impex Co., Ltd. (Hangzhou, China) and Sunflower oil from Countdown (Auckland, New Zealand). High molecular weight chitosan (CS, MW: 310000-375000 Da), phosphate buffered saline (PBS) tablets, glutaraldehyde (GA) (Grade II, 25% in H<sub>2</sub>O), Span® 80 (viscosity 1000-2000 mPa.s), ethanol (absolute, for HPLC, ≥99.8%), toluene (analytical standard), sodium hydroxide (≥98%, anhydrous pellets) and acetic acid (analytical standard) were obtained from Sigma-Aldrich (Auckland, New Zealand). All other used chemicals were analytical grade.

### 6.2.2. Microspheres and hydrogel preparation

#### 6.2.2.1. Microspheres formulation

CS microspheres with/without LNG were prepared by a water-in-oil emulsion method (Jameela et al., 1998; Zou et al., 2015). CS solution (2% w/v) was prepared under acidic condition (1% v/v acetic acid). LNG powder was accurately weighed and added into CS solution to obtain a 10% w/v concentration. The mixture was homogenised under stirring at 1000 rpm for 30 min. The homogenised emulsion (30 mL) was gradually dropped into an oil bath (300 mL) with 4.5 mL Span 80 as emulsifier under consistent stirring for spherulitising. Glutaraldehyde-saturated toluene (GST) (60 mL) was immediately added to crosslink the microsphere under stirring and an additional 12mL GA (25%) was rapidly added at the end of 30 min in order to minimise loss of drug. After solidification, microspheres were collected by centrifugation and washed twice with 10 ml of 0.1N sodium hydroxide to remove the residues of GA and oil.

The particles were then washed three times with 10 ml deionised water and subjected to vacuum drying at room temperature. CS microspheres without LNG were prepared as control.

#### 6.2.2.2. Hydrogel preparation

PVA hydrogels were prepared via physical crosslinking introduced by freeze-thaw cycles (Fukumori & Nakaoki, 2013, 2014, 2015; Hassan & Peppas, 2000; Xiao & Yang, 2006). PVA powder was accurately weighed and dissolved in distilled water at 85°C for 2h (three concentrations were prepared: 10, 15 and 20% w/v). PVA solutions were cooled to room temperature before the following treatments. LNG-CS microspheres (125-300  $\mu\text{m}$ ) were accurately weighed (microsphere concentration in PVA solution: 5.71 mg/ml) and mixed with PVA solutions under stirring at room temperature. These mixtures were transferred into 24-well plate moulds (Sigma-Aldrich, New Zealand) and immediately frozen by liquid nitrogen to avoid sedimentation of the microspheres. Subsequently, all samples were treated with five cycles of freeze-thaw processes (16 h of freezing at -20°C and 8 h of thaw at room temperature) and finally vacuum dried at room temperature. Subsequently, samples were annealed at 130°C for 2 h. Each PVA hydrogel contained 8.8 mg of LNG. Microsphere-free PVA hydrogels were prepared as control.

#### 6.2.3. Morphological assessment

The particle size range analysis and collection of size fragments were carried out using standard test sieves (63, 125 and 300  $\mu\text{m}$ ; FRITSCH, Germany). The percent weight distribution was plotted against size range (Jameela et al., 1998). The particle size distributions of microspheres from each size range were determined using a Malvern

Mastersizer particle size analyser (Hydro2000, Malvern Panalytical, United Kingdom). Measurements were repeated in triplicate and presented as mean  $\pm$  SD. Polydispersity Index (PDI) of the microspheres was calculated based on Eq.(6-1) (Clayton, Salameh, Wereley, & Kinzer-Ursem, 2016):

$$PDI = \left(\frac{\sigma}{d}\right)^2 \quad (6-1)$$

where  $\sigma$  is the standard deviation (SD) of the particle diameter distribution, and  $d$  is the mean particle diameter.

Surface and cryo-fractured cross-section scanning electron images of microspheres and hydrogels were obtained using a Schottky field emission SEM (SU-70, Hitachi, United Kingdom) under a working voltage of 5 kV. Prior to SEM, samples were placed on metallic stubs and coated with platinum under vacuum for 100 seconds for microspheres and 20 seconds for hydrogels using an ion sputter coater (E-1045, Hitachi, United Kingdom) for visualisation.

#### 6.2.4. Drug loading

To assess the drug loading of LNG-CS microspheres and PVA hydrogels, the microspheres (or powdered PVA hydrogels with microspheres) were accurately weighed and dispersed in 10 mL absolute ethanol. The samples were sonicated in an ice bath for 3 min with 20% output power (450w) using an Ultrasonic Processor (FS-450N, Ultrasonics, China) and subsequently filtered with a 0.45  $\mu$ m Teflon syringe filter (F2500-3, Thermo Scientific, United States). LNG was analysed by high performance liquid chromatography (HPLC) using LC-20AT liquid chromatography LC-20AT HT auto sampler, DGU-20A5 degasser, RF-10A XL UV/VIS detector (Shimadzu USA manufacturing Inc, USA) equipped with a GraceSmart RP 18, 3  $\mu$ m,

50 mm x 2.1 mm reverse phase chromatography column. A mixture of acetonitrile: 0.1% formic acid in water (33:67) was used as mobile phase at a flow rate of 1 mL/min and injection volume of 2  $\mu$ L with UV detection at 240 nm. A chromatogram of LNG peak is shown in Figure 6-1. A calibration curve ( $Y=1.406 \times 10^{-4}X$ ,  $R^2=0.9998$ ) was obtained with standard solutions of 0, 0.125, 0.25, 0.50, 1.00, 2.00, 4.00, 8.00 and 16.00  $\mu$ g/mL.”

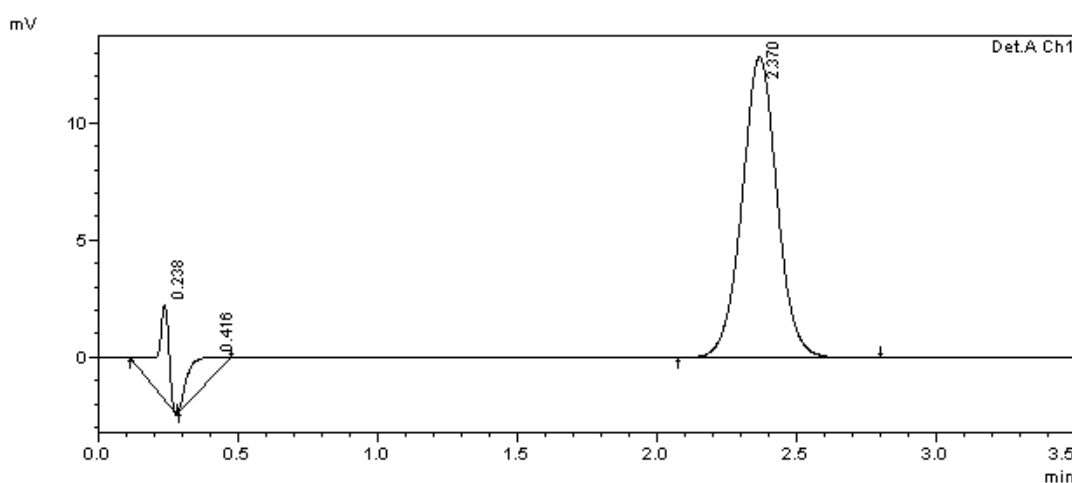


Figure 6-1. The chromatogram obtained with LNG peak eluting at 2.370 mins.

The measurements were repeated in triplicate and presented as mean  $\pm$  SD. Drug loading was determined using Eq.(6-2) (D. Li et al., 2013; Shen & Burgess, 2012):

$$\text{Drug loading (\%)} = \frac{\text{weight of drug}}{\text{weight of polymer} + \text{drug}} \times 100 \quad (6-2)$$

### 6.2.5. Swelling and water absorption of PVA hydrogel

The equilibrium swelling ratio (ESR) of PVA hydrogels with/without LNG-CS microspheres in deionised water at room temperature was determined using a gravimetric method (Khurma et al., 2006). Samples were weighed and submerged in the swelling medium. At predetermined time intervals, samples were withdrawn and blotted with tissue paper to remove the extra surface water. The blotted samples were

immediately weighed to determine the wet weight. The experiments were continued until equilibrium was achieved. The measurements were repeated in triplicate and presented as mean  $\pm$  SD. The  $E_{SR}$  was calculated using Eq.(6-3):

$$E_{SR}(\%) = \frac{W_t - W_d}{W_d} \times 100 \quad (6-3)$$

where  $W_t$  is the weight of wet hydrogel at a particular time (t),  $W_d$  is the weight of dry hydrogel before swelling. The equilibrium water content (EWC) was calculated using Eq.(6-4):

$$E_{WC}(\%) = \frac{W_e - W_d}{W_e} \times 100 \quad (6-4)$$

where  $W_e$  is the weight of hydrogel at equilibrium state.

### 6.2.6. *In vitro* drug release

*In vitro* LNG release from CS microspheres and microsphere-embedded PVA hydrogels were studied in a simulated physiologically medium (PBS buffer, pH=7.4) under sink conditions. For the LNG-CS microspheres, samples were accurately weighed and inserted into a dialysis membrane (cut off 3500 MWCO) bag to avoid floating. The dialysis bag was filled with 1 mL PBS buffer and then placed in a screw top tube containing 49 mL PBS buffer. For the microsphere-hydrogel samples, drug release was studied in 50 mL PBS buffer solution. All samples were shaken at 100 rpm at 37°C. At predetermined time intervals, 20 mL of the incubation media from each sample was collected and an equal amount of fresh media was added into each release system to maintain the total volume and sink conditions. The concentration of LNG in the release media was determined by HPLC as described in Section 2.4. The cumulative amount of LNG released was plotted against time for each sample. LNG-

free CS microspheres and microsphere-free PVA hydrogels were used as controls.

The experiment performed in triplicate with data presented as mean  $\pm$  SD.

### 6.2.7. Kinetic models

To study the release kinetics and mechanism of LNG release from microsphere and microsphere-hydrogel systems, data fitted to the below models:

Zero-order model (Dash et al., 2010):

$$Q_t = Q_0 + K_0 t \quad (6-5)$$

where  $Q_t$  is the amount of drug released at time  $t$ ,  $Q_0$  is the initial amount of drug in the solution, and  $K_0$  is the zero-order release constant expressed in the units of concentration/time. Zero-order model describes a system where the release rate of incorporated drug is independent of its concentration (Shaikh et al., 2015).

Korsmeyer–Peppas model (Dash et al., 2010):

$$Q_t/Q_\infty = K_{KP} t^n \quad (6-6)$$

where  $Q_t/Q_\infty$  is a fraction of drug released at time  $t$ ,  $K_{KP}$  is the release rate constant and  $n$  is the release exponent. This relationship describes drug release from a polymeric system such as hydrogel. Only data up to 60% drug release was used to fit into this kinetic model.

### 6.2.8. Spectral analysis of chemical interactions

Fourier-transform infrared (FTIR) spectroscopy was used to characterise the presence of specific chemical groups and their interactions in the samples using a Nicolet iS10 FTIR spectrophotometer (Thermo Scientific, USA) in attenuated total reflectance

(ATR) mode using a diamond ATR crystal. The spectra of the samples were recorded in the range of 4000-400  $\text{cm}^{-1}$  with an average of 64 scans at a resolution of 4  $\text{cm}^{-1}$ .

#### 6.2.9. Differential scanning calorimetry (DSC) analysis

The crystallinity and thermal properties of hydrogels and microspheres were characterised using DSC (DSC Q1000, TA Instruments, New Zealand). The samples were weighed and sealed in aluminium pans before the DSC test. The tests were performed under nitrogen atmosphere at a heating rate of 10  $^{\circ}\text{C}/\text{min}$  between the temperature range of 30-250  $^{\circ}\text{C}$ .



## 6.3. Results and discussion

### 6.3.1. Characterisation of CS microspheres

As a first step for the development of hybrid hydrogels, the CS microspheres were prepared by GA crosslinking by the Schiff base reaction between amino groups of CS and aldehyde groups of GA (Zou et al., 2015). The Schiff base reaction can happen intermolecularly or intramolecularly to form a polymer network leading to the formation of CS microspheres (Figure 6-2). This process enabled to load the drug LNG within these CS microspheres as described in section 6.2.2.1. The micro-emulsion process resulted in spherical size particles as shown in Figure 6-3. In absence of drug, the CS microsphere had smooth surface morphology. However, after drug loading it became relatively rough. After microsphere incorporation into PVA hydrogel, LNG-CS microspheres remained spherical as shown in Figure 6-4 e.

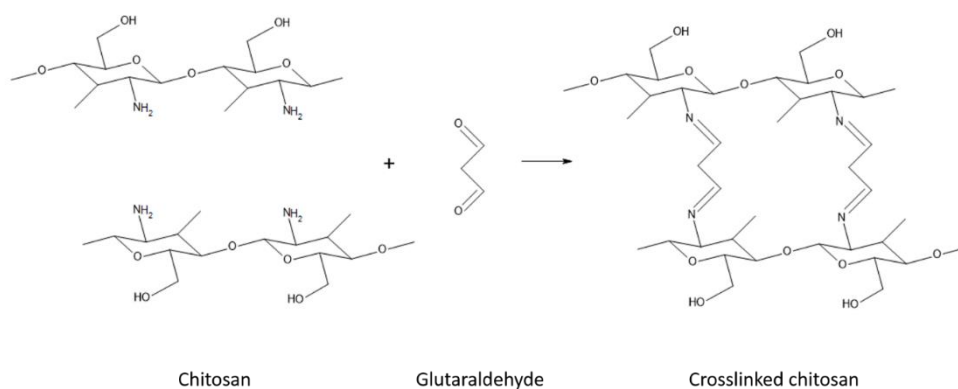


Figure 6-2. Aldehyde-crosslinking reaction of chitosan (CS) by glutaraldehyde (GA).

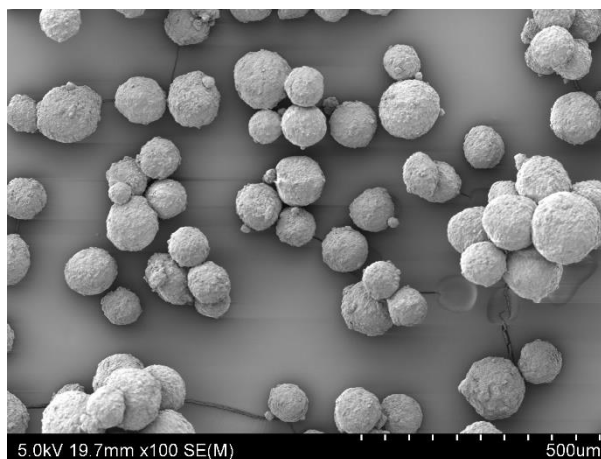


Figure 6-3. SEM micrograph of Levonorgestrel (LNG)-loaded and glutaraldehyde (GA)-crosslinked chitosan (CS) microspheres in the size range of 125-300  $\mu\text{m}$ .

As can be seen in Figure 6-3, all CS microspheres were spherical in shape. Smaller microspheres below the size range were found to adhere to larger microspheres. Regarding microsphere surface characteristics, LNG-free CS microspheres (Figure 6-4 a, c) appeared smoother compared to LNG-CS microspheres (Figure 6-4 b, d, f) which had a rough surface. These can be related to the drug molecules themselves, which were being physically entrapped in the CS matrix and presented a phase separation due to their hydrophobic property.

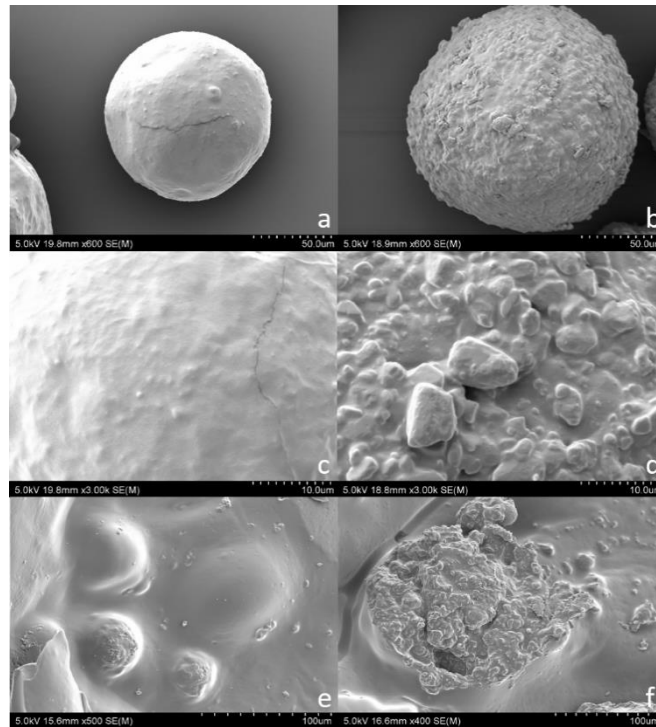


Figure 6-4. SEM micrographs of a) levonorgestrel (LNG)-free chitosan (CS) microsphere, b) LNG-loaded CS microsphere, c) surface of LNG-free CS microsphere, d) surface of LNG-loaded CS microsphere, e) LNG-loaded CS microsphere embedded in poly (vinyl alcohol) (PVA) hydrogel and f) cross-section of LNG-CS microsphere.

The dry CS-LNG microspheres produced by this micro-emulsion process followed by vacuum drying were separated into three size fractions  $<63\ \mu\text{m}$ ,  $63\text{--}125\ \mu\text{m}$ ,  $125\text{--}300\ \mu\text{m}$  using a standard sieving procedure. The weight fraction of dry microsphere are summarised in Table 6-1. Majority of these microspheres were below  $300\ \mu\text{m}$ , while only 1.81% of the microspheres were larger than  $300\ \mu\text{m}$  size. Out of these three fractions ( $<300\ \mu\text{m}$ ), 72% was between  $125\text{--}300\ \mu\text{m}$ , 15% was between  $63\text{--}125\ \mu\text{m}$  and 11% was smaller than  $63\ \mu\text{m}$ .

Particle size distribution of these three separated fractions were determined using Malvern Mastersizer particle size analyser in aqueous medium. As a result, the particles were hydrated and expanded in size. The average diameter of hydrated microspheres from each size ranges was  $113$ ,  $151$  and  $188\ \mu\text{m}$  corresponding to dry

microspheres <63  $\mu\text{m}$ , between 63-125  $\mu\text{m}$  and between 125-300  $\mu\text{m}$ , respectively (Table 6-1).

PDI values of the microspheres in the size range of <63, 63-125 and 125-300  $\mu\text{m}$  were  $1.23 \times 10^{-4}$ ,  $2.25 \times 10^{-4}$  and  $2.81 \times 10^{-5}$ , respectively (Figure 6-5), much less than 0.1 (Clayton et al., 2016). Hence, the particle size distribution analysis suggests that the micro-emulsion process was capable of forming monodispersed microspheres in all these three size ranges with good uniformity.

Table 6-1. Particle size parameters of levonorgestrel (LNG)-loaded chitosan (CS) microspheres.

	Size range ( $\mu\text{m}$ )	Fraction (%)	Average hydrated diameter ( $\mu\text{m}$ )
Microsphere	<63	$10.72 \pm 0.59$	$112.54 \pm 1.25$
	63-125	$15.44 \pm 0.74$	$151.03 \pm 2.26$
	125-300	$72.02 \pm 1.51$	$188.08 \pm 1.00$

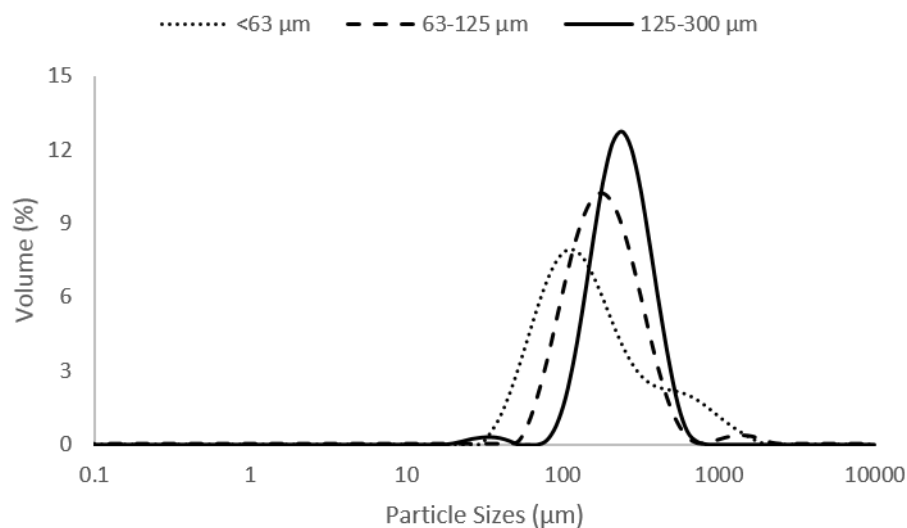


Figure 6-5. Particle size distribution of levonorgestrel (LNG)-loaded chitosan (CS) microsphere from different size ranges: dotted line represents microspheres < 63  $\mu\text{m}$ , dashed line represents microspheres of 63-125  $\mu\text{m}$  and solid line represents microspheres of 125-300  $\mu\text{m}$ .

The effect of drug loading in these microspheres were further evaluated and the results are presented in Table 6-2. There is a noticeable increment in drug loading by increasing the microsphere size.

Table 6-2. Drug loading of chitosan (CS) microspheres and poly (vinyl alcohol) (PVA) hydrogels.

	Formulation	Drug loading (%)
Microsphere	<63 $\mu\text{m}$	$56.93 \pm 6.47$
	63-125 $\mu\text{m}$	$68.58 \pm 5.64$
	125-300 $\mu\text{m}$	$77.12 \pm 6.53$
Microsphere-hydrogel	10% PVA	$3.71 \pm 0.75$
	15% PVA	$3.05 \pm 0.07$
	20% PVA	$2.74 \pm 0.05$

As a final step for developing the hybrid hydrogel, these drug loaded microspheres (LNG-CS) were encapsulated in PVA hydrogel. Various PVA concentrations were used to prepare these hybrid hydrogels. At a given microsphere size range (125-300  $\mu\text{m}$ ), increasing the PVA concentration decreased the drug loading capacity (Table 2). Hence, both microsphere size and the concentration of PVA are found to be the controlling factors for optimising the drug loading and to formulate the hybrid hydrogels.

### 6.3.2. Characterisation of the hydrogel

In this study, PVA hydrogels were prepared through freeze-thaw cycling since it has been reported that freeze-thaw cycling can significantly increase water stability of PVA hydrogels (Fukumori & Nakaoki, 2013, 2014, 2015; Kamoun et al., 2017; Kenawy et al., 2014; L. Zhang et al., 2011). Aqueous solutions of PVA prepared with different PVA concentrations were subjected to five freeze-thaw cycles and the crosslinking was achieved physically by the crystallisation step. Translucent and elastic PVA hydrogels were formed with well-maintained cylinder shape as shown in Figure 6-6 a. Vacuum drying shrunk the structure due to water-loss, however, the cylindrical geometry was maintained. As shown in Figure 6-6 c, the incorporation of

CS microspheres introduced light yellowish colour in the PVA hydrogels due to the inherent colour of CS. After annealing treatment, the coloration of CS was promoted by the high temperature as the dry heating produced chromophores related to the crosslinking of  $\text{NH}_2$  groups in CS (Lim, Khor, & Ling, 1999).

Whilst high hydrolysis grade PVA powder (98.5-99.2%) and relatively high concentrations (10-20% w/v) of PVA is sufficient for the preparation of hydrogels by one treatment cycle of freeze-thaw nevertheless, all hydrogels were treated with five freeze-thaw cycles. Increasing freeze-thaw cycles have been reported to improve the stability of PVA hydrogel and slow down drug release (Fukumori & Nakaoki, 2013, 2014; Galeska et al., 2005). This could be because small crystallites formed during the freeze-thaw treatment in the gel may act as nucleation sites for crystallisation during the water-evaporation process (Fukumori & Nakaoki, 2015). Thus, in this study the crystallinity of PVA hydrogels was enhanced by five freeze-thaw cycles. Consequently, a more compact internal structure was obtained as the polymer chains were packed with crystals with reduced internal spaces. An annealing process was subsequently applied to increase the crystallinity by introducing the aggregation of the PVA polymer chains and consequently increase the crystal regions (Fukumori & Nakaoki, 2014).

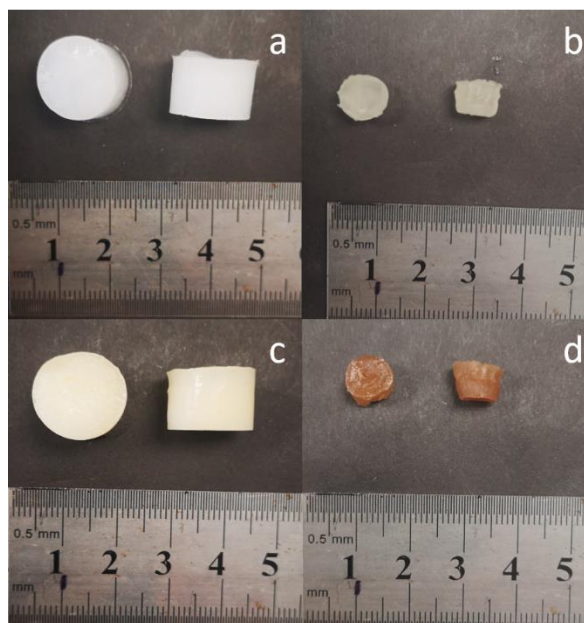


Figure 6-6. Poly (vinyl alcohol) (PVA) hydrogel scaffolds (PVA concentration:15%): a) Microsphere-free fresh hydrogel after five freeze-thaw cycles, b) Microsphere-free dried hydrogel after annealing, c) microspheres-loaded (125-300  $\mu\text{m}$ ) fresh hydrogel after five freeze-thaw cycles and d) microspheres-loaded (125-300  $\mu\text{m}$ ) dried hydrogel after annealing.

All PVA hydrogels prepared with five freeze-thaw cycles had sufficient structural integrity to be physically handled. The internal microstructures were examined by SEM as shown in Figure 6-7. Increasing PVA concentrations resulted in noticeable morphological changes in the internal structure of hydrogels. In fact, higher PVA concentration resulted in reduced porosity due to a higher crosslinking density.

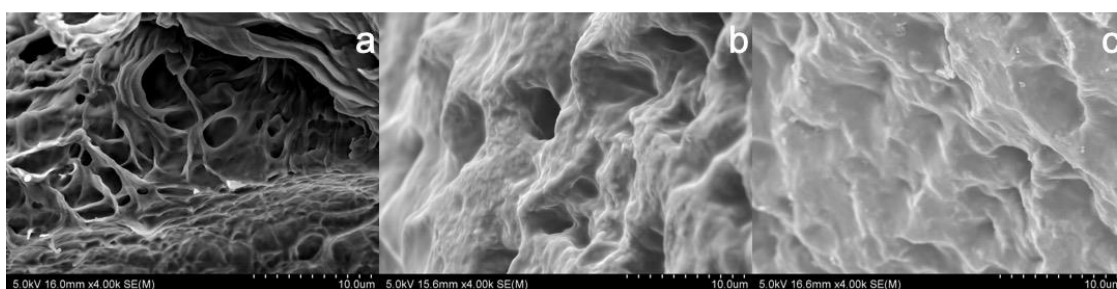


Figure 6-7. SEM micrographs of dried and annealed poly (vinyl alcohol) (PVA) hydrogels prepared with different PVA concentrations: a) 10%, b) 15% and c) 20% w/v.

### 6.3.3. Swelling studies

One of the important parameters of a hydrogel-based drug delivery system is its swelling behaviour as it has a significant effect on the release rate of incorporated

drugs. Swelling of hydrogels is mainly caused by the free-water (water molecules that don't take part in hydrogel bonding with polymer molecules) content in a hydrogel (Khurma et al., 2006). The swelling degree of hydrogels depends on the crosslinking density and degree of crystallinity in the hydrogel (Abitbol, Johnstone, Quinn, & Gray, 2011). In this study, various PVA concentrations were used to prepare the hydrogels. The drug loaded microspheres (LNG-CS) were encapsulated in PVA hydrogel followed by freeze-thawing process to control the drug release rate and to achieve the dimensional stability of the gel. The gels were further processed by annealing treatment to fine tune the drug release rate and the dimensional stability. Effects of different parameters, such as PVA concentrations, annealing treatment and loading of microspheres on the swelling behaviours and water content of PVA hydrogel scaffolds were investigated to optimise the hydrogel formulation. As can be seen in Figure 6-8, the annealing process significantly reduced the swelling capacity of hydrogels due to the presence of physical interactions in the matrix and increased crystallinity, as shown by FTIR and DSC. This behaviour was not notably affected by the incorporation of microspheres into formulations.



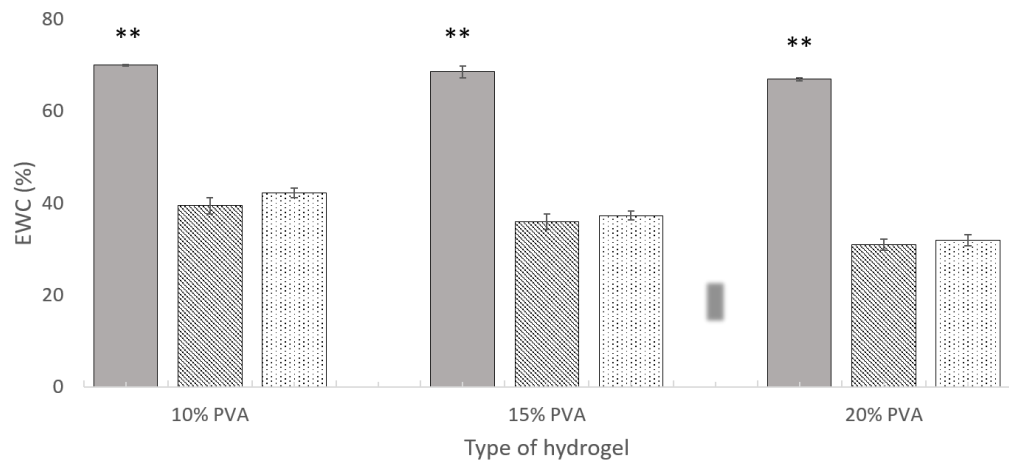


Figure 6-8. Equilibrium water content (EWC) of poly (vinyl alcohol) (PVA) hydrogels: solid bars correspond to the unannealed PVA hydrogels without microspheres, gradient-filled bars correspond to the annealed PVA hydrogels without microspheres and dot-filled bars correspond to the annealed PVA hydrogels with microspheres ( $n=3 \pm \text{SD}$ ). \*\*:  $p < 0.01$ .

The effect of PVA concentration on the water content and degree of swelling are shown in Figure 6-8 and Figure 6-9 respectively. Hydrogels with lower PVA concentrations exhibited faster swelling rate and higher water-absorbing capacity. The hydrogels prepared with lowest PVA concentration (10% PVA) reached equilibrium swelling state (232%) in 72 h while the highest (20% PVA) took about 144 h to reach 202%. The EWC of these PVA hydrogels were 70, 69 and 67% for 10, 15 and 20% PVA content, respectively (Figure 6-8). The higher crosslinking density and reduced porosity in the hydrogels with increasing PVA concentrations can explain their reduced swelling rate and lower water absorbency, which is validated with the observations of reduced porosity in higher PVA concentrations in SEM (Figure 6-7).

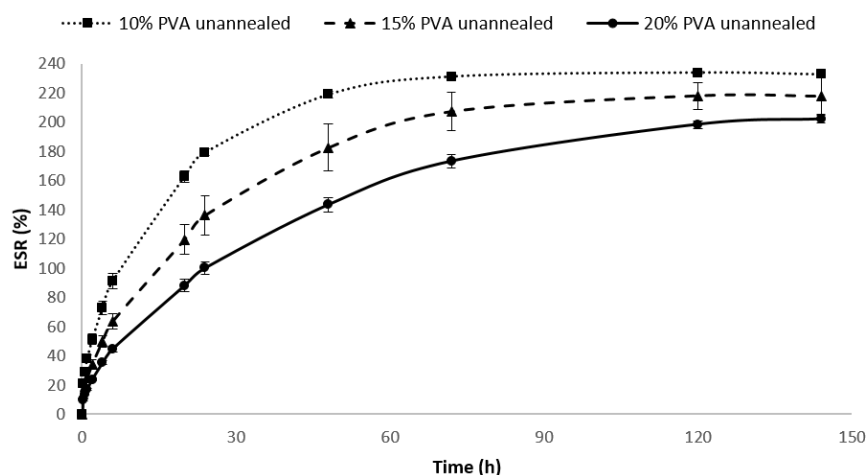


Figure 6-9. Equilibrium swelling ratio (ESR) of unannealed poly (vinyl alcohol) (PVA) hydrogels prepared by five cycles of freeze-thawing without microspheres: dotted line represents 10% PVA hydrogel, dashed line represents 15% PVA hydrogel and solid line represents 20% PVA hydrogel ( $n=3 \pm \text{SD}$ ).

The effect of annealing treatment on the swelling degree of PVA hydrogels is shown in Figure 6-9 and Figure 6-10. Compared to unannealed hydrogels (Figure 6-9), the PVA hydrogels with annealing treatment showed significantly reduced swelling degree and water content. After annealing, the ESR dropped down to 65, 56 and 45% (Figure 6-10) while the EWC values were decreased to 40, 36 and 31% for 10, 15 and 20% PVA content, respectively (Figure 6-8). The annealing process results in the formation of crystal regions in the hydrogels, which is confirmed by DSC results. These crystalline regions can act as nucleation sites to hold molecules more closely, subsequently resulting in a denser hydrogel structure with lesser free-water molecules to penetrate into the gel network (K. Chen et al., 2018; Park et al., 2012). This finding supports the observations in DSC, where the degree of crystallinity was enhanced by annealing treatment.

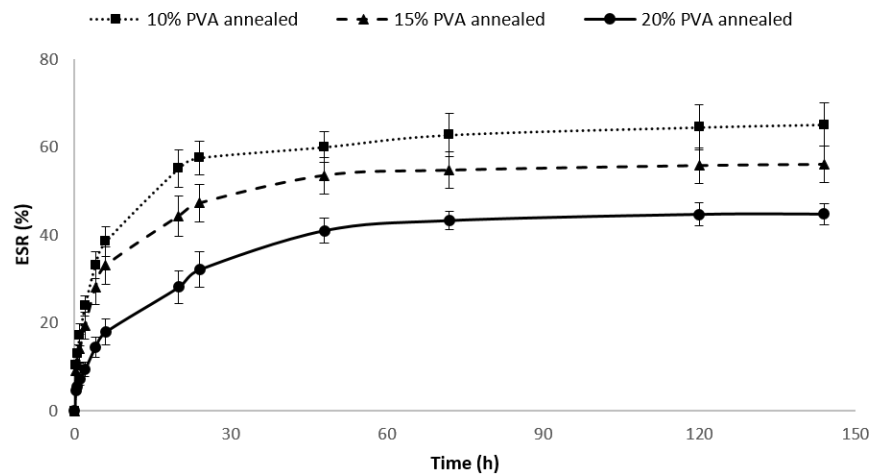


Figure 6-10. Equilibrium swelling ratio (ESR) of freeze-thawed followed by annealed hydrogels without microspheres: dotted line represents 10% PVA hydrogel, dashed line represents 15% PVA hydrogel and solid line represents 20% PVA hydrogel ( $n=3 \pm \text{SD}$ ).

The swelling behaviours of PVA hydrogels loaded with LNG-CS microspheres are shown in Figure 6-11. Compared to microsphere-free hydrogels, the swelling degree and EWC of microsphere-loaded PVA hydrogels stay at equal level with only a slight increase. A Paired Two Sample for Means T-Test to identify the difference in ESR and EWC between microsphere-free and microsphere-loaded PVA hydrogels indicate that microsphere-loaded PVA hydrogels exhibit a greater degree of swelling than microsphere-free hydrogels while there was no significant difference in the final water content ( $p$  values for ESR:  $1.82 \times 10^{-4}$ ,  $7.96 \times 10^{-3}$  and  $7.55 \times 10^{-4}$ ; for EWC: 0.065, 0.498 and 0.589 for 10, 15 and 20% PVA, respectively). For microsphere-loaded hydrogels, the ESR values were 73, 60 and 47%, and the EWC 42, 38 and 32% for 10, 15 and 20% PVA hydrogels, respectively. This result indicates the microspheres made by crosslinked CS, as a material capable of swelling, contributes to improve the swelling of the hybrid system. However, due to the low weight percentage of microspheres and the restriction of surrounding PVA hydrogel matrix, the water content contribution from microspheres is minimal.

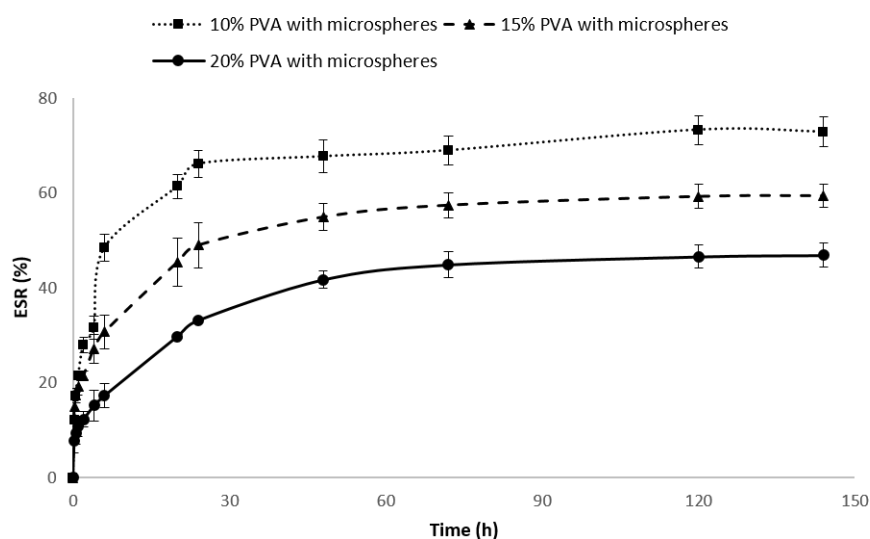


Figure 6-11. Equilibrium swelling ratio (ESR) of annealed poly (vinyl alcohol) (PVA) hydrogels prepared by five cycles of freeze-thawing with levonorgestrel (LNG)-chitosan (CS) microspheres: dotted line represents 10% PVA hydrogel, dashed line represents 15% PVA hydrogel and solid line represents 20% PVA hydrogel ( $n=3 \pm \text{SD}$ ).

#### 6.3.4. *In vitro* drug release

*In vitro* release profiles of LNG from microsphere systems are presented in Figure 6-12, indicating that all formulations showed sustained release over a period of 163 days. Particularly notable is the low burst release and near zero-order release pattern for all formulations, which can be attributed to the low solubility of LNG at experimental condition (in PBS buffer at pH 7.4) and the washing step when preparing microspheres which removed the surface drug. The release patterns from LNG-CS microspheres were inversely proportional to the size of microspheres. Release from microspheres of smaller size was faster and greater than that from microspheres of larger size. Small microspheres have shorter length of diffusion path for drug particles and larger surface area to volume ratio that provide a larger contact area with the release medium (Weiluan Chen, Palazzo, Hennink, & Kok, 2016). Over a period of 163 days, 44, 36 and 28% of LNG were released from the CS-LNG microspheres in the size ranges of <63, 63-125 and 125-300  $\mu\text{m}$ , respectively. Based on the exhibited

release profiles, the LNG-CS microspheres in size range of 125-300  $\mu\text{m}$  were chosen to be incorporated into PVA hydrogels to further prolong the release of LNG.

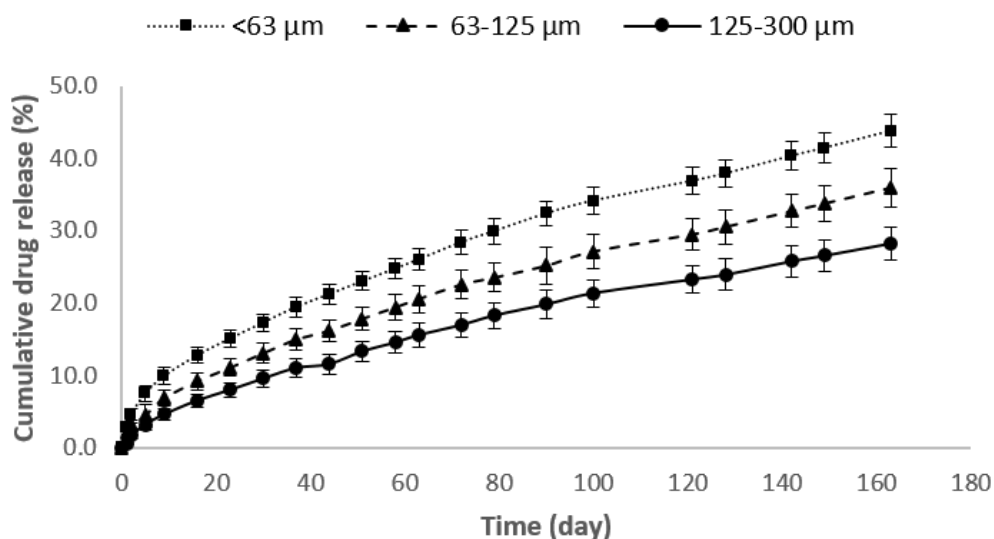


Figure 6-12. *In vitro* release of levonorgestrel (LNG) from microsphere system based on different size ranges of microspheres: dotted line represents microspheres < 63  $\mu\text{m}$ , dashed line represents microspheres of 63-125  $\mu\text{m}$  and solid line represents microspheres of 125-300  $\mu\text{m}$  ( $n=3 \pm \text{SD}$ ).

*In vitro* release of LNG from microsphere-hydrogel systems are shown in Figure 6-13, where more controlled and extended release profiles were obtained compared to the microsphere system alone. Similar to the release behaviours from microspheres, near zero-order release patterns without burst release were also observed in microsphere-hydrogel systems. As a comparison, the microsphere embedded in 20% PVA hydrogel released only 9% of LNG over a period of 100 days, whereas 22% of LNG was released from the same microspheres without incorporation into PVA hydrogel. This can be explained by PVA hydrogels acting as an additional barrier to release, elongating the diffusion pathway of the drug and limiting its contact with release medium. Another explanation is that the microcrystalline domains of PVA hydrogel may form at the surface of the microspheres as the microsphere can also acts as the nucleation site to promote the crystallisation of PVA in freeze-thawing process. In

this way, the crystallised PVA surroundings considerably diminished the accessibility of the release medium to the microspheres, and accordingly slowed down the polymer degradation and release rate of the drug (Galeska et al., 2005). The crystallisation was confirmed from DSC results. A small dosage of LNG can give effectively contraception such as Skyla implant which release 14  $\mu\text{g/day}$  for three-year contraception. This lower release from PVA hydrogels still provide a daily release of 16.7-20.1  $\mu\text{g/implant}$  in the first 23 days, followed by a consistent release of 7.05-7.80  $\mu\text{g/day/implant}$ . Basically two implants could provide enough therapeutic effect.

As shown in Figure 6-13, the release profiles from microsphere-hydrogel systems were affected by the PVA concentrations. Slower and lesser drug release was observed with higher concentrations of PVA. Over a period of 100 days, the microsphere-hydrogel systems released 14, 11 and 9 % of LNG from 10, 15 and 20% PVA hydrogels, correspondingly. The higher polymer concentration resulted in higher crosslinking density and crystallinity in the freeze-thawing process, which is in accordance with swelling and DSC studies. Consequently, a more compact structure was formed in these hydrogels (as shown in Figure 6-7) that entrapped the microspheres more tightly and hindered the contact of release medium or the diffusion of drug. Thus, 20% PVA would be suggested as the optimised formulation to prolong the drug release.

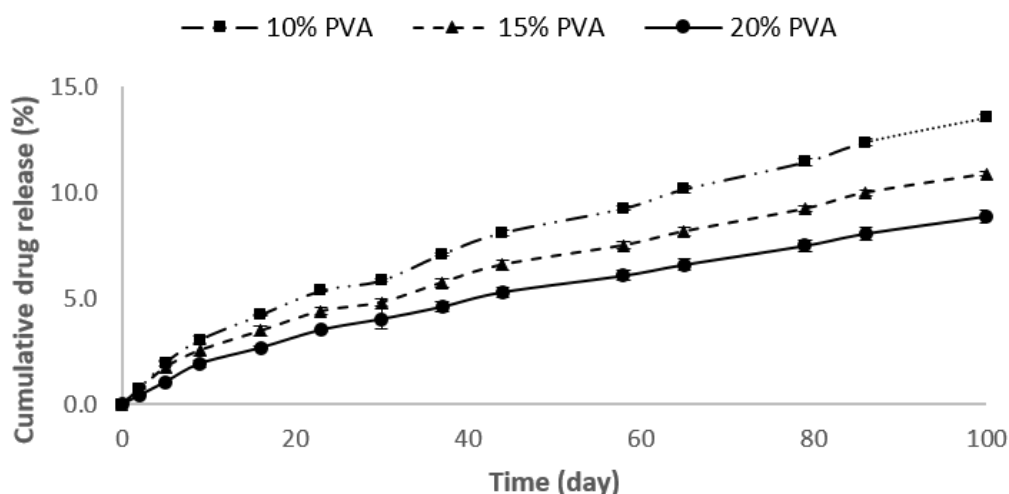


Figure 6-13. *In vitro* release of levonorgestrel (LNG) from microsphere-hydrogel system based on different poly (vinyl alcohol) (PVA) concentrations: dotted line represents 10% PVA hydrogel, dashed line represents 15% PVA hydrogel and solid line represents 20% PVA hydrogel ( $n=3 \pm \text{SD}$ ).

The development of zero-order release systems capable of delivering drugs for prolonged periods are necessary for various pharmaceutical applications. As shown in Figure 6-12 and Figure 6-13, approximately zero order release profiles were obtained in all formulations with  $R^2$  values as 0.9441, 0.9581 and 0.9646 for microsphere systems in the size range of <63, 63-125 and 125-300  $\mu\text{m}$ , and 0.9705, 0.9680 and 0.9686 for microsphere-hydrogel systems with 10, 15 and 20% PVA hydrogels, respectively. The release data were also fitted nicely into Korsmeyer-Peppas model, with  $R^2$  values as 0.9984, 0.9974 and 0.9770 for microsphere systems in the size range of <63, 63-125 and 125-300  $\mu\text{m}$ , and 0.9893, 0.9910 and 0.9877 for microsphere-hydrogel systems with 10, 15 and 20% PVA hydrogels, respectively. The Korsmeyer-Peppas model is typically applied to a hydrophilic and porous polymer system that sorbs the penetrant (water or solvent) and desorbs the incorporated drug (J Siepmann & Peppas, 2001). The values of the diffusional exponent “ $n$ ” determined the mechanism of LNG released from microsphere and microsphere-hydrogel systems: i) when  $n$  approximates to 0.45, a Fickian transport

(anomalous) is implied, indicating that the release is controlled by diffusion; ii) when  $0.45 < n < 0.89$ , a superposition of both phenomena (anomalous transport) is suggested; iii) when  $n = 0.89$ , zero order (case II transport) (Korsmeyer et al., 1983). In this study, the values of  $n$  are in the range of 0.45-0.89 (0.52, 0.56 and 0.71 for microsphere systems in the size range of <63, 63-125 and 125-300  $\mu\text{m}$ , and 0.69, 0.66 and 0.74 for microsphere-hydrogel systems with 10, 15 and 20% PVA hydrogels, respectively), indicating both Fickian transport and case II transport coexisted in the release profiles of LNG. As supported by SEM observations (Figure 6-7 and Figure 6-14), the porous structures existed in PVA hydrogels and microspheres act as the channels for the diffusion of incorporated drug, leading to a diffusion-controlled Fickian transport. The polymer relaxation caused by swelling of PVA and CS matrix resulted in the swelling-controlled case II transport. Based on these observations, the diffusion- and swelling- controlled release mechanisms may coexist for the controlled release of LNG from the microsphere and microsphere-hydrogel systems.



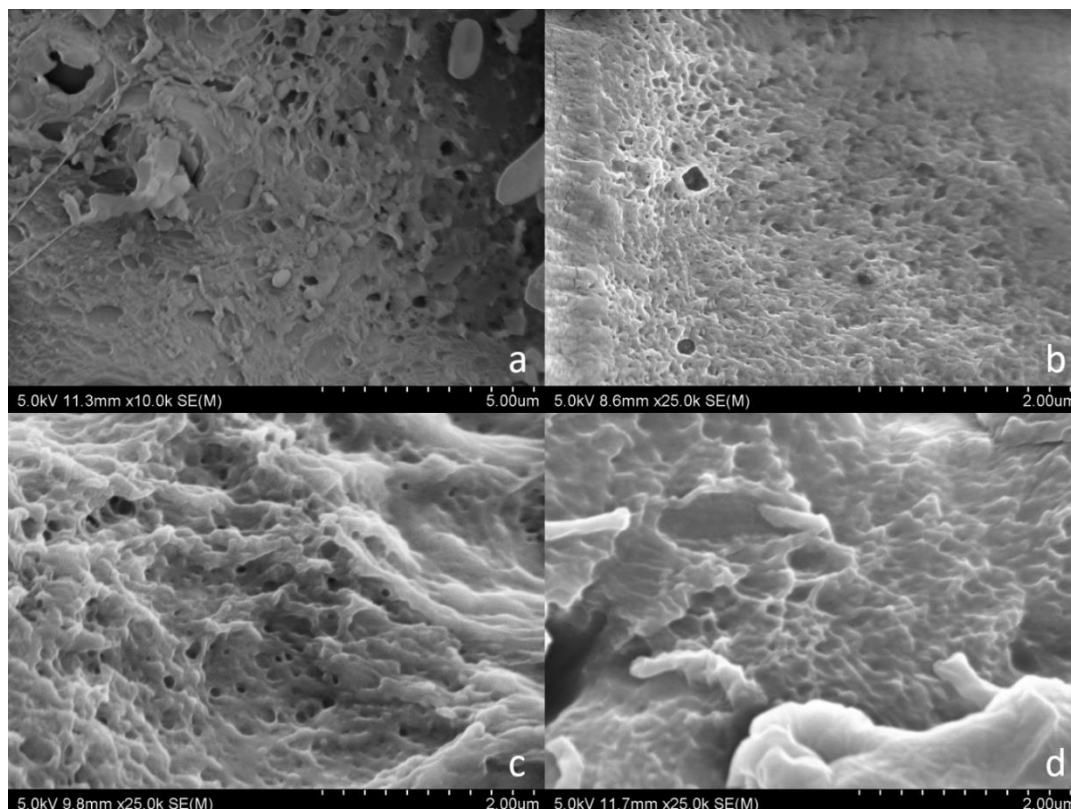


Figure 6-14. SEM micrographs of samples after dissolution test: a) levonorgestrel (LNG)-loaded chitosan (CS) microsphere, b) 10% poly(vinyl alcohol) (PVA) hydrogel, c) 15% PVA hydrogel and d) 20% PVA hydrogel.

### 6.3.5. Spectral analysis

Samples were analysed by FTIR (Figure 6-15) in order to characterise the presence of specific chemical groups from used chemicals and to identify interactions.

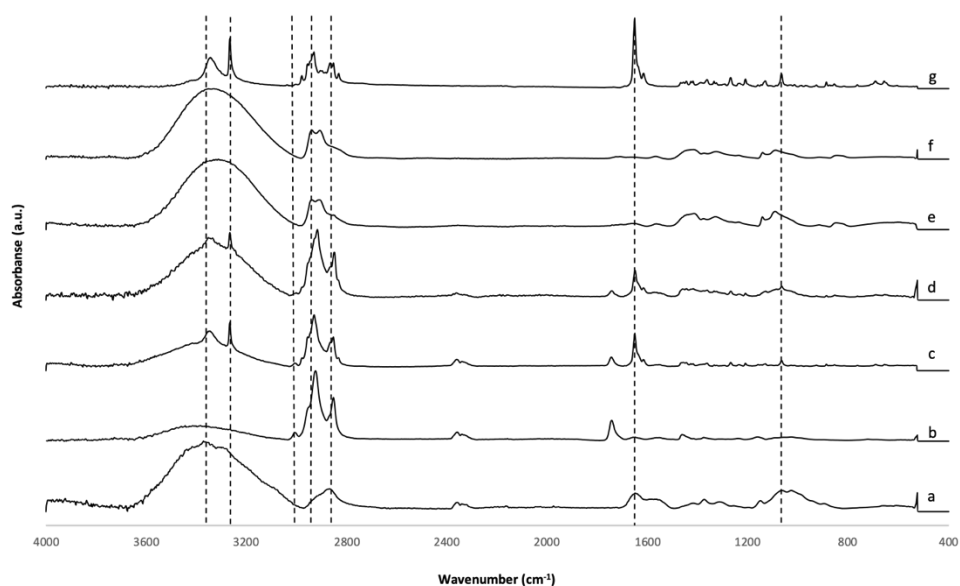


Figure 6-15. FTIR spectra of (a) chitosan (CS), (b) levonorgestrel (LNG)-free chitosan (CS) microspheres, (c) LNG-loaded CS microsphere, (d) LNG-loaded CS microsphere (125-300  $\mu\text{m}$ ) embedded in 20% poly (vinyl alcohol) (PVA) hydrogel, (e) 20% PVA hydrogel, (f) PVA and (g) LNG.

Pure CS (Figure 6-15 a) showed the characteristic bands:  $3372\text{ cm}^{-1}$  (O-H and N-H stretching vibration),  $2868\text{ cm}^{-1}$  (C-H stretching vibration),  $1417\text{ cm}^{-1}$  (O-H and C-H bending vibration),  $1375\text{ cm}^{-1}$  ( $\text{CH}_3$  bending vibration),  $1151\text{ cm}^{-1}$  (C-O-C bending vibration) and  $1066\text{ cm}^{-1}$  (C-OH stretching vibration) (Baldino, Concilio, Cardea, De Marco, & Reverchon, 2015). Some major changes were observed in the spectrum of crosslinked CS microspheres (Figure 6-15 b) compared with that of pure CS. The broad band O-H and N-H stretching at  $3372\text{ cm}^{-1}$  was reduced and shifted to  $3387\text{ cm}^{-1}$ , as the intermolecular hydrogen bonds were destroyed by the crosslinking reaction (Zou et al., 2015). The peak at  $2868\text{ cm}^{-1}$  changed to two sharp peaks at  $2927\text{ cm}^{-1}$  and  $2855\text{ cm}^{-1}$ , referring to the C-H asymmetric and symmetric stretching respectively (B. Li et al., 2013). The crosslinking reaction can be confirmed by the Schiff base formation as verified by the  $1657\text{ cm}^{-1}$  and  $1557\text{ cm}^{-1}$  bands correlated with C=N and  $\text{NH}_2$  groups, correspondingly (Baldino et al., 2015). The Schiff base (imine group) formation is introduced by the nucleophilic reaction of the amino groups from CS

with the aldehydic groups from GA as shown in Figure 6-16 (Baldino et al., 2015). After embedding the LNG-CS microspheres in the PVA hydrogel, all characteristic peaks from CS microspheres/drug were present with no changes in the band positions (Figure 6-15 d), indicating the absence of interactions between microsphere, drug and hydrogel matrix.

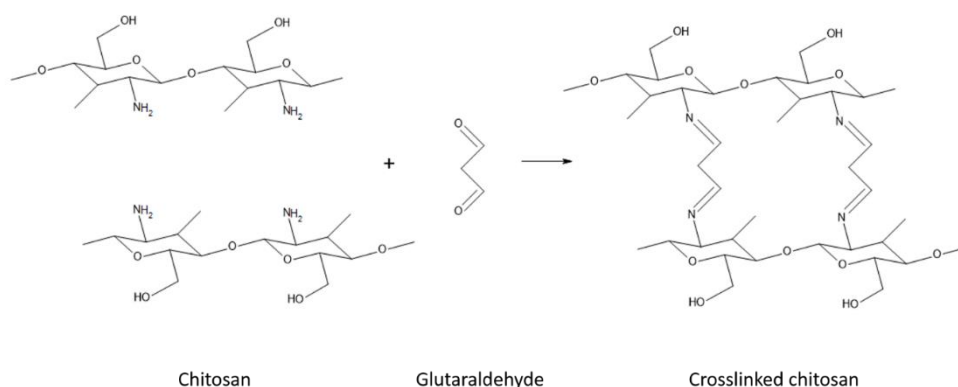


Figure 6-16. Aldehyde crosslinking reaction of chitosan by glutaraldehyde.

The major peaks related to hydroxyl and acetate groups were observed in pure PVA (Figure 6-15 f) and PVA hydrogel spectrum (Figure 6-15 e). A broad band around  $3329\text{ cm}^{-1}$  was linked to O–H stretching from the hydrogen bonded band (Figueiredo et al., 2009). The vibration bands between  $3000\text{ cm}^{-1}$  and  $2840\text{ cm}^{-1}$  were related to the C–H stretching of alkyl groups (Qi et al., 2015). The peak at  $1142\text{ cm}^{-1}$  referred to the C–O stretching vibration, which mostly corresponds to crystallinity of the PVA (J. Y. Chang et al., 2000; Kenawy et al., 2014; Qi et al., 2015). After freeze-thaw crosslinking, there was no significant changes in spectrum between the pure PVA and PVA hydrogel. However, it can be seen that the broad bands corresponding to O–H stretching shifted from  $3329\text{ cm}^{-1}$  to  $3312\text{ cm}^{-1}$ , indicating more hydrogen bonds were formed during freeze-thaw crosslinking (M. Huang et al., 2012). Moreover, the intensity of the peak at  $1142\text{ cm}^{-1}$  referred to the C–O stretching was increased in the

PVA hydrogel, indicating the crystallinity was increased after the freeze-thaw and annealing treatments (M. Huang et al., 2012). This result has endorsed the findings based on the crystallinity in DSC assessment.

In the case of LNG (Figure 6-15 g), the characteristic peaks were found at  $3345\text{ cm}^{-1}$  and  $3267\text{ cm}^{-1}$  corresponding to O-H stretching vibration, and  $1652\text{ cm}^{-1}$  due to C=O stretching of carbonyl groups (Bao et al., 2018; Manoukian et al., 2018). All the characteristic peaks of LNG were present in the polymer matrix without any noticeable peak shift or widening after being incorporated in the CS microspheres (Figure 6-15 c) and subsequently when embedded in the PVA hydrogel (Figure 6-15 d). This indicates no molecular interaction between the drug and polymers. As explained by the FTIR results, it corroborates that the drug was only physically entrapped in the microsphere matrix. This result indicates the rough surfaces observed in the LNG-CS microspheres in SEM are likely drug particles physically entrapped in the CS matrix (Figure 6-4).

#### 6.3.6. Thermal analysis

Processes involving thermal treatments, such as freezing, thawing and annealing, can affect the properties of crystalline substances as they undergo changes in the degree of molecular motion during the process cycle (Ray & Cooney, 2018). Hence, DSC studies were performed to further analyse the molecular interactions between drug and host polymers as well as the crystallinity of PVA hydrogels.

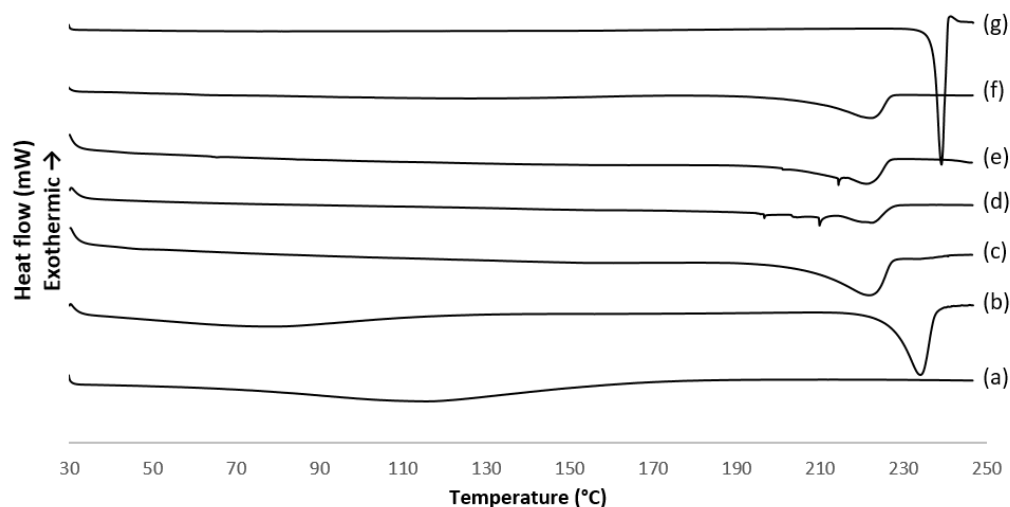


Figure 6-17. DSC thermograms of (a) chitosan (CS), (b) levonorgestrel (LNG)-loaded CS microspheres, (c) annealed 20% poly(vinyl alcohol) (PVA) hydrogel with LNG-loaded CS microspheres, (d) annealed 20% PVA hydrogel, (e) unannealed 20% PVA hydrogel, (f) PVA and (g) LNG.

Chitosan (Figure 6-17 a) showed a large and broad peak at about 80-150°C, due to the dehydration of the polymer. In the LNG-loaded CS microspheres (Figure 6-17 b), the dehydration band was reduced and shifted to lower temperatures (50-110°C), indicating a reduction in moisture levels after drying and annealing processes. The endothermic peak at 234°C corresponding to the melting point of LNG was also observed in the LNG-loaded CS microspheres, confirming the presence of LNG in its crystalline form within the CS microspheres. Compared to free LNG, a slight shift of the melting point from 239°C was observed in the LNG-loaded CS microspheres. This can be attributed to the influence of CS on the crystallisation of LNG within the microspheres (Schulz, Fussnegger, & Bodmeier, 2011).

Although FTIR results suggest that the freeze-thaw and annealing treatments led to an increased crystallinity of PVA (Fukumori & Nakaoki, 2015), the data on crystalline structure of PVA hydrogels may disclose further insights to a better understanding

between structures and properties of PVA hydrogels. The degree of crystallinity ( $X_c$ ) of PVA hydrogel was calculated using Eq. (7) as the ratio between the heat of fusion ( $\Delta H_m$ ) of the PVA samples and the thermodynamic enthalpy of melting a 100% crystalline PVA ( $\Delta H_c = 138.6 \text{ J/g}$ ) (Hassan & Peppas, 2000).

$$X_c(\%) = \frac{\Delta H_m}{\Delta H_c} \times 100 \quad (7)$$

The PVA hydrogel prepared by freeze-thaw cycles (Figure 6-17 e) exhibited increased crystallinity of 48% compared to 40% crystallinity in the pristine PVA (Figure 6-17 f) The result suggests that freeze-thaw treatment promotes the ordering of the polymer to form crosslinking conjunctions and thus promoting crystallisation.

Annealing treatment on PVA hydrogels has been reported to increase their crystallinity and water stability (Fathi, Atyabi, Imani, & Alinejad, 2011). In this study, the degree of crystallinity increased from 48% in unannealed PVA hydrogel (Figure 6-17 e) to 54% after annealing treatment (Figure 6-17 d). This is because crystallisation is promoted by annealing process, as crystallites form during freeze-thaw cycling act as the nucleation sites for further crystal growth during annealing (Figure 6-18). It is worth noting that compared to free PVA (Figure 6-17 f), multiple endothermic peaks existed in freeze-thawed PVA hydrogel (Figure 6-17 d and e). This is likely because microcrystallines before freeze-thawing and annealing were lesser and looser, while the number of crystal regions increased after freeze-thaw and annealing treatments, where more endothermic peaks were observed. Moreover, those endothermic peaks were shifting to lower temperatures after freeze-thawing and annealing, which may partly be because these crystals became more ordered and

packed during freeze-thaw and annealing treatments. The reduced crystal size resulted in a relatively lower melting temperature for those packed crystals while the growing number of crystal regions led to increased heat of fusion (Fathi et al., 2011).

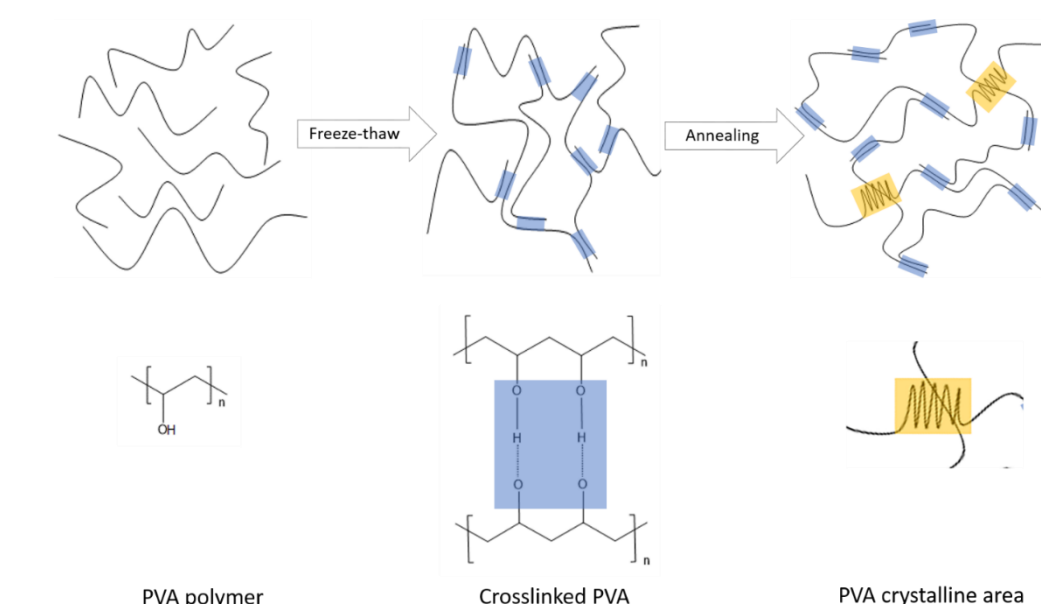


Figure 6-18. Crosslinked poly (vinyl alcohol) (PVA) hydrogel by hydrogen bonding and crystallisation by annealing.

After introducing microspheres into PVA hydrogel (Figure 6-17 c), the melting peak was sharpened and multiplied compared to microsphere-free PVA hydrogel (Figure 6-17 d), representing a more ordered crystal structure formed thus more energy required for melting. It is note-worthy that the small and sharp multiple endothermic peaks observed in microsphere-free hydrogels were disappeared in the microsphere loaded PVA hydrogel. The microspheres possibly prevent the formation of early phase crystal formation. In case of microsphere-loaded PVA hydrogel, the endothermic peak corresponds to LNG melting point encapsulated within the CS microspheres was masked by PVA hydrogel. However, a weak broad shoulder endotherm was observed at 233°C in the microsphere-loaded PVA hydrogel corresponding to the melting peak of LNG.

## 6.4. Conclusion

In this study, a long-term and controlled release system consisting of CS microspheres embedded into PVA hydrogels was developed and characterised for the delivery of LNG contraceptive. CS microspheres, as the first drug reservoir, were prepared by chemical crosslinking of GA and subsequently partitioned in three size ranges (<63, 63-125 and 125-300  $\mu\text{m}$ ), and the particle size distribution analysis showed that all microspheres in each size range were monodisperse. Based on the drug loading and release profile, an optimised size range 125-300  $\mu\text{m}$  was chosen to be incorporated in to PVA hydrogels. SEM images of microspheres loaded PVA hydrogels showed that they remained spherical in the matrix and that the higher concentration of PVA reduced the porosity in the hydrogel matrix as more crosslinked network and crystallisation can be formed in the hydrogel prepared with higher PVA concentrations. FTIR results confirmed the chemical crosslinking of CS and physical crosslinking of PVA by hydrogen bonds. The drug, LNG, was physically entrapped in the CS matrix as indicated by FTIR results and SEM micrographs. DSC results supported that the crystallinity of PVA was increased by freeze-thawing and annealing treatments. Swelling studies showed that increasing PVA concentrations and annealing treatment resulted in reduced swelling degree and water content, while loading of microspheres into the PVA hydrogel led to a slight increase in swelling degree. Approximately zero-order release profiles without burst release were obtained from both microsphere and microsphere- hydrogel systems. The *in vitro* release data were fitted into Korsmeyer-Peppas model, indicating that the diffusion- and swelling-controlled release mechanisms may coexist for the controlled release of LNG from the microsphere and microsphere-hydrogel systems. In conclusion, the data obtained



in this study points out to the possibility of developing zero-order release systems for the delivery of long-term contraception by using chitosan microspheres embedded in PVA hydrogels, and a representative formulation with optimised processing conditions was presented.

## 6.5. Reference

- Abitbol, T., Johnstone, T., Quinn, T. M., & Gray, D. G. (2011). Reinforcement with cellulose nanocrystals of poly (vinyl alcohol) hydrogels prepared by cyclic freezing and thawing. *Soft Matter*, 7(6), 2373-2379.
- Ahsan, S. M., Thomas, M., Reddy, K. K., Sooraparaju, S. G., Asthana, A., & Bhatnagar, I. (2017). Chitosan as biomaterial in drug delivery and tissue engineering. *International journal of biological macromolecules*, 110, 97-109.
- Baldino, L., Concilio, S., Cardea, S., De Marco, I., & Reverchon, E. (2015). Complete glutaraldehyde elimination during chitosan hydrogel drying by SC-CO<sub>2</sub> processing. *The Journal of Supercritical Fluids*, 103, 70-76.
- Bao, Q., Gu, B., Price, C. F., Zou, Y., Wang, Y., Kozak, D., . . . Burgess, D. J. (2018). Manufacturing and characterization of long-acting levonorgestrel intrauterine systems. *International journal of pharmaceutics*, 550(1-2), 447-454.
- Bhardwaj, U., Sura, R., Papadimitrakopoulos, F., & Burgess, D. J. (2007). Controlling acute inflammation with fast releasing dexamethasone-PLGA microsphere/PVA hydrogel composites for implantable devices. *Journal of diabetes science and technology*, 1(1), 8-17.
- Bhardwaj, U., Sura, R., Papadimitrakopoulos, F., & Burgess, D. J. (2010). PLGA/PVA hydrogel composites for long-term inflammation control following sc implantation. *International journal of pharmaceutics*, 384(1-2), 78-86.
- Buntner, B., Nowak, M., Kasperczyk, J., Ryba, M., Grieb, P., Walski, M., . . . Bero, M. (1998). The application of microspheres from the copolymers of lactide and  $\epsilon$ -caprolactone to the controlled release of steroids. *Journal of Controlled Release*, 56(1-3), 159-167.
- Chang, G., Chen, Y., Li, Y., Li, S., Huang, F., Shen, Y., & Xie, A. (2015). Self-healable hydrogel on tumor cell as drug delivery system for localized and effective therapy. *Carbohydrate polymers*, 122, 336-342.
- Chang, J. Y., Godovsky, D., Han, M., Hassan, C., Kim, J., Lee, B., . . . Yoo, T. (2000). *Biopolymers· PVA Hydrogels Anionic Polymerisation Nanocomposites* (Vol. 153): Springer Science & Business Media.

- Chen, K., Chen, G., Wei, S., Yang, X., Zhang, D., & Xu, L. (2018). Preparation and property of high strength and low friction PVA-HA/PAA composite hydrogel using annealing treatment. *Materials Science and Engineering: C*, 91, 579-588.
- Chen, W., Hou, Y., Tu, Z., Gao, L., & Haag, R. (2017). pH-degradable PVA-based nanogels via photo-crosslinking of thermo-preinduced nanoaggregates for controlled drug delivery. *Journal of Controlled Release*, 259, 160-167.
- Chen, W., Palazzo, A., Hennink, W. E., & Kok, R. J. (2016). Effect of particle size on drug loading and release kinetics of gefitinib-loaded PLGA microspheres. *Molecular pharmaceutics*, 14(2), 459-467.
- Clayton, K. N., Salameh, J. W., Wereley, S. T., & Kinzer-Ursem, T. L. (2016). Physical characterization of nanoparticle size and surface modification using particle scattering diffusometry. *Biomicrofluidics*, 10(5), 054107.
- Croxatt, H. B. (2002). Progestin implants for female contraception. *Contraception*, 65(1), 15-19.
- Dash, S., Murthy, P. N., Nath, L., & Chowdhury, P. (2010). Kinetic modeling on drug release from controlled drug delivery systems. *Acta Poloniae Pharmaceutica*, 67(3), 217-223.
- Dhanaraju, M. D., Vema, K., Jayakumar, R., & Vamsadhara, C. (2003). Preparation and characterization of injectable microspheres of contraceptive hormones. *International journal of pharmaceutics*, 268(1-2), 23-29.
- El-Feky, G. S., Sharaf, S. S., El Shafei, A., & Hegazy, A. A. (2017). Using chitosan nanoparticles as drug carriers for the development of a silver sulfadiazine wound dressing. *Carbohydrate polymers*, 158, 11-19.
- Fan, L., Yang, H., Yang, J., Peng, M., & Hu, J. (2016). Preparation and characterization of chitosan/gelatin/PVA hydrogel for wound dressings. *Carbohydrate polymers*, 146, 427-434.
- Fathi, E., Atyabi, N., Imani, M., & Alinejad, Z. (2011). Physically crosslinked polyvinyl alcohol–dextran blend xerogels: morphology and thermal behavior. *Carbohydrate polymers*, 84(1), 145-152.
- Figueiredo, K., Alves, T. L., & Borges, C. P. (2009). Poly (vinyl alcohol) films crosslinked by glutaraldehyde under mild conditions. *Journal of applied polymer science*, 111(6), 3074-3080.

- Freiberg, S., & Zhu, X. (2004). Polymer microspheres for controlled drug release. *International journal of pharmaceutics*, 282(1-2), 1-18.
- Friend, D. R. (2016). Development of controlled release systems over the past 50 years in the area of contraception. *Journal of Controlled Release*, 240, 235-241.
- Fukumori, T., & Nakaoki, T. (2013). Significant improvement of mechanical properties for polyvinyl alcohol film prepared from freeze/thaw cycled gel. *Open Journal of Organic Polymer Materials*, 3(4), 110.
- Fukumori, T., & Nakaoki, T. (2014). High - tensile - strength polyvinyl alcohol films prepared from freeze/thaw cycled gels. *Journal of applied polymer science*, 131(15).
- Fukumori, T., & Nakaoki, T. (2015). High strength poly (vinyl alcohol) films obtained by drying and then stretching freeze/thaw cycled gel. *Journal of applied polymer science*, 132(1).
- Galeska, I., Kim, T.-K., Patil, S. D., Bhardwaj, U., Chattopadhyay, D., Papadimitrakopoulos, F., & Burgess, D. J. (2005). Controlled release of dexamethasone from PLGA microspheres embedded within polyacid-containing PVA hydrogels. *The American Association of Pharmaceutical Scientists (AAPS) journal*, 7(1), E231-E240.
- Hassan, C. M., & Peppas, N. A. (2000). Structure and morphology of freeze/thawed PVA hydrogels. *Macromolecules*, 33(7), 2472-2479.
- Hickey, T., Kreutzer, D., Burgess, D., & Moussy, F. (2002). Dexamethasone/PLGA microspheres for continuous delivery of an anti-inflammatory drug for implantable medical devices. *Biomaterials*, 23(7), 1649-1656.
- Huang, M., Cai, D., Liu, Y., Sun, J., Wang, J., Qin, C., . . . Kazuo, Y. (2012). Investigation of a-PVA/s-PVA hydrogels prepared by freezing-thawing method. *Fibers and Polymers*, 13(8), 955-962.
- Jameela, S., Kumary, T., Lal, A., & Jayakrishnan, A. (1998). Progesterone-loaded chitosan microspheres: a long acting biodegradable controlled delivery system. *Journal of Controlled Release*, 52(1-2), 17-24.
- Kamoun, E. A., Kenawy, E.-R. S., & Chen, X. (2017). A review on polymeric hydrogel membranes for wound dressing applications: PVA-based hydrogel dressings. *Journal of advanced research*, 8(3), 217-233.

- Kashikar, V., Dhole, S., Kandekar, U., & Khose, P. (2014). Study of mucoadhesive microsphere of pirfenidone for nasal drug delivery. *Asian Journal of Pharmaceutics (AJP): Free full text articles from Asian J Pharm*, 8(1).
- Kenawy, E.-R., Kamoun, E. A., Eldin, M. S. M., & El-Meligy, M. A. (2014). Physically crosslinked poly (vinyl alcohol)-hydroxyethyl starch blend hydrogel membranes: Synthesis and characterization for biomedical applications. *Arabian Journal of Chemistry*, 7(3), 372-380.
- Khurma, J. R., Rohindra, D. R., & Nand, A. V. (2006). Synthesis and properties of hydrogels based on chitosan and poly (vinyl alcohol) crosslinked by genipin. *Journal of Macromolecular Science, Part A: Pure and Applied Chemistry*, 43(4-5), 749-758.
- Kobayashi, M., Chang, Y.-S., & Oka, M. (2005). A two year in vivo study of polyvinyl alcohol-hydrogel (PVA-H) artificial meniscus. *Biomaterials*, 26(16), 3243-3248.
- Korsmeyer, R. W., Gurny, R., Doelker, E., Buri, P., & Peppas, N. A. (1983). Mechanisms of solute release from porous hydrophilic polymers. *International journal of pharmaceutics*, 15(1), 25-35.
- Li, B., Shan, C.-L., Zhou, Q., Fang, Y., Wang, Y.-L., Xu, F., . . . Xie, G.-L. (2013). Synthesis, characterization, and antibacterial activity of cross-linked chitosan-glutaraldehyde. *Marine drugs*, 11(5), 1534-1552.
- Li, D., Guo, G., Fan, R., Liang, J., Deng, X., Luo, F., & Qian, Z. (2013). PLA/F68/dexamethasone implants prepared by hot-melt extrusion for controlled release of anti-inflammatory drug to implantable medical devices: I. Preparation, characterization and hydrolytic degradation study. *International journal of pharmaceutics*, 441(1), 365-372.
- Li, J. K., Wang, N., & Wu, X. S. (1998). Poly (vinyl alcohol) nanoparticles prepared by freezing–thawing process for protein/peptide drug delivery. *Journal of Controlled Release*, 56(1-3), 117-126.
- Lim, L. Y., Khor, E., & Ling, C. E. (1999). Effects of dry heat and saturated steam on the physical properties of chitosan. *Journal of Biomedical Materials Research*, 48(2), 111-116.
- Long, J., Nand, A. V., Ray, S., Mayhew, S., White, D., Bunt, C. R., & Seyfoddin, A. (2018). Development of customised 3D printed biodegradable projectile for

- administering extended-release contraceptive to wildlife. *International journal of pharmaceutics*, 548(1), 349-356.
- Ma, G., Song, C., Sun, H., Yang, J., & Leng, X. (2006). A biodegradable levonorgestrel-releasing implant made of PCL/F68 compound as tested in rats and dogs. *Contraception*, 74(2), 141-147.
- Machado, S. R., Lunardi, L. O., Tristão, A. P., & Marchetti, J. M. (2009). Preparation and characterization of D, L-PLA loaded 17- $\beta$ -Estradiol valerate by emulsion/evaporation methods. *Journal of microencapsulation*, 26(3), 202-213.
- Mallapragada, S. K., Peppas, N. A., & Colombo, P. (1997). Crystal dissolution - controlled release systems. II. Metronidazole release from semicrystalline poly (vinyl alcohol) systems. *Journal of Biomedical Materials Research*, 36(1), 125-130.
- Manoukian, O. S., Arul, M. R., Sardashti, N., Stedman, T., James, R., Rudraiah, S., & Kumbar, S. G. (2018). Biodegradable polymeric injectable implants for long - term delivery of contraceptive drugs. *Journal of applied polymer science*, 135(14), 46068.
- Park, J.-S., Kim, H.-A., Choi, J.-B., Gwon, H.-J., Shin, Y.-M., Lim, Y.-M., . . . Nho, Y.-C. (2012). Effects of annealing and the addition of PEG on the PVA based hydrogel by gamma ray. *Radiation Physics and Chemistry*, 81(7), 857-860.
- Poon, L., Wilson, L. D., & Headley, J. V. (2014). Chitosan-glutaraldehyde copolymers and their sorption properties. *Carbohydrate polymers*, 109, 92-101.
- Qi, X., Hu, X., Wei, W., Yu, H., Li, J., Zhang, J., & Dong, W. (2015). Investigation of Salecan/poly (vinyl alcohol) hydrogels prepared by freeze/thaw method. *Carbohydrate polymers*, 118, 60-69.
- Ray, S., & Cooney, R. P. (2018). Thermal degradation of polymer and polymer composites *Handbook of Environmental Degradation of Materials* (Third ed., pp. 185-206): Elsevier.
- Schulz, M., Fussnegger, B., & Bodmeier, R. (2011). Influence of adsorbents in transdermal matrix patches on the release and the physical state of ethinyl estradiol and levonorgestrel. *European Journal of Pharmaceutics and Biopharmaceutics*, 77(2), 240-248.

- Shaikh, H. K., Kshirsagar, R., & Patil, S. (2015). Mathematical models for drug release characterization: a review. *World Journal Of Pharmacy And Pharmaceutical Sciences*, 4(04), 324-338.
- Shen, J., & Burgess, D. J. (2012). Accelerated in vitro release testing of implantable PLGA microsphere/PVA hydrogel composite coatings. *International journal of pharmaceutics*, 422(1-2), 341-348.
- Shulman, L. P. (2011). The state of hormonal contraception today: benefits and risks of hormonal contraceptives: combined estrogen and progestin contraceptives. *American journal of obstetrics and gynecology*, 205(4), S9-S13.
- Shulman, L. P., Nelson, A. L., & Darney, P. D. (2004). Recent developments in hormone delivery systems. *American journal of obstetrics and gynecology*, 190(4), S39-S48.
- Siepmann, J., & Peppas, N. (2001). Modeling of drug release from delivery systems based on hydroxypropyl methylcellulose (HPMC). *Advanced drug delivery reviews*, 48(2-3), 139-157.
- Sinha, V., Singla, A. K., Wadhawan, S., Kaushik, R., Kumria, R., Bansal, K., & Dhawan, S. (2004). Chitosan microspheres as a potential carrier for drugs. *International journal of pharmaceutics*, 274(1-2), 1-33.
- Soni, S. R., & Ghosh, A. (2017). Exploring pullulan-poly (vinyl alcohol) interpenetrating network microspheres as controlled release drug delivery device. *Carbohydrate polymers*, 174, 812-822.
- Stegeman, B. H., de Bastos, M., Rosendaal, F. R., van Hylckama Vlieg, A., Helmerhorst, F. M., Stijnen, T., & Dekkers, O. M. (2013). Different combined oral contraceptives and the risk of venous thrombosis: systematic review and network meta-analysis. *British Medical Journal*, 347, f5298.
- Szymańska, E., & Winnicka, K. (2015). Stability of chitosan—a challenge for pharmaceutical and biomedical applications. *Marine drugs*, 13(4), 1819-1846.
- Vellayappan, M., Venugopal, J., Ramakrishna, S., Ray, S., Ismail, A., Mandal, M., . . . Jaganathan, S. (2016). Electrospinning applications from diagnosis to treatment of diabetes. *Royal Society of Chemistry Advances*, 6(87), 83638-83655.
- Wang, S., Zhang, L., Lin, F., Sa, X., Zuo, J., Shao, Q., . . . Zeng, S. (2005). Controlled release of levonorgestrel from biodegradable poly (D, L-lactide-co-glycolide)

- microspheres: in vitro and in vivo studies. *International journal of pharmaceutics*, 301(1-2), 217-225.
- West, G., Heard, D., & Caulkett, N. (2014). *Zoo animal and wildlife immobilization and anesthesia*: John Wiley & Sons.
- Wu, J. C.-C., Ray, S., Gizdavic-Nikolaidis, M., Uy, B., Swift, S., Jin, J., & Cooney, R. P. (2014). Nanostructured bioactive material based on polycaprolactone and polyaniline fiber-scaffolds. *Synthetic Metals*, 198, 41-50.
- Wu, L., Janagam, D. R., Mandrell, T. D., Johnson, J. R., & Lowe, T. L. (2015). Long-acting injectable hormonal dosage forms for contraception. *Pharmaceutical research*, 32(7), 2180-2191.
- Xiao, C., & Yang, M. (2006). Controlled preparation of physical cross-linked starch-g-PVA hydrogel. *Carbohydrate polymers*, 64(1), 37-40.
- Yu, S., Zhang, X., Tan, G., Tian, L., Liu, D., Liu, Y., . . . Pan, W. (2017). A novel pH-induced thermosensitive hydrogel composed of carboxymethyl chitosan and poloxamer cross-linked by glutaraldehyde for ophthalmic drug delivery. *Carbohydrate polymers*, 155, 208-217.
- Zhang, L., Wang, Z., Xu, C., Li, Y., Gao, J., Wang, W., & Liu, Y. (2011). High strength graphene oxide/polyvinyl alcohol composite hydrogels. *Journal of Materials Chemistry*, 21(28), 10399-10406.
- Zou, X., Zhao, X., Ye, L., Wang, Q., & Li, H. (2015). Preparation and drug release behavior of pH-responsive bovine serum albumin-loaded chitosan microspheres. *Journal of Industrial and Engineering Chemistry*, 21, 1389-1397.



# Chapter 7

*General discussion*

## 7.1. Thesis summary

This thesis aimed to develop a novel 3D printed BDDS for wildlife applications. It began with a literature review (Chapter 2) about FDM 3D printing and its applications in drug delivery. Considering the easy fabrication process and acceptable mechanical strength, FDM it was our first choice to print BDDS.

A prototype of 3D printed BDDS was developed in Chapter 3, confirming the feasibility of using FDM to print drug-loaded ballistic projectiles. This prototype showed good ballistic and sustained *in vitro* drug release properties. In the following chapter, an attempt was made to improve the projectile prototype so to: i) develop a multi-compartment model of ballistic projectile capable of loading multiple drugs (as shown in Figure 1-2). Considering the penetration trauma cannot be avoided in a BDDS, assisting drugs such as anti-inflammatory and anaesthetic medicines are necessary to be delivered along with the main contraception, ii) a long-term contraception is essential to reduce the administration frequency. The *in vitro* P4 release from the prototype in Chapter 3 provided a sustained release over five months, which would be enough for a seasonal contraception. However, a long-term contraception (3-5 years) is preferred in particular wildlife applications.

In Chapter 4, the anti-inflammatory drug DEX was formulated with PVA hydrogels. In the BDDS, this formulation is to be placed in the subulate cap of the projectile to reduce inflammation around the penetration trauma. The developed DEX-PVA formulation can also be used to control acute and/or chronic inflammation after surgical or implantation procedures in humans and animals.

In Chapter 5, the anaesthetic drug LDC was formulated with CS-PEC hydrogel and then 3D printed as a flexible mesh. In the BDDS, this formulation is to be wrapped around the inner wall of the cylindrical body of the projectile which helps to reduce the pain after ballistic delivery. This formulation can be also used as a customised wound dressing providing fast pain relief and a moist environment for better healing.

In Chapter 6, to develop a slow-release delivery system for LNG, a two barriers approach was investigated where the drug was initially microencapsulated and further embedded in a PVA hydrogel. In the BDDS, this formulation is to be moulded as a cylindrical insert and be accommodated in the hollow projectile body (Figure 1-1). The individual application of this chapter is to be used as a long-term biodegradable contraception implant.

## 7.2. Core chapter philosophies

**Chapter 2- Literature review:** *Application of fused deposition modelling (FDM) method of 3D printing in drug delivery.*

Recent innovations in the field of 3D printing have led to a wide range of research into its applications in pharmaceutical and medical areas. Since FDA approved the first 3D printed medicine in 2015, there has been considerable increase in the number of studies addressing 3D printing of medicines. However, there is a relative paucity of literature reviews specifically relating to the potential of FDM 3D printing, as the most common 3D printing technology, in drug delivery applications. This is perhaps because this area is relatively new and has not yet been widely applied. Thus, considering the need for compiling information about the application of FDM in drug delivery, this chapter was written to provide comprehensive information about mechanisms, practical considerations, material selection and applications of FDM applied in drug delivery. It is hoped that this review will contribute to a deeper understanding of the potential and practical capability of FDM as a novel and versatile manufacturing technique for creating customised drug delivery devices that are capable of incorporating accurate doses of medicine(s) and providing controlled drug released profiles.

**Chapter 3- Research paper:** *Development of customised 3D printed biodegradable projectile for administering extended-release contraceptive to wildlife.*

After identifying the feasibility of FDM to fabricate drug-loaded scaffolds, this chapter was set to develop a prototype ballistic projectile. This study is one of the first

attempts to build a 3D printed ballistic drug delivery system. A biodegradable projectile containing different doses of contraceptive P4 was prepared using FDM 3D printing. Hot melt extrusion, as one of the more practical ways of loading drug into filaments, was adopted in this chapter to prepare 1.75 mm PLA filaments with different concentrations of P4. The *in vitro* drug release profile indicated a controlled and sustained release of P4 over a period of five months. The short-term contraception formulation developed in this chapter provides a potential solution for wildlife managements where seasonal contraception is needed, such as for feral horses in the central North Island of New Zealand. Penetration assessment confirmed that the drug loaded PLA projectiles provided sufficient specific kinetic energy required to penetrate thin and medium-thickness skins.

**Chapter 4 - Research paper:** *Controlled release of dexamethasone from poly (vinyl alcohol) hydrogel.*

To control and reduce the inflammation due to trauma inflicted by ballistic delivery, this chapter aimed to develop a formulation providing a slow release of anti-inflammatory drug DEX. PVA hydrogel was employed as the drug carrier since it can be easily loaded into the hollow space of a projectile cap for ballistic drug delivery. After penetration impact, the diffusion of drug with body fluids would be achieved through the expanded/exploded projectile shell. PVA use is further supported by there being examples of various applications such as anti-inflammatory implants in postoperative care or hydrogel coatings for implantable devices. Sustained and controlled release profiles of DEX over one month could be achieved through

regulating the crosslinking density of PVA hydrogel. The findings from this chapter has added to the growing body of hydrogel drug carriers and offered a possibility for exploring the incorporation of hydrogel formulations into 3D printed devices.

**Chapter 5- Research paper:** *A 3D printed chitosan-pectin hydrogel wound dressing containing lidocaine hydrochloride*

Upon ballistic drug delivery and penetration of the projectile through the skin, measures have to be in place to alleviate pain. This chapter aimed to formulate a 3D printed wound dressing to provide a quick burst of an anaesthetic drug as pain relief. Here, an extrusion-based 3D printing method with mechanical positive displacement dispensing system was used which differs from FDM by the absence of the need to heat and melt filaments, using powders instead. The 3D printed hydrogel showed good flexibility and customisability with the possibility to be wrapped around the inner wall of the cylindrical body of the projectile. The high swelling ratio and water absorption of the material can be beneficial for absorbing exudates and maintaining a moist environment for wound healing. As expected, the thermosensitive CS-PEC hydrogel delivered a fast release of LDC in 5h, potentially providing an effective pain relief on fresh wound/trauma. The hydrogels also exhibited excellent self-adhesion to the skin, signifying their potentials to be used individually as customised hydrogel wound dressings can be tailored to size, thickness or drug dose based on specific applications.

**Chapter 6- Research paper:** *Development of a long-term contraceptive implant with levonorgestrel loaded chitosan microspheres embedded in poly (vinyl alcohol) hydrogel*

One of the major objectives of this thesis was to develop a long-term controlled release system for wildlife contraception that can be easily incorporated into the projectile. Thus, in the final experimental chapter, a combined system of CS microspheres embedded in PVA hydrogel was developed and characterised for this purpose. A novel delivery system was created capable of extending the release of LNG to up to three years. The sol-gel property of hydrogel drug carrier can potentially facilitate its accommodation in the cylindrical body of the projectile.

### 7.3. Limitations

#### 7.3.1. *In vivo* studies for individual formulations

Being limited to animal availability issues and restricted budget, this thesis did not evaluate *in vivo* drug release for each individual drug formulation. *In vivo* assessment is essential in drug formulation development before moving forward to clinical tests as it provides practical insights to understand the actual effects in a living body. An essential step forward is to work on bridging the gap between *in vitro* release profiles and *in vivo* release behaviours. The following are recommended to be considered in any future *in vivo* study: i) to study the *in vivo* release of P4 from the P4-PLA prototype (Chapter 3) by measuring the plasma concentration of P4 in treated animals, ii) to evaluate the contraception efficacy of P4-PLA system (Chapter 3), iii) To evaluate the *in vivo* release of DEX, LDC and LNG (Chapter 4-6) from the final ballistic model by determining the plasma concentrations of these drugs in animals, iv) to evaluate the anti-inflammatory effect of DEX (Chapter 4) by comparing the inflammation and healing rate of the ballistic trauma in the animals that are treated with DEX-included and DEX-excluded projectiles, v) to assess the pain relief effect of LDC (Chapter 5) and vi) to evaluate the long-term contraception efficacy of LNG by a track study of incidence parturition in the administered animals.

However, it is important to point out that there have been thousands of studies published where *in vitro* studies have been used to determine drug release rates under specific conditions, identify release kinetics, predicting the timeframe of drug release and to simulate and forecast *in vivo* behaviour. Besides, *in vitro/in vivo* correlations have been adequately studied and published, especially for microspheres and



polymeric systems (Photos, Bacakova, Discher, Bates, & Discher, 2003; Shen & Burgess, 2015; Zolnik & Burgess, 2008).

### 7.3.2. Characterisation of the assembled projectile

The final projectile, as shown in Figure 1-2, can be easily assembled as a BDDS with customised size/shape for different projectors and animal species by taking the advantages of 3D printing. The ballistic assessments were limited in this thesis due to limited accessibility to projectors/facilities and restrictive firearm licenses in New Zealand.

The lack of *in vivo* animal study of the final projectile adds further caution regarding generalizing the findings of this thesis. It is desired that in the near future further studies can gain insights regarding *in vivo* performance of this 3D printed BDDS.

## 7.4. Future work

There are many potential opportunities for future ballistic drug delivery research and applications, especially 3D printed projectiles with capabilities of customising their size, shape, drug and doses. The ideas developed in this thesis offer a solution to wildlife management and should be pursued further.

For instance, the surged population of Kaimanawa wild horses in the central North Island in New Zealand presents a perceived threat to the fragile ecosystem in their habitat. These feral horses put a heavy burden on the wetlands and tussock lands in Kaimanawa through grazing and trampling. Published by the Department of Conservation (DOC) in New Zealand, many typical plants including eleven special plants known to only exist in this area have been threatened. Various strategies have been implemented to control the population of Kaimanawa horses, including annual mustering and counting followed by slaughtering which has been controversial with animal support groups. In such situations, the short-term contraceptive device developed in Chapter 3 (P4-PLA projectile) finds practical applications. This prototype could provide an effective contraception over the breeding season with a single shot delivery.

For the improved ballistic prototype with long-term contraception developed in chapter 6 (LNG-loaded CS microspheres embedded in PVA hydrogel), one of the practical future application is for the contraception of koalas in Kangaroo Island as mentioned in Chapter 1. The flexibility and customisability of 3D printing allow us to fabricate the right size of projectile and accurate dose of contraceptives for koalas. With a ballistic delivery system, it will not be necessary to capture koalas. Indeed,

this project has sparked considerable interests from the people responsible for the management of koalas in Kangaroo Island when presented in the Australasian Wildlife Management Society (AWMS) annual conference in 2016.

The prototype developed in Chapter 6 (long-term contraceptive implant) has also shown valuable potential for future applications. In fact, a collaboration between Dr Seyfoddin's Drug Delivery Research Group, the University of Melbourne in Australia and Waitemata District Health Board in New Zealand has been established for developing controlled-release and sustained-release formulations of oestrogen for neonatal applications.

## 7.5. Conclusion

This thesis set out to develop a 3D printed ballistic drug delivery system capable to administer multiple drugs with controlled release performances, and to formulate those drugs with independent applications. A prototype of ballistic projectile was developed to administer short-term contraception, and then improved as a multi-compartment model to deliver multiple drugs. Three pharmaceutical formulations were subsequently framed as sustained-released anti-inflammation, wound dressings with fast-released pain relief and long-term contraception. The unique assemble/individual design will bring high possibility of transforming the promising potential of this study into practical solutions to make an important contribution to both of the maintenance of wildlife and the development of controlled drug delivery systems.

## 7.6. References

- Photos, P. J., Bacakova, L., Discher, B., Bates, F. S., & Discher, D. E. (2003). Polymer vesicles in vivo: correlations with PEG molecular weight. *Journal of Controlled Release*, 90(3), 323-334.
- Shen, J., & Burgess, D. J. (2015). In vitro–in vivo correlation for complex non-oral drug products: where do we stand? *Journal of Controlled Release*, 219, 644-651.
- Zolnik, B. S., & Burgess, D. J. (2008). Evaluation of in vivo–in vitro release of dexamethasone from PLGA microspheres. *Journal of Controlled Release*, 127(2), 137-145.

## Reference list

## References

- Abitbol, T., Johnstone, T., Quinn, T. M., & Gray, D. G. (2011). Reinforcement with cellulose nanocrystals of poly (vinyl alcohol) hydrogels prepared by cyclic freezing and thawing. *Soft Matter*, 7(6), 2373-2379.
- Abu-Huwaij, R., Assaf, S., Salem, M., & Sallam, A. (2007). Mucoadhesive dosage form of lidocaine hydrochloride: I. Mucoadhesive and physicochemical characterization. *Drug development and industrial pharmacy*, 33(8), 855-864.
- Ahmed, S., & Ikram, S. (2016). Chitosan based scaffolds and their applications in wound healing. *Achievements in the Life Sciences*, 10(1), 27-37.
- Ahsan, S. M., Thomas, M., Reddy, K. K., Sooraparaju, S. G., Asthana, A., & Bhatnagar, I. (2017). Chitosan as biomaterial in drug delivery and tissue engineering. *International journal of biological macromolecules*, 110, 97-109.
- Alemzadeh, I., & Vossoughi, M. (2002). Controlled release of paraquat from poly vinyl alcohol hydrogel. *Chemical Engineering and Processing: Process Intensification*, 41(8), 707-710.
- Andrade, G. I., Barbosa-Stancioli, E. F., Mansur, A. A. P., Vasconcelos, W. L., & Mansur, H. S. (2008). Small-angle X-ray scattering and FTIR characterization of nanostructured poly (vinyl alcohol)/silicate hybrids for immunoassay applications. *Journal of materials science*, 43(2), 450-463.
- Ang, T. H., Sultana, F. S. A., Hutmacher, D. W., Wong, Y. S., Fuh, J. Y. H., Mo, X. M., . . . Teoh, S. H. (2002). Fabrication of 3D chitosan-hydroxyapatite scaffolds using a robotic dispensing system. *Materials Science and Engineering: C*, 20(1-2), 35-42.
- Archana, D., Dutta, J., & Dutta, P. (2013). Evaluation of chitosan nano dressing for wound healing: Characterization, in vitro and in vivo studies. *International journal of biological macromolecules*, 57, 193-203.

## References

- Arnold, C. B., Serra, P., & Piqué, A. (2007). Laser direct-write techniques for printing of complex materials. *Materials Research Society Bulletin*, 32(01), 23-31.
- Baino, F., Ferraris, S., Miola, M., Perero, S., Verné, E., Coggiola, A., . . . Ferraris, M. (2016). Novel antibacterial ocular prostheses: Proof of concept and physico-chemical characterization. *Materials Science and Engineering: C*, 60, 467-474.
- Baldino, L., Concilio, S., Cardea, S., De Marco, I., & Reverchon, E. (2015). Complete glutaraldehyde elimination during chitosan hydrogel drying by SC-CO<sub>2</sub> processing. *The Journal of Supercritical Fluids*, 103, 70-76.
- Bao, Q., Gu, B., Price, C. F., Zou, Y., Wang, Y., Kozak, D., . . . Burgess, D. J. (2018). Manufacturing and characterization of long-acting levonorgestrel intrauterine systems. *International journal of pharmaceutics*, 550(1-2), 447-454.
- Beever, E. A., Huntsinger, L., & Petersen, S. L. (2018). Conservation challenges emerging from free-roaming horse management: A vexing social-ecological mismatch. *Biological conservation*, 226, 321-328.
- Bhardwaj, U., Sura, R., Papadimitrakopoulos, F., & Burgess, D. J. (2007). Controlling acute inflammation with fast releasing dexamethasone-PLGA microsphere/PVA hydrogel composites for implantable devices. *Journal of diabetes science and technology*, 1(1), 8-17.
- Bhardwaj, U., Sura, R., Papadimitrakopoulos, F., & Burgess, D. J. (2010). PLGA/PVA hydrogel composites for long-term inflammation control following sc implantation. *International journal of pharmaceutics*, 384(1-2), 78-86.
- Boateng, J. S., Matthews, K. H., Stevens, H. N., & Eccleston, G. M. (2008). Wound healing dressings and drug delivery systems: a review. *Journal of pharmaceutical sciences*, 97(8), 2892-2923.



- Brockelman, W. Y., & Kobayashi, N. K. (1971). Live capture of free-ranging primates with a blowgun. *The Journal of Wildlife Management*, 852-855.
- Buntner, B., Nowak, M., Kasperczyk, J., Ryba, M., Grieb, P., Walski, M., . . . Bero, M. (1998). The application of microspheres from the copolymers of lactide and  $\epsilon$ -caprolactone to the controlled release of steroids. *Journal of Controlled Release*, 56(1-3), 159-167.
- Bush, M. (1992). Remote drug delivery systems. *Journal of Zoo and Wildlife Medicine*, 159-180.
- Butscher, A., Bohner, M., Hofmann, S., Gauckler, L., & Müller, R. (2011). Structural and material approaches to bone tissue engineering in powder-based three-dimensional printing. *Acta Biomaterialia*, 7(3), 907-920.
- Cerchiara, T., Luppi, B., Bigucci, F., & Zecchi, V. (2003). Effect of chitosan on progesterone release from hydroxypropyl- $\beta$ -cyclodextrin complexes. *International journal of pharmaceutics*, 258(1), 209-215.
- Chang, G., Chen, Y., Li, Y., Li, S., Huang, F., Shen, Y., & Xie, A. (2015). Self-healable hydrogel on tumor cell as drug delivery system for localized and effective therapy. *Carbohydrate polymers*, 122, 336-342.
- Chang, J. Y., Godovsky, D., Han, M., Hassan, C., Kim, J., Lee, B., . . . Yoo, T. (2000). *Biopolymers: PVA Hydrogels Anionic Polymerisation Nanocomposites* (Vol. 153): Springer Science & Business Media.
- Chen, H., Fuhlbrigge, T., Zhang, G., & Masood, S. (2007). Application of fused deposition modelling in controlled drug delivery devices. *Assembly automation*, 27(3), 215-221.

## References

- Chen, K., Chen, G., Wei, S., Yang, X., Zhang, D., & Xu, L. (2018). Preparation and property of high strength and low friction PVA-HA/PAA composite hydrogel using annealing treatment. *Materials Science and Engineering: C*, 91, 579-588.
- Chen, W., Hou, Y., Tu, Z., Gao, L., & Haag, R. (2017). pH-degradable PVA-based nanogels via photo-crosslinking of thermo-preinduced nanoaggregates for controlled drug delivery. *Journal of Controlled Release*, 259, 160-167.
- Chen, W., Palazzo, A., Hennink, W. E., & Kok, R. J. (2016). Effect of particle size on drug loading and release kinetics of gefitinib-loaded PLGA microspheres. *Molecular pharmaceutics*, 14(2), 459-467.
- Chia, H. N., & Wu, B. M. (2015). Recent advances in 3D printing of biomaterials. *Journal of biological engineering*, 9(1), 1.
- Chiang, Z.-C., Yu, S.-H., Chao, A.-C., & Dong, G.-C. (2012). Preparation and characterization of dexamethasone-immobilized chitosan scaffold. *Journal of bioscience and bioengineering*, 113(5), 654-660.
- Christie, R., Findley, D., Dunfee, M., Hansen, R., Olsen, S., & Grainger, D. (2006). Photopolymerized hydrogel carriers for live vaccine ballistic delivery. *Vaccine*, 24(9), 1462-1469.
- Chung, J. H., Naficy, S., Yue, Z., Kapsa, R., Quigley, A., Moulton, S. E., & Wallace, G. G. (2013). Bio-ink properties and printability for extrusion printing living cells. *Biomaterials Science*, 1(7), 763-773.
- Clayton, K. N., Salameh, J. W., Wereley, S. T., & Kinzer-Ursem, T. L. (2016). Physical characterization of nanoparticle size and surface modification using particle scattering diffusometry. *Biomicrofluidics*, 10(5), 054107.
- Croisier, F., & Jérôme, C. (2013). Chitosan-based biomaterials for tissue engineering. *European Polymer Journal*, 49(4), 780-792.

## References

- Croxatt, H. B. (2002). Progestin implants for female contraception. *Contraception*, 65(1), 15-19.
- Dash, S., Murthy, P. N., Nath, L., & Chowdhury, P. (2010). Kinetic modeling on drug release from controlled drug delivery systems. *Acta Poloniae Pharmaceutica*, 67(3), 217-223.
- Davies, N. M., Fair, S. J., Hadgraft, J., & Kellaway, I. W. (1991). Evaluation of mucoadhesive polymers in ocular drug delivery. I. Viscous solutions. *Pharmaceutical research*, 8(8), 1039-1043.
- Desai, S. J., Simonelli, A., & Higuchi, W. (1965). Investigation of factors influencing release of solid drug dispersed in inert matrices. *Journal of pharmaceutical sciences*, 54(10), 1459-1464.
- Dhanaraju, M. D., Vema, K., Jayakumar, R., & Vamsadhara, C. (2003). Preparation and characterization of injectable microspheres of contraceptive hormones. *International journal of pharmaceutics*, 268(1-2), 23-29.
- El-Feky, G. S., Sharaf, S. S., El Shafei, A., & Hegazy, A. A. (2017). Using chitosan nanoparticles as drug carriers for the development of a silver sulfadiazine wound dressing. *Carbohydrate polymers*, 158, 11-19.
- El Maghraby, G. M., Barry, B. W., & Williams, A. C. (2008). Liposomes and skin: from drug delivery to model membranes. *European Journal of Pharmaceutical Sciences*, 34(4), 203-222.
- ElHag, M., Coghlan, K., Christmas, P., Harvey, W., & Harris, M. (1985). The anti-inflammatory effects of dexamethasone and therapeutic ultrasound in oral surgery. *British journal of oral and maxillofacial surgery*, 23(1), 17-23.

## References

- Espalin, D., Arcaute, K., Rodriguez, D., Medina, F., Posner, M., & Wicker, R. (2010). Fused deposition modeling of patient-specific polymethylmethacrylate implants. *Rapid Prototyping Journal*, 16(16), 164-173.
- Falconer, J. L., Christie, R. J., Pollard, E. J., Olsen, S. C., & Grainger, D. W. (2016). Live RB51 vaccine lyophilized hydrogel formulations with increased shelf life for practical ballistic delivery. *International journal of pharmaceutics*, 498(1), 187-194.
- Fan, L., Yang, H., Yang, J., Peng, M., & Hu, J. (2016). Preparation and characterization of chitosan/gelatin/PVA hydrogel for wound dressings. *Carbohydrate polymers*, 146, 427-434.
- Farzadi, A., Waran, V., Solati-Hashjin, M., Rahman, Z. A. A., Asadi, M., & Osman, N. A. A. (2015). Effect of layer printing delay on mechanical properties and dimensional accuracy of 3D printed porous prototypes in bone tissue engineering. *Ceramics International*, 41(7), 8320-8330.
- Fathi, E., Atyabi, N., Imani, M., & Alinejad, Z. (2011). Physically crosslinked polyvinyl alcohol–dextran blend xerogels: morphology and thermal behavior. *Carbohydrate polymers*, 84(1), 145-152.
- Ferris, C. J., Gilmore, K. J., & Wallace, G. G. (2013). Modified gellan gum hydrogels for tissue engineering applications. *Soft Matter*, 9(14), 3705-3711.
- Figueiredo, K., Alves, T. L., & Borges, C. P. (2009). Poly (vinyl alcohol) films crosslinked by glutaraldehyde under mild conditions. *Journal of applied polymer science*, 111(6), 3074-3080.
- Fiorica, C., Palumbo, F. S., Pitarresi, G., Bongiovì, F., & Giammona, G. (2017). Hyaluronic acid and beta cyclodextrins films for the release of corneal epithelial cells and dexamethasone. *Carbohydrate polymers*, 166, 281-290.

## References

- Fitzgerald, S. (2015). FDA Approves First 3D-Printed Epilepsy Drug Experts Assess the Benefits and Caveats. *Neurology Today*, 15(18), 26-27.
- Freiberg, S., & Zhu, X. (2004). Polymer microspheres for controlled drug release. *International journal of pharmaceutics*, 282(1-2), 1-18.
- Friend, D. R. (2016). Development of controlled release systems over the past 50 years in the area of contraception. *Journal of Controlled Release*, 240, 235-241.
- Fukumori, T., & Nakaoki, T. (2013). Significant improvement of mechanical properties for polyvinyl alcohol film prepared from freeze/thaw cycled gel. *Open Journal of Organic Polymer Materials*, 3(4), 110.
- Fukumori, T., & Nakaoki, T. (2014). High - tensile - strength polyvinyl alcohol films prepared from freeze/thaw cycled gels. *Journal of applied polymer science*, 131(15).
- Fukumori, T., & Nakaoki, T. (2015). High strength poly (vinyl alcohol) films obtained by drying and then stretching freeze/thaw cycled gel. *Journal of applied polymer science*, 132(1).
- Galeska, I., Kim, T.-K., Patil, S. D., Bhardwaj, U., Chattopadhyay, D., Papadimitrakopoulos, F., & Burgess, D. J. (2005). Controlled release of dexamethasone from PLGA microspheres embedded within polyacid-containing PVA hydrogels. *The American Association of Pharmaceutical Scientists (AAPS) journal*, 7(1), E231-E240.
- Garlotta, D. (2001). A Literature Review of Poly(Lactic Acid). *Journal of Polymers & the Environment*, 9(2), 63-84.
- Gehrke, S. H., & Lee, P. I. (1990). Hydrogels for drug delivery systems. *Drugs and the pharmaceutical sciences*, 41, 333-392.

## References

- Gemeinhart, R. A., Chen, J., Park, H., & Park, K. (2000). pH-sensitivity of fast responsive superporous hydrogels. *Journal of Biomaterials Science, Polymer Edition*, 11(12), 1371-1380.
- Genina, N., Holländer, J., Jukarainen, H., Mäkilä, E., Salonen, J., & Sandler, N. (2016). Ethylene vinyl acetate (EVA) as a new drug carrier for 3D printed medical drug delivery devices. *European Journal of Pharmaceutical Sciences*, 90, 53-63.
- Gethin, G. (2007). The significance of surface pH in chronic wounds. *Wounds uk*, 3(3), 52.
- Gnanasambandam, R., & Proctor, A. (2000). Determination of pectin degree of esterification by diffuse reflectance Fourier transform infrared spectroscopy. *Food chemistry*, 68(3), 327-332.
- Goole, J., & Karim, A. (2016). 3D printing in pharmaceuticals: A new tool for designing customized drug delivery systems. *International journal of pharmaceuticals*, 499(1-2), 376-394.
- Gosain, A., & DiPietro, L. A. (2004). Aging and wound healing. *World journal of surgery*, 28(3), 321-326.
- Goyanes, A., Buanz, A. B. M., Basit, A. W., & Gaisford, S. (2014b). Fused-filament 3D printing (3DP) for fabrication of tablets. *International journal of pharmaceuticals*, 476(1-2), 88-92.
- Goyanes, A., Buanz, A. B. M., Hatton, G. B., Gaisford, S., & Basit, A. W. (2014a). 3D printing of modified-release aminosalicylate (4-ASA and 5-ASA) tablets. *European Journal of Pharmaceuticals and Biopharmaceuticals*, 89, 157-162.
- Goyanes, A., Chang, H., Sedough, D., Hatton, G. B., Wang, J., Buanz, A., . . . Basit, A. W. (2015). Fabrication of controlled-release budesonide tablets via desktop (FDM) 3D printing. *International journal of pharmaceuticals*, 496(2), 414-420.

## References

- Goyanes, A., Wang, J., Buanz, A., Martínez-Pacheco, R., Telford, R., Gaisford, S., & Basit, A. W. (2015b). 3D printing of medicines: Engineering novel oral devices with unique design and drug release characteristics. *Molecular pharmaceutics*, 12(11), 4077-4084.
- Groenendyk, M., & Gallant, R. (2013). 3D printing and scanning at the Dalhousie University Libraries: a pilot project. *Library Hi Tech*, 31(1), 34-41.
- Gross, B. C., Erkal, J. L., Lockwood, S. Y., Chen, C., & Spence, D. M. (2014). Evaluation of 3D printing and its potential impact on biotechnology and the chemical sciences. *Analytical chemistry*, 86(7), 3240-3253.
- Gu, D., O'Connor, A. J., GH Qiao, G., & Ladewig, K. (2017). Hydrogels with smart systems for delivery of hydrophobic drugs. *Expert opinion on drug delivery*, 14(7), 879-895.
- Gupta, P., Vermani, K., & Garg, S. (2002). Hydrogels: from controlled release to pH-responsive drug delivery. *Drug discovery today*, 7(10), 569-579.
- Haigh, J., & Hopf, H. (1976). The blowgun in veterinary practice: its uses and preparation. *Journal of the American Veterinary Medical Association*, 169(9), 881-883.
- Hall, S. E., Nixon, B., & Aitken, R. J. (2017). Non-surgical sterilisation methods may offer a sustainable solution to feral horse (*Equus caballus*) overpopulation. *Reproduction, Fertility and Development*, 29(9), 1655-1666.
- Hassan, C. M., & Peppas, N. A. (2000). Structure and morphology of freeze/thawed PVA hydrogels. *Macromolecules*, 33(7), 2472-2479.
- Heimdal, K., Hirschberg, H., Slettebø, H., Watne, K., & Nome, O. (1992). High incidence of serious side effects of high-dose dexamethasone treatment in patients

## References

- with epidural spinal cord compression. *Journal of neuro-oncology*, 12(2), 141-144.
- Henderson, A. M. (1993). Ethylene-vinyl acetate (EVA) copolymers: a general review. *The Institute of Electrical and Electronics Engineers Electrical Insulation Magazine*, 9(1), 30-38.
- Hendricks, M. D., & Treadway, L. N. (2015). Dart gun: Google Patents.
- Hickey, T., Kreutzer, D., Burgess, D., & Moussy, F. (2002). Dexamethasone/PLGA microspheres for continuous delivery of an anti-inflammatory drug for implantable medical devices. *Biomaterials*, 23(7), 1649-1656.
- Higuchi, T. (1963). Mechanism of sustained - action medication. Theoretical analysis of rate of release of solid drugs dispersed in solid matrices. *Journal of pharmaceutical sciences*, 52(12), 1145-1149.
- Hill, S., Varker, A. S., Karlage, K., & Myrdal, P. B. (2009). Analysis of drug content and weight uniformity for half-tablets of 6 commonly split medications. *Journal of Managed Care Pharmacy*, 15(3), 253-261.
- Hoffman, A. S. (2012). Hydrogels for biomedical applications. *Advanced drug delivery reviews*, 64, 18-23.
- Holländer, J., Genina, N., Jukarainen, H., Khajeheian, M., Rosling, A., Mäkilä, E., & Sandler, N. (2016). Three-dimensional printed PCL-based implantable prototypes of medical devices for controlled drug delivery. *Journal of pharmaceutical sciences*, 105(9), 2665-2676.
- Huang, M., Cai, D., Liu, Y., Sun, J., Wang, J., Qin, C., . . . Kazuo, Y. (2012). Investigation of a-PVA/s-PVA hydrogels prepared by freezing-thawing method. *Fibers and Polymers*, 13(8), 955-962.



## References

- Huang, X., & Brazel, C. S. (2001). On the importance and mechanisms of burst release in matrix-controlled drug delivery systems. *Journal of Controlled Release*, 73(2-3), 121-136.
- Hutmacher, D. W., Sittering, M., & Risbud, M. V. (2004). Scaffold-based tissue engineering: rationale for computer-aided design and solid free-form fabrication systems. *Trends in Biotechnology*, 22(7), 354-362.
- Islam, A., & Yasin, T. (2012). Controlled delivery of drug from pH sensitive chitosan/poly (vinyl alcohol) blend. *Carbohydrate polymers*, 88(3), 1055-1060.
- Jameela, S., Kumary, T., Lal, A., & Jayakrishnan, A. (1998). Progesterone-loaded chitosan microspheres: a long acting biodegradable controlled delivery system. *Journal of Controlled Release*, 52(1-2), 17-24.
- Jin, S. G., Kim, K. S., Kim, D. W., Kim, D. S., Seo, Y. G., Go, T. G., . . . Choi, H.-G. (2016). Development of a novel sodium fusidate-loaded triple polymer hydrogel wound dressing: Mechanical properties and effects on wound repair. *International journal of pharmaceutics*, 497(1-2), 114-122.
- Jonathan, G., & Karim, A. (2016). 3D printing in pharmaceuticals: A new tool for designing customized drug delivery systems. *International Journal of Pharmaceutics*, 499(1-2), 376-394.  
doi:<http://dx.doi.org/10.1016/j.ijpharm.2015.12.071>
- Kalra, A., Lowe, A., & Al-Jumaily, A. (2016). Mechanical Behaviour of Skin: A Review. *Journal of Material Science & Engineering*, 5(4), 254-260.
- Kamoun, E. A., Kenawy, E.-R. S., & Chen, X. (2017). A review on polymeric hydrogel membranes for wound dressing applications: PVA-based hydrogel dressings. *Journal of advanced research*, 8(3), 217-233.

## References

- Karageorgiou, V., & Kaplan, D. (2005). Porosity of 3D biomaterial scaffolds and osteogenesis. *Biomaterials*, 26(27), 5474-5491.
- Kashikar, V., Dhole, S., Kandekar, U., & Khose, P. (2014). Study of mucoadhesive microsphere of pirfenidone for nasal drug delivery. *Asian Journal of Pharmaceutics (AJP): Free full text articles from Asian J Pharm*, 8(1).
- Kaur, A., & Kaur, G. (2012). Mucoadhesive buccal patches based on interpolymer complexes of chitosan–pectin for delivery of carvedilol. *Saudi Pharmaceutical Journal*, 20(1), 21-27.
- Kayal, S., & Ramanujan, R. (2010). Doxorubicin loaded PVA coated iron oxide nanoparticles for targeted drug delivery. *Materials Science and Engineering: C*, 30(3), 484-490.
- Kenawy, E.-R., Kamoun, E. A., Eldin, M. S. M., & El-Meligy, M. A. (2014). Physically crosslinked poly (vinyl alcohol)-hydroxyethyl starch blend hydrogel membranes: Synthesis and characterization for biomedical applications. *Arabian Journal of Chemistry*, 7(3), 372-380.
- Kevadiya, B. D., Joshi, G. V., Mody, H. M., & Bajaj, H. C. (2011). Biopolymer–clay hydrogel composites as drug carrier: host–guest intercalation and in vitro release study of lidocaine hydrochloride. *Applied Clay Science*, 52(4), 364-367.
- Khaled, S. A., Burley, J. C., Alexander, M. R., Yang, J., & Roberts, C. J. (2015). 3D printing of tablets containing multiple drugs with defined release profiles. *International journal of pharmaceutics*, 494(2), 643-650.
- Khurma, J. R., Rohindra, D. R., & Nand, A. V. (2006). Synthesis and properties of hydrogels based on chitosan and poly (vinyl alcohol) crosslinked by genipin. *Journal of Macromolecular Science, Part A: Pure and Applied Chemistry*, 43(4-5), 749-758.

## References

- Kim, E. G., Kim, B. S., & Kim, D. S. (2007). Physical properties and morphology of polycaprolactone/starch/pine - leaf composites. *Journal of applied polymer science*, 103(2), 928-934.
- Kim, T. H., Park, Y. H., Kim, K. J., & Cho, C. S. (2003). Release of albumin from chitosan-coated pectin beads in vitro. *International journal of pharmaceutics*, 250(2), 371-383.
- King, T. L., & Brucker, M. C. (2010). *Pharmacology for women's health*: Jones & Bartlett Publishers.
- Klode, J., Schöttler, L., Stoffels, I., Körber, A., Schadendorf, D., & Dissemmond, J. (2011). Investigation of adhesion of modern wound dressings: a comparative analysis of 56 different wound dressings. *Journal of the European Academy of Dermatology and Venereology*, 25(8), 933-939.
- Kobayashi, M., Chang, Y.-S., & Oka, M. (2005). A two year in vivo study of polyvinyl alcohol-hydrogel (PVA-H) artificial meniscus. *Biomaterials*, 26(16), 3243-3248.
- Kochhar, J. S., Lim, W. X. S., Zou, S., Foo, W. Y., Pan, J., & Kang, L. (2013). Microneedle integrated transdermal patch for fast onset and sustained delivery of lidocaine. *Molecular pharmaceutics*, 10(11), 4272-4280.
- Kokabi, M., Sirousazar, M., & Hassan, Z. M. (2007). PVA-clay nanocomposite hydrogels for wound dressing. *European Polymer Journal*, 43(3), 773-781.
- Korsmeyer, R. W., Gurny, R., Doelker, E., Buri, P., & Peppas, N. A. (1983). Mechanisms of solute release from porous hydrophilic polymers. *International journal of pharmaceutics*, 15(1), 25-35.
- Kowalonek, J. (2017). Studies of chitosan/pectin complexes exposed to UV radiation. *International journal of biological macromolecules*, 103, 515-524.

## References

- Kreeger, T. J. (1997). Overview of delivery systems for the administration of contraceptives to wildlife. *Contraception in wildlife management*. Washington, DC: US Government Printing Office, 29-48.
- Kumar, A., Pandey, M., Koshy, M., & Saraf, S. A. (2010). Synthesis of fast swelling superporous hydrogel: effect of concentration of crosslinker and acidisol on swelling ratio and mechanical strength. *International Journal of Drug Delivery*, 2(2), 135-140.
- Kumari, A., Yadav, S. K., & Yadav, S. C. (2010). Biodegradable polymeric nanoparticles based drug delivery systems. *Colloids and surfaces B: Biointerfaces*, 75(1), 1-18.
- Kunasekaran, V., & Krishnamoorthy, K. (2015). Experimental Design for the Optimization of Nanoscale Solid Lipid Particles Containing Rasagiline Mesylate. *Journal of Young Pharmacists Vol*, 7(4), 285.
- Labet, M., & Thielemans, W. (2009). Synthesis of polycaprolactone: a review. *Chemical Society Reviews*, 38(12), 3484-3504.
- Larrañeta, E., Barturen, L., Ervine, M., & Donnelly, R. F. (2018). Hydrogels based on poly (methyl vinyl ether-co-maleic acid) and Tween 85 for sustained delivery of hydrophobic drugs. *International journal of pharmaceutics*, 538(1-2), 147-158.
- Larrañeta, E., Stewart, S., Ervine, M., Al-Kasasbeh, R., & Donnelly, R. F. (2018). Hydrogels for Hydrophobic Drug Delivery. Classification, Synthesis and Applications. *Journal of functional biomaterials*, 9(1), 13.
- Lee, C. H., & Bae, Y. C. (2015). Effect of salt on swelling behaviors of thermosensitive hydrogels: applicability of the nonrandom contact model. *Macromolecules*, 48(12), 4063-4072.

## References

- Leimann, F. V., Biz, M. H., Kaufmann, K. C., Maia, W. J., Honçalves, O. H., Cardozo Filho, L., . . . Araújo, P. H. H. d. (2015). Characterization of progesterone loaded biodegradable blend polymeric nanoparticles. *Ciência Rural*, 45(11), 2082-2088.
- Leong, K., Cheah, C., & Chua, C. (2003). Solid freeform fabrication of three-dimensional scaffolds for engineering replacement tissues and organs. *Biomaterials*, 24(13), 2363-2378.
- Li, B., Shan, C.-L., Zhou, Q., Fang, Y., Wang, Y.-L., Xu, F., . . . Xie, G.-L. (2013). Synthesis, characterization, and antibacterial activity of cross-linked chitosan-glutaraldehyde. *Marine drugs*, 11(5), 1534-1552.
- Li, D., Guo, G., Fan, R., Liang, J., Deng, X., Luo, F., & Qian, Z. (2013). PLA/F68/dexamethasone implants prepared by hot-melt extrusion for controlled release of anti-inflammatory drug to implantable medical devices: I. Preparation, characterization and hydrolytic degradation study. *International journal of pharmaceutics*, 441(1), 365-372.
- Li, J. K., Wang, N., & Wu, X. S. (1998). Poly (vinyl alcohol) nanoparticles prepared by freezing–thawing process for protein/peptide drug delivery. *Journal of Controlled Release*, 56(1-3), 117-126.
- Li, L., Saedan, M., Feng, W., Fuh, J., Wong, Y., Loh, H., . . . Lu, L. (2009). Development of a multi-nozzle drop-on-demand system for multi-material dispensing. *Journal of Materials Processing Technology*, 209(9), 4444-4448.
- Li, X., Bian, W., Li, D., Lian, Q., & Jin, Z. (2011). Fabrication of porous beta-tricalcium phosphate with microchannel and customized geometry based on gel-casting and rapid prototyping. *Proceedings of the institution of mechanical engineers, Part H: journal of engineering in medicine*, 225(3), 315-323.

## References

- Lim, L. Y., Khor, E., & Ling, C. E. (1999). Effects of dry heat and saturated steam on the physical properties of chitosan. *Journal of Biomedical Materials Research*, 48(2), 111-116.
- Long, J., Gholizadeh, H., Lu, J., Bunt, C., & Seyfoddin, A. (2017). Application of fused deposition modelling (FDM) method of 3D printing in drug delivery. *Current pharmaceutical design*, 23(3), 433-439.
- Long, J., Nand, A. V., Ray, S., Mayhew, S., White, D., Bunt, C. R., & Seyfoddin, A. (2018). Development of customised 3D printed biodegradable projectile for administrating extended-release contraceptive to wildlife. *International journal of pharmaceutics*, 548(1), 349-356.
- Ma, G., Song, C., Sun, H., Yang, J., & Leng, X. (2006). A biodegradable levonorgestrel-releasing implant made of PCL/F68 compound as tested in rats and dogs. *Contraception*, 74(2), 141-147.
- Machado, S. R., Lunardi, L. O., Tristão, A. P., & Marchetti, J. M. (2009). Preparation and characterization of D, L-PLA loaded 17- $\beta$ -Estradiol valerate by emulsion/evaporation methods. *Journal of microencapsulation*, 26(3), 202-213.
- Malana, M. A., & Zohra, R. (2013). The release behavior and kinetic evaluation of tramadol HCl from chemically cross linked Ter polymeric hydrogels. *DARU Journal of Pharmaceutical Sciences*, 21(1), 10.
- Mallapragada, S. K., Peppas, N. A., & Colombo, P. (1997). Crystal dissolution - controlled release systems. II. Metronidazole release from semicrystalline poly (vinyl alcohol) systems. *Journal of Biomedical Materials Research*, 36(1), 125-130.
- Mallepally, R. R., Bernard, I., Marin, M. A., Ward, K. R., & McHugh, M. A. (2013). Superabsorbent alginate aerogels. *The Journal of Supercritical Fluids*, 79, 202-208.

## References

- Maniruzzaman, M., Boateng, J. S., Snowden, M. J., & Douroumis, D. (2012). A review of hot-melt extrusion: process technology to pharmaceutical products. *International Scholarly Research Notices pharmaceuticals*, 2012.
- Manoukian, O. S., Arul, M. R., Sardashti, N., Stedman, T., James, R., Rudraiah, S., & Kumbar, S. G. (2018). Biodegradable polymeric injectable implants for long - term delivery of contraceptive drugs. *Journal of applied polymer science*, 135(14), 46068.
- Mansur, H. S., Sadahira, C. M., Souza, A. N., & Mansur, A. A. (2008). FTIR spectroscopy characterization of poly (vinyl alcohol) hydrogel with different hydrolysis degree and chemically crosslinked with glutaraldehyde. *Materials Science and Engineering: C*, 28(4), 539-548.
- Mashak, A., Mobedi, H., & Mahdavi, H. (2015). A Comparative Study of Progesterone and Lidocaine Hydrochloride Release from Poly (L-lactide) Films. *Pharmaceutical Sciences*, 21(2), 77.
- McCullough, E. J., & Yadavalli, V. K. (2013). Surface modification of fused deposition modeling ABS to enable rapid prototyping of biomedical microdevices. *Journal of Materials Processing Technology*, 213(6), 947-954.
- McKenzie, M., Betts, D., Suh, A., Bui, K., Kim, L. D., & Cho, H. (2015). Hydrogel-based drug delivery systems for poorly water-soluble drugs. *Molecules*, 20(11), 20397-20408.
- Melocchi, A., Parietti, F., Loreti, G., Maroni, A., Gazzaniga, A., & Zema, L. (2015). 3D printing by fused deposition modeling (FDM) of a swellable/erodible capsular device for oral pulsatile release of drugs. *Journal of Drug Delivery Science and Technology*, 30, 360-367.

## References

- Mishra, R. K., Datt, M., & Banthia, A. K. (2008). Synthesis and characterization of pectin/PVP hydrogel membranes for drug delivery system. *Aaps Pharmscitech*, 9(2), 395-403.
- Miyai, T., Ito, A., Tamazawa, G., Matsuno, T., Sogo, Y., Nakamura, C., . . . Satoh, T. (2008). Antibiotic-loaded poly- $\epsilon$ -caprolactone and porous  $\beta$ -tricalcium phosphate composite for treating osteomyelitis. *Biomaterials*, 29(3), 350-358.
- Mohanty, A. K., Misra, M., & Drzal, L. T. (2005). *Natural fibers, biopolymers, and biocomposites*: Chemical Rubber Company Press.
- Moroni, L., de Wijn, J. R., & van Blitterswijk, C. A. (2006). 3D fiber-deposited scaffolds for tissue engineering: Influence of pores geometry and architecture on dynamic mechanical properties. *Biomaterials*, 27(7), 974-985.
- Moulton, S. E., & Wallace, G. G. (2014). 3-dimensional (3D) fabricated polymer based drug delivery systems. *Journal of Controlled Release*, 193, 27-34.
- Nand, A. V., Ray, S., Travas-Sejdic, J., & Kilmartin, P. A. (2012). Characterization of polyethylene terephthalate/polyaniline blends as potential antioxidant materials. *Materials Chemistry and Physics*, 134(1), 443-450.
- Nanda, S., Sood, N., Reddy, B., & Markandeywar, T. S. (2013). Preparation and characterization of poly (vinyl alcohol)-chondroitin sulphate hydrogel as scaffolds for articular cartilage regeneration. *Indian Journal of Materials Science*, 2013.
- Neufeld, L., & Bianco-Peled, H. (2017). Pectin–chitosan physical hydrogels as potential drug delivery vehicles. *International journal of biological macromolecules*, 101, 852-861.



## References

- Niebergall, P., Milosovich, G., & Goyan, J. (1963). Dissolution rate studies II. Dissolution of particles under conditions of rapid agitation. *Journal of pharmaceutical sciences*, 52(3), 236-241.
- Nikam, V. K., Kotade, K. B., Gaware, V. M., Dhamak, R., Somwanshi, S. B., & Khadse, A. N. (2011). Eudragit a versatile polymer: a review. *Pharmacol online*, 1(1), 152-164.
- Nordby, M. H., Kjøniksen, A.-L., Nyström, B., & Roots, J. (2003). Thermoreversible gelation of aqueous mixtures of pectin and chitosan. *Rheology. Biomacromolecules*, 4(2), 337-343.
- Numpilai, T., Witoon, T., Chareonpanich, M., & Limtrakul, J. (2017). Impact of physicochemical properties of porous silica materials conjugated with dexamethasone via pH-responsive hydrazone bond on drug loading and release behavior. *Applied Surface Science*, 396, 504-514.
- Nuttelman, C. R., Mortisen, D. J., Henry, S. M., & Anseth, K. S. (2001). Attachment of fibronectin to poly (vinyl alcohol) hydrogels promotes NIH3T3 cell adhesion, proliferation, and migration. *Journal of Biomedical Materials Research*, 57(2), 217-223.
- Ofokansi, K. C., & Kenechukwu, F. C. (2013). Formulation development and evaluation of drug release kinetics from colon-targeted ibuprofen tablets based on Eudragit RL 100-chitosan interpolyelectrolyte complexes. *International Scholarly Research Notices: Pharmaceutics*, 2013.
- Okan, D., Woo, K., Ayello, E. A., & Sibbald, G. (2007). The role of moisture balance in wound healing. *Advances in skin & wound care*, 20(1), 39-53.
- Oliveira, J. E., Medeiros, E. S., Cardozo, L., Voll, F., Madureira, E. H., Mattoso, L. H. C., & Assis, O. B. G. (2013). Development of poly (lactic acid) nanostructured

## References

- membranes for the controlled delivery of progesterone to livestock animals. *Materials Science and Engineering: C*, 33(2), 844-849.
- Olsen, S. C., Christie, R., Grainger, D., & Stoffregen, W. (2006). Immunologic responses of bison to vaccination with *Brucella abortus* strain RB51: Comparison of parenteral to ballistic delivery via compressed pellets or photopolymerized hydrogels. *Vaccine*, 24(9), 1346-1353.
- Paradossi, G., Cavalieri, F., Chiessi, E., Spagnoli, C., & Cowman, M. K. (2003). Poly (vinyl alcohol) as versatile biomaterial for potential biomedical applications. *Journal of Materials Science: Materials in Medicine*, 14(8), 687-691.
- Park, J.-S., Kim, H.-A., Choi, J.-B., Gwon, H.-J., Shin, Y.-M., Lim, Y.-M., . . . Nho, Y.-C. (2012). Effects of annealing and the addition of PEG on the PVA based hydrogel by gamma ray. *Radiation Physics and Chemistry*, 81(7), 857-860.
- Peppas, N., Bures, P., Leobandung, W., & Ichikawa, H. (2000). Hydrogels in pharmaceutical formulations. *European Journal of Pharmaceutics and Biopharmaceutics*, 50(1), 27-46.
- Peppas, N., & Simmons, R. (2004). Mechanistic analysis of protein delivery from porous poly (vinyl alcohol) systems. *Journal of Drug Delivery Science and Technology*, 14(4), 285-289.
- Peppas, N. A., Hilt, J. Z., Khademhosseini, A., & Langer, R. (2006). Hydrogels in biology and medicine: from molecular principles to bionanotechnology. *Advanced materials*, 18(11), 1345-1360.
- Peppas, N. A., & Wright, S. L. (1998). Drug diffusion and binding in ionizable interpenetrating networks from poly (vinyl alcohol) and poly (acrylic acid). *European Journal of Pharmaceutics and Biopharmaceutics*, 46(1), 15-29.

## References

- Perrie, Y., & Rades, T. (2010). *Pharmaceutics—Drug Delivery and Targeting: Fastrack*, Pharmaceutical Press: London.
- Photos, P. J., Bacakova, L., Discher, B., Bates, F. S., & Discher, D. E. (2003). Polymer vesicles in vivo: correlations with PEG molecular weight. *Journal of Controlled Release*, 90(3), 323-334.
- Pietrzak, K., Isreb, A., & Alhnan, M. A. (2015). A flexible-dose dispenser for immediate and extended release 3D printed tablets. *European Journal of Pharmaceutics and Biopharmaceutics*, 96, 380-387.
- Poon, L., Wilson, L. D., & Headley, J. V. (2014). Chitosan-glutaraldehyde copolymers and their sorption properties. *Carbohydrate polymers*, 109, 92-101.
- Prasad, L. K., & Smyth, H. (2015). 3D Printing technologies for drug delivery: a review. *Drug development and industrial pharmacy*, 42(7), 1019-1031.
- Qi, X., Hu, X., Wei, W., Yu, H., Li, J., Zhang, J., & Dong, W. (2015). Investigation of Salecan/poly (vinyl alcohol) hydrogels prepared by freeze/thaw method. *Carbohydrate polymers*, 118, 60-69.
- Rai, B., Teoh, S.-H., Hutmacher, D., Cao, T., & Ho, K. (2005). Novel PCL-based honeycomb scaffolds as drug delivery systems for rhBMP-2. *Biomaterials*, 26(17), 3739-3748.
- Ray, S., & Cooney, R. P. (2012). Thermal degradation of polymer and polymer composites *Handbook of environmental degradation of materials* (Second ed.).
- Ray, S., & Cooney, R. P. (2018). Thermal degradation of polymer and polymer composites *Handbook of Environmental Degradation of Materials* (Third ed., pp. 185-206): Elsevier.

- Reis, C. P., Neufeld, R. J., & Veiga, F. (2017). Preparation of Drug-Loaded Polymeric Nanoparticles *Nanomedicine in Cancer* (pp. 197-240): Pan Stanford.
- Reis, E. F. d., Campos, F. S., Lage, A. P., Leite, R. C., Heneine, L. G., Vasconcelos, W. L., . . . Mansur, H. S. (2006). Synthesis and characterization of poly (vinyl alcohol) hydrogels and hybrids for rMPB70 protein adsorption. *Materials Research, 9*(2), 185-191.
- Repka, M. A., Gutta, K., Prodduturi, S., Munjal, M., & Stodghill, S. P. (2005). Characterization of cellulosic hot-melt extruded films containing lidocaine. *European Journal of Pharmaceutics and Biopharmaceutics, 59*(1), 189-196.
- Rodrigues, L. B., Leite, H. F., Yoshida, M. I., Saliba, J. B., Junior, A. S. C., & Faraco, A. A. (2009). In vitro release and characterization of chitosan films as dexamethasone carrier. *International journal of pharmaceutics, 368*(1), 1-6.
- Roozbahani, M., Kharaziha, M., & Emadi, R. (2017). pH sensitive dexamethasone encapsulated laponite nanoplatelets: Release mechanism and cytotoxicity. *International journal of pharmaceutics, 518*(1-2), 312-319.
- Rossi, F., Perale, G., & Masi, M. (2016). *Controlled Drug Delivery Systems: Towards New Frontiers in Patient Care*: Springer.
- Rutkowski, J. V., & Levin, B. C. (1986). Acrylonitrile - butadiene - styrene copolymers (ABS): Pyrolysis and combustion products and their toxicity—a review of the literature. *Fire and materials, 10*(3 - 4), 93-105.
- Sachs, E., Cima, M., Williams, P., Brancazio, D., & Cornie, J. (1992). Three dimensional printing: rapid tooling and prototypes directly from a CAD model. *Journal of Engineering for Industry, 114*(4), 481-488.
- Salgado, M., Rodríguez-Rojo, S., Reis, R. L., Cocero, M. J., & Duarte, A. R. C. (2017). Preparation of barley and yeast  $\beta$ -glucan scaffolds by hydrogel foaming:

- Evaluation of dexamethasone release. *The Journal of Supercritical Fluids*, 127, 158-165.
- Saurí, J., Millán, D., Suñé-Negre, J., Colom, H., Ticó, J., Miñarro, M., . . . García-Montoya, E. (2014). Quality by design approach to understand the physicochemical phenomena involved in controlled release of captopril SR matrix tablets. *International journal of pharmaceutics*, 477(1), 431-441.
- Sawant, P. D., Luu, D., Ye, R., & Buchta, R. (2010). Drug release from hydroethanolic gels. Effect of drug's lipophilicity (log P), polymer–drug interactions and solvent lipophilicity. *International journal of pharmaceutics*, 396(1-2), 45-52.
- Schmedlen, R. H., Masters, K. S., & West, J. L. (2002). Photocrosslinkable polyvinyl alcohol hydrogels that can be modified with cell adhesion peptides for use in tissue engineering. *Biomaterials*, 23(22), 4325-4332.
- Schulz, M., Fussnegger, B., & Bodmeier, R. (2011). Influence of adsorbents in transdermal matrix patches on the release and the physical state of ethinyl estradiol and levonorgestrel. *European Journal of Pharmaceutics and Biopharmaceutics*, 77(2), 240-248.
- Scoutaris, N., Alexander, M. R., Gellert, P. R., & Roberts, C. J. (2011). Inkjet printing as a novel medicine formulation technique. *Journal of Controlled Release*, 156(2), 179-185.
- Sébastien, F., Stéphane, G., Copinet, A., & Coma, V. (2006). Novel biodegradable films made from chitosan and poly (lactic acid) with antifungal properties against mycotoxinogen strains. *Carbohydrate polymers*, 65(2), 185-193.
- Seeley, S. K., Seeley, J. V., Telehowski, P., Martin, S., Tavakoli, M., Colton, S. L., . . . Atkinson, P. J. (2004). Volume and surface area study of tobramycin-

## References

- polymethylmethacrylate beads. *Clinical orthopaedics and related research*, 420, 298-303.
- Selimis, A., Mironov, V., & Farsari, M. (2015). Direct laser writing: Principles and materials for scaffold 3D printing. *Microelectronic Engineering*, 132, 83-89.
- Senatov, F., Niaza, K., Zadorozhnyy, M. Y., Maksimkin, A., Kaloshkin, S., & Estrin, Y. (2016). Mechanical properties and shape memory effect of 3D-printed PLA-based porous scaffolds. *Journal of the mechanical behavior of biomedical materials*, 57, 139-148.
- Seyfoddin, A., Shaw, J., & Al-Kassas, R. (2010). Solid lipid nanoparticles for ocular drug delivery. *Drug delivery*, 17(7), 467-489.
- Shah, D., Shah, Y., & Pradhan, R. (1997). Development and evaluation of controlled-release diltiazem HCl microparticles using cross-linked poly (vinyl alcohol). *Drug development and industrial pharmacy*, 23(6), 567-574.
- Shaikh, H. K., Kshirsagar, R., & Patil, S. (2015). Mathematical models for drug release characterization: a review. *World Journal Of Pharmacy And Pharmaceutical Sciences*, 4(04), 324-338.
- Shakespeare, P. (2001). Burn wound healing and skin substitutes. *Burns*, 27(5), 517-522.
- Shapiro, L., Eason, C., Bunt, C., Hix, S., Aylett, P., & MacMorran, D. (2016). Efficacy of encapsulated sodium nitrite as a new tool for feral pig management. *Journal of pest science*, 89(2), 489-495.
- Shen, J., & Burgess, D. J. (2012). Accelerated in vitro release testing of implantable PLGA microsphere/PVA hydrogel composite coatings. *International journal of pharmaceutics*, 422(1-2), 341-348.

## References

- Shen, J., & Burgess, D. J. (2015). In vitro–in vivo correlation for complex non-oral drug products: where do we stand? *Journal of Controlled Release*, 219, 644-651.
- Shulman, L. P. (2011). The state of hormonal contraception today: benefits and risks of hormonal contraceptives: combined estrogen and progestin contraceptives. *American journal of obstetrics and gynecology*, 205(4), S9-S13.
- Shulman, L. P., Nelson, A. L., & Darney, P. D. (2004). Recent developments in hormone delivery systems. *American journal of obstetrics and gynecology*, 190(4), S39-S48.
- Sibbald, R., Williamson, D., Orsted, H., Campbell, K., Keast, D., Krasner, D., & Sibbald, D. (2000). Preparing the wound bed--debridement, bacterial balance, and moisture balance. *Ostomy/Wound Management*, 46(11), 14-22.
- Siepmann, J., & Peppas, N. (2001). Modeling of drug release from delivery systems based on hydroxypropyl methylcellulose (HPMC). *Advanced drug delivery reviews*, 48(2-3), 139-157.
- Siepmann, J., & Peppas, N. A. (2011). Higuchi equation: derivation, applications, use and misuse. *International journal of pharmaceuticals*, 418(1), 6-12.
- Singhvi, G., & Singh, M. (2011). In-vitro drug release characterization models. *International Journal of Pharmaceutical Studies and Research*, 2(1), 77-84.
- Sinha, V., Singla, A. K., Wadhawan, S., Kaushik, R., Kumria, R., Bansal, K., & Dhawan, S. (2004). Chitosan microspheres as a potential carrier for drugs. *International journal of pharmaceuticals*, 274(1-2), 1-33.
- Sinitsya, A., Čopíková, J., Prutyanov, V., Skoblya, S., & Machovič, V. (2000). Amidation of highly methoxylated citrus pectin with primary amines. *Carbohydrate polymers*, 42(4), 359-368.

## References

- Skowrya, J., Pietrzak, K., & Alhnan, M. A. (2015). Fabrication of extended-release patient-tailored prednisolone tablets via fused deposition modelling (FDM) 3D printing. *European Journal of Pharmaceutical Sciences*, 68, 11-17.
- Smith, K. (2017). Assessing koala (*Phascolarctos cinereus*) population density for management on French Island, Victoria.
- Snyder, R. J., Fife, C., & Moore, Z. (2016). Components and quality measures of DIME (devitalized tissue, infection/inflammation, moisture balance, and edge preparation) in wound care. *Advances in skin & wound care*, 29(5), 205.
- Soni, S. R., & Ghosh, A. (2017). Exploring pullulan-poly (vinyl alcohol) interpenetrating network microspheres as controlled release drug delivery device. *Carbohydrate polymers*, 174, 812-822.
- Stegeman, B. H., de Bastos, M., Rosendaal, F. R., van Hylckama Vlieg, A., Helmerhorst, F. M., Stijnen, T., & Dekkers, O. M. (2013). Different combined oral contraceptives and the risk of venous thrombosis: systematic review and network meta-analysis. *British Medical Journal*, 347, f5298.
- Szymańska, E., & Winnicka, K. (2015). Stability of chitosan—a challenge for pharmaceutical and biomedical applications. *Marine drugs*, 13(4), 1819-1846.
- Tamburic, S., & Craig, D. Q. (1997). A comparison of different in vitro methods for measuring mucoadhesive performance. *European Journal of Pharmaceutics and biopharmaceutics*, 44(2), 159-167.
- Tan, D., Maniruzzaman, M., & Nokhodchi, A. (2018). Advanced pharmaceutical applications of Hot-Melt Extrusion coupled with Fused Deposition Modelling (FDM) 3D printing for personalised drug delivery. *Pharmaceutics*, 10(4), 203.



## References

- Tavakoli, J., & Tang, Y. (2017). Honey/PVA hybrid wound dressings with controlled release of antibiotics: Structural, physico-mechanical and in-vitro biomedical studies. *Materials Science and Engineering: C*, 77, 318-325.
- Tentor, F. R., de Oliveira, J. H., Scariot, D. B., Lazarin-Bidoia, D., Bonafe, E. G., Nakamura, C. V., . . . Martins, A. F. (2017). Scaffolds based on chitosan/pectin thermosensitive hydrogels containing gold nanoparticles. *International journal of biological macromolecules*, 102, 1186-1194.
- Teo, E. Y., Ong, S.-Y., Chong, M. S. K., Zhang, Z., Lu, J., Moochhala, S., . . . Teoh, S.-H. (2011). Polycaprolactone-based fused deposition modeled mesh for delivery of antibacterial agents to infected wounds. *Biomaterials*, 32(1), 279-287.
- Thakral, S., Thakral, N. K., & Majumdar, D. K. (2013). Eudragit®: a technology evaluation. *Expert opinion on drug delivery*, 10(1), 131-149.
- Tiwari, G., Tiwari, R., Sriwastawa, B., Bhati, L., Pandey, S., Pandey, P., & Bannerjee, S. K. (2012). Drug delivery systems: An updated review. *International journal of pharmaceutical investigation*, 2(1), 2.
- Treanor, J. J., Johnson, J. S., Wallen, R. L., Cilles, S., Crowley, P. H., Cox, J. J., . . . Plumb, G. E. (2010). Vaccination strategies for managing brucellosis in Yellowstone bison. *Vaccine*, 28, F64-F72.
- Vellayappan, M., Venugopal, J., Ramakrishna, S., Ray, S., Ismail, A., Mandal, M., . . . Jaganathan, S. (2016). Electrospinning applications from diagnosis to treatment of diabetes. *Royal Society of Chemistry Advances*, 6(87), 83638-83655.
- Ventura, I., & Bianco-Peled, H. (2015). Small-angle X-ray scattering study on pectin–chitosan mixed solutions and thermoreversible gels. *Carbohydrate polymers*, 123, 122-129.
- Villanueva, J. M. (2007). Vaginal health products: Google Patents.

## References

- Wahlquist, C. (2017). Kangaroo Island koala cull rejected by South Australian government. Retrieved from <https://www.theguardian.com/australia-news/2017/aug/28/kangaroo-island-koala-cull-rejected-by-south-australian-government>
- Wan, L. S., & Lim, L. (1992). Drug release from heat-treated polyvinyl alcohol films. *Drug development and industrial pharmacy*, 18(17), 1895-1906.
- Wang, S., Zhang, L., Lin, F., Sa, X., Zuo, J., Shao, Q., . . . Zeng, S. (2005). Controlled release of levonorgestrel from biodegradable poly (D, L-lactide-co-glycolide) microspheres: in vitro and in vivo studies. *International journal of pharmaceutics*, 301(1-2), 217-225.
- Wang, T., Turhan, M., & Gunasekaran, S. (2004). Selected properties of pH - sensitive, biodegradable chitosan - poly (vinyl alcohol) hydrogel. *Polymer International*, 53(7), 911-918.
- Warnke, P. H., Seitz, H., Warnke, F., Becker, S. T., Sivananthan, S., Sherry, E., . . . Douglas, T. (2010). Ceramic scaffolds produced by computer - assisted 3D printing and sintering: Characterization and biocompatibility investigations. *Journal of Biomedical Materials Research Part B: Applied Biomaterials*, 93(1), 212-217.
- West, G., Heard, D., & Caulkett, N. (2014). *Zoo animal and wildlife immobilization and anesthesia*: John Wiley & Sons.
- Whittle, K., Kieser, J., Ichim, I., Swain, M., Waddell, N., Livingstone, V., & Taylor, M. (2008). The biomechanical modelling of non-ballistic skin wounding: blunt-force injury. *Forensic science, medicine, and pathology*, 4(1), 33-39.
- Wiedner, E., Lindsay, W., & Isaza, R. (2012). Management of zebras and zebra hybrids (zebroids). *Compendium*, 34, E1-E4.

## References

- Wilson, C., Olejnik, O., & Hardy, J. (1983). Precorneal drainage of polyvinyl alcohol solutions in the rabbit assessed by gamma scintigraphy. *Journal of Pharmacy and Pharmacology*, 35(7), 451-454.
- Wilson, M. E., & Coulson, G. (2016). Comparative efficacy of levonorgestrel and deslorelin contraceptive implants in free-ranging eastern grey kangaroos (*Macropus giganteus*). *Wildlife Research*, 43(3), 212-219.
- Wittaya-areekul, S., Prahsarn, C., & Sungthongjeen, S. (2006). Development and in vitro evaluation of chitosan-Eudragit RS 30D composite wound dressings. *AAPS PharmSciTech*, 7(1), E215-E220.
- Wittbrodt, B., & Pearce, J. M. (2015). The effects of PLA color on material properties of 3-D printed components. *Additive Manufacturing*, 8, 110-116.
- Wood, A. J., & Barnes, P. J. (1995). Inhaled glucocorticoids for asthma. *New England Journal of Medicine*, 332(13), 868-875.
- Wrona, M., Cran, M. J., Nerín, C., & Bigger, S. W. (2017). Development and characterisation of HPMC films containing PLA nanoparticles loaded with green tea extract for food packaging applications. *Carbohydrate polymers*, 156, 108-117.
- Wu, J. C.-C., Ray, S., Gizdavic-Nikolaidis, M., Uy, B., Swift, S., Jin, J., & Cooney, R. P. (2014). Nanostructured bioactive material based on polycaprolactone and polyaniline fiber-scaffolds. *Synthetic Metals*, 198, 41-50.
- Wu, L., Janagam, D. R., Mandrell, T. D., Johnson, J. R., & Lowe, T. L. (2015). Long-acting injectable hormonal dosage forms for contraception. *Pharmaceutical research*, 32(7), 2180-2191.
- Xiao, C., & Yang, M. (2006). Controlled preparation of physical cross-linked starch-g-PVA hydrogel. *Carbohydrate polymers*, 64(1), 37-40.

## References

- Yeom, C.-K., & Lee, K.-H. (1996). Pervaporation separation of water-acetic acid mixtures through poly (vinyl alcohol) membranes crosslinked with glutaraldehyde. *Journal of membrane science*, 109(2), 257-265.
- Yin, M.-J., Yamamoto, Y., & Gaynor, R. B. (1998). The anti-inflammatory agents aspirin and salicylate inhibit the activity of I $\kappa$ B kinase- $\beta$ . *Nature*, 396, 77-80.
- Yu, S., Zhang, X., Tan, G., Tian, L., Liu, D., Liu, Y., . . . Pan, W. (2017). A novel pH-induced thermosensitive hydrogel composed of carboxymethyl chitosan and poloxamer cross-linked by glutaraldehyde for ophthalmic drug delivery. *Carbohydrate polymers*, 155, 208-217.
- Zein, I., Hutmacher, D. W., Tan, K. C., & Teoh, S. H. (2002). Fused deposition modeling of novel scaffold architectures for tissue engineering applications. *Biomaterials*, 23(4), 1169-1185.
- Zhang, C., Zhao, K., Hu, T., Cui, X., Brown, N., & Boland, T. (2008). Loading dependent swelling and release properties of novel biodegradable, elastic and environmental stimuli-sensitive polyurethanes. *Journal of Controlled Release*, 131(2), 128-136.
- Zhang, L., Wang, Z., Xu, C., Li, Y., Gao, J., Wang, W., & Liu, Y. (2011). High strength graphene oxide/polyvinyl alcohol composite hydrogels. *Journal of Materials Chemistry*, 21(28), 10399-10406.
- Zhang, X., Tang, K., & Zheng, X. (2016). Electrospinning and crosslinking of COL/PVA nanofiber-microsphere containing salicylic acid for drug delivery. *Journal of Bionic Engineering*, 13(1), 143-149.
- Zhang, Z., Yu, J., Zhou, Y., Zhang, R., Song, Q., Lei, L., & Li, X. (2018). Supramolecular nanofibers of dexamethasone derivatives to form hydrogel for topical ocular drug delivery. *Colloids and surfaces B: Biointerfaces*, 164, 436-443.

## References

- Zolnik, B. S., & Burgess, D. J. (2008). Evaluation of in vivo–in vitro release of dexamethasone from PLGA microspheres. *Journal of Controlled Release*, 127(2), 137-145.
- Zou, X., Zhao, X., Ye, L., Wang, Q., & Li, H. (2015). Preparation and drug release behavior of pH-responsive bovine serum albumin-loaded chitosan microspheres. *Journal of Industrial and Engineering Chemistry*, 21, 1389-1397.